MACROEVOLUTIONARY TRENDS IN PALAEOZOIC ACTINOPTERYGIANS

by

STRUAN A. C. HENDERSON

A thesis submitted to the University of Birmingham for the degree of DOCTOR OF PHILOSOPHY

Department of Earth Sciences

School of Geography, Earth and Environmental Sciences

College of Life and Environmental Sciences

University of Birmingham

March 2023

UNIVERSITY OF
BIRMINGHAM

University of Birmingham Research Archive

e-theses repository

This unpublished thesis/dissertation is copyright of the author and/or third parties. The intellectual property rights of the author or third parties in respect of this work are as defined by The Copyright Designs and Patents Act 1988 or as modified by any successor legislation.

Any use made of information contained in this thesis/dissertation must be in accordance with that legislation and must be properly acknowledged. Further distribution or reproduction in any format is prohibited without the permission of the copyright holder.

Abstract

The Actinopterygii (ray-finned fishes) are a highly successful group of bony fish that dominate modern-day aquatic vertebrate faunas. Though ubiquitous today, actinopterygians were a minor component of fish faunas during the Devonian 'Age of Fishes', when they were overshadowed by agnathans, placoderms and sarcopterygians. The Devonian to Carboniferous transition saw a major shift, with extinctions of placoderms and sarcopterygians paving the way for the diversification of actinopterygians and their establishment as the primary group of fishes by the end of the Permian. The mechanisms of this rise and lasting dominance through the Palaeozoic are poorly understood, however, a suite of compounding factors obscure early actinopterygian spatiotemporal diversity trends, character evolution and relationships. This thesis presents a comprehensive database of Palaeozoic actinopterygian occurrences, identifying major sampling and taxonomic biases influencing face-value trends in diversity. Trends generally track sampling, and there is overwhelming geographic bias towards Europe and North America. Biases are so prolific that sampling standardisation methods fail to recover biologically meaningful palaeodiversity trends beyond a genuine increase following the end-Devonian mass extinction. A small number of poorly defined, widespread genera mask significant taxonomic and morphological diversity. Description of two Carboniferous actinopterygians using CT scanning reveals hidden morphologies and highlights the relative oversight of Carboniferous actinopterygians: a specimen known for over 100 years from the most heavily sampled region of the Palaeozoic record is recognised as a new taxon. This oversight also contributes to phylogenetic uncertainty, as absence of distinct groups in phylogenetic analyses potentially obfuscates character evolution

in the stem-actinopterygians seeding the crown and early, stem-members of extant clades. Despite the seemingly large scale of the problems facing understanding of early actinopterygian evolution, the means of addressing them is clear: taxonomic revision of key genera; expansion of phylogenetic datasets; increased sampling of underrepresented regions; and focus on localised diversity patterns.

Acknowledgements

My first and greatest thanks go to my supervisor Sam Giles, whose endless support and guidance are what have made this thesis possible. Sam not only provided incredible academic supervision but embraced my need for flexibility, especially through difficult times during the COVID pandemic. Sam was also instrumental in helping me prior to my PhD and in encouraging me to undertake a doctorate, for which I am truly grateful. Without her I wouldn't have gotten very far at all. I would also like to thank my co-supervisor Richard Butler for his helpful suggestions and advice throughout the course of my PhD. A special thanks are also due to Emma Dunne, who in many ways acted as an unofficial supervisor during my PhD and whose contributions I greatly appreciate.

So many people assisted me throughout the course of my PhD. I would like to thank Graeme Lloyd, Hannah Byrne, Lisa Schnetz, Martin Brazeau, Matt Friedman, Richard Dearden, Rodrigo Figueroa, Roger Close, Stephan Lautenschlager and Thomas Clements for their insightful discussions and help with software. Particular thanks go to Richard Dearden and Hannah Byrne for our chats, which inevitably digressed from fossil fishes onto ~~far more interesting~~ other topics. Thank you to Christian Kammerer, Victor Goyannes Dill Orrico and Katie Collins for advice about nightmare-inducing taxonomy, and very special thanks to Emma Bernard, Zerina Johanson, Stig Walsh, David Gelsthorpe, Matt Riley and Tim Smithson for collections access and help with specimens. I also thank the Royal Society for funding my PhD research. To all of the other graduate students—Luke, Nicola, Bridget, Alastair, Emma H, JP, Davey and Andy—you made going to work a pleasure during my time in

Birmingham, thank you. I am also particularly grateful for Jake, Iacopo, Soph and Phil, our unanimous despair about actinopterygians made me smile often and kept me going.

I would also like to acknowledge the unknown individuals who worked in the coal mines that many of the specimens I have researched in this thesis came from. In the process of researching the provenance of some specimens I came across tragic accounts of what was a gruelling, and sadly sometimes lethal, way to earn a living.

Shout-out to my friends, whose consistent inquiries as to how long I have left on my PhD were always appreciated. To the Quarantinas – thanks for some fantastic times over the past few years, I rest easy knowing Kiel will always be mine. To the Eavers – I'm genuinely so thankful for the constant contact, it's been a source of much mirth and helped me get through these five years.

Finally, this thesis would have been impossible without the support of my family. Mum and Dad: nothing I have done would have been possible without you, you have fostered my love for palaeontology my entire life and held my hand every step of the way; this thesis is as much yours as it is mine. To my brothers, my best friends, you were always there for me too and I will always cherish our shared moments over the past five years, they lifted me when I needed it. Freddie, my little boy, you taught me more about life and love than I ever thought possible, thank you for giving me perspective and reminding me to have fun. And to my partner, Imogen, you are the roots that gave me the strength to finish this thesis. You have been alongside me at every stage and reflecting on how we've grown together over the last five years brings me as much joy as tea in bed brings you. I love you all.

"Time will not allow of the full treatment of the fishes of the Coal Measures."

– Herbert Bolton, January 18th, 1896.

List of papers

The following papers were published during the course of my doctoral study at the University of Birmingham and are incorporated into this thesis:

HENDERSON, S., DUNNE, E.M., FASEY, S.A. and GILES, S., 2023. The early diversification of ray-finned fishes (Actinopterygii): hypotheses, challenges and future prospects. *Biological Reviews*, 98(1), 284-315. https://doi.org/10.1111/brv.12907.

HENDERSON, S., DUNNE, E.M. and GILES, S., 2022. Sampling biases obscure the early diversification of the largest living vertebrate group. *Proceedings of the Royal Society B*, 289(1985), 20220916. https://doi.org/10.1098/rspb.2022.0916.

Table of Contents

1 Introduction 1
1.1 Actinopterygians – the quintessential bony fishes 1
1.2 Origins and rise of the ray-fins 7
1.3 History of actinopterygian research 12
1.4 Palaeodiversity and sampling bias 15
1.5 Objectives 18
2 The early diversification of ray-finned fishes (Actinopterygii): hypotheses, challenges and future prospects 20
2.1 Introduction 20
2.2 Current hypotheses of Palaeozoic actinopterygian diversity 23
2.2.1 Past studies 23
2.2.2 Devonian diversity patterns 27
2.2.3 Carboniferous diversity patterns 29
2.2.4 Permian diversity patterns 33
2.3 Materials and methods 35
2.3.1 Data preparation 35
2.3.2 Occurrence data 35
2.3.3 Collectors' curves 37
2.4 Results 37
2.4.1 Occurrence data 37
2.4.2 Distribution of Palaeozoic actinopterygians 42
2.4.2.1 United Kingdom and the Republic of Ireland 42
2.4.2.2 Western Europe 44
2.4.2.3 Central Europe 46
2.4.2.4 Eastern Europe 47
2.4.2.5 North America 48
2.4.2.6 Africa 49
2.4.2.7 Asia 50
2.4.2.8 South America 51
2.4.2.9 Oceania 52
2.4.3 Collectors' curves 52
2.5 Challenges to deciphering the Palaeozoic actinopterygian fossil record accurately 57

2.5.1 Fossil record biases 57
2.5.1.1 Geological biases 58
2.5.1.2 Geographic and spatial biases 59
2.5.1.3 Taphonomic biases 61
2.5.2 Taxonomic issues 64
2.5.3 Phylogenetic issues 67
2.6 Conclusions 72
3 Sampling biases obscure the early diversification of the largest living vertebrate group 77
3.1 Introduction 77
3.2 Methods 80
3.2.1 Data preparation 80
3.2.2 Alpha diversity (local richness) 82
3.2.3 Sampling standardisation and diversity estimation 83
3.3 Results 84
3.3.1 Alpha diversity (local richness) 84
3.3.2 Palaeomaps and geographical spread 86
3.3.2.1 Devonian 86
3.3.2.2 Carboniferous 88
3.3.2.3 Permian 89
3.3.3 Palaeodiversity estimates 90
3.3.3.1 Coverage-based rarefaction 90
3.3.3.2 Squares 91
3.3.3.3 Split-and-sum tests 93
3.4 Discussion 93
3.4.1 Biogeographic trends and biases 93
3.4.2 Palaeozoic actinopterygian diversity patterns 96
3.4.3 Unevenness in the actinopterygian fossil record 99
3.5 Conclusion and future directions 103
4 A reinvestigation of the cranial anatomy and taxonomy of *Phanerosteon* (=*Carboveles*) *ovensi* using computed tomography 106
4.1 Introduction 106
4.2 Materials and Methods 110
4.2.1 Specimens 110
4.2.2 Geological context 111

4.2.3 CT scanning 112
4.2.4 Institutional abbreviations 112
4.2.5 Comparative material 112
4.2.6 Anatomical abbreviations 113
4.2.7 Anatomical terminology 113
4.3 Systematic palaeontology 113
4.4 Description 117
4.4.1 Skull roof 117
4.4.2 Infraorbitals 118
4.4.3 Upper jaws and palate 119
4.4.4 Lower jaws 125
4.4.5 Shoulder girdle, operculogular system and gill skeleton 127
4.5 Discussion 128
4.5.1 Updates to previous descriptions 128
4.5.2 Morphological changes in the Carboniferous 132
4.5.3 Ecological expansions 134
4.6 Conclusions 137
5 A new genus and species of actinopterygian from the Upper Carboniferous (Bashkirian) of Northern England 138
5.1 Introduction 138
5.2 Materials and Methods 142
5.2.1 Specimens 142
5.2.2 Geological context 143
5.2.3 CT scanning 143
5.2.4 Institutional abbreviations 144
5.2.5 Comparative material 144
5.2.6 Phylogenetic analyses 144
5.2.7 Anatomical abbreviations 147
5.2.8 Anatomical terminology 149
5.3 Systematic palaeontology 149
5.4 Description 152
5.4.1 Dermal cranial elements 152
5.4.2 Braincase 157
5.4.3 Parasphenoid 162

5.4.4 Endocast 162
5.4.5 Upper jaws and palate 165
5.4.6 Lower jaws 168
5.4.7 Hyoid and gill skeleton 169
5.4.8 Pectoral girdle 176
5.4.9 Pelvic girdle 180
5.4.10 Fins 181
5.4.11 Axial skeleton 182
5.4.12 Squamation 185
5.5 Phylogenetic results 185
5.6 Discussion 190
5.6.1 Taxonomic reassessment 190
5.6.2 Comparative morphology 194
5.6.3 Phylogenetically forgotten fishes 199
5.7 Conclusion 200
6 Summary and Future Directions 202
6.1 Summary 202
6.2 The importance of taxonomic and descriptive study 204
6.3 Future palaeodiversity studies 205
6.4 Progress in phylogenetic investigation 208
References 213
Appendices 258
A Supplementary Information from Henderson *et al*. (2023) 258
A.1 Occurrence and interval data 258
A.2 Supplementary Figures 259
B Supplemental Material from Henderson *et al*. (2022) 261
B.1 Occurrence data and code 261
B.2 Supplementary Figures 262
C Supplementary Information for Chapter 5 273
C.1 Additional images of MM L.1696 273
C.2 Taxon list for phylogenetic analyses 274
C.3 Character list for phylogenetic analyses 278
C.4 *Mesonichthys aitkeni* genus and species diagnoses 322
C.5 Supplementary Figures 323

List of Figures

Figure 1.1: Simplified cladogram showing the relationships of extant actinopterygian clades 2

Figure 1.2: Simplified cladogram showing relationships of vertebrates 6

Figure 1.3: A simplified Palaeozoic timescale, showing early osteichthyan and actinopterygian fossils and key global Palaeozoic events 8

Figure 2.1: Diversity of Palaeozoic actinopterygians through time presented in previous studies..... 24

Figure 2.2: Raw counts of Palaeozoic actinopterygian genera and sampling proxies from the Paleobiology Database..... 26

Figure 2.3: Geographic spread of actinopterygians occurrences entered in the Paleobiology Database 30

Figure 2.4: Raw counts of Palaeozoic actinopterygian genera and sampling proxies from occurrence data..... 38

Figure 2.5: Raw counts of Palaeozoic actinopterygian genera and species in standard International Commission on Stratigraphy (ICS) stages 40

Figure 2.6: Geographic spread of actinopterygians occurrences 43

Figure 2.7: Distribution of widespread actinopterygian genera..... 45

Figure 2.8: Collector's curve of Palaeozoic actinopterygians 53

Figure 2.9: Network of phylogenetic analyses of Palaeozoic actinopterygians 68

Figure 2.10: Phylogenetic analyses of Palaeozoic actinopterygians 70

Figure 3.1: Local richness Palaeozoic actinopterygians..... 85

Figure 3.2: Palaeomaps of local richness..... 87

Figure 3.3: Coverage-based rarefaction estimates..... 91

Figure 3.4: Squares diversity estimates..... 92

Figure 4.1: Specimens of *Phanerosteon* 109

Figure 4.2: Lateral view of NHMUK PV P.13184 118

Figure 4.3: Left lateral view of NHMUK PV P.13184 120

Figure 4.4: Infraorbitals of NHMUK PV P.13184 121

Figure 4.5: Upper jaw of NHMUK PV P.13184 122

Figure 4.6: Right upper and lower jaw of NHMUK PV P.13184 123

Figure 4.7: Parasphenoid of NHMUK PV P.13184 124

Figure 4.8: Clavicle and cleithrum of NHMUK PV P.13184 127

Figure 4.9: Specimens of *Phanerosteon* showing differences in tail morphology ... 131

Figure 5.1: Locality and stratigraphic context of 'new taxon' MM L.1696 141

Figure 5.2: Photograph and renders of 'new taxon' MM L.1696 153

Figure 5.3: Cranium of 'new taxon' MM L.1696 154

Figure 5.4: Braincase of 'new taxon' MM L.1696 156

Figure 5.5: Jaws and palate of 'new taxon' MM L.1696 167

Figure 5.6: Hyoid and gill skeleton of 'new taxon' MM L.1696 170

Figure 5.7: Rearticulated braincase, jaws, hyoid and gill skeleton of 'new taxon' MM L.1696 173

Figure 5.8: Shoulder girdle and pectoral endoskeleton of 'new taxon' MM L.1696. 177

Figure 5.9: Pelvic girdle of 'new taxon' MM L.1696 181

Figure 5.10: Axial elements of 'new taxon' MM L.1696 183

Figure 5.11: Results of parsimony analysis 186

Figure 5.12: Results of Bayesian analysis (50% majority rule) 188

Figure 5.13: Results of Bayesian analysis (All compatable clades) 189

Figure 5.14: Treespace 190

Figure 5.15: Comparative anatomy of *Mesonichthys aitkeni* 192

Figure 5.16: Hyomandibular morphology of selected actinopterygians 197

1 Introduction

1.1 Actinopterygians – the quintessential bony fishes

The Actinopterygii, or ray-finned fishes, today account for more than 36,000 species and the overwhelming majority of aquatic vertebrate biodiversity (Nelson *et al.*, 2016). Scientific research continues to grow this number, having added 3,478 new species in the past ten years (Fricke *et al.*, 2023). This astonishing taxonomic diversity includes fishes which range in size from the miniscule stout infantfish (*Schindleria brevipinguis*), measuring only 6.5 mm long (Watson & Walker, 2004), to the monstrous 8 m long oarfish (*Regalecus glesne*; Benfield *et al.*, 2013) and gargantuan 2,300 kg giant sunfish (*Mola alexandrine*; Sawai & Nyegaard, 2022). Ray-fins are essential members of modern ecosystems and occur in nearly every aquatic habitat on Earth, including some of the most extreme, such as hypersaline lakes (Magadi tilapia, *Alcolapia grahami*; Kavembe *et al.*, 2016), pitch-black caves (the blind cavefish, *Cryptotora thamicola*; Flammang *et al.*, 2016), the deepest parts of the ocean at depths of over 8,000 m (Mariana snailfish, *Pseudoliparis swirei*; Linley *et al.*, 2016; Gerringer *et al.*, 2017), and even 5,200 m altitude thermal hot springs (Tibetan stone loach, *Triplophysa stolickai*; Kottelat, 2012). Staggering morphological disparity, with forms as disparate as seahorses and eels, also mirrors the taxonomic, niche and habitat diversity of ray-fins.

The vast majority of extant actinopterygians belong to the hyperdiverse group Teleostei, which has dominated fish faunas since at least the Cretaceous period (Friedman, 2022). Prior to this, however, non-teleost lineages accounted for a greater

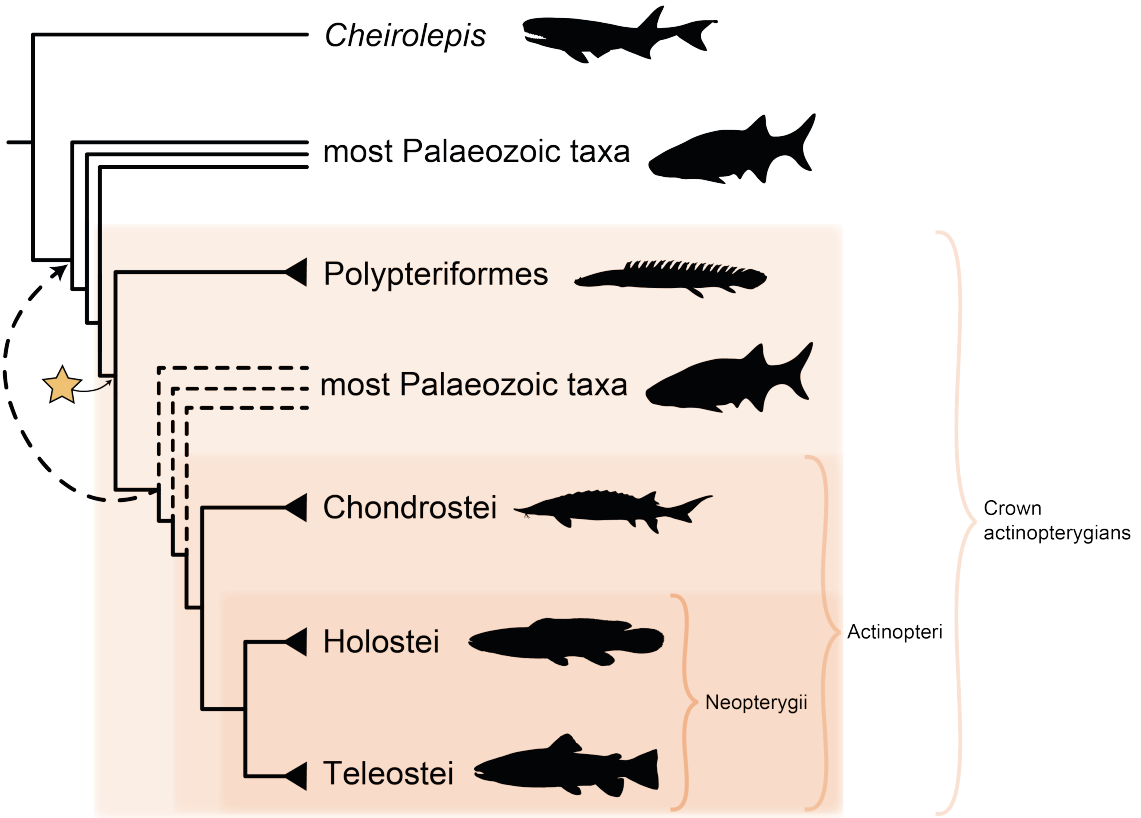


Figure 1.1: Simplified cladogram showing the relationships of extant actinopterygian clades, *Cheirolepis* and most Palaeozoic actinopterygians. Dotted line indicates hypothesised placement of Palaeozoic taxa within the crown in most analyses prior to that of Giles *et al.* (2017), with the arrow indicating the shift to the stem. The star indicates the actinopterygian crown node. *Cheirolepis* represented by *Cheirolepis trailli*; Palaeozoic taxa represented by *Mimipiscis toombsi*; Polypteriformes represented by *Polypterus bichir*; Chondrostei represented by *Acipenser oxyrhynchus*; Holostei represented by *Amia calva*; Teleostei represented by *Salmo trutta*. Silhouettes from phylopic.org, with thanks to Brian Choo, Carlos Cano-Barbacil, Michael Keesey and Yan Wong.

proportion of diversity. The Holostei, consisting of the Halecomorphi (bowfins) and Ginglymodi (gars) (Grande & Bemis, 1998; Grande, 2010; López-Arbarello *et al.*, 2016; Brito, Alvarado-Ortega & Meunier, 2017), are sister to the Teleostei (Arratia, 1997, 1999, 2001). Together, holosteans and teleosts form the Neopterygii (Fig. 1.1); both groups were prominent in the Jurassic (Lambers, 1999; Clarke & Friedman, 2018). Paddlefish and sturgeons comprise the Chondrostei, which are sister to neopterygians (Fig. 1.1). Indeed, the chondrostean stem-lineage, populated by the Mesozoic

chondrosteids and peipiaosteids, is contemporaneous with their neopterygian counterparts (Grande & Bemis, 1991, 1996; Grande *et al.*, 2002; Grande & Hilton, 2006; Hilton & Forey, 2009). Polypteriformes (bichirs and reedfish) are the earliest diverging extant actinopterygian lineage (Hughes *et al.*, 2018; Dornburg & Near, 2021), sister to the Actinopteri (the clade comprised of the Chondrostei and Neopterygii).

Early cladistic and phylogenetic studies placed only the Devonian actinopterygian *Cheirolepis* outside the actinopterygian crown (Fig. 1.1; Patterson, 1982; Gardiner, 1984; Gardiner & Schaeffer, 1989; Taverne, 1997; Coates, 1999; Gardiner, Schaeffer & Masserie, 2005), despite this resulting in an unpopulated stem-lineage lasting over 285 million years (Dutheil, 1999). A consequence of this placement was that the remainder of extinct actinopterygians branched within the crown group, a result which propagated throughout subsequent phylogenetic studies (Xu & Gao, 2011; Xu *et al.*, 2014). Recently, a major revision of phylogenetic datasets recognised the Triassic group Scanilepiformes as stem-polypteriforms (Giles *et al.*, 2017). This not only massively shortened the length of the empty polypteriform stem-lineage but shifted most Palaeozoic taxa onto the actinopterygian stem (Fig. 1.1), corroborating a handful of prior studies (Cloutier & Arratia, 2004; Mickle *et al.*, 2009).

Relationships between early actinopterygians and their position relative to the extant lineages are extremely volatile, however, with major changes resulting from minor modifications to taxa and characters. In many analyses, stem-actinopterygians form a large polytomy (Latimer & Giles, 2018; Figueroa, Friedman & Gallo, 2019; Stack & Gottfried, 2021). In others, separate clades of pre- and post-Devonian taxa branch successively from the stem (Giles *et al.*, 2017; Wilson *et al.*, 2018; Argyriou *et al.*, 2018; Argyriou *et al.*, 2022; Figueroa *et al.*, 2021; Ren & Xu, 2021), which suggests relatively

few lineages crossed the Devonian-Carboniferous boundary. The most recent studies challenge this view and point towards greater diversification prior to the boundary, with numerous lineages crossing into the Carboniferous (Giles *et al.*, 2023). A significant issue with existing matrices, however, is that many hypothesised clades from the literature are absent (e.g. Aeduellidae [Heyler, 1969, 1977, 2000; Gottfried, 1987; Štamberg, 2007, 2018; Mickle, 2011], Haplolepidae [Westoll, 1944; Lowney, 1980a, 1983; Huber, 1992; Elliott, 2014], Ptycholepidae [Aldinger, 1937; Brough, 1939; Gardiner, 1967; Gardiner & Schaeffer, 1989; Bürgin, 1992; Romano *et al.*, 2019]) or have not had their monophyly explicitly tested (Eurynotiformes [Sallan & Coates, 2013; Friedman *et al.*, 2018]), resulting in a failure to capture the totality of early actinopterygian diversity in a comprehensive phylogenetic hypothesis. Thus, missing data may be causing unpredictable or inaccurate sequences of character evolution. While missing data may contribute to contrasting and unresolved topologies, the problem is exacerbated by ambiguity in character sets defining stem-actinopterygian relationships and widespread homoplasy.

In the context of an extensive, unresolved stem and highly morphologically derived extant lineages, defining actinopterygian characteristics is difficult. While the group's name derives from the Ancient Greek terms for 'ray' (*aktis*) and 'fins' (*ptérux*), fin rays are not exclusive to ray-finned fishes (Friedman & Brazeau, 2010). Instead, modern ray-fins share various features related to their soft-tissue anatomy and physiology (Friedman, 2015), though these may not necessarily apply to the actinopterygian total group (i.e. early fossil forms). For example, recent studies show that some aspects of brain development and morphology common to living actinopterygian clades (Nieuwenhuys, 1982) are absent in fossilised actinopterygian

brains (though other aspects of brain morphology such as modified rhombencephalic meningeal tissues remain shared; Figueroa *et al.*, 2023). Exceptionally preserved fossil actinopterygians conserving soft-tissue are extremely rare, however, and characters distinguishing early actinopterygians from closely related fishes are necessarily based on hard-tissue morphology that is more typically preserved in the fossil record, despite subsequent losses or absence in living species. These synapomorphies were outlined by Friedman (2015) as: 1) no jugal sensory canal; 2) median aortic canal (enclosed dorsal aorta) in neurocranium; 3) narrow interorbital septum of neurocranium consisting of a single sheet of bone; 4) no basal plates; 5) haemal spines longer than caudal radials; 6) acrodin; 7) fenestra in palatoquadrate for basipterygoid articulation; 8) perforate pectoral propterygium; and 9) multiple superimposed layers of enamel ("ganoine"). However, new CT-based techniques have altered our understanding of the morphology of the earliest actinopterygians and complicated the picture of their evolution. Redescriptions of *Cheirolepis trailli* (Giles *et al.*, 2015b) and *Meemannia eos* (Lu *et al.*, 2016) showed that only two characters represented clear actinopterygian synapomorphies: 1) supratemporals extending posterior to the parietals; and 2) the presence of an endocranial lateral cranial canal (though the absence of a surface for the parasymphysial whorl on the lower jaw likely represents an additional synapomorphy; Lu *et al.*, 2016). The characters listed by Friedman (2015) instead define successive nodes excluding *Meemannia* (1, 4, 5, 7, and 9 above) and *Cheirolepis* (2, 3, 6 and 8 above; Lu *et al.*, 2016: fig. 4).

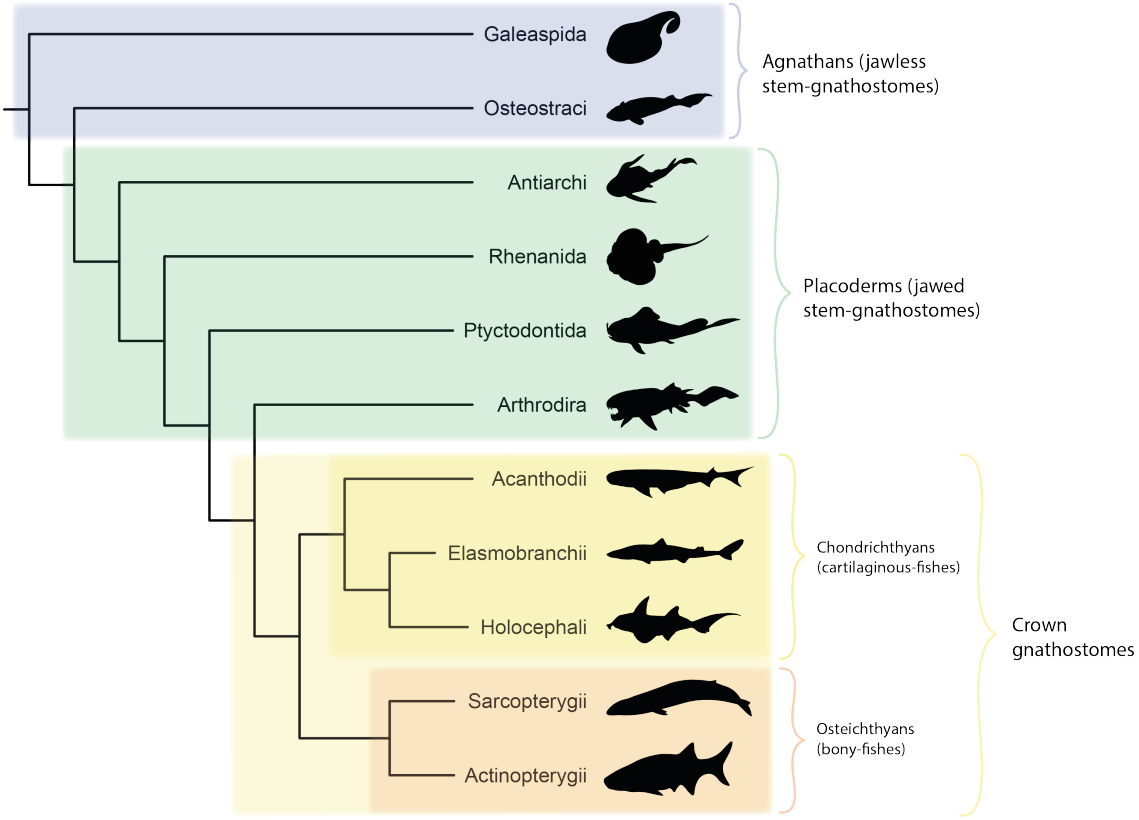


Figure 1.2: Simplified cladogram showing relationships of vertebrates, adapted from (Brazeau and Friedman, 2015; Qiao *et al.*, 2016; Zhu *et al.*, 2022). Agnathans – blue; chondrichthyans – yellow; osteichthyans – orange; placoderms – green. Galeaspida represented by *Hanyangaspis guodingshanensis*; Osteostraci represented by *Hemicyclaspis*; Antiarchi represented by *Bothriolepis canadensis*; Rhenanida represented by *Gemuendina stuerzti*; Ptyctodontida represented by *Materpiscis attenboroughi*; Arthrodira represented by *Dunkleosteus*; Acanthodii represented by *Acanthodes bronni*; Elasmobranchii represented by *Squalus acanthias*; Holocephali represented by *Callorhinchus milii*; Sarcopterygii represented by *Balaenoptera musculus*; Actinopterygii represented by *Mimipiscis toombsi*. Silhouettes from phylopic.org, with thanks to Brian Choo, Ghedoghedo, Ignacio Contreras, Maija Karala, Nobu Tamura, Phillipe Janvier, Steven Coombs and Tony Ayling.

Meemannia illustrates the complexity of identifying definitive actinopterygian characters and differentiating them from close relatives, as it was originally placed within the Sarcopterygii (Zhu *et al.*, 2006; Zhu *et al.*, 2010). The Sarcopterygii, or lobe-finned fishes, include the coelacanths, lungfish, and all tetrapods, and are the sister-group to Actinopterygii (Fig. 1.2). Together, these groups belong to the Osteichthyes

(bony-fishes), which in turn is sister to the Chondrichthyes (cartilaginous-fishes, including both extinct groups such as the Acanthodii and living sharks and rays). Outside this group of crown gnathostomes (chondrichthyans and osteichthyans) are successively diverging lineages of jawed and jawless fishes, belonging to paraphyletic groups of ‘placoderms’ and ‘agnathans’ (Fig. 1.2; Brazeau and Friedman, 2015; Qiao *et al.*, 2016; Zhu *et al.*, 2022). These lineages have no direct extant descendants, and are therefore stem-gnathostomes, as they branch between crown gnathostomes and the next most closely related extant agnathan clade: Cyclostomi (hagfishes and lampreys; Miyashita *et al.*, 2019). In fact, it is these other groups of fishes, and not the ray-fins we today recognise as ‘quintessentially fishy’, who gave the Devonian period the title of ‘the Ages of Fishes’. It is in the shadows of agnathans, placoderms, acanthodians and sarcopterygians that early actinopterygians swam.

1.2 Origins and rise of the ray-fins

The most recent time-scaled phylogeny of actinopterygians (Giles *et al.*, 2023) that explicitly uses fossils within the analysis to calibrate nodes estimates the age of the actinopterygian total-group to be close to the Ordovician-Silurian boundary (~443.8 Ma, Fig. 1.3; Gradstein *et al.*, 2020). Despite this, the earliest microfossils suggested to represent actinopterygian scales do not occur until the late Silurian. The scale-based taxa *Naxilepis gracilis* and *Ligulaepis yunnanensis* occur in the early Ludfordian of Yunnan, China, and were initially described as actinopterygians (Wang & Dong, 1989) though they only exhibit scale characteristics shared by early osteichthyans and not

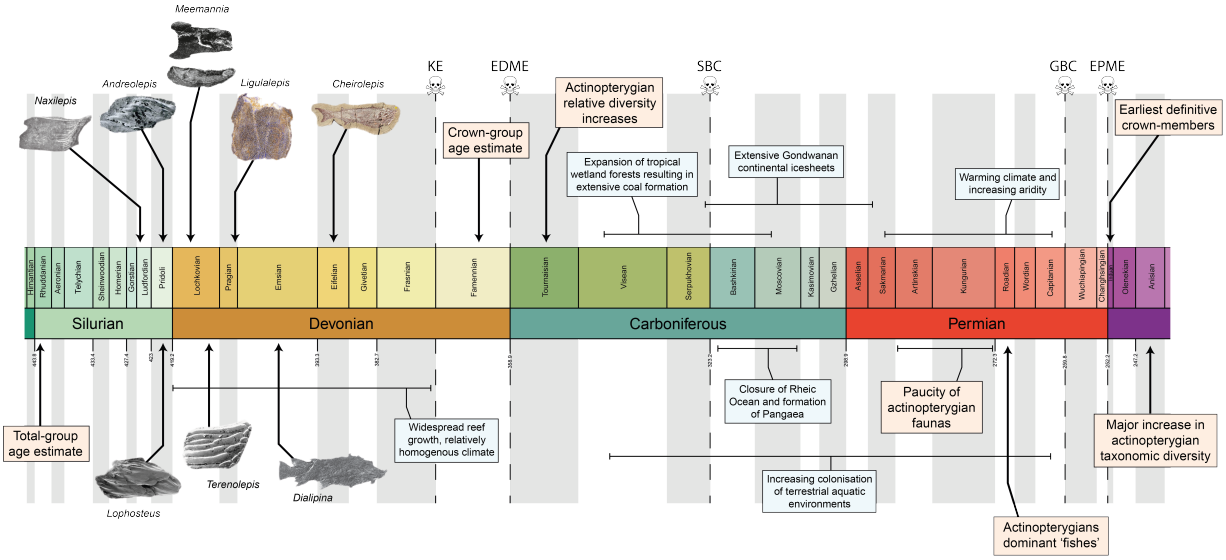


Figure 1.3: A simplified Palaeozoic timescale, showing early osteichthyan and actinopterygian fossils (Schultze, 1968; Wang & Dong, 1989; Burrow, 1995; Basden & Young, 2001; Märss, 2001; Schultze & Cumbaa, 2001; Schultze & Märss, 2004), key events in actinopterygian evolutionary history (Friedman & Sallan, 2012; Friedman, 2015; Giles *et al.*, 2023), and key global Palaeozoic events (Qie *et al.*, 2019). EDME – End-Devonian Mass Extinction; EPME – End-Permian Mass Extinction; GBC – Guadalupian Biodiversity Crisis; KE – Kellwasser Event; SBC – Serpukhovian Biodiversity Crisis.

features diagnostic of Actinopterygii (Botella *et al.*, 2007; Friedman & Brazeau, 2010; Giles *et al.*, 2015c). This is also true of later scale taxa from the Pridoli (Silurian) and Lochkovian (Devonian), including *Andreolepis hedei* (Märss, 2001), *Lophosteus superbus* (Schultze & Märss, 2004) and *Terenolepis turnerae* (Burrow, 1995).

From the late 19th century until 2016, the oldest definitive actinopterygian was considered to be the Middle Devonian taxon *Cheirolepis trailli* from Old Red Sandstone deposits of Scotland (Fig. 1.3; Traquair, 1875; Pearson & Westoll, 1979). The late 20th and 21st century discovery of numerous definitive sarcopterygians, the sister group to Actinopterygii, in the late Silurian and earliest Devonian evidenced the necessary existence of actinopterygians and left a major gap in the actinopterygian fossil record (Chang, 1982; Zhu & Fan, 1995; Zhu & Yu, 2002; Lu & Zhu, 2009). The redescription

of *Meemannia eos* from the Lochkovian of China as an actinopterygian by Lu *et al.* (2016) closed this gap (Fig. 1.3), although early Devonian actinopterygians remain very rare relative to sarcopterygians and other gnathostome fishes. Only two other occurrences have been suggested as representing actinopterygians during the near 20-million-year gap separating *Meemannia* and *Cheirolepis*: *Ligulalepis toombsi* (and associated braincase material tentatively referred to the species), from the Lower Devonian of Australia (Fig. 1.3; Schultze, 1968; Basden and Young, 2001; Clement *et al.*, 2018), and *Dialipina salgueiroensis*, from the Lower Devonian of Canada (Fig. 1.3; Schultze, 1968; Schultze and Cumbaa, 2001). As with the earlier scale taxa, however, these taxa lack any actinopterygian synapomorphies and more likely represent stem-osteichthyans (Friedman & Brazeau, 2010; Brazeau & Friedman, 2015).

Two distinct actinopterygian species of *Moythomasia* are present in the late Givetian-early Frasnian Bergisch-Gladbach fauna (Ørvig, 1960; Choo, 2015), though the first instance of multiple definitive actinopterygian genera from a single fauna is in the Frasnian Gogo Formation Lagerstätte of Australia, one of the largest barrier reef systems present in the fossil record (Long & Trinajstic, 2010, 2017; Trinajstic *et al.*, 2022). In fact, prior to the Famennian, temperature differences between polar and equatorial regions were slight, allowing extensive reef development even at mid-high palaeolatitudes (Fig. 1.3; Copper and Scotese, 2003). Absence of actinopterygians from many Devonian reef deposits points towards genuine rarity of actinopterygians in the Devonian, and those that were present were morphologically conservative (Anderson *et al.*, 2011; Deakin *et al.*, 2022). While cooling temperatures (Joachimski & Buggisch, 2002; Joachimski *et al.*, 2009; Huang *et al.*, 2018) and oceanic anoxia (Bond *et al.*, 2013; Carmichael *et al.*, 2014; Zhang *et al.*, 2020) are hypothesised to

have caused a mass extinction in marine invertebrates at the Frasnian-Famennian boundary (Kellwasser Event), vertebrates appear to pass through the event unscathed (Sallan & Coates, 2010). Instead, the Devonian-Carboniferous boundary (Hangenberg Event) represents a major mass extinction for vertebrates (Sallan & Coates, 2010; Assemat *et al.*, 2022), as well as many marine invertebrate groups (Sepkoski, 1996; Alroy *et al.*, 2008; Tolokonnikova & Ernst, 2021; Hou *et al.*, 2022).

Devonian actinopterygians were clearly outnumbered by other fishes (sarcopterygians, placoderms, acanthodians), but the transition to the Carboniferous saw this imbalance reversed (Sallan & Coates, 2010). By the Permian, actinopterygians were the overwhelmingly dominant aquatic fishes (Friedman, 2022: fig. 2). The transition from placoderm-sarcopterygian dominant to actinopterygian-chondrichthyan dominant faunas brought about by the end-Devonian mass extinction event (Sallan & Coates, 2010; Friedman & Sallan, 2012; Sallan & Galimberti, 2015) is marked not only by an increase in taxonomic diversity, but also morphological change. Early Carboniferous actinopterygians occupy a wider range of morphospace (Sallan & Friedman, 2012) and tend to be smaller (Sallan & Galimberti, 2015; Giles *et al.*, 2023) than Devonian actinopterygians, though trends in actinopterygian body size through the extinction event remain unclear (Giles *et al.*, 2023). The initial rise of actinopterygians occurs alongside changing climatic conditions, such as low atmospheric CO_2, major glaciation in the Southern Hemisphere, and coincident sea-level changes (Fig. 1.3; McGhee *et al.*, 2012; Montañez and Poulsen, 2013; Wang *et al.*, 2013; Montañez, 2016; Qie *et al.*, 2019; Aretz *et al.*, 2020; Griffis *et al.*, 2023). Evidence from the broader marine record suggests that these conditions were ideal for widespread taxa occupying broad niches (Qie *et al.*, 2019). Indeed, as with the

Frasnian-Famennian Kellwasser Event, the Serpukhovian Biodiversity Crisis (Sepkoski, 1996; McGhee *et al.*, 2012) appears to have had little impact on actinopterygians (Patterson, 1994; Blieck, 2011).

Unlike modern faunas, however, actinopterygians were not the overwhelmingly dominant fish group; chondrichthyans also accounted for a significant proportion of fish diversity in the Carboniferous (Sallan & Coates, 2010). The extent to which this may reflect differences in taxonomic practice and the distinctiveness of microfossils (many chondrichthyan taxa are identifiable based on isolated remains, which is not the case for actinopterygians; Ivanov & Lucas, 2019; Ginter & Wilk, 2021) is unclear. Nonetheless, chondrichthyan face-value and subsampled diversity declines significantly throughout the late Palaeozoic (Schnetz, 2022), while actinopterygians account for increasingly higher proportions of fish taxa (Friedman, 2015). Actinopterygian taxic diversity does apparently decrease in the Permian, though actinopterygians still greatly outnumber sarcopterygian bony-fishes (Romano *et al.*, 2016). Importantly, this trough may not reflect 'true' diversity decline, but rather geological bias resulting from an absence of deposits, associated with the formation of Pangaea (Friedman & Sallan, 2012; Stampfli *et al.*, 2013). Overall, it is unclear whether the Permian actinopterygian record is sufficient to determine clear trends, let alone the effect of major events such as the Guadalupian Biodiversity Crisis which impacted the marine invertebrate and tetrapod records (Clapham *et al.*, 2009; Day *et al.*, 2015; Lucas, 2017; Rampino & Shen, 2021).

Aquatic vertebrate faunas in the Mesozoic increasingly begin to resemble modern ones dominated by teleost actinopterygians (Friedman, 2022), with a further reduction in chondrichthyan relative diversity following the end-Permian mass

extinction (Romano *et al.*, 2016). Mesozoic faunas yield the first identifiable members of the extant clades (Fig. 1.3)—polypteriforms (Xu & Gao, 2011; Xu *et al.*, 2014; Giles *et al.*, 2017), chondrosteans (Grande *et al.*, 2002; Grande & Hilton, 2006; Hilton & Forey, 2009), holosteans (Grande & Bemis, 1998; Grande, 2010; López-Arbarello *et al.*, 2016) and teleosts (Arratia, 2013; Tintori *et al.*, 2015)—while overall face-value taxonomic diversity also increases (Romano *et al.*, 2016). Node age estimates from both molecular and palaeontological timescaling (Clarke *et al.*, 2016; Giles *et al.*, 2023), however, suggest that the roots of this diversification and the actinopterygians' rise to dominance lie firmly in the Palaeozoic.

1.3 History of actinopterygian research

The first Palaeozoic actinopterygian specimens were described over 200 years ago by Henri-Marie Ducrotay de Blainville (Blainville, 1818; Brignon, 2019), and thus predate even the use of the term 'palaeontology' (Blainville, 1822); for historical context, this was only three years after the Battle of Waterloo, and the year that Emily Brontë, Frederick Douglass and Karl Marx were born. Agassiz subsequently dropped the two genera erected by Blainville, *Palaeothrissum* and *Stromateus*, and incorporated them into *Palaeoniscum* and *Platysomus*, respectively, in his seminal work '*Recherches sur les poissons fossiles*' (Agassiz, 1833-1844), which laid the foundations for palaeoichthyology. Work on fossil actinopterygians blossomed in the second half of the 19th century thanks to contributions from many European and North American naturalists (Giebel, 1848; Egerton, 1850, 1856; King, 1850; Newberry, 1856; Eichwald, 1861; Kirkby, 1864; Young, 1866; Newberry & Worthen, 1870; Hancock & Howse, 1870; Hancock & Atthey, 1872; Frič, 1879; Rzehak, 1881) and the considerable work

of British ichthyologists Arthur Smith Woodward and Ramsay Traquair (Traquair, 1877-1914; Woodward, 1889-1901; Lloyd & Friedman, 2013).

Notably, the interests of these naturalists coincided with the increasing industrialisation of western Europe and North America. Earth's coal deposits are primarily Carboniferous and Permian in age (Cleal & Thomas, 2005; Schachat *et al.*, 2023) and due to widespread Carboniferous forestation in Euamerica and burial of large quantities of organic matter (Nelsen *et al.*, 2016) extensive deposits occur in present-day Europe and North America (Opluštil & Cleal, 2007). Discoveries of Carboniferous fishes were therefore in no small part a by-product of the economic demand for coal to fuel global industry (Knick Harley, 1989; Clark & Jacks, 2007). Miners extracting coal from the late Palaeozoic deposits of Europe and North America regularly stumbled upon fossilised remains of fishes, many of which were collected by mine owners or private collectors and found their way into museum collections (Page, 1977). It is important to note, however, that the institutions which enabled many of these early naturalists' work are deeply rooted in a colonial past (Manias, 2015; Das & Lowe, 2018; Vogel, 2019; Raja *et al.*, 2022) at a time when European imperialism was at its peak (Aldrich, 2009).

While undoubtedly pioneering, this early work was the root of clear biases in the Palaeozoic record of actinopterygians. It was common practice to erect new species on the basis of minor morphological differences, while at the same time encompassing them in poorly defined genera (cf. *Amblypterus* Agassiz, *Elonichthys* Giebel, *Palaeoniscum* Agassiz, *Platysomus* Agassiz, *Rhadinichthys* Traquair). This bias propagated throughout the 19th and 20th centuries, with subsequent authors erecting higher-level taxonomic groups (e.g. Amblypteridae, Palaeoniscidae and Platysomidae)

on the basis of these animals and still describing most Palaeozoic actinopterygians under the blanket term ‘palaeoniscoids’ (Sallan, 2014). Furthermore, many 20th and 21st century studies focused extensively on Devonian actinopterygians (Sallan, 2014), despite the abundance of Carboniferous forms curated in museum collections. Recent redescriptions are beginning to address these problems (Coates & Tietjen, 2018; Friedman *et al.*, 2018; Schindler, 2018), revealing that existing genera (and their broad definitions) superficially conceal considerable taxonomic and morphological diversity. The availability of new techniques, such as CT scanning, combined with the abundance of historically overlooked Carboniferous and Permian taxa housed in museum collections provide ample opportunities to reinvestigate early actinopterygians. New descriptions of Palaeozoic actinopterygians (often utilising CT scanning) continue to outpace redescriptions and taxonomic revision, however (Giles *et al.*, 2015b, 2023; Elliott, 2016; Štamberg, 2016b; Mickle, 2017, 2018; Wilson *et al.*, 2018; Choo *et al.*, 2019; Bakaev & Kogan, 2020; Figueroa *et al.*, 2021; Newman *et al.*, 2021; Stack & Gottfried, 2021), evidencing researchers’ preference to describe new taxon and adding ‘novelty bias’ to the record (Alroy, 2010b).

Concentration of both historical and recent work in Europe and North America also causes geographic bias in sampling, as well as a consequent concentration of this knowledge (‘scientific colonialism’; Raja *et al.*, 2022). As yet, no study has quantitatively investigated biases impacting the Palaeozoic actinopterygian record (Friedman & Sallan, 2012).

1.4 Palaeodiversity and sampling bias

As well as erecting numerous genera that exist to this day, Agassiz (1833-1844) also presented the first representation of trends in palaeodiversity through time, focusing on various groups of fishes (including actinopterygians as part of the 'Ordre des Ganoïdes'). However, subsequent studies attempting to quantify the diversity of actinopterygians did not occur until the latter 20th century (Thomson, 1977; Patterson, 1994) and used compendia of the fossil record (Romer, 1966; Benton, 1993) to plot actinopterygian family- or genus-level diversity. These studies closely followed seminal studies critically examining face-value Phanerozoic taxonomic diversity more broadly and investigating the role of uneven temporal and spatial sampling in variation of diversity through time (Valentine & Peddicord, 1967; Valentine, 1968; Raup, 1972, 1976; Sepkoski *et al.*, 1981).

Crucially, this marked the beginning of research on "sources of error" (i.e. biases) impacting palaeodiversity (Raup, 1972) and stimulated a proliferation of studies seeking to tease apart signal from bias, including the effect of interval lengths (Foote, 1994; Guillerme & Cooper, 2018; Dean *et al.*, 2020), Lagerstätten (Benson & Butler, 2011; Butler *et al.*, 2013; Romano *et al.*, 2016; Flannery Sutherland *et al.*, 2019; de Celis *et al.*, 2021), species-area relationships (Sepkoski, 1976; Barnosky, Carrasco & Davis, 2005; Close *et al.*, 2017), sediment or outcrop availability (Smith, 2001; Peters, 2005; Peters & Heim, 2010; Smith & McGowan, 2011; Hannisdal & Peters, 2011; Smith, Lloyd & McGowan, 2012; Dunhill *et al.*, 2014; Dunhill *et al.*, 2018), and taxonomic group preference (Whitaker & Kimmig, 2020) on palaeodiversity. Numerous subsequent studies also realised fossil record biases stemming from other sources not

highlighted by Raup (1972), such as depositional palaeoenvironment (Zuschin *et al.*, 2011; Dunhill *et al.*, 2014; Cleary *et al.*, 2015, 2020; Romano *et al.*, 2016), size (Behrensmeyer, 1988; Williams & Lucas, 2013; Brown *et al.*, 2013), and taphonomy (Hendy, 2011; Muscente *et al.*, 2017; Purnell *et al.*, 2018; Flannery Sutherland *et al.*, 2019), all of which impact the eventual face-value record.

Emergent in recent literature focusing on the impact of bias on palaeodiversity are the impact of significant spatial biases and historical sources of anthropogenic bias. Research showing significant spatial structuring of both the marine and terrestrial Phanerozoic fossil records (Vilhena and Smith, 2013; Benson *et al.*, 2016; Close *et al.*, 2020a, 2020b; Flannery-Sutherland, Silvestro and Benton, 2022) challenges interpretations of 'global' fossil records (Vermeij & Leighton, 2003). Increasingly, it is clear that 'global' fossil records are in fact amalgamations of regional fossil records, each subject to heterogenous processes (including varied biasing factors) acting at different spatial and temporal scales (Benson *et al.*, 2021; Flannery-Sutherland *et al.*, 2022). Importantly, these biases do not occur in isolation; in fact, interactions are likely to be prolific. For example, historical and ongoing palaeontological research in North America and Europe, initially facilitated by exploitative and industrial practices and today enabled by historical precedent, institutional prestige and availability of funding (Raja *et al.*, 2022), has contributed significantly to the spatial structuring of the fossil record, with occurrences through time heavily concentrated in these regions (Allison & Briggs, 1993; Vilhena & Smith, 2013; Benson *et al.*, 2021; Ye & Peters, 2023). Other regions of the world are significantly underrepresented, in terms of occurrences per sedimentary rock map area, relative to western Europe and North America (Ye & Peters, 2023). The vast majority of knowledge (including many physical specimens,

regardless of their provenance) is also concentrated in North America and Europe, and publications on palaeodiversity are mainly driven by researchers at North American and European institutions (Raja *et al.*, 2022). Additionally, collections of fossil specimens that have aggregated over the past 200 years are likely influenced by collector biases, with collectors favouring the best-preserved specimens and discarding others, and/or preferentially collecting only specimens from particular taxonomic groups (Dunne, 2020).

Alongside studies highlighting fossil record biases came methodological development of statistical techniques seeking to tease genuine biological signal out of the face-value fossil record. Residual modelling approaches use the relationship between face-value diversity and a sampling proxy to identify instances when diversity was higher or lower than expected, given the level of sampling (Smith & McGowan, 2007; Lloyd, 2011). However, this technique fails when sampling is poor, is generally dependent on the chosen sampling proxy, and cannot 'correct' sampling biases (Dunhill *et al.*, 2014, 2018; Brocklehurst, 2015; Sakamoto *et al.*, 2017). Subsampling and rarefaction techniques are alternatives that standardise and allow comparison between samples (Bush *et al.*, 2004; Alroy *et al.*, 2008; Close *et al.*, 2018; Alroy, 2020). Classical (or size-based) rarefaction (Sanders, 1968) subsamples down to an equal number of data points (occurrences in the palaeodiversity literature; Lloyd & Friedman, 2013), but has been found to be inappropriate for palaeodiversity studies as it flattens diversity curves and compresses richness ratios (Alroy, 2010a, 2010b; Chao and Jost, 2012). Coverage-based rarefaction (also called shareholder quorum subsampling) instead standardises samples to equal coverage, a measure of the completeness of a sample based on the frequency with which taxa occur (Alroy, 2010a, 2010b, 2010c;

Jost, 2010; Chao and Jost, 2012; Close *et al.*, 2018). This method is susceptible to unevenness (Alroy, 2020), though so are all richness estimators in cases where sampling is relatively poor (Close *et al.*, 2018). Finally, extrapolation methods attempt to extrapolate out from the available data to obtain diversity estimates. While numerous extrapolators exist, some are more appropriate than others: TRiPS (Starrfelt & Liow, 2016) has major faults (Alroy, 2020), while squares (Alroy, 2018) and correct first-order jackknife perform well in many instances (Alroy, 2020). Most of these sampling standardisation techniques were, however, developed for use in the ecological literature, and the most appropriate method for estimating palaeodiversity is unclear (Dillon *et al.*, 2023). At present, coverage-based rarefaction and squares appear to be the best available estimators for palaeodiversity studies (Alroy, 2020; Benson *et al.*, 2021).

1.5 Objectives

The objectives of this thesis are to: 1) generate an occurrence database of Palaeozoic actinopterygians; 2) analyse the occurrence data to examine trends in palaeodiversity; 3) identify significant biases influencing the Palaeozoic actinopterygian fossil record; and 4) add to the body of descriptive literature on often overlooked Carboniferous actinopterygians. To achieve these goals, I compiled the occurrence data through museum visits and literature reviews, used digital methods to generate 3D anatomical models of specimens, utilised advances in statistical methods to analyse diversity data and prepared a phylogenetic matrix for analyses. In doing so I also identify key issues facing research on the Palaeozoic actinopterygian fossil record and highlight ways for future work to address these problems.

In Chapter 2 (published in *Biological Reviews*) I review past hypotheses of Palaeozoic actinopterygian diversity, present a new occurrence database and discuss challenges facing research on Palaeozoic actinopterygians.

In Chapter 3 (published in *Proceedings of the Royal Society B*) I examine temporal and palaeogeographic trends in Palaeozoic actinopterygian local richness, apply sampling standardisation methods to occurrence data and identify significant biases impacting our perception of actinopterygian diversity.

In Chapter 4 I redescribe a specimen of early Carboniferous (Tournaisian) actinopterygian, *Carboveles ovensi*, based on CT-segmented data and discuss morphological evolution in actinopterygians across the Devonian-Carboniferous boundary.

In Chapter 5 I describe a new taxon from the late Carboniferous (Bashkirian) of England and highlight unexpected anatomical features pertaining to the hyoid and branchial arches. I add taxa and characters to an expanded phylogenetic matrix, conduct a phylogenetic analysis that also visualises treespace explored by different methods, and highlight key barriers to improving our understanding of early actinopterygian relationships.

2 The early diversification of ray-finned fishes (Actinopterygii): hypotheses, challenges and future prospects

This chapter is a reformatted version of the following paper, published in *Biological Reviews*. I compiled the occurrence, collectors' curve and phylogenetic data, prepared the figures and wrote the manuscript. EMD and I wrote the code analysing the data. SAF is making the data available on the Paleobiology Database. SG provided guidance on all aspects. All authors revised the manuscript and approved the published version. The editorial 'we' is used throughout the text to reflect these contributions.

HENDERSON, S., DUNNE, E.M., FASEY, S.A. and GILES, S., 2023. The early diversification of ray-finned fishes (Actinopterygii): hypotheses, challenges and future prospects. *Biological Reviews*, 98(1), 284-315. https://doi.org/10.1111/brv.12907.

2.1 Introduction

Reconstructions of deep-time biodiversity patterns are critical to understanding the evolution of life of Earth. However, deciphering whether these patterns represent true changes in biodiversity is a key challenge for palaeobiologists (Raup, 1972, 1976; Sepkoski, 1981; Alroy *et al.*, 2008). The past 20 years have seen rapid growth in the number of quantitative studies employing fossil occurrence data to estimate patterns

of diversity in vertebrate groups. The majority of work on vertebrate diversity through time focuses on either individual taxonomic groups of tetrapods (e.g. Alroy, 2009; Benson *et al.*, 2010; Mannion *et al.*, 2011, 2019; Butler *et al.*, 2011; Butler *et al.*, 2013; Brocklehurst, Kammerer and Fröbisch, 2013; Pearson *et al.*, 2013; Cleary *et al.*, 2015, 2018, 2020; Bennett *et al.*, 2018; Cantalapiedra *et al.*, 2018; Cantalapiedra *et al.*, 2021; Brown *et al.*, 2019; Driscoll *et al.*, 2019; Celis *et al.*, 2020) and fishes (Sallan & Coates, 2010; Koot, 2013; Lloyd & Friedman, 2013; Sansom *et al.*, 2015; Romano *et al.*, 2016), or large-scale analyses of all tetrapods using publicly available, community-led databases such as the Paleobiology Database (PBDB; paleobiodb.org) (Sahney *et al.*, 2010; Close *et al.*, 2017, 2019, 2020*a*; Dunne *et al.*, 2018; Dunne, 2020). These studies have allowed insight into evolutionary dynamics in deep time, the assembly of ancient and modern ecosystems, and revealed major changes in diversification, extinction, and paleoecology. For example, studies of Palaeozoic vertebrates have illuminated the rise of jawed vertebrates from the Silurian to the Devonian (Sansom *et al.*, 2015), a major shift from placoderm- and sarcopterygian-dominated faunas to chondrichthyan- and actinopterygian-dominated faunas after the end-Devonian mass extinction (Sallan & Coates, 2010), and changes in Palaeozoic tetrapod diversity in relation to palaeoenvironments (Dunne *et al.*, 2018; Pardo *et al.*, 2019).

Despite accounting for roughly half of extant vertebrate species (Nelson *et al.*, 2016), research on the diversity of actinopterygians over long evolutionary timescales comprises only a fraction of macroevolutionary studies. Ray-finned fishes likely evolved in the Silurian (Zhu *et al.*, 2009) with the crown group originating close to the Devonian–Carboniferous boundary (Giles *et al.*, 2017), but diversity dynamics throughout the Palaeozoic are poorly understood due to the limited number of studies

utilising occurrence-based data sets. This reflects a broader palaeontological trend of understudy into the fossil record of fishes (Friedman & Sallan, 2012). Notable exceptions include diversity and faunal analyses of Middle Devonian to Mississippian gnathostomes (Sallan & Coates, 2010); an analysis of British fish richness (Lloyd & Friedman, 2013); and a study on Permo-Triassic osteichthyans (Romano *et al.*, 2016). Other studies have used compendia of first and last appearances to plot counts through time (Benton, 1993; Patterson, 1994; Sepkoski, 2002; Blieck, 2011; Friedman & Sallan, 2012). Additional studies examine patterns of biodiversity across long periods of time using publicly available occurrence data (e.g. PBDB), although they present aggregated data of numerous groups of 'fishes', or an even broader set of taxa such as nektonic metazoans (e.g. Whalen & Briggs, 2018; Harper *et al.*, 2020; Close *et al.*, 2020*b*).

While these studies present an important first foray into understanding Palaeozoic actinopterygian evolution, there have been limited syntheses that take the accuracy of the ray-fin fossil record into account, which is a major barrier to reconstructing long-term evolutionary patterns. Previous attempts either focus on the UK and include non-actinopterygian fishes (Lloyd & Friedman, 2013), do not cover the entire Palaeozoic (Sallan & Coates, 2010; Romano *et al.*, 2016), or are broader in scope without as much focus on the suitability of data and barriers to interpreting diversity patterns (Sallan, 2014). Friedman & Sallan (2012) note the lack of such investigation for fishes, and, through a qualitative survey, suggest that geological and taxonomic biases likely impact studies of the diversity of fishes through time. Here, we summarise the current state of research on the Palaeozoic fossil record of actinopterygians and present a new occurrence database spanning the Palaeozoic in

an attempt to answer the following questions: (1) how has our understanding of the Palaeozoic actinopterygian fossil record changed over time; (2) what are the trends in face-value diversity through the Palaeozoic; (3) how do sampling and other biases affect our understanding of Palaeozoic actinopterygian diversity through time; and (4) how do taxonomic problems and existing phylogenetic analyses hinder our interpretation of the Palaeozoic actinopterygian fossil record?

2.2 Current hypotheses of Palaeozoic actinopterygian diversity

2.2.1 Past studies

Although our understanding of patterns of actinopterygian diversity lags behind that of other groups, a number of studies over the past few decades have investigated fish diversity at different taxonomic levels and geological scales (Fig. 2.1). Initially, these approaches used published compendia to generate family- and/or genus-level diversity curves. The first major attempt (Thomson, 1977) used data from Romer's (1966) compendium to plot genus- and family-level diversity of Phanerozoic 'fishes' (Acanthodii, Agnatha, Chondrichthyes, Chondrostei, Holostei, Placodermi, Sarcopterygii and Teleostei; Fig. 2.1E). In subsequent years, several studies used family-level data from Benton (1993) to investigate osteichthyan diversity through the Palaeozoic. Patterson (1994) plotted diversity curves for osteichthyans as well as stem-actinopterygians, stem-neopterygians and stem-teleosts, encompassing all

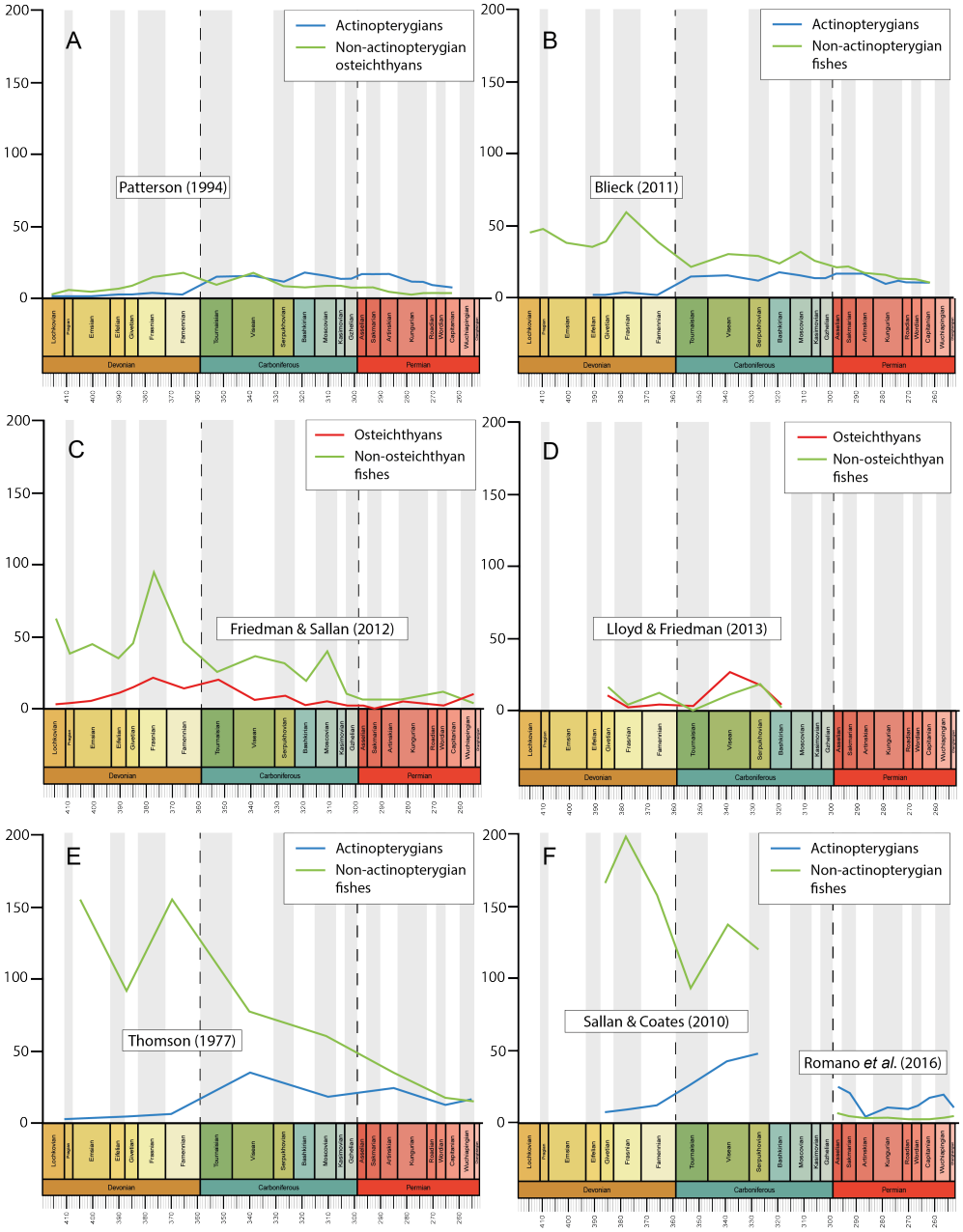


Figure 2.1: Diversity of Palaeozoic fishes through time presented in previous studies. (A) family-level diversity curves of actinopterygians and non-actinopterygian osteichthyans (Patterson, 1994; using data from Benton, 1993). (B) Family-level diversity curves of actinopterygians and non-actinopterygian fishes (Blieck, 2011; using data from Benton, 1993). (C) Genus-level diversity of marine osteichthyans and non-osteichthyan fishes, excluding conodonts (Friedman & Sallan, 2012; using data from Sepkoski, 2002). (D) Genus-level diversity of British osteichthyans and non-osteichthyan fishes (Lloyd & Friedman, 2013). (E) Genus-level diversity of actinopterygians and non-actinopterygian fishes (Thomson, 1977; using data from Romer, 1966). (F) Genus-level diversity of actinopterygians and non-actinopterygian fishes (Sallan & Coates, 2010; Romano *et al.*, 2016).

Palaeozoic actinopterygians included in the parent data set (Fig. 2.1A). Blieck (2011; Fig. 2.1B) and Benton (2014: fig. 2.11) also used data compiled by Benton (1993) to

plot family-level diversity curves of vertebrates from the Ordovician to Triassic, though did not focus on actinopterygians. Additionally, Friedman & Sallan (2012) used an existing marine data set (Sepkoski, 2002) to present genus-level diversity patterns of all ‘fishes’ (vertebrates excluding Tetrapoda and including Conodonta) throughout the Phanerozoic (Fig. 2.1C).

Other attempts have used literature-based data sets to interrogate patterns of diversity. Sallan & Coates (2010) assembled a data set of gnathostome occurrences from 66 localities spanning the Middle Devonian (Givetian) to early Carboniferous (Serpukhovian) and presented diversity curves of gnathostomes (Acanthodii, Actinopterygii, Chondrichthyes, Placodermi, Sarcopterygii, Tetrapoda; Fig. 2.1F). Lloyd & Friedman (2013) compiled data from a variety of sources, both as a means of comparing data sets (Agassiz, 1833-1844; Carroll, 1988; Benton, 1993; Sepkoski, 2002; Paleobiology Database, downloaded on 31/05/12) and to investigate the diversity of Phanerozoic ‘fishes’ (excluding Conodonta) with a particular focus on the fossil record of Great Britain (Fig. 2.1D). Romano *et al.* (2016) and Vázquez & Clapham (2017) compiled data sets that commence in the Asselian (early Permian) and encompass osteichthyans (Actinistia, Dipnoi, Holostei, ‘Palaeopterygii’, ‘Subholostei’ and Teleosteomorpha: Romano *et al.*, 2016; Fig. 2.1F) and marine fishes [Osteichthyes (excluding Dipnoi) and Chondrichthyes (excluding Acanthodii); Vázquez & Clapham, 2017].

As in Lloyd & Friedman (2013), a large proportion of recent diversity studies for fossil groups utilise occurrence data from the PBDB, a public resource that is voluntarily maintained by an international group of palaeontologists. However, most

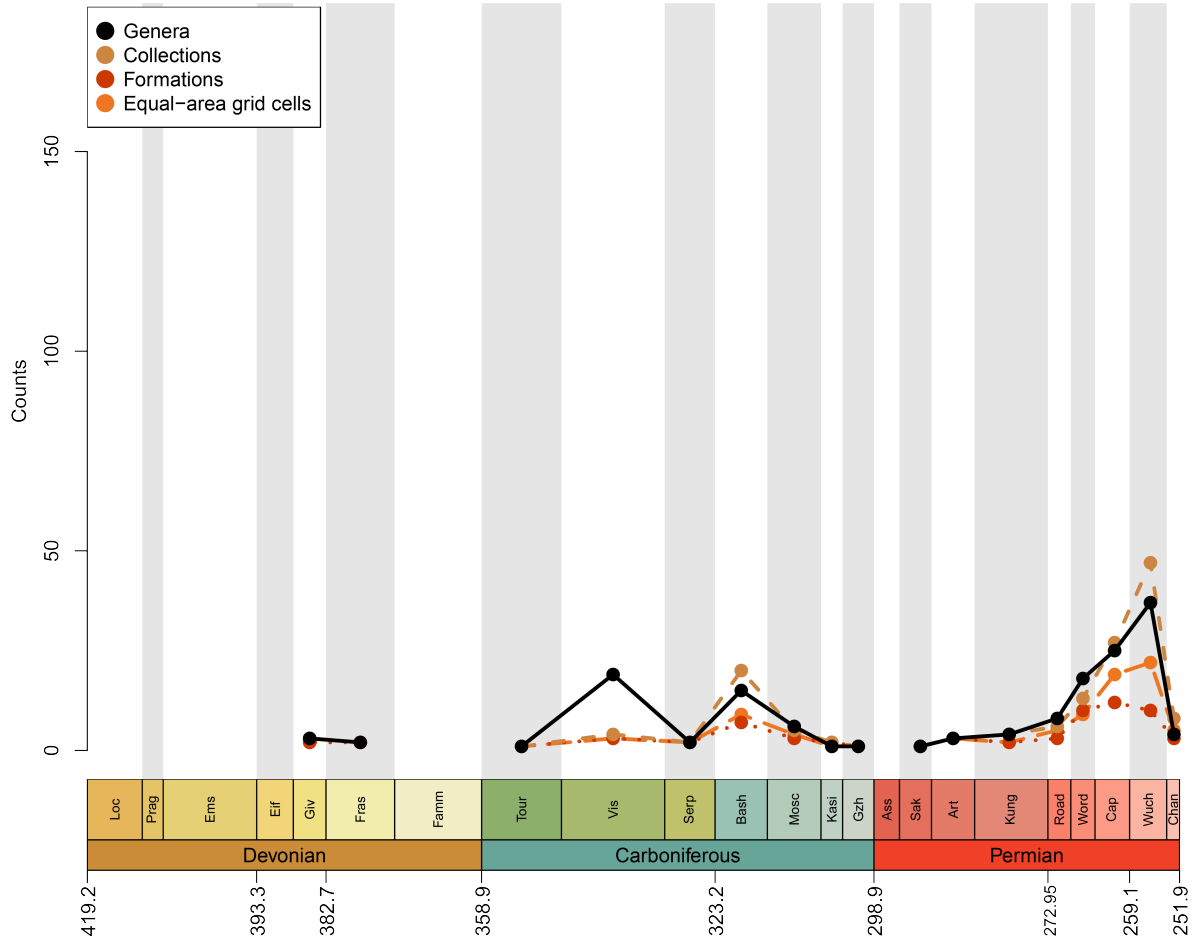


Figure 2.2: Raw counts of Palaeozoic actinopterygian genera (black, solid line), collections (brown, short dashed line), formations (red, dotted line) and equal-area grid cells (orange, long dashed line) entered in the Paleobiology Database (PBDB).

diversity studies on actinopterygians have relied on published compendia or data sets compiled directly from the literature, i.e. without use of the PBDB [see Vázquez & Clapham (2017) for an exception]. There have not yet been enough efforts to enter occurrence data for osteichthyans, and particularly actinopterygians, into the PBDB to represent their record accurately, as discussed by Lloyd & Friedman (2013) and evidenced by current PBDB Palaeozoic actinopterygian diversity curves for genera, collections, formations and equal-area grid cells (Fig. 2.2). Several periods throughout the Devonian and early Permian lack entries entirely, and no time period contains more

than 50 occurrences: the average number of occurrences is less than eight per interval, while the median is three. Diversity levels appear to fluctuate wildly during the Carboniferous before a precipitous rise and steep drop in the Changhsingian. The PBDB data presented here (Fig. 2.2) is intended as a snapshot of the currently available occurrence data, highlighting that research effort to contribute Palaeozoic actinopterygian occurrences to the database has thus far been minimal. Improving this record represents a priority for future studies, and efforts are currently underway to expand the actinopterygian PBDB record.

The studies introduced above differ greatly in their sampling and spread of taxa, but collectively they provide an indication of the general patterns of changes in actinopterygian diversity through time, as summarised below and in Figs. 2.1 and 2.2.

2.2.2 Devonian diversity patterns

All studies covering the Devonian depict very low counts of actinopterygians (Thomson, 1977: fig. 7; Patterson, 1994: fig. 1; Sallan & Coates, 2010: fig. 1; Blieck, 2011: fig. 2) (Fig. 2.1), and PBDB occurrences are lacking (Fig. 2.2). Thomson (1977), Patterson (1994) and Sallan & Coates (2010) show a gradual rise from the Middle to Late Devonian. Blieck (2011), however, figures a small peak in the Frasnian, likely due to the Gogo and Gladbach faunas (Sallan & Coates, 2010), while only a handful of genera from the Givetian and Frasnian (and none in the Famennian) have been entered into the PBDB. Only four genera (eight species) of actinopterygians are entered in the PBDB for the entire Devonian; fewer than the number described in the literature for just the Famennian (Dunkle, 1964; Dunkle & Schaeffer, 1973; Taverne, 1997; Daeschler, 2000; Prokofiev, 2002; Friedman & Blom, 2006).

While new taxa are still being described, actinopterygians appear to be genuinely rare in Devonian deposits, especially relative to other taxa (Friedman, 2015: fig. 4). Reclassification of *Meemannia* Zhu *et al.* 2004 as a ray-finned fish rather than a lobe-finned fish (Lu *et al.*, 2016) filled a conspicuous temporal gap in early actinopterygian evolution, but this taxon remains the only actinopterygian known amongst roughly 20 species from this locality. Choo *et al.* (2019) recently described a new genus of actinopterygian from the highly diverse Frasnian Gogo Formation, which is known primarily for its placoderm and sarcopterygian faunas. Although ray fins account for only five species out of around 50 Gogo taxa (Long & Trinajstic, 2010, 2017; Sallan & Coates, 2010: fig. 2) they comprise a large proportion of specimens, indicating faunal abundance despite taxonomic paucity. Even more recently, Newman *et al.* (2021) described a new species of *Cheirolepis* Agassiz 1835 from the Givetian of Svalbard, found alongside roughly 20 non-actinopterygian fishes. Similarly, a new site from the Famennian of Belgium has yielded microremains of an undescribed actinopterygian, amidst large numbers of other vertebrates (Olive *et al.*, 2015*a*,*b*, 2016, 2020).

Recent work on historically undersampled regions has revealed numerous new taxa, although overall taxonomic diversity of actinopterygians remains relatively low throughout the Devonian. Isolated jaw elements, body impressions and scales from Famennian deposits in South Africa likely represent a single actinopterygian amid a diverse array of other fishes (Gess & Whitfield, 2020), while renewed prospecting in the contemporary Maïder Basin of Morocco has produced remains of a single articulated actinopterygian (Frey *et al.*, 2018) amongst its well-known placoderm and chondrichthyan assemblages. New South American discoveries include evidence of a

stegotrachelid actinopterygian from the Frasnian of Colombia (Olive *et al.*, 2019), the first actinopterygian remains from the Devonian of the Parnaíba Basin of Brazil (Pais de Rezende *et al.*, 2021), and a new circumpolar species from the Middle Devonian (Figueroa *et al.*, 2021). As in other localities, non-actinopterygian fishes dominate these faunas (Janvier, 2007; Janvier & Maisey, 2010; Figueroa & Machado, 2018). The low diversity of actinopterygians also correlates with their limited morphological disparity, contrasting with the vast array of anatomies, and presumably ecologies, exhibited by Devonian sarcopterygians and placoderms (Anderson *et al.*, 2011). While important for understanding the early evolution of the group, these scattered reports of new Devonian taxa are unlikely to change existing overarching hypotheses of actinopterygian diversity: as minor faunal components represented by a small number of taxa relative to other fish groups.

2.2.3 Carboniferous diversity patterns

Previous diversity studies consistently report a large increase in actinopterygian taxonomic diversity in the earliest Carboniferous following the end-Devonian mass extinction (EDME). This increase is somewhat reflected in the data currently entered in the PBDB, although entries are extremely limited both taxonomically (only 51 taxa from 92 localities are entered) and geographically (all but one of the entries are from USA and UK localities; Fig. 2.3B). Thomson's (1977) counts of 'chondrostean' genera (which encompasses all Devonian and Carboniferous actinopterygians) rise sharply in the Mississippian, as does Patterson's (1994) stem-actinopteran family-level count. Sallan & Coates (2010) show this significant change in absolute and relative diversity most clearly in their presentation of faunal composition from the Devonian into the Carboniferous (Sallan & Coates, 2010: fig. 2; see also Friedman, 2015: fig. 4). This

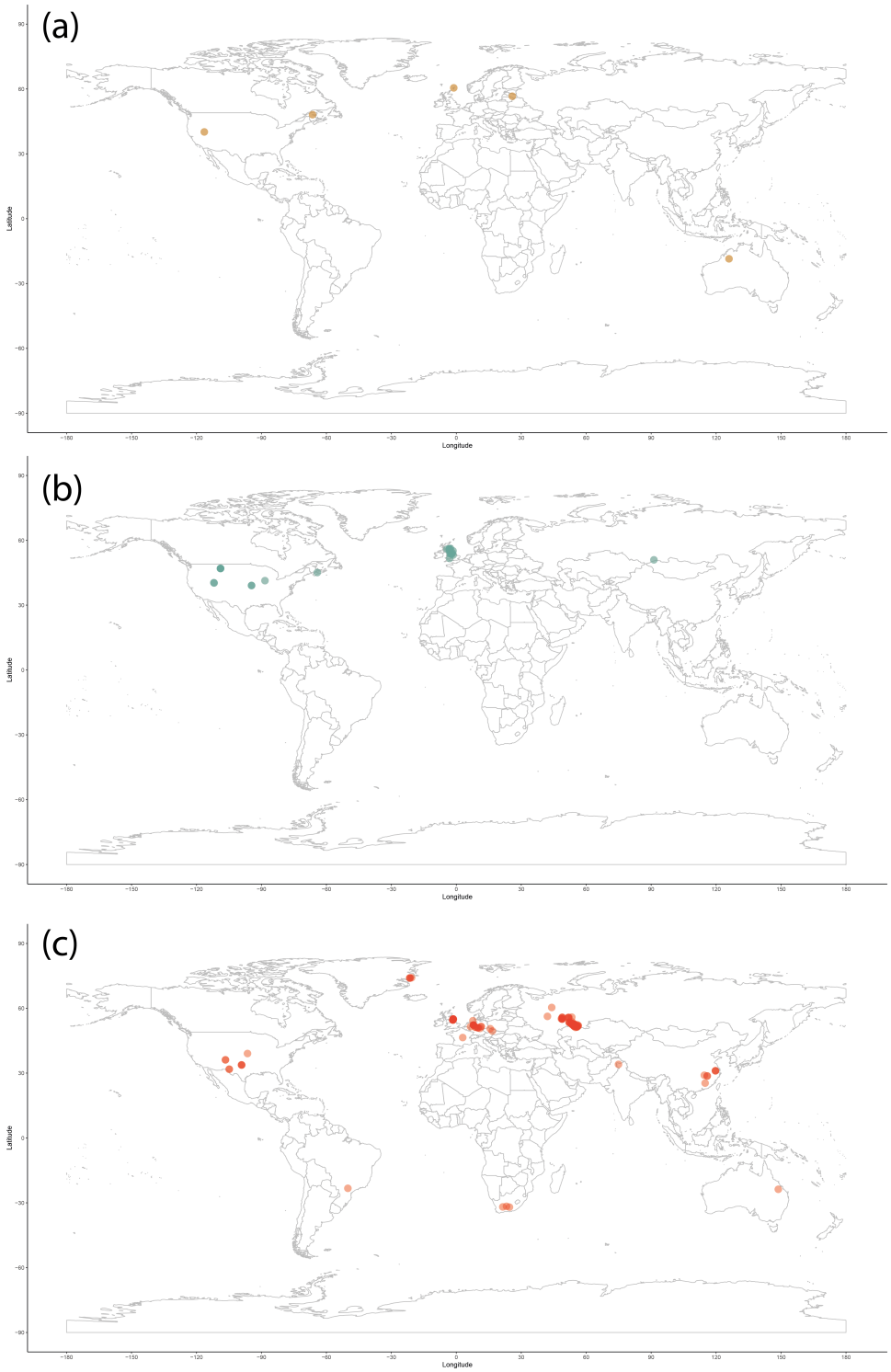


Figure 2.3: Geographic spread of actinopterygians occurrences entered in the Paleobiology Database (PBDB) for the (A) Devonian; (B) Carboniferous; and (C) Permian.

sharp rise is especially notable because the early Carboniferous (Tournaisian and early Visean) coincides with ‘Romer’s Gap’, an apparent hiatus in the fossil record of

tetrapods (and other animals) variably explained as either a period of poor sampling (Romer, 1956), low atmospheric oxygen (Ward *et al.*, 2006) or recovery following the EDME (Sallan & Coates, 2010). Recent concerted efforts have begun to populate Romer's Gap, indicating that poor sampling accounted for most of the apparent paucity of the record (Clack *et al.*, 2019; Otoo *et al.*, 2019). The diversification of actinopterygians immediately following the EDME likely represents an adaptive radiation seeded by very few – or perhaps just one – actinopterygian lineages (Sallan & Friedman, 2012; Sallan, 2014; Giles *et al.*, 2017), although this hypothesis has not been explicitly tested. The contrast between diverse (e.g. in Russia; Alekseev *et al.*, 1994) and depleted (e.g. in Morocco; Frey *et al.*, 2018) early Tournaisian faunas exemplifies the uncertainty of the relative contributions of extinction recovery, poor sampling and spatial bias to the observed fossil record, although potential differences between local environmental conditions are an important consideration.

Raw genus diversity increases into the Visean from Tournaisian levels in most previous analyses (Patterson, 1994; Sallan & Coates, 2010; Blieck, 2011) and the PBDB (Fig. 2.2). The fossil record of Great Britain exhibits a particularly extreme increase in osteichthyan richness, most likely due to the very richly sampled Visean deposits of Scotland (Dineley & Metcalf, 1999). Such high sampling in the Visean of Scotland results from a concentration of a wide range of aquatic palaeoenvironments (fluvial, lacustrine, deltaic, marine) in a region heavily explored for fossil fuels near major population centres, and with extensive coastline that has eroded overlying Quaternary sediments (Waters *et al.*, 2011*a*). The rise in richness coincides with a proliferation of new morphologies and ecologies, likely *via* multiple independent acquisitions of key traits such as durophagy, deep-, and eel-like-bodies (Sallan &

Friedman, 2012; Sallan, 2012, 2014; Sallan & Coates, 2013; Friedman, 2015; Friedman *et al.*, 2018). This gradual rise in richness, accompanied by morphological and functional diversification, may represent a classic extinction recovery and adaptive radiation (Sallan & Friedman, 2012; Sallan, 2014).

Previous studies describe conflicting patterns of actinopterygian raw diversity into the Serpukhovian. Patterson (1994) and Blieck (2011) report a decrease in family counts, in contrast to a slight increase in genus counts in Sallan & Coates (2010). The diversity curve of Thomson (1977) only separates data into Mississippian and Pennsylvanian bins, and therefore lacks the temporal resolution to allow comparison. Discrepancy between the trends in Sallan & Coates (2010), Patterson (1994) and Blieck (2011) may be due to poor higher-level taxonomy in actinopterygians. For example, the highly diverse Bear Gulch fauna likely drives the rise in actinopterygian diversity in Sallan & Coates (2010), but this is not captured in higher-level family counts due to the aggregation of genera in broad, ill-defined families. Additionally, the Serpukhovian decrease in PBDB occurrence data contrasts with other studies (e.g. Sallan & Coates, 2010) and is, in part, due to inconsistencies between regional substages and International Commission on Stratigraphy (ICS) stages. For example, in the PBDB, Bear Gulch localities are included in the Bashkirian due to the age range of the Arnsbergian, but more accurately should be placed in the Serpukhovian bin.

It is difficult to reconstruct patterns of diversity in the late Carboniferous due to an absence of published data compilations across the Pennsylvanian. Sallan & Coates' (2010) range ends at the Mississippian, while Romano *et al.*'s (2016) data begin in the Asselian. Thomson's (1977) genus counts decrease from the Mississippian to the Pennsylvanian, however family counts of actinopterygians increase from the

Serpukhovian to the Bashkirian (Patterson, 1994; Blieck, 2011). For the Moscovian–Gzhelian the only data for actinopterygians are the family counts derived from Benton (1993); these show gradual decreases from the Bashkirian to the Moscovian, and again from the Moscovian to plateau in the Kasimovian and Gzhelian (Patterson, 1994; Blieck, 2011). Importantly, counts of families remain at roughly the same level as they were in the Tournaisian and Visean. Counts of osteichthyan genera are not discernible for this period in Friedman & Sallan (2012: fig. 2), and there are no Kasimovian or Gzhelian occurrences in the British fossil record (Lloyd & Friedman, 2013). Counts of genera in the PBDB decrease throughout the Pennsylvanian (Fig. 2.2), although this also appears to be a result of low data entry: Pennsylvanian PBDB actinopterygian occurrences derive from important localities for other groups [e.g. Linton for early tetrapods (Hook and Baird, 1986); Mazon Creek for arthropods (Clements, Purnell and Gabbott, 2019)].

Reported overall trends in actinopterygian diversity in the Carboniferous are consequently unclear. Genus-level counts are suggestive of a gradual rise throughout the Mississippian (Sallan & Coates, 2010), with a subsequent drop in the Pennsylvanian (Thomson, 1977). This contrasts with family counts, which are relatively stable except for minor deviations in the Serpukhovian and Bashkirian.

2.2.4 Permian diversity patterns

Genus- and family-level counts in previous studies agree on the general trend of actinopterygian diversity in the Permian, although differ at finer timescales. The highest counts are observed in the early Permian in curves derived from Benton's (1993) data set (Patterson, 1994; Blieck, 2011) and Thomson's (1977) genus-level data. Occurrence-based data sets also show a peak in the early Permian, although limited

to the Asselian and Sakmarian, likely driven by freshwater Lagerstätte (Romano *et al.*, 2016). However, very few early Permian occurrences of actinopterygians have been entered into the PBDB (Fig. 2.2), although the geographic spread of occurrences in the Permian PBDB is substantially greater than the Devonian or Carboniferous (Fig. 2.3C). Genus- and family-level trends deviate from one another in the Artinskian: the family curve stays more or less stable, whereas genus richness decreases substantially. Family-level counts drop in the Kungurian and remain roughly at this level, with minor fluctuations, until the end-Permian. Genus richness in Thomson's (1977) curves for 'chondrostean' genus richness drop in the middle Permian and rise slightly in the late Permian; the late Permian also sees the first appearance of holosteans. Counts in the finer-scale data set of Romano *et al.* (2016) rise gradually from the Roadian–Wuchiapingian, reaching close to early Permian levels before dropping in the Changhsingian. Unlike the early Permian, PBDB data closely reflect the trends of Romano *et al.* (2016) in large part due to targeted entry of marine fishes for studies relating to the End-Permian Mass Extinction (e.g. by Vázquez and Clapham, 2017). It is clear, however, that the substantial freshwater actinopterygian fossil record from the late Carboniferous-early Permian (Beltan, 1978, 1981; Forey & Young, 1985; Murray, 2000; Soler-Gijón & Moratalla, 2001; Evans, 2005; Štamberg & Zajíc, 2008; Šimůnek and Cleal, 2020) has not yet been entered into the PBDB.

While previous studies have established a broad understanding of general diversity trends in the Palaeozoic, patterns differ depending on the taxonomic level and geological scale investigated, and there has not yet been a through-Palaeozoic study focussing solely on actinopterygians. At present, publicly available occurrence

databases lack the level of detail required for reconstructing long-term diversity through the Palaeozoic, necessitating the collation of occurrences spanning the Palaeozoic.

2.3 Materials and methods

2.3.1 Data preparation

Global occurrences of Palaeozoic Actinopterygii were compiled from the published literature. Taxonomically indeterminate occurrences (i.e. those that could not be confidently assigned to a valid genus or species) were excluded, as were occurrences that were represented solely by scales or teeth (i.e. only body fossils were retained). The cleaned data set comprises 1,611 occurrences, representing 468 species belonging to 225 genera, from 507 unique geographic locations. We recognise that databases compiled from the published literature are subject to bias (Alroy, 2010*a*,*b*,*c*; Clapham *et al.*, 2016; Close *et al.*, 2018), however collating and examining occurrences present in the literature provides a foundation upon which to build. The database includes taxon identity, locality name, locality coordinates, stratigraphy, region and country, age (ICS stage and regional substage), authority naming the taxon and the year the species was described. These data are available as online supporting information (Table S1) and are in the process of being uploaded to the PBDB.

2.3.2 Occurrence data

The length of stratigraphic stages drastically differs within the Palaeozoic. For example, the Kasimovian is 3.3 million years (Myr) in length, compared to the 15.8 Myr long Visean. As the length of intervals may impact richness trends (Raup, 1972; Smith and McGowan, 2011). occurrence data were placed in composite intervals of roughly

equal length (~9 Myr) intervals following Close *et al.* (2017, 2020*a,b*), as well as in standard stratigraphic stages (Lochkovian–Changhsingian). In order to form equal length intervals, some stratigraphic stages were combined (e.g. the Kasimovian and Gzhelian) and others were split (e.g. the Visean) (Table S2). Interval ranges were updated to reflect most recent stage boundaries according to the ICS (Cohen, Harper and Gibbard, 2021). Equal-length intervals were compared with standard stratigraphic stages to obtain an indication of the effect of interval length on diversity counts.

Face-value (= raw, uncorrected, or observed) genus and species richness at 'global' scales are presented with the proviso that face-value diversity counts may be highly misleading. While 'global' curves likely represent the extent of spatial sampling rather than global palaeodiversity (Close *et al.*, 2017, 2020*a*,*b*), face-value richness counts allow for comparison with previous diversity curves (e.g. Thomson, 1977; Sallan & Coates, 2010; Romano *et al.*, 2016) and for an initial exploration of gross Palaeozoic actinopterygian diversity. 'Global' (gamma scale) face-value richness curves were computed using sampled-in-bin counts of occurrences. Counts of geographic localities and geological units (unique formations, members, groups, etc.) were used to provide an indication of sampling effort. Occupied equal-area grid cells, i.e. the number of 50 km^2 cells on a global map (constructed using the *dggridR* R package; Barnes, 2021) that contained unique localities, were calculated as a further measure of sampling. Localities were plotted on a modern world map to show the scope of present-day sampling.

Linear regressions were conducted to investigate the relationship between counts of taxa and various sampling metrics (localities, formations and equal-area grid

cells), as well as with sea level through time (data from Hannisdal & Peters, 2011). All analyses were conducted within R 4.1.0 (R Core Team, 2020).

2.3.3 Collectors' curves

We extracted taxonomic identity, country, authority naming the taxon and the year the species was described from the occurrence database, resulting in a total of 516 species. Collector's curves showing cumulative counts of the total number of species described through time globally and within the UK were then plotted.

2.4 Results

2.4.1 Occurrence data

Overall diversity trends in the equal length genus-level, raw occurrence data set are hard to discern (Fig. 2.4A), but genus richness is highest during the late Permian (Lopingian; Wuchiapingian) and mid-Carboniferous (Serpukhovian). The lowest levels are seen in the Devonian: only a single taxon is identified in the Lochkovian (Lu *et al.*, 2016), and, aside from contentious scale-based taxa, no ray-finned fish are known from Pragian or Emsian deposits. Richness increases marginally from the Eifelian and Givetian to the Frasnian, remaining flat in the Famennian. Counts increase substantially from the Famennian to the Tournaisian, before decreasing again substantially in the early Visean (Chadian-Holkerian) and rising in the late Visean (Asbian–Brigantian). A peak in the Serpukhovian is followed by a decrease in counts in the Bashkirian and the Moscovian and another modest rise across the Carboniferous-Permian boundary. A large decrease in the Artinskian sees raw genus

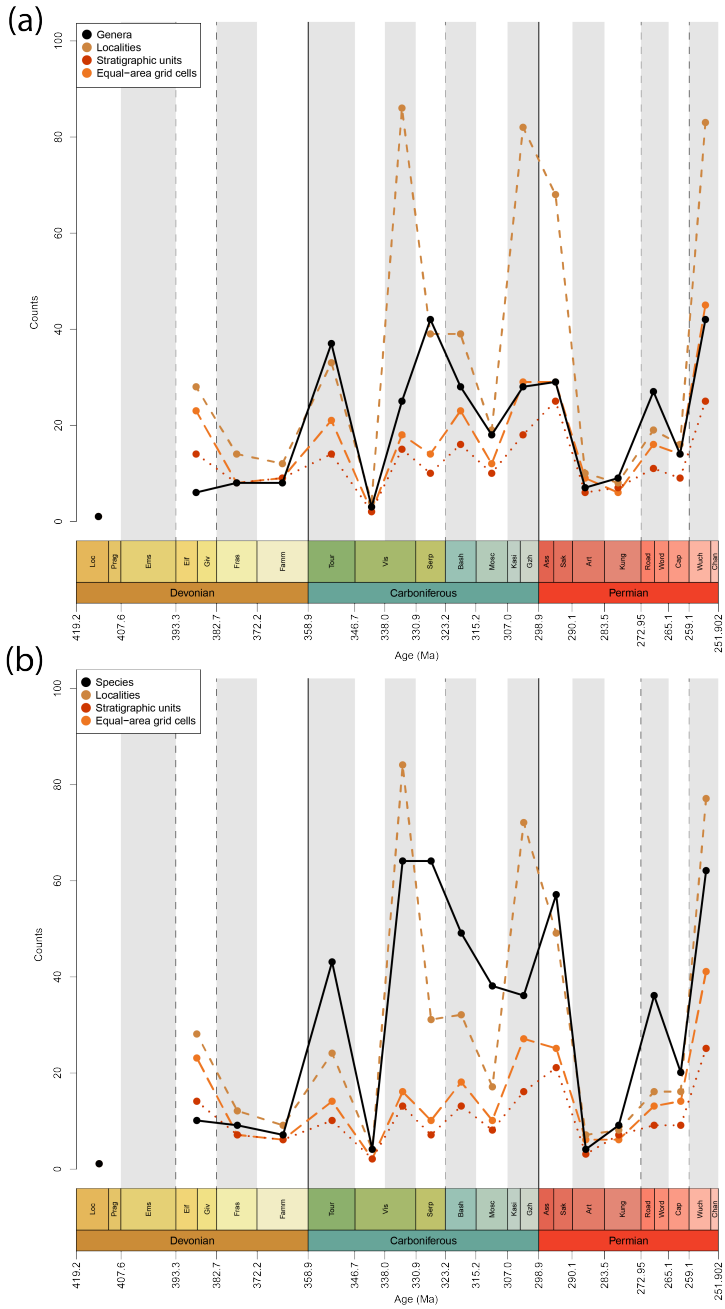


Figure 2.4: Raw counts of Palaeozoic actinopterygian (A) genera and (B) species (black, solid line) in roughly equal-length intervals (see Table S2). Collections (brown, short dashed line), formations (red, dotted line) and equal-area grid cells (orange, long dashed line) are also plotted.

counts return to late Devonian levels. Counts increase again from the Artinskian trough to the Wordian, followed by a fall in the Capitanian and final peak in the Lopingian.

Raw species richness broadly follows the same pattern, though with some notable departures (Fig. 2.4B). The highest species counts are in the late Visean

(Asbian–Brigantian) and Serpukhovian, although are only marginally lower in the Lopingian (Wuchiapingian and Changsinghian) and earliest Permian (Asselian and Sakmarian). In contrast to patterns of genus richness, species richness decreases slightly from the Middle to the Late Devonian. Furthermore, Kasimovian and Gzhelian species richness is lower than the Moscovian, meaning that, unlike in the raw genus counts, richness noticeably increases across the Carboniferous to Permian boundary.

Comparison of counts of taxa in roughly equal-length stages with counts in ICS stages shows that the choice of sampling interval strongly influences richness trends (Figs 4 and 5). Devonian trends for genus and species richness are similar (Fig. 2.5A), however trends in the early Carboniferous and Permian differ, with ICS stage counts instead largely resembling (as expected) previous studies analysing these periods (e.g. Sallan & Coates, 2010; Romano *et al.*, 2016). Genus richness is highest in the Serpukhovian, however a notable departure from previous hypotheses is the Tournaisian peak in genus richness followed by a drop in the Visean. This results from a discrepancy in the age of the diverse Waaipoort Formation: previous work counted these deposits as Visean (Sallan & Coates, 2010), suggesting a gradual rise in richness through the Mississippian, while recent studies shift the age back to the Tournaisian (Lakin *et al.*, 2016), in turn altering Mississippian richness trends. There is then a general decline throughout the Pennsylvanian that reaches a trough in the final interval of the Carboniferous, the Gzhelian (Fig. 2.5A). Richness then decreases in the Asselian and rises in the Sakmarian before a drop in the Artinskian (the lowest count of genera throughout the Carboniferous and Permian). Genus richness then fluctuates through the Kungurian (increase from Artinskian), Roadian (decrease from Kungurian), Wordian (increase from Roadian), Capitanian (decrease from Wordian),

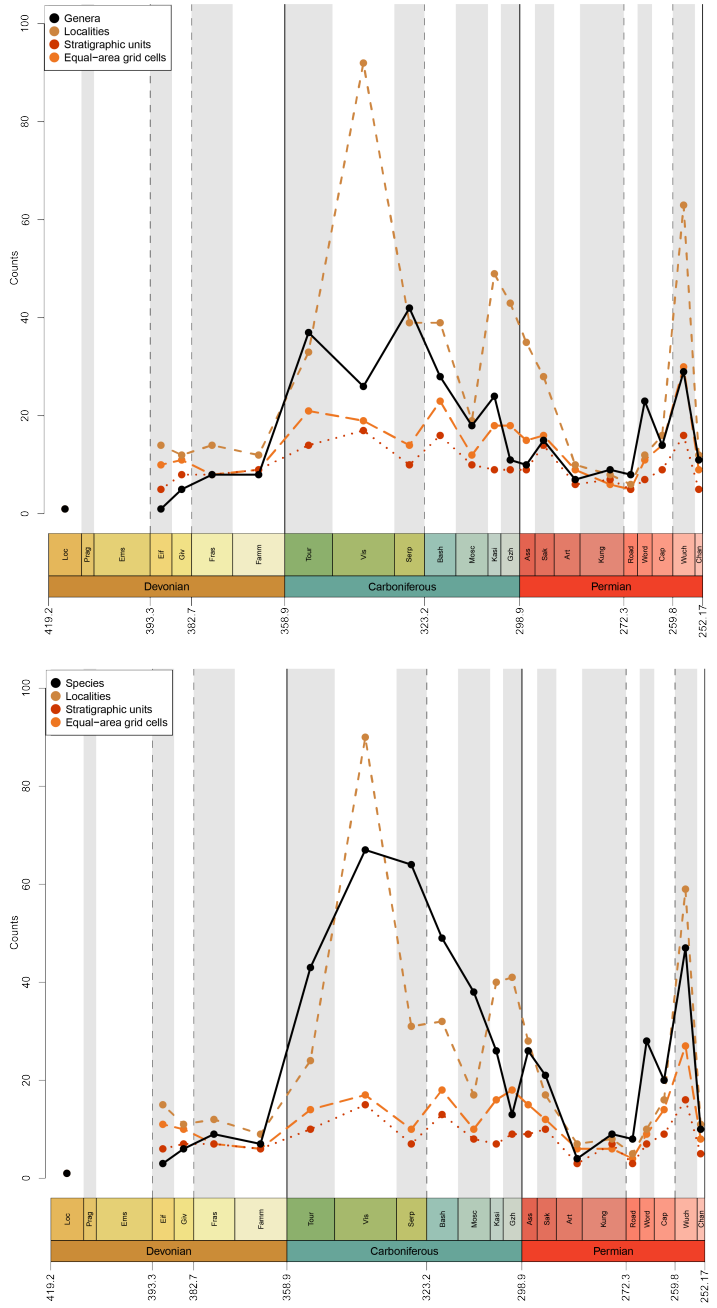


Figure 2.5: Raw counts of Palaeozoic actinopterygian (A) genera and (B) species (black, solid line) in standard International Commission on Stratigraphy (ICS) stages. Collections (brown, short dashed line), formations (red, dotted line) and equal-area grid cells (orange, long dashed line) are also plotted.

Wuchiapingian (increase from Capitanian) and Changhsingian (decrease from Wuchiapingian); these trends are broadly similar to Romano *et al.* (2016). Species richness trends are generally the same (albeit exaggerated) as those of genus

richness, excepting the Visean, which becomes the most speciose interval of the Palaeozoic (Fig. 2.5B).

Face-value richness at both genus and species level closely tracks proxies for sampling effort; where the number of localities, formations and equal-area grid cells are high, richness is also high (Fig. 2.4). Notable exceptions to this trend are the Eifelian-Givetian and Serpukhovian. Discrepancy in the Eifelian–Givetian is due to the widespread occurrence of *Cheirolepis* at a time when actinopterygians had very low relative diversity. In the Serpukhovian, high genus counts despite a decrease in sampling metrics is a result of the diverse Bear Gulch fauna (Lund, Greenfest-Allen and Grogan, 2012). In addition, three large peaks in counts of localities in the late Visean, Kasimovian and Gzhelian and Asselian and Sakmarian are a result of intense sampling of localised regions with homogenous contemporary faunas (e.g. Midland Valley of Scotland, Visean [Dineley & Metcalf, 1999]; Boskovice Graben, late Carboniferous and early Permian [Štamberg, 2007; Štamberg & Zajíc, 2008]), and thus do not correspond with peaks in genus richness. However, there are species-level richness counts peaks in the late Visean and Asselian and Sakmarian (Fig. 2.4B).

First inspection reveals multiple sources of bias in the Palaeozoic actinopterygian fossil record. The clear differences between the species- and genus-level curves highlight issues with problematic ‘waste-basket’ genera containing vast numbers of species, while overall face-value richness appears to track sampling metrics. Regressions (Appendix Fig. A.1) show that genus richness positively correlates with number of localities (R^2 = 0.47, p = 0.003, Appendix Fig. A.1A), stratigraphic units (R^2 = 0.34, p = 0.019, Appendix Fig. A.1B) and occupied equal-area grid cells (R^2 = 0.39, p = 0.009, Appendix Fig. A.1C). Removing the highly diverse Bear

Gulch and Glencartholm assemblages strengthens these relationships. As expected, interval length does not correlate with richness when using roughly equal-length intervals (R^2 = 0.16, p = 0.128, Appendix Fig. A.1D). Overall genus richness also significantly correlates with sea level (R^2 = 0.47, p = 0.003, Appendix Fig. A.1E). This relationship persists when analysing isolated counts of freshwater genera (R^2 = 0.44, p = 0.005, Appendix Fig. A.1F), although counts of marine genera do not significantly correlate with sea level (R^2 = 0.15, p = 0.135, Appendix Fig. A.1G). This significant correlation, with both overall genera and freshwater genera, disappears when the Devonian stages are removed (R^2 = 0.14, p = 0.205, Appendix Fig. A.1H; R^2 = 0.20, p = 0.129, Appendix Fig. A.1I).

2.4.2 Distribution of Palaeozoic actinopterygians

A global map of occurrences gives a broad overview of the distribution of actinopterygian localities through the Devonian, Carboniferous and Permian (Fig. 2.6), showing that published occurrences are overwhelmingly located in Europe and North America. Here we break down the global data in order to (*a*) understand better the distributions of actinopterygians through the Palaeozoic and (*b*) identify widespread taxa or regions that share taxonomic affinities.

2.4.2.1 United Kingdom and the Republic of Ireland

Eifelian and Givetian occurrences in the well-known Orcadian basin precede a nearly continuous Carboniferous record of actinopterygians in the British Isles, which persists until the end of the Moscovian. This is followed by a total lack of occurrences, likely due to increasingly arid conditions and uplift from the Variscan Orogeny, until the extensively sampled Wuchiapingian deposits of the Raisby and Marl Slate Formations (Westoll, 1934, 1941*b*).

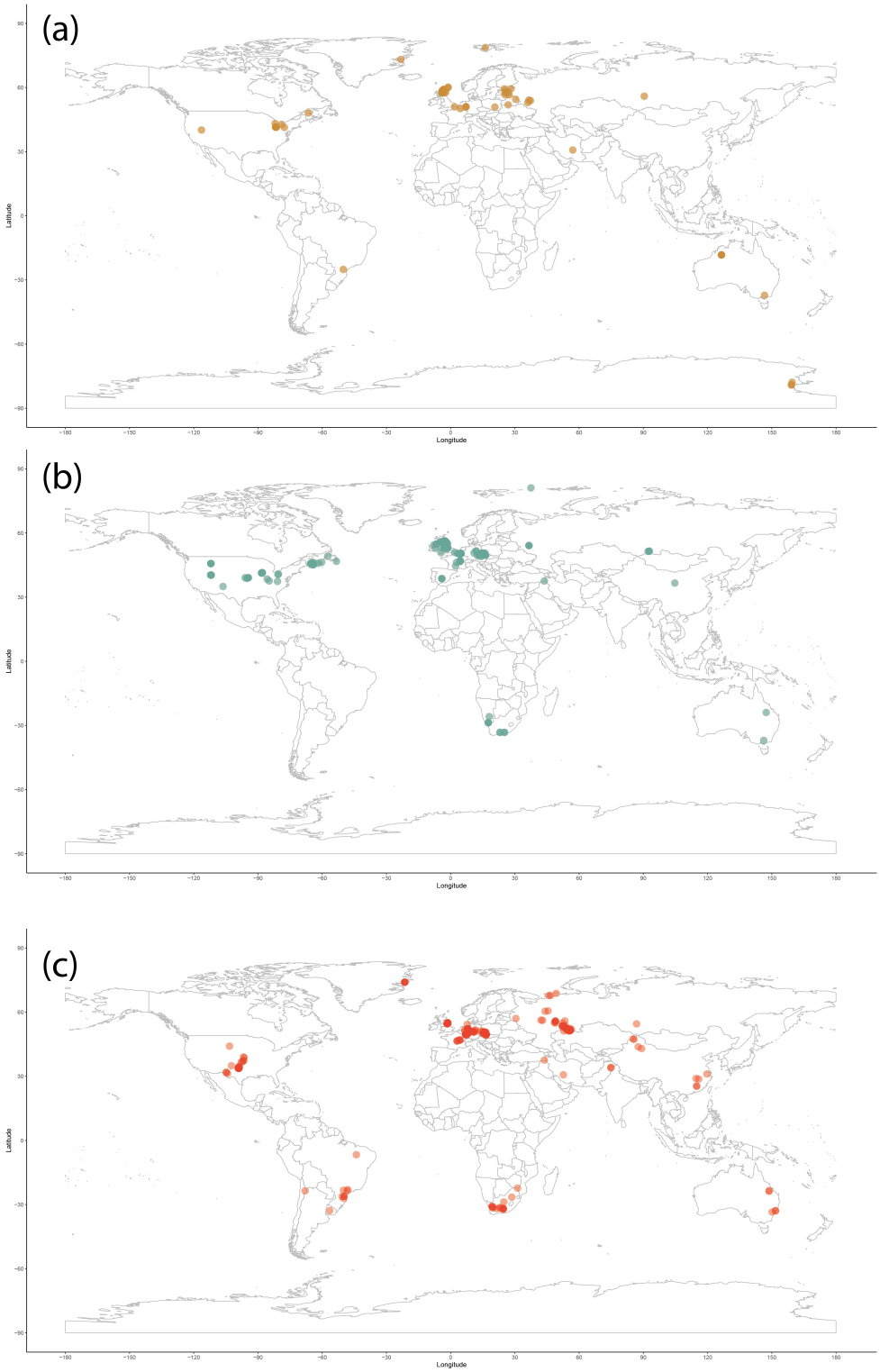


Figure 2.6: Geographic spread of actinopterygians occurrences in the (A) Devonian; (B) Carboniferous; and (C) Permian.

The earliest Devonian taxon from this region, *Cheirolepis* from the Eifelian of Scotland (Pearson and Westoll, 1979), is also present in North America (Arratia &

Cloutier, 1996, 2004), the Baltic (Mark-Kurik, 2000) and Spitsbergen (Newman *et al.*, 2021), while *Stegotrachelus* (Givetian; Swartz, 2009) may also occur in Colombia (Olive *et al.*, 2019) and was thought to be present in central Europe (Ørvig, 1960) until revision of that material as *Moythomasia* (Choo, 2015). Some Tournaisian actinopterygians in the British Isles are present at other isolated Northern Hemisphere localities, for example in the Tournaisian of Russia (Lebedev, 1996) and Serpukhovian of the USA (Lowney, 1980b). However, by far the most common genera throughout the Carboniferous are '*Elonichthys*' and *Rhadinichthys*, which are also geographically widespread (Fig. 2.7C, G). While there are some endemic genera that are locally widespread and present at many localities [e.g. *Eurynotus*, *Nematoptychius* (Traquair, 1908; Moy-Thomas & Dyne, 1938; Friedman *et al.*, 2018)], the other most common Carboniferous occurrences in British and Irish deposits are of globally distributed genera (*Platysomus*, *Palaoniscum*, *Acrolepis*, Fig. 2.7A, E, F). The late Permian fish fauna (Marl Slate and Raisby Formations) is very similar to that of contemporary German deposits (Kupferschiefer and Zechstein formations; Westoll, 1941*a*).

2.4.2.2 Western Europe

In Western Europe, isolated occurrences in the Frasnian, Famennian, Tournaisian, Visean, Serpukhovian and Bashkirian precede more considerable numbers of occurrences in the Kasimovian, Asselian and Sakmarian (Fig. 2.6). These late Carboniferous and early Permian Western European localities yield taxa that are shared with contemporary central European deposits, including *Paramblypterus*, '*Elonichthys*', *Progyrolepis*, *Bourbonnella* and *Aeduella* (Štamberg, 2006; Štamberg & Zajíc, 2008). Of these genera, *Bourbonnella* and *Progyrolepis* are also present in the USA (Dunkle, 1946; Dalquest & Kocurko, 1988; Mickle, 2011), while numerous other

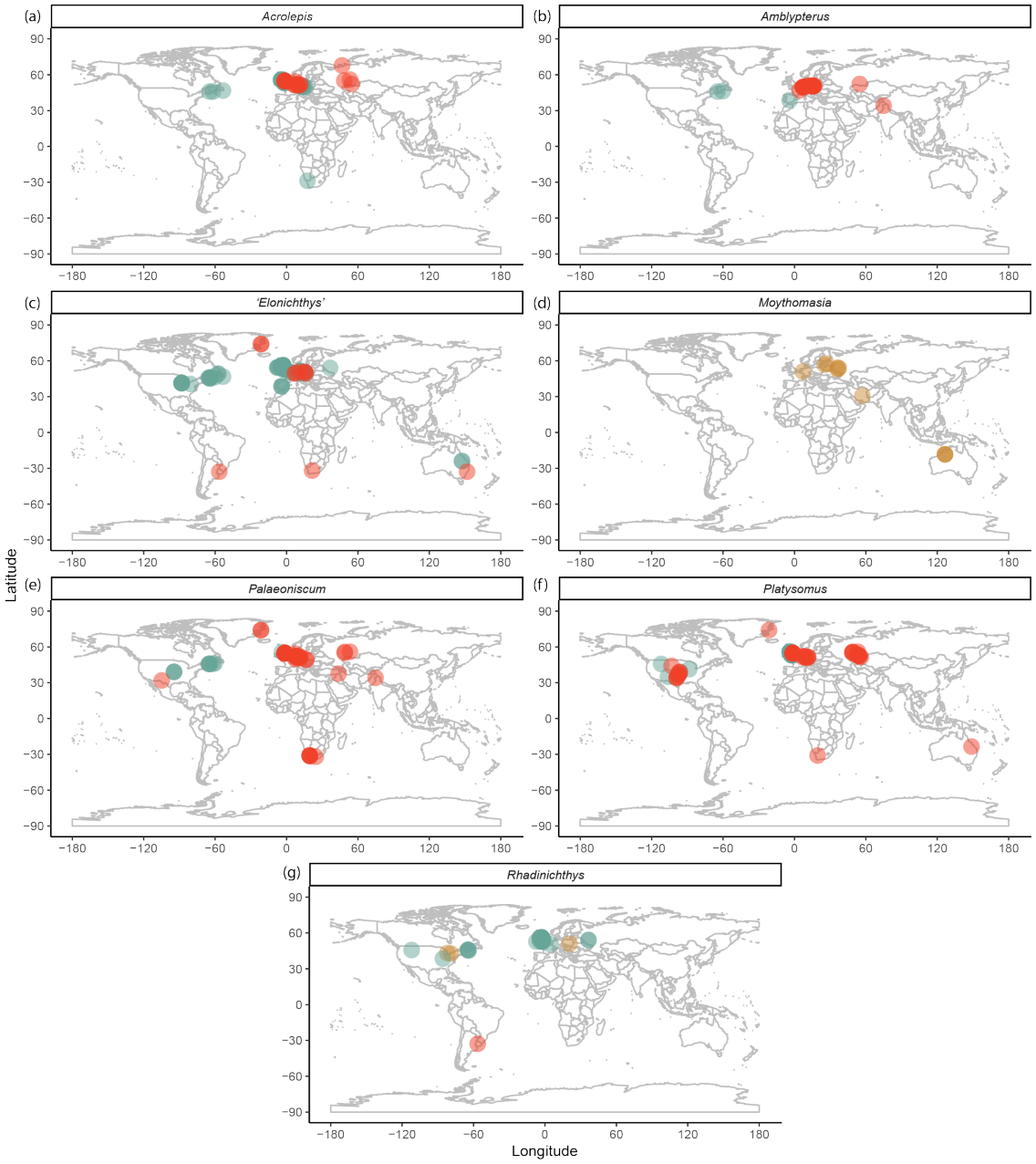


Figure 2.7: Distribution of the most speciose and widespread actinopterygian genera, with occurrences coloured according to the ICS colours for the period in which they occur (Devonian – brown; Carboniferous – green; Permian – red): (A) *Acrolepis*; (B) *Amblypterus*; (C) '*Elonichthys*'; (D) *Moythomasia*; (E) *Palaeoniscum*; (F) *Platysomus*; and (G) *Rhadinichthys*. Palaeomaps of Devonian, Carboniferous, Permian in Supplemental Material A.2.

genera found in Western Europe are also widespread: *Cheirodus* (Bashkirian, France; Derycke *et al.*, 1995) also occurs in the UK (Visean–Bashkirian; Traquair, 1890); *Gonatodus* (Visean, Belgium) in the Carboniferous of the UK (Gardiner, 1967) and

latest Devonian of the USA (Hannibal, 2020); *Mesonichthys* (Serpukhovian, France; Derycke *et al.*, 1995) in the UK (Bashkirian; Elliott, 2016) and Uruguay (early Permian; Beltan, 1978); *Pygopterus* (Bashkirian, Belgium; Derycke *et al.*, 1995) in Germany, Greenland and the UK [all Wuchiapingian (King, 1850; Woodward, 1891; Aldinger, 1937; Holzapfel & Malzahn, 1984; Diedrich, 2009; Hosgör & Štamberg, 2014)]; and *Rhadinichthys* (Serpukhovian, Belgium; Derycke *et al.*, 1995) is present across the globe (Fig. 2.7G).

2.4.2.3 Central Europe

Devonian occurrences in Germany and Poland (Givetian–Frasnian) represent the earliest in Central Europe, with a subsequent gap encompassing the entirety of the early Carboniferous. Actinopterygians later occur in the Moscovian, Kasimovian and Gzhelian, with particularly large numbers of occurrences in the latter two stages [largely in Czechia, with a few occurrences in the Gzhelian of Germany (Štamberg & Zajíc, 2008; Schindler, 2018)]. The early Permian of Czechia and Germany are also extensively sampled. Isolated Artinskian and Kungurian occurrences precede a hiatus until the considerable counts in the Wuchiapingian of Germany, stemming from the famous Kupferschiefer and Zechstein formations. In total these deposits contribute a reasonable number of genera to the global count.

Two Devonian genera (*Moythomasia*, *Rhadinichthys*) are present at numerous localities globally (Fig. 2.7D, G), although the third, *Stegotrachelus*, is only present in the Givetian of Scotland (Swartz, 2009). '*Elonichthys*', *Palaeoniscum*, *Amblypterus* and *Acrolepis*, all of which have notably global distributions (Fig. 2.7A–C, E), comprise a large number of occurrences in Central Europe. Intense sampling of Central European deposits has resulted in abundant occurrences of locally widespread taxa. Many of

these taxa are endemic to the region [*Spinarichthys*, *Rhabdolepis*, *Zaborichthys* (Štamberg, 1991, 2016*a*; Štamberg & Zajíc, 2008; Schindler, 2018*b*)], and others occur at isolated localities outside Central Europe (e.g. *Sphaerolepis*, USA; Olson, 1967) or in the broader palaeogeographic region encompassing present-day Europe and North America (e.g. *Aeduella*, *Bourbonnella*, *Paramblypterus*, *Progyrolepis*, *Pygopterus*).

2.4.2.4 Eastern Europe

Actinopterygians are reported from the Eifelian, Givetian, Frasnian and Famennian and Tournaisian of Eastern Europe and European Russia, though Eifelian and Givetian remains are fragmentary. Occurrences are absent from the remainder of the Carboniferous, and only a single Kungurian occurrence is known. In stark contrast, the middle and late Permian of Russia are heavily sampled, with numerous occurrences in the Roadian, Wordian, Capitanian and Wuchiapingian.

Devonian occurrences yield the globally distributed *Cheirolepis* (Mark-Kurik, 2000) and *Moythomasia* (Fig. 2.7D; Sallan & Coates, 2010) for the most part, with only a single endemic genus, *Krasnoyarichthys* (Prokofiev, 2002). Widespread genera are also present in the Tournaisian [e.g. '*Elonichthys*', *Rhadinichthys*: Fig. 2.7C, G (Alekseev *et al.*, 1994; Yankevich & Minikh, 1998; Golubev, 2001; Minikh & Minikh, 2009; Minikh *et al.*, 2016)], albeit alongside a notable number of unique genera [e.g. *Oxypteriscus*, *Ministrella*, *Palaeobergia* (Berg, 1958; Matveeva, 1958)]. A small number of genera are in common with the Tournaisian of the UK (*Aetheretmon*, *Strepheoschema*; Lebedev, 1996) and Siberian Russia (*Ganolepis*, *Grassator*; Lebedev, 1996).

Similarly, the middle Permian occurrences range on a spectrum from endemic to widespread genera. *Platysomus* has the highest number of occurrences (Fig. 2.7F),

and *Acrolepis* and *Palaeoniscum* (Fig. 2.7A, E; Golubev, 2001; Tverdokhlebov *et al.*, 2005; Minikh & Minikh, 2009; Nurgaliev *et al.*, 2015; Bakaev & Kogan, 2020) are also common. *Varialepis* and *Alilepis* are present in contemporary middle Permian deposits from the USA (Ivanov *et al.*, 2013; Ivanov *et al.*, 2020) while other frequently occurring genera are endemic and span multiple stages (e.g. *Toyemia*, *Isadia*, *Geryonichthys*, *Kargalichthys*; Tverdokhlebov *et al.*, 2005).

2.4.2.5 North America

Relatively few actinopterygians occur in the Devonian of North America, with limited occurrences in the Givetian, Frasnian and Famennian. Tournaisian occurrences predominantly derive from Canada [comprising an assortment of globally widespread genera such as *Acrolepis*, '*Elonichthys*', and *Rhadinichthys*: Fig. 2.7A, C, G (Rygel *et al.*, 2006; Mickle, 2017)]. Visean localities are rare. By contrast, the Serpukhovian is highly diverse, although all but two of the Serpukhovian occurrences are from Bear Gulch deposits (Weems & Windolph, 1986; Mickle, 2018). There are occurrences throughout the Pennsylvanian, however the majority occur in the Moscovian [Mazon and Yellow Creek localities (Newberry, 1856; Schultze & Bardack, 1987)].

Occurrences are limited throughout the early and middle Permian, mirroring the overall Palaeozoic actinopterygian record. There are no late Permian occurrences in continental North America, although Wuchiapingian deposits containing actinopterygians are present in Greenland (Aldinger, 1937). '*Elonichthys*', *Platysomus* and *Palaeoniscum* comprise three of the four most abundantly occurring genera in North America. In addition, the collective occurrences of these genera in North America range from the earliest Carboniferous to the end-Permian proving them not only

geographically (Fig. 2.7C, E, F) but temporally widespread. However, *Rhadinichthys* and *Acrolepis* are more restricted temporally in North America than their other global occurrences (Fig. 2.7A, G). The overwhelming majority of Bear Gulch taxa – the source of most of North American actinopterygian diversity – are endemic to the locality, although a small number of genera are present elsewhere [e.g. *Mesopoma* and *Phanerosteon* (Traquair, 1881; White, 1927; Moy-Thomas & Dyne, 1938; Moy-Thomas, 1938; Gardiner, 1985)]. More broadly, actinopterygian genera from North America are also present in numerous European deposits: *Alilepis* (Russia; Minikh *et al.*, 2016), *Bourbonnella* [Czechia, France, Spain (Heyler, 1977; Soler-Gijón & Moratalla, 2001; Štamberg, 2007)], *Parahaplolepis* (UK; Elliott, 2014, 2016), *Progyrolepis* [Czechia, Spain, France (Forey & Young, 1985; Heyler, 2000; Soler-Gijón & Moratalla, 2001; Štamberg & Zajíc, 2008)], *Pyritocephalus* [Czechia, UK (Štamberg, 1991; Elliott, 2014)], *Sphaerolepis* (Czechia; Štamberg & Zajíc, 2008)] and *Varialepis* (Russia; Nurgaliev *et al.*, 2015).

2.4.2.6 Africa

African occurrences predominantly derive from South African deposits, with a scattering of contributions from Namibia and Zimbabwe. These sparse occurrences are separated by large temporal gaps: actinopterygians are only reported from the Tournaisian, Gzhelian (or Asselian, age is uncertain; Murray, 2000), Artinskian, Capitanian and Changhsingian (Fig. 2.6). The diverse Tournaisian fauna of the Waaipoort Formation is endemic, with no taxa found at any other Palaeozoic locality (Gardiner, 1969; Evans, 2005). Indeed, the majority of African taxa are endemic [Gzhelian-Changhsingian, e.g. *Namaichthys* (Gürich, 1923; Murray, 2000); Changhsingian, e.g. *Bethesdaichthys* and *Kompasia* (Bender, 2001, 2004)], although

they are occasionally accompanied by widespread genera such as *Palaeoniscum* [Changhsingian, *P. bainii* (Egerton, 1856); Artinskian, *P. capensis* (Murray, 2000; Evans, 2005)], '*Elonichthys*' (*E. whaitsi*; Jubb & Gardiner, 1975), *Acrolepis* (Gzhelian or Asselian, *A.* sp.; Murray, 2000) and *Platysomus* (Artinskian, *P.* sp.; Evans, 2005) (Fig. 2.7A, C, E, F). *Watsonichthys* (a genus present in Visean and Serpukhovian deposits of Scotland) is also reported in the Gzhelian (or Asselian) and Artinskian of southern Africa (Jubb & Gardiner, 1975; Evans, 2005).

2.4.2.7 Asia

Despite the earliest actinopterygian occurring in the Devonian (Lochkovian) of China (Lu *et al.*, 2016), actinopterygians subsequently only occur in China in the Bashkirian (Lu, 2002) and late Permian (Wang *et al.*, 2007). Other central and eastern Asian occurrences partially populate this gap: Famennian and Tournaisian occurrences are present in Siberia, while deposits from eastern Kazakhstan (most notably those of the Kalyn-Kara; Kazantseva-Selezneva, 1980, 1981) yield actinopterygians from the late Carboniferous and early Permian. Some indeterminate actinopterygians also occur in the Devonian of South East Asia (Wang *et al.*, 2010). Together, these occurrences constitute a low proportion of global counts of genera. None of the taxa present in these regions, with one exception [*Saurichthys*, found in both late Permian Chinese and Russian deposits (Liu & Wei, 1988; Tverdokhlebov *et al.*, 2005; Minikh & Minikh, 2009)], are found in any other Palaeozoic locality or time stage.

By contrast, occurrences in the Famennian, Tournaisian and Capitanian of the Middle East [Iran and Turkey (Hampe *et al.*, 2013; Hosgör & Štamberg, 2014)] and Middle Permian of South Asia (India; Bandyopadhyay, 1999) yield a small number of

genera (*Amblypterus*, *Canobius*, *Moythomasia*, *Palaeoniscum*, *Pygopterus*, and *Rhadinichthys*), all of which are found in numerous other regions of the world (Fig. 2.7).

2.4.2.8 South America

Until recently, taxonomically determinate occurrences of Palaeozoic actinopterygians in South America were restricted to the Permian. The recent discovery of an actinopterygian from the Middle Devonian of Brazil (Figueroa *et al.*, 2021) extends the record back some 83 million years (excluding indeterminate late Devonian occurrences; Arratia & Cione, 1996), resulting in a substantial occurrence gap. South American actinopterygians occur throughout the Permian, yet apart from the diverse Rio Negro (San Gregorio Formation) fauna from Uruguay (Beltan, 1978), these occurrences stem from a few, disparate, isolated localities, and produce comparatively low numbers of genera.

The vast majority of South America taxa are endemic to the region, with some notable exceptions. The Rio Negro fauna contains species of two very common genera – *Rhadinichthys* (*R. rioniger*) and '*Elonichthys*' ('*E.*' *macropercularis*) [Fig. 2.7C, G (Beltan, 1978; Cione *et al.*, 2010)] – as well as less-common genera that are nonetheless also present in more fully sampled regions. *Mesonichthys* (*M. antipodeus* from Rio Negro) is also present in the Carboniferous (Serpukhovian–Moscovian) of Belgium and the UK (Derycke *et al.*, 1995; Elliott, 2016), and *Coccocephalichthys* (*C. tesselatus* from Rio Negro) is present in both the UK (Bashkirian; Poplin and Véran, 1996) and USA (Gzhelian; Poplin, 1974).

2.4.2.9 Oceania

The only occurrences from Oceania are from Australia, where actinopterygians are present in the Devonian [Givetian and Frasnian (Long, 1988; Long & Trinajstic, 2010)] and early Carboniferous [Tournaisian and Visean (Long, 1988; Holland *et al.*, 2006)], followed by a ~65 Myr gap until the mid-late Permian [Capitanian, Wuchiapingian and Changhsingian (Woodward, 1931; Campbell & Phuoc, 1983)]. This gap may be a result of extensive continental icesheets given the proximity to the southern palaeopole, as well as the uplift of the Eastern Highlands. Relatively few genera comprise these occurrences, the majority of which are endemic (e.g. *Mimipiscis*, *Ebenaqua*, *Mansfieldiscus*), although there are also occurrences of the widespread genera *Moythomasia* (*M. durgaringa*) and '*Elonichthys*' ('*E.*' *davidi*) (Fig. 2.7C, D). Notably, the Frasnian is the most diverse stage due to the Gogo Formation localities, which yield nearly as many genera as the remainder of the Palaeozoic occurrences.

2.4.3 Collectors' curves

We compiled collector's curves for Palaeozoic actinopterygians to examine whether the asymptote observed by Lloyd & Friedman (2013) for the British fossil fish record is upheld when restricted to Palaeozoic actinopterygians and is extended beyond Great Britain. An asymptote is observed when considering Palaeozoic actinopterygians from the British Isles (Fig. 2.8). The number of described taxa starts to plateau in the late 19th century, largely due to the foundational monographic descriptions of Agassiz (1833-1844) and Traquair (1877*b*). A slight increase in recent years indicates a resurgence of interest focussed around computed tomography (CT) based

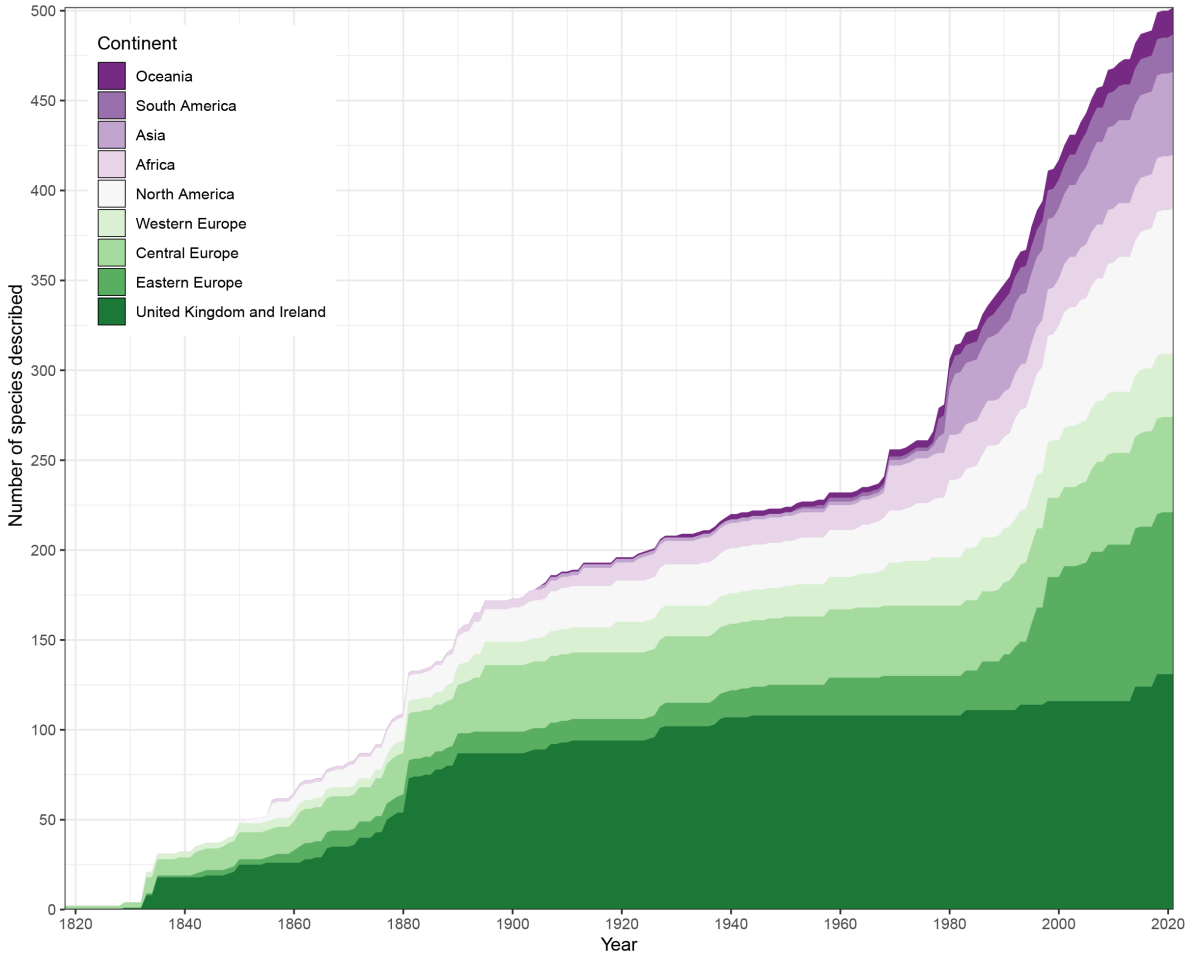


Figure 2.8: Collector's curve of the global Palaeozoic actinopterygian fossil record, divided by present-day geographic region.

redescriptions and taxonomic splitting of classic taxa held in museums (e.g. Coates & Tietjen, 2018), as well as new collection and local taxonomic reviews (e.g. Elliott, 2014, 2016). While unlikely to alter large-scale diversity patterns (Lloyd & Friedman, 2013) this uptick is suggestive of further hidden diversity in the fossil record of Palaeozoic actinopterygians in Great Britain, particularly with regard to redescription of material that has been untouched since the 19th and early 20th century.

The global collector's curve, however, presents a very different trend (Fig. 2.8). During the 19th century, the global curve roughly tracks that of the British curve, albeit with slightly higher cumulative counts. This is in part due to the works of Agassiz (1833-

1844) and Traquair (1877-1912), who also described actinopterygians from Belgium, France and Germany, with other important contributions from the USA and Europe (e.g. Newberry, 1856; Hancock & Atthey, 1872; Frič, 1879). Throughout the 20th century, however, the global curve departs from the British curve, continuing to rise steadily. Part of this can be traced to significant contributions from Aldinger (1937) and Gardiner (1969), who described new taxa from Greenland and South Africa, respectively. From the late 1960s the global collector's curve accelerates at a faster and steadier rate than at any time previously, corroborating statements that the fossil record of Palaeozoic actinopterygians is undersampled (Sallan & Coates, 2010).

This accelerated rate of descriptions is a combined result of a steady description of isolated occurrences (e.g. Daeschler, 2000; Prokofiev, 2002; Friedman & Blom, 2006; Long *et al.*, 2008; Mickle & Bader, 2009; Mickle, 2011, 2017, 2018; Choo, 2015; Giles *et al.*, 2015; Figueroa *et al*., 2021; Newman *et al.*, 2021; Štamberg & Steyer, 2021) as well as descriptions of new, diverse, highly productive fish faunas such as Bear Gulch (Lowney, 1980b; Lund & Poplin, 1997; Lund, 2000; Poplin & Lund, 2000; Mickle *et al.*, 2009; Grogan & Lund, 2015), Mazon Creek (Schultze & Bardack, 1987), the Waaipoort Formation (Gardiner, 1969), Rio Negro (Beltan, 1989), Kalyn-Kara (Kazantseva-Selezneva, 1981) and the Gogo Formation (Gardiner & Bartram, 1977; Choo *et al.*, 2009; Choo *et al.*, 2019; Choo, 2012).

A geographical breakdown of the regions yielding new actinopterygian genera and localities reveals that Europe and North America are the most intensely sampled regions in the Palaeozoic actinopterygian fossil record. New European fishes account for the largest increase in descriptions in the last three decades, while contributions from North America are also increasing, although the mechanisms differ between

Europe and North America. For example, increased sampling of multiple localities has contributed to the rising rate of new descriptions from Europe. Extensive work in Central Europe (Štamberg, 2007, 2010, 2013, 2016*a*,*b*, 2021; Štamberg & Zajíc, 2008; Choo, 2015) and European Russia (Minikh, 1992, 1998; Esin, 1995; Yankevich & Minikh, 1998; Minikh & Minikh, 2009; Minikh *et al.*, 2016; Bakaev & Kogan, 2020) in recent years is responsible for the increase from these regions (Fig. 2.8). Actinopterygians are also being described from new British (Elliott, 2016) and Western European (Giles *et al.*, 2015; Štamberg & Steyer, 2021) deposits. By contrast, the majority of new species from North America stem from focussed efforts on well-known localities, such as Bear Gulch (Lowney, 1980b; Lund & Melton, 1982; Lund & Poplin, 1997, 1999; Lund, 2000; Poplin & Lund, 2000, 2002; Mickle *et al.*, 2009; Grogan & Lund, 2015), Kinney Brick Quarry (Gottfried, 1987, 1992; Bardack, 1992; Zidek, 1992; Williams & Lucas, 2013; Stack *et al.*, 2021), and Mazon Creek (Bardack, 1979; Schultze & Bardack, 1987). Comparatively few taxa derive from more depauperate localities (Mickle, 2017, 2018; Wilson *et al.*, 2018).

While historically understudied regions are producing new taxa, sampling and descriptions from well-sampled regions are still outpacing them. The relative proportion of descriptions from African deposits has decreased, as, except for a handful of taxa from the Beaufort Group (e.g. Bender, 2001, 2002, 2004, 2005), no taxa have been described since the mid-20th century (Gardiner, 1969). New fishes from Siberia (Kazantseva-Selezneva, 1980) and Kazakhstan (Kazantseva-Selezneva, 1981) boost counts of taxa from Asia in the late-20th century, with new descriptions published steadily in subsequent years (Poplin *et al.*, 1991; Prokofiev, 2002, 2005; Zhu *et al.*, 2006; Wang *et al.*, 2007). Descriptions from South America follow a similar pattern,

with an early burst (Beltan, 1978) followed by irregular but sustained contributions (Malabarba, 1988; Beltan, 1989; Cox & Hutchinson, 1991; Richter & Breitkreuz, 1997; Martha, 2002; Figueiredo & Carvalho, 2004; Hamel, 2005; Dias, 2012; Figueroa *et al.*, 2021), notably from the Paraná Basin of Brazil (Cox & Hutchinson, 1991; Figueiredo & Carvalho, 2004; Hamel, 2005; Dias, 2012). Descriptions from Oceania (comprised exclusively of Australian fishes [Woodward, 1931, 1940; Gardiner & Bartram, 1977; Campbell & Phuoc, 1983; Long, 1988; Choo *et al.*, 2009, 2019; Choo, 2012]) consistently comprise a very small proportion of the global collectors' curve.

New actinopterygian taxa are being erected both from newly discovered deposits and through revisiting and revising existing museum collections. It is likely that further diversity is hiding in the extensive collections of museums in historically well-sampled regions (e.g. Natural History Museum, London; American Museum of Natural History, New York City) – Mickle (2017) notes hundreds of specimens of early Carboniferous genera (*Rhadinichthys* and *Elonichthys*) in North American museums. Notably, museum collections will be crucial in augmenting occurrence data, as they likely contain vastly more unique localities than are recorded in the primary literature (by over an order of magnitude; Marshall *et al.*, 2018). In parallel, sampling of new localities in underrepresented regions is likely to yield new taxa as the sampling universe expands (Raup, 1972; Close *et al.*, 2018). The widespread adoption of CT scanning will continue to facilitate valuable redescriptions and taxonomic revisions of such material and remains an important avenue for research (Giles & Friedman, 2014; Giles *et al.*, 2015, 2017; Pradel *et al.*, 2016; Coates & Tietjen, 2018; Friedman *et al.*, 2018; Argyriou *et al.*, 2018; Figueroa *et al.*, 2019). Both new exploration and revisiting

museum collections will be important in increasing our understanding of Palaeozoic actinopterygians.

2.5 Challenges to deciphering the Palaeozoic actinopterygian fossil record accurately

2.5.1 Fossil record biases

A major obstacle to interpreting the evolution of Palaeozoic actinopterygians accurately is the various forms of biases that pervade their fossil record, which are related to geological, geographic and anthropogenic factors. Investigations into the effect of geological, spatial and taphonomic biases on the actinopterygian fossil record are in their infancy, and the extent to which observed patterns of diversity are driven by biases is far from understood. Previous studies posit that changes in richness of the fossil fish record through time likely represent changes in sampling (Friedman & Sallan, 2012). Furthermore, the number of occupied grid cells has been suggested as the best proxy for explaining the richness of all fishes in the fossil record of Great Britain, although osteichthyan richness does not correlate with any proxy (Lloyd & Friedman, 2013). Actinopterygian richness in the Palaeozoic, however, tracks sampling proxies such as localities, formations and equal-area grid cells (Fig. 2.4). A common suggestion in the literature is that the late Palaeozoic record is poorly sampled, particularly in terms of marine deposits, and that this leads to low levels of diversity (Hurley *et al.*, 2007; Near *et al.*, 2012; Broughton *et al.*, 2013). Freshwater occurrences of actinopterygians dominate much of the Permian (Romano *et al.*, 2016; Smithwick & Stubbs, 2018) and some of this skew away from marine deposits may have been linked

to the formation of Pangaea and coincident reductions in coastline (Friedman & Sallan, 2012). Pinpointing the extent to which geological, spatial and taphonomic biases drive the actinopterygian record is a critical next step in understanding the evolution of actinopterygians in the Palaeozoic.

2.5.1.1 Geological biases

The extent to which observed patterns of diversity are the result of rock record biases and correlate with metrics such as the numbers of formations, rock volume or outcrop area is the subject of much debate (Benton, 2015). There are three main hypothesised mechanisms for correlation: (1) a true bias, where diversity patterns are truly dependent on the rock record (Smith, 2001; Peters & Foote, 2001); (2) common cause, where another factor such as sea level (and associated extent of shallow marine sea area and presence of epicontinental seas) drives correlations between the rock and fossil records (Peters, 2005, 2006; Peters & Heim, 2010, 2011; Hannisdal & Peters, 2011); and (3) redundancy, where the effects of sampling on the fossil record and *vice versa* are redundant (Benton *et al.*, 2011, 2013). Lloyd & Friedman (2013) reject the common cause hypothesis for fishes of Great Britain, but the mechanisms acting on the actinopterygian fossil record remain uncertain. The global actinopterygian fossil record includes both marine and freshwater components, which can be further divided into different zones (e.g. benthic assemblages [Sallan *et al.*, 2018]; open ocean *versus* shallow marine [Benson *et al.*, 2010]) that may be subject to different drivers. For example, non-marine area negatively correlates with diversity of shallow marine Mesozoic tetrapods, while contemporaneous open ocean diversity correlates with fossiliferous formations (Benson *et al.*, 2010). Diversity of European marine mammals in the Cenozoic also does not correlate with rock outcrops (Marx, 2009). The

actinopterygian record therefore represents an interesting test of the relative effects of these hypotheses. Analysis of actinopterygian richness in regions with adequate macrostratigraphic data (e.g. in North America; Peters *et al.*, 2018) may help to constrain the effect of geological biases acting on the Palaeozoic record. Richness in the Palaeozoic certainly correlates with geological proxies for sampling metrics (Fig. 2.4 and Appendix Fig. A.1), although the extent to which spatial bias impacts all of these metrics (including richness) is important to consider.

2.5.1.2 Geographic and spatial biases

Europe and North America are the most intensely sampled regions in the marine animal fossil record (Close *et al.*, 2020*b*). The vast majority of Palaeozoic actinopterygian occurrences are also from Europe and North America (Fig. 2.6), with important, although limited, occurrences from South America, Australia and Africa: this distribution is likely due to sampling intensity rather than true diversity. Sampling in the Devonian (Fig. 2.6A) and Carboniferous (Fig. 2.6B) is more restricted than the Permian (Fig. 2.6C), which may result from researcher biases towards the end-Permian mass extinction and the general rise of terrestrial tetrapods. This same pattern is seen in terrestrial vertebrates of the same age (e.g. Dunne *et al.*, 2018). Bias towards Europe and North America hark back to the early descriptions of actinopterygians (particularly from the UK), which are intimately linked to extensive mining, extraction and industrialisation of these regions during the 19th and early 20th centuries (e.g. Agassiz, 1833-1844; King, 1850; Jackson, 1851). More broadly, recent work demonstrates just how important (neo-)colonialism and global socio-economics are as contributing factors to the global skew in palaeontological research outputs and therefore occurrence data (Raja *et al.*, 2022). Variation in taxonomic practice can also impact

richness counts depending on the number of researchers working on certain groups and time periods, and whether these researchers are the same for all time periods (Lloyd *et al.*, 2012*a*,*b*). This variation may contribute to higher diversity in Europe relative to other continental regions (Close *et al.*, 2020*b*), although higher diversity is also likely intimately linked to historical factors and ongoing scientific colonialism (Raja *et al.*, 2022).

Spatial biases also have a substantial impact on diversity trends at global scales due to temporal variability in the fossil content, fossil quantity, and palaeogeographical coverage of assemblages. The 'global' fossil record of any group in fact consists of occurrences distributed heterogeneously in space and time (Benson *et al.*, 2016; Close *et al.*, 2017, 2020*a*,*b*), and is better conceptualised as the sum of multiple regional records with different attributes (Close *et al.*, 2020*a*). Diversity curves representing 'global' counts of taxa may therefore not be a true representation of the peaks and troughs in diversity of a group through time, but instead a combined record of the regional diversity in sampled areas. The effect of this is such that changes in diversity through time likely mainly mirror changes in the spatial extent of the groups' fossil record between sampled intervals (Close *et al.*, 2020*a*,*b*). Notably, the common cause (Peters, 2005, 2006; Peters & Heim, 2010, 2011; Hannisdal & Peters, 2011) and redundancy (Benton *et al.*, 2011, 2013; Dunhill *et al.*, 2014; Benton, 2015) hypotheses do not explain this substantial source of sampling bias (Benson *et al.*, 2016; Close *et al.*, 2017, 2018, 2019, 2020*a*).

This is not to say that studies of the 'global' fossil record of specific taxonomic groups are uninformative, only that patterns must be carefully examined and interpreted with the knowledge that they likely exhibit significant spatial structuring.

Diversity at the regional scale will be informative in determining specific drivers of, and biases in, the diversity signal (Crampton *et al.*, 2003; Dunhill *et al.*, 2012, 2013, 2014; Close *et al.*, 2020*a*), as will examining differences between diversity measures (e.g. alpha and beta diversity), which can also be spatially dependent (Womack *et al.*, 2021).

Different spatial biases acting on the freshwater and marine records may also variably impact different diversity estimates, dependent on the attributes of the sampled regions (Lagomarcino & Miller, 2012). For example, the species–area effect (Hallam and Wignall, 1999; Peters, 2005, 2007; Hannisdal & Peters, 2011; Close *et al.*, 2020*b*) may play a role in levels of marine actinopterygian diversity, linked to changes in sea level and associated features (Lagomarcino & Miller, 2012; Jones *et al.*, 2021), whereas other factors may drive freshwater actinopterygian diversity. Furthermore, the impacts of spatial and temporal variation in the establishment and reduction of epeiric seas (Peters, 2007) and reefs (Kiessling *et al.*, 2010) may play a role in determining diversity of actinopterygians through the Palaeozoic. These potential contributing factors would combine to result in complex drivers of regional heterogeneity in the actinopterygian fossil record, that can now be investigated with occurrence data.

2.5.1.3 Taphonomic biases

Variation in the taphonomy of actinopterygian occurrences also likely influences interpretations of the Palaeozoic actinopterygian fossil record, but the impact of taphonomic processes and biases on this record has not been investigated. Taphonomic biases not only obscure underlying biological signals and impact perceived diversity, but likely influence understanding of other aspects of actinopterygian evolution, such as the degree of functional disparity or ecospace

occupation (Smithwick & Stubbs, 2018). The effects of detrimental taphonomic processes varies geographically, between environments and with time (Brett, 1995; Zohar *et al.*, 2008; Walker *et al.*, 2020), although low-energy, anoxic environments in which individuals were buried rapidly are usually those that best preserve vertebrates, i.e. Lagerstätten (Pardo *et al.*, 2020). Lagerstätten play more of a role in biasing preservation in the marine record than the terrestrial (Muscente *et al.*, 2017), and they clearly influence taxonomic diversity (Benson *et al.*, 2010; Benson & Butler, 2011; Butler *et al.*, 2011; Flannery Sutherland *et al.*, 2019).

As with spatial biases, this may result in different preservational drivers of apparent diversity in the marine and non-marine Palaeozoic; the majority of Lagerstätten (defined by the presence of high concentrations of fossil material [Konzentrat], exceptional preservation [Konservat], or both) yielding actinopterygians are indeed marine (e.g. Bear Gulch Konzenstrat Lagerstätte [Grogan & Lund, 2002; Lund *et al.*, 2012]; Glencartholm Konzenstrat Lagerstätte [Schram, 1983; Briggs & Gall, 1990]; Gogo Konzenstrat and Konservat Lagerstätte [Trinajstic *et al.*, 2022]; Kinney Brick Quarry Konservat Lagerstätte [Lucas *et al.*, 2021]; Mazon Creek Konservat Lagerstätte [Clements *et al.*, 2019]; Miguasha Konservat and Konzenstrat Lagerstätte [Cloutier *et al.*, 2011]), with comparatively few non-marine sites (e.g. Montceau-les-Mines Konservat Lagerstätte; Perrier & Charbonnier, 2014). Lagerstätten may skew diversity trends towards specific intervals, however they also provide unique snapshots of ecosystems in these intervals providing key information not only on taxonomic diversity, but also relative abundance within biota. For example, while actinopterygians were species-poor relative to other vertebrates in the Devonian (Friedman, 2015), they are relatively abundant in the Gogo Formation (Trinajstic *et al.*, 2022).

In recent years, literature has emerged on quantifying the skeletal completeness of the fossil record of various vertebrate groups using both character-completeness metrics (e.g. Mannion & Upchurch, 2010; Brocklehurst & Fröbisch, 2014; Cashmore *et al.*, 2020) and specimen-based completeness metrics (e.g. Cleary *et al.*, 2015; Tutin & Butler, 2017; Driscoll *et al.*, 2019). To date, only one study has investigated completeness in a group of fishes (Schnetz *et al.*, 2022), finding that the acanthodian fossil record is comprised predominantly of isolated remains and is among the least complete vertebrate records (measured as skeletal completeness). Completeness of specimens was significantly higher in freshwater deposits than marine, in contrast to the fossil record of marine tetrapod clades, which appears to be more complete than those of terrestrial tetrapods (Cleary *et al.*, 2015; Tutin & Butler, 2017; Driscoll *et al.*, 2019). Higher completeness in marine tetrapods is attributed to higher sedimentation rates in the marine realm, whereas anoxic conditions and low turbulence are suggested to be responsible for higher freshwater completeness in acanthodians (Schnetz *et al.*, 2022). Quantification of the level of skeletal completeness in actinopterygians will help determine whether completeness of the actinopterygian record exhibits similar traits to the acanthodian or tetrapod records and aid interpretations of the biases acting on the fossil record, especially regarding marine *versus* freshwater fishes.

An additional taphonomic factor that may detrimentally impact our understanding of the actinopterygian fossil record is degree of preservation related to the size of specimens. There are data to suggest that larger organisms are much more likely to preserve than smaller organisms (Benson, 2018; Pardo *et al.*, 2020), while larger, more robust specimens can be associated with higher quality preservation

(Cooper *et al.*, 2006). The extent to which this applies to aquatic vertebrates is little understood, but this is likely to be of importance to actinopterygians: Sallan and Galimberti (2015) suggested that ray-finned fish were small in the aftermath of the EDME. As the early Carboniferous coincides with the origin of the actinopterygian crown (Giles *et al.*, 2017), and small ancestors are thought to have seeded most actinopterygian clades (Romano *et al.*, 2016; Guinot & Cavin, 2018), a bias against preservation of smaller organisms may contribute to the failure to identify or sample early members of these radiations. Furthermore, taphonomic factors have been shown to destroy small actinopterygian bones in particular (Smith *et al.*, 1988) further confounding our ability to interpret the early actinopterygian fossil record correctly.

2.5.2 Taxonomic issues

Deep-seated problems with Palaeozoic actinopterygian taxonomy exacerbate low levels of actinopterygian genus richness, despite high numbers of species and considerable morphological variation within these genera. Many genera from this period have apparently global distributions and stratigraphic ranges spanning nearly the entirety of the Carboniferous and Permian (Fig. 2.7; Gardiner, 1993; Sepkoski, 2002), which may be an artefact of reduced researcher effort in this period in favour of earlier Devonian forms, or later Mesozoic forms (Sallan, 2014). As a result, many mid-late Palaeozoic actinopterygians have not been the subject of detailed taxonomic work.

Carboniferous and Permian actinopterygians received the most attention from researchers in the 19th and early 20th centuries. While much of this work was ground-breaking and laid the foundations for palaeoichthyology, there are substantial problems with some outcomes of the research, notably the existence of wide-ranging, poorly defined genera. Often, initial descriptions of taxa were brief and erected new genera

with a heavy reliance on the shape of the body (e.g. deep-bodied, fusiform, slender) and scale morphology (Agassiz, 1833-1844; Traquair, 1877-1912, 1879; Moy-Thomas & Dyne, 1938). This led to poorly defined genus diagnoses, often containing large numbers of dubiously related species – species whose characteristics sometimes even contradicted generic diagnoses. Some of the most notable problem genera – also termed 'waste-baskets' (Evans, 2005) and 'trash fish' (Coates & Tietjen, 2018) – are '*Elonichthys*' Giebel 1848 (44 species), *Rhadinichthys* Traquair 1877 (30 species), *Platysomus* Agassiz 1843 (20 species), *Amblypterus* Agassiz 1843 (18 species), *Palaeoniscum* Blainville 1818 (18 species) and *Acrolepis* Agassiz 1843 (14 species) (Mickle, 2017), although others exhibit similar issues (e.g. *Moythomasia* Gross 1950). Higher-level taxonomic groups based on these genera, which are almost exclusively erected with generic diagnoses (Sallan, 2014), suffer from the same problems.

In addition to being taxonomically ambiguous, these few Palaeozoic actinopterygian genera likely obscure a significant proportion of genus-level diversity. Redescriptions and redefined diagnoses are necessary in order to reveal the true taxonomic diversity hiding within these genera. Recently, '*Elonichthys*' was redefined to include just three species (Schindler, 2018*a*) from Central European late Carboniferous and early Permian deposits. Consequently, the temporal and spatial extent of the genus has been drastically reduced, and nearly 50 other species of '*Elonichthys*', ranging from the Tournaisian to the Wuchiapingian, are invalid and represent other taxa currently unaccounted for in genus-level diversity analysis. More broadly, while apparently widespread by modern continental configuration (Fig. 2.6), palaeogeographic distributions of problem genera are more concentrated due to the proximity of Western Europe and North America in the Palaeozoic (Scotese, 2021).

That these regions, where the majority of species within problem genera occur (Fig. 2.7), were geographically contiguous in the Palaeozoic exacerbates the geographic research bias associated with greater sampling of North America and Europe. Shared presence of numerous groups of actinopterygians [e.g. haplolepids, eurynotiforms, aeduelliforms (Sallan & Coates, 2013; Elliott, 2014, 2016; Hodnett & Lucas, 2015)] in present-day North America and Western Europe indicates a close link, though it is possible that this similarity is artificial and may simply reflect the absence of samples from elsewhere.

In recent years, new anatomical information revealed by CT scanning has prompted several reinvestigations of the validity of Palaeozoic taxa. Coates & Tietjen (2018) recently redescribed a Bashkirian actinopterygian and moved it to *Trawdenia* n. gen. This specimen was originally referred to *Mesopoma*, a taxon erected by Traquair (1890) in an attempt to separate species belonging to *Canobius* and *Rhadinichthys*. Traquair subsequently retracted the genus (Traquair, 1912), before Moy-Thomas & Dyne (1938) restored it (see Coates, 1993, 1998; Coates & Tietjen, 2018). *Trawdenia* exemplifies both the root cause of the problem with many Carboniferous and Permian actinopterygian genera – a diagnosis based on characteristics prevalent in other late Palaeozoic actinopterygians and lacking unambiguous synapomorphies – and also the route to resolving the problem: detailed redescription to identify unique characters aided by currently available technology such as CT scanning. Reinvestigation of Palaeozoic material is not simply an exercise in correcting taxonomy, however. Coates (1999) and Coates & Tietjen's (2018) work revealed previously hidden features of the endocast and pectoral fin in a specimen that had been known to the literature for over a century. The case of *Trawdenia*, as well as

others such as *Eurynotus crenatus* (Friedman *et al.*, 2018) and *Brazilichthys macrognathus* (Figueroa *et al.*, 2019), clearly demonstrate that reinvestigation can reveal not only hidden taxa, but untold anatomical and ecological diversity.

2.5.3 Phylogenetic issues

Relationships of the four extant actinopterygian clades (Cladistia, Chondrostei, Holostei, Teleostei) has reached a point of consensus through both molecular (e.g. Betancur-R *et al.*, 2017; Hughes *et al.*, 2018; Dornburg & Near, 2021) and morphological (e.g. Patterson, 1982; Gardiner & Schaeffer, 1989; Coates, 1998; Cloutier & Arratia, 2004; Grande, 2010; Xu *et al.*, 2014; Giles *et al.*, 2017) research. Sallan (2014) provided a detailed summary of previous hypotheses of living clades and the basis for this consensus. Friedman (2015) synthesises attempts to place Palaeozoic actinopterygians relative to extant clades, highlighting that the relationships of extinct actinopterygians, both in relation to each other and to extant clades, remain unclear.

The cladistic analysis of Gardiner & Schaeffer (1989), which built significantly on prior work by Gardiner (1984), represented a seminal study for investigations into Palaeozoic actinopterygian relationships (Friedman, 2015). Gardiner & Schaeffer (1989) organised early actinopterygians into groups (e.g. the *Moythomasia* Group, the *Platysomus* Group), which they tentatively posited to be monophyletic, in order to determine actinopterygian phylogeny. Although the monophyly of these groups was rarely upheld in later work, this analysis and the anatomical characters it established forms the basis for almost all future phylogenetic studies (e.g. Coates, 1999; Dietze, 2000; Poplin & Lund, 2000; Cloutier & Arratia, 2004; Poplin & Dutheil, 2005; Friedman & Blom, 2006; Swartz, 2009; Fig. 2.9). The history of phylogenetic work on

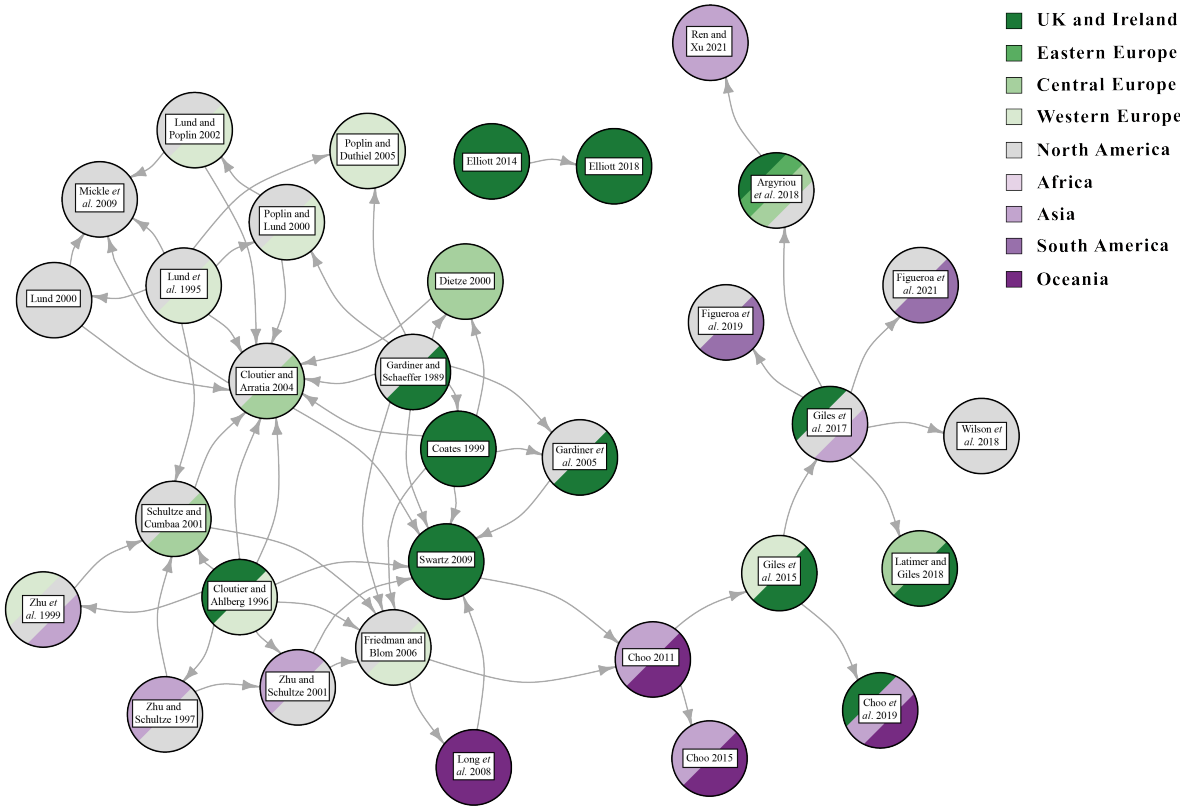


Figure 2.9: Network depicting the flow of characters to and from phylogenetic analyses of Palaeozoic actinopterygians. Nodes are coloured according to the geographic region in which authors' listed institutions (in the primary article) are located.

actinopterygians mirrors the geographic biases related to sampling of actinopterygian occurrences, with clear bias towards the regions in which research groups are located (Fig. 2.9).

Subsequent analyses have attempted to determine the relationships of primitive actinopterygians relative to extant clades (e.g. Cloutier & Arratia, 2004) or focussed solely on Palaeozoic actinopterygian interrelationships (e.g. Friedman & Blom, 2006). Although most analyses draw on multiple sources, two main subsequent 'lineages' of analyses have arisen, both with a focus shifted towards relationships of actinopterygians rather than early bony fishes. Cloutier & Arratia (2004), which attempted a major synthesis of existing character matrices, sourcing characters from

previous cladistic and phylogenetic studies, heavily influenced Mickle *et al*. (2009) and Swartz (2009), while Friedman & Blom (2006) became the basis of Choo (2012) and all subsequent analyses derived from that matrix (Giles *et al.*, 2015, 2017; Argyriou *et al.*, 2018; Choo *et al.*, 2019; Figueroa *et al.*, 2019, 2021; Fig. 2.9). Giles *et al.* (2017) significantly expanded and revised this derived matrix with the aim of interrogating relationships between living and fossil actinopterygian lineages.

Other matrices focus on a particular fauna or geographic region. Most notable amongst these are efforts to investigate the relationships of Bear Gulch actinopterygians, which include limited taxa from outside this deposit (Lund *et al.*, 1995; Lund, 2000; Fig. 2.9). Cloutier & Arratia (2004) attempted to integrate these analyses with other early actinopterygian and osteichthyan matrices. This was further expanded by Mickle *et al.* (2009; Fig. 2.10B; and in an unpublished thesis: Mickle, 2012), who included more Bear Gulch forms and several other taxa (e.g. *Roslerichthys*; Hamel, 2005). Separately, Elliott (2016; Fig. 2.10D) conducted an analysis of Scottish Bashkirian actinopterygians, sampling traditionally underrepresented groups (such as haplolepids) while excluding all other Palaeozoic actinopterygians.

In general, expansions of these matrices has focused on increasing taxon sampling of actinopterygian groups that are already represented and adding more crownward taxa (Latimer & Giles, 2018; Argyriou *et al.*, 2018; Ren & Xu, 2021), rather than including previously excluded Palaeozoic taxa. Numerous proposed Palaeozoic actinopterygian clades are yet to be included fully in phylogenetic analyses despite high support in the literature (e.g. eurynotiforms [Sallan & Coates, 2013; Friedman *et al.*, 2018]), and many others remain represented by a single terminal (e.g. platysomids; Giles *et al*., 2017). Hypotheses of relationships have been shown to change

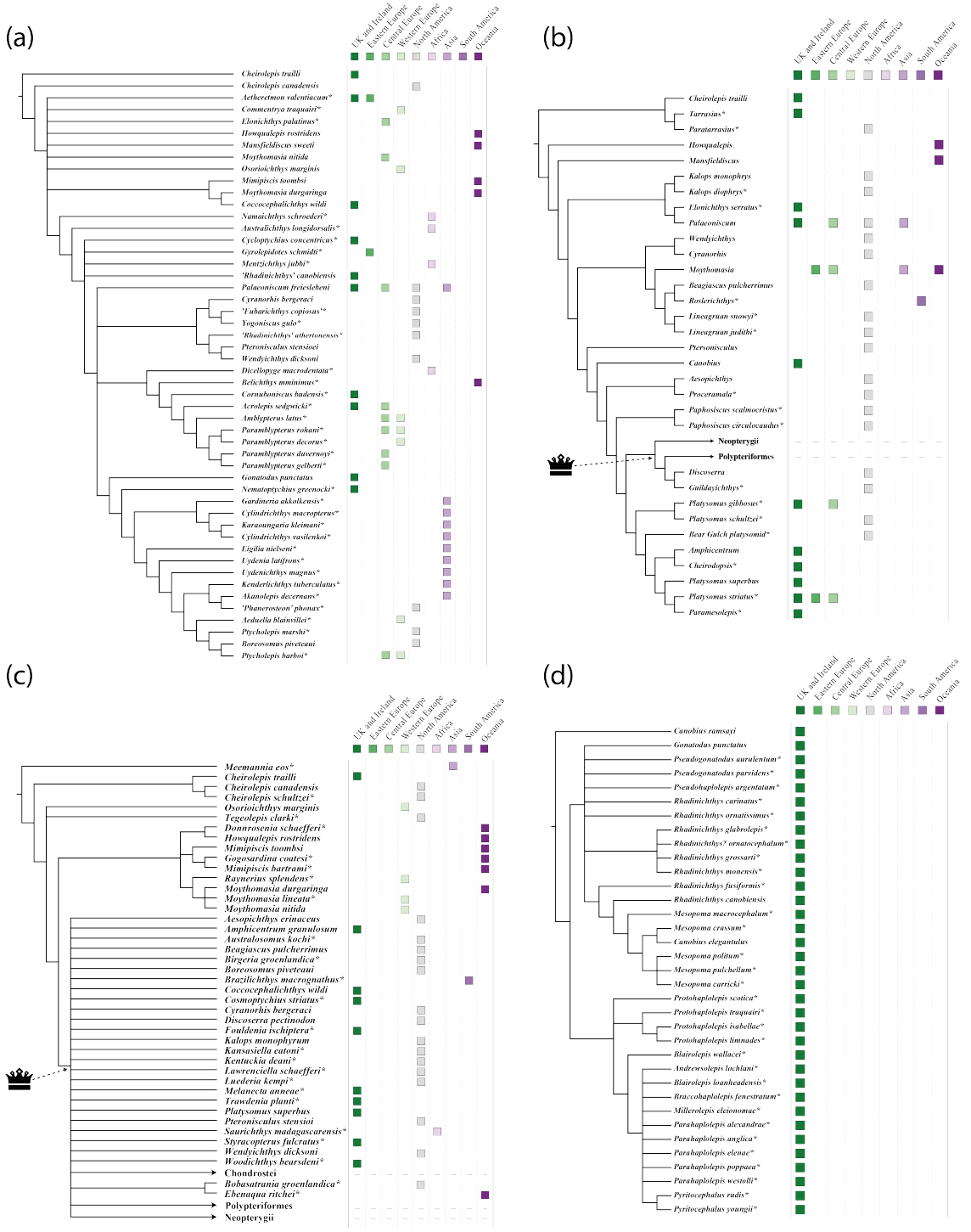


Figure 2.10: Phylogenetic analyses of Palaeozoic actinopterygian relationships showing the geographic distribution of sampled taxa: (A) Dietze (2000); (B) Mickle et al. (2009); (C) Figueroa et al. (2019); and (D) Elliott (2016). The actinopterygian crown node is indicated in analyses that include extant taxa. Asterisks (*) indicate taxa not included in the other depicted analyses to show the lack of overlap between data sets.

substantially when additional taxa from underrepresented taxonomic groups are included [e.g. saurichthyids (Argyriou *et al.*, 2018); dapediids and pycnodonts (Latimer

& Giles, 2018)], resulting in topologies and divergence timelines inconsistent with past molecular (Betancur-R *et al*., 2017; Hughes *et al*., 2018; Dornburg & Near, 2021) and morphological (Cloutier & Arratia, 2004; Grande, 2010; Xu *et al*., 2014; Giles *et al.*, 2017) consensus, suggesting that this skewed representation may be a major source of uncertainty in the early actinopterygian tree.

Other sources of bias are noticeable, especially temporal and geographic imbalances. Most analyses contain roughly even numbers of Devonian and Carboniferous taxa (Coates, 1999; Cloutier & Arratia, 2004; Gardiner *et al.*, 2005; Giles *et al.*, 2017; Figueroa *et al*., 2021), despite there being an order of magnitude more species described from the Carboniferous (Fig. 2.4). Permian taxa are largely excluded, despite the nearly equivalent numbers of Permian species relative to the Carboniferous (Fig. 2.4). Furthermore, most analyses heavily sample fishes from British, North American and Australian deposits (Fig. 2.10). Dietze (2000; Fig. 2.10A) is a notable exception that incorporates underrepresented taxonomic groups (e.g. amplypterids) and geographic regions (e.g. Africa, Asia, Central Europe), although very few subsequent analyses have built upon this widespread sampling of taxa. A synthesis and integration of disparate phylogenetic analyses that focus on individual groups or regions (e.g. Dietze, 2000; Elliott, 2016) with broader analyses that attempt to span the actinopterygian radiation (e.g. Giles *et al.*, 2017; Figueroa *et al.*, 2019, 2021; Ren & Xu, 2021) is sorely needed. Among the most recent iterations of the Giles *et al*. (2017) matrix are studies beginning to expand the geographic spread of taxa by including actinopterygians from South America (Figueroa *et al.*, 2019, 2021). Importantly, when sampling expands beyond taxa from the Euro-American realm,

support for past hypotheses of relationships among stem-actinopterygians collapses (Fig. 2.10C).

Lack of an adequate representation of known morphologies, clades and geographic regions in character matrices is drastically preventing an accurate understanding of Palaeozoic actinopterygians (Friedman, 2015). While revisions to early cladistic and phylogenetic analyses (Gardiner & Schaeffer, 1989; Coates, 1999) have resulted in the shift of the majority of Palaeozoic taxa from the actinopterygian crown to the stem (Cloutier & Arratia, 2004; Mickle *et al.,* 2009; Giles *et al.* 2017), the relationships between the numerous diverse clades within the Palaeozoic are still highly unstable. As well as expanding the geographic range encompassed by taxa, it will be important to address existing imbalances in geographic sampling before analysing important phylogeographic aspects of actinopterygian evolution (such as dispersal rates), as variation in sampling can greatly influence results (Gardner, Surya and Organ, 2019).

2.6 Conclusions

(1) Comprehensive occurrence-based data sets are necessary for examining biases in the fossil record and deducing accurate diversity trends (Alroy, 2020), while robust phylogenies are crucial for detailed macroevolutionary analyses (Soul & Wright, 2021). Fishes are rarely the subject of such analyses, but present ample opportunities for investigating evolutionary dynamics through the Palaeozoic. A priority for Palaeozoic actinopterygian research is to record occurrences in the PBDB and update regional substage ages; efforts to do so are in progress.

(2) Actinopterygian richness fluctuates throughout the Palaeozoic, but raw counts largely appear to be tracking sampling proxies. Europe and North America are oversampled in comparison to most Global South regions, and sampling and spatial biases have a clear influence on the record. Targeted sampling of underrepresented regions (e.g. mid- to high-palaeolatitudes in the Carboniferous), time periods and environments (e.g. marine environments in the Late Carboniferous–Middle Permian) will be necessary to redress this imbalance. Concurrently, detailed sampling of well-known regions will allow for more accurate diversity analyses of local and regional subsets, which are a critical avenue for research considering issues regarding analysis of 'global' fossil records. This detailed sampling should take the form of cataloguing museum collections in such regions (as well as more broadly) given the likelihood that they contain a large number of occurrences that are not recorded in the primary literature, and thus not entered into occurrence databases (Marshall *et al.*, 2018).

(3) Our occurrence-level database for Palaeozoic actinopterygians paves the way for examining biases in the fossil record and deducing accurate diversity trends. In particular, analytical methods of sampling standardisation (Chao, 1984; Chao & Jost, 2012; Alroy, 2017, 2018, 2020; Close *et al.*, 2020*a*; Jones *et al.*, 2021) and application of diversity estimation at different scales (Close *et al.*, 2019) represent a priority for future studies (Alroy, 2010*a*,*b*; Close *et al.*, 2018). Incorporation of macrostratigraphic data may help facilitate a synthesis of the various biases impacting the actinopterygian fossil record.

(4) Historical poor taxonomic practices mask valuable taxonomic and morphological diversity in Palaeozoic actinopterygians (Coates & Tietjen, 2018; Schindler, 2018*a*). Re-evaluation of 'waste-basket' taxa, aided by CT scanning,

represent the foundation for many other studies. Taxonomic revisions will result in a tightening of the geographic and temporal ranges of these widespread genera, which in turn will help to deduce accurate patterns of palaeodiversity (Close *et al.*, 2018), palaeogeographic dispersal (Cavin, 2008; Gardner *et al.*, 2019) and regional connectedness (Stigall *et al.*, 2017). Redescriptions also aid the identification of early members of extant actinopterygian clades (Giles *et al.*, 2017), thus paving the way for a better understanding of the evolutionary dynamics between clades (Clarke *et al.*, 2016) as actinopterygians became dominant in aquatic habitats (Sallan & Coates, 2010; Friedman, 2015).

(5) Existing phylogenetic character matrices are plagued by similar biases to the overall fossil record, heavily oversampling North American and European fishes, and expanding the geographic and temporal range of phylogenies must represent a priority. Continued addition of taxa and well-formulated characters (Brazeau, 2011), as well as better methods for dealing with inapplicable characters (Brazeau *et al.*, 2019; Goloboff *et al.*, 2021), will generate robust hypotheses of relationships with which to investigate key evolutionary events. Greater incorporation of techniques such as tip-dating may be able to tease apart relationships suspected to result from homoplasy (Lee & Yates, 2018), for example the multiple deep-bodied radiations of Palaeozoic actinopterygians.

(6) The mechanisms underlying actinopterygian diversification following the end-Devonian mass extinction and their subsequent evolutionary dynamics through the Palaeozoic remain largely unknown, in part due to the lack of stable phylogenetic hypotheses of relationships and occurrence databases. Having these data in hand will

enable a wide range of analysis, from inference-based methods to phylogenetic comparative methods to palaeogeographical dispersal:

(*a*) Reliable and representative phylogenies are an important component of biogeographic network analyses (Button *et al.*, 2017; Dunne *et al.*, 2018; Kubo, 2019), and alternative estimates of diversity such as lineages counts through time (also referred to as phylogenetic diversity; Ezcurra and Butler, 2018) that would complement taxic estimates of diversity.

(*b*) Application of phylogenetic comparative methods has the potential to identify adaptive radiations (Close *et al.*, 2015; Ezcurra & Butler, 2018; Felice & Goswami, 2018; Halliday *et al.*, 2019; Simões *et al.*, 2020). Actinopterygians appear to diversify explosively in the early Carboniferous, but the lack of comprehensive phylogenetic analysis prevents testing of whether this best fits a model of classic extinction recovery, adaptive radiation, or ecological release (Schluter, 2000; Sallan & Friedman, 2012; Friedman & Sallan, 2012; Slater, 2013). In tandem, investigating survivorship and selectivity through mass extinctions, such as the end-Devonian, among and between lineages (Soul & Friedman, 2017; Allen *et al.*, 2019) may reveal more detail on the effects of mass extinctions (Sallan & Friedman, 2012; Sallan & Galimberti, 2015). Deep-bodied Palaeozoic actinopterygians also represent an obvious test case for exploring these techniques, for example by quantifying convergence and teasing this apart from shared history (Speed & Arbuckle, 2017; Arbour & Zanno, 2020).

(*c*) Previous work has examined shifts between marine and non-marine habitats in other fossil groups (and coincident changes in morphology and

disparity; Lamsdell, 2016). By combining palaeoecological observations from occurrence data with reliable phylogenetic hypotheses, it will be possible to examine habitat transitions and trends in actinopterygian ecology and biogeography through time (Lamsdell *et al.*, 2017). In addition, previous ancestral-state based hypotheses of crown-group actinopterygian habitats have inferred both a freshwater (Carrete Vega & Wiens, 2012) and marine (Betancur-R *et al.*, 2015; Guinot & Cavin, 2018) origin for actinopterygians (although the result indicates that a freshwater origin is due to the absence of fossil data in the analysis). Given recent upheavals in established schemes of phylogenetic relationships, with a particular effect on deep-branching members of stem groups (e.g. Giles *et al.*, 2017), ancestral state reconstructions should be reassessed. As it may be physiologically easier to adapt from one environment to another (Betancur-R *et al.*, 2015), it would be prudent to explore the use of asymmetric transition models as recently used to investigate the evolution of oviparity and viviparity in squamates (Blackburn, 2015).

Collectively, these investigations will greatly expand our understanding of the early evolution and rise to dominance of the most speciose extant vertebrate clade, the Actinopterygii.

3 Sampling biases obscure the early diversification of the largest living vertebrate group

This chapter is a reformatted version of the following paper, published in *Proceedings of the Royal Society B*. I compiled the occurrence, conducted the analyses, prepared the figures and wrote the manuscript. EMD and I wrote the code analysing the data. All authors revised the manuscript and approved the published version. The editorial 'we' is used throughout the text to reflect these contributions.

HENDERSON, S., DUNNE, E.M. and GILES, S., 2022. Sampling biases obscure the early diversification of the largest living vertebrate group. Proceedings of the Royal Society B, 289(1985), 20220916. https://doi.org/10.1098/rspb.2022.0916.

3.1 Introduction

There are around 32,000 species of living ray-finned fishes (actinopterygians), amounting to over half of extant vertebrate diversity, and split roughly evenly between marine and freshwater environments (Nelson *et al.*, 2016). Ray-finned fishes originated in the Palaeozoic, which saw major evolutionary events and changes in the vertebrate fauna, such as the emergence of jaws (Sansom *et al.*, 2015), major extinctions of vertebrate groups (Sallan & Coates, 2010), and the move onto land (Clack, 2012). Despite these pivotal changes, and a long history of research on actinopterygians, there are relatively few macroevolutionary studies investigating diversity trends in their early evolution, and all examine face-value patterns of taxonomic richness (Thomson,

1977; Patterson, 1994; Sallan & Coates, 2010; Blieck, 2011; Romano *et al.*, 2016; Henderson *et al.*, 2021).

Few studies investigate whether the Palaeozoic ray-fin fossil record is adequate for investigating diversity patterns or whether it is severely biased (Sallan & Coates, 2010; Friedman & Sallan, 2012; Romano *et al.*, 2016). Notably, biases may impact the marine and freshwater record differently. For example, trends in Permian freshwater osteichthyan diversity are altered by inclusion of Lagerstätten in analyses, while trends in the marine realm remain consistent with or without Lagerstätten (Romano *et al.*, 2016). However, this difference is likely due to the temporal distribution of marine and freshwater Lagerstätten rather than a causal effect related to palaeoenvironment. Despite apparent limitations of the early actinopterygian record, a series of hypotheses have been proposed on the basis of face-value readings of the record. Low taxonomic diversity in the Devonian followed by an explosive increase in the early Carboniferous is generally interpreted as representing a genuine biological signal, on the basis of relative increases in the actinopterygian faunal component (Sallan & Coates, 2010; Friedman & Sallan, 2012). In the later Palaeozoic, some authors qualitatively suggest that low Permian diversity is linked to the rarity of suitable deposits (Hurley *et al.*, 2007), while others disagree and attribute the decline in richness among freshwater taxa to the loss of extensive Euramerican freshwater habitats (Romano *et al.*, 2016). It has further been proposed that the consistent ecomorphologies in typical Palaeozoic actinopterygians hint at constraints on diversification into new ecologies and habitats and thus low richness (Friedman & Sallan, 2012). To date, however, previous studies only present face-value counts of actinopterygians through time without employing recent advances in methodologies to estimate diversity trends. An exception to this

(Romano *et al.*, 2016) performed coverage-based rarefaction to compare the Permian and Triassic as a whole, rather than to estimate diversity trends through time.

Assessing the degree to which fossil record biases affect interpretations of richness is critical to obtaining an accurate estimate of diversity trends (Raup, 1972; Sepkoski, 1981; Alroy *et al.*, 2008). These biases can be geological (Peters, 2005; Wall *et al.*, 2011), geographic (Close *et al.*, 2017, 2020a, 2020b), or anthropogenic (Upchurch *et al.*, 2011; Raja *et al.*, 2022) in nature, and recent analyses show that 'global' fossil records are intimately linked to the spatial extent of that record (Close *et al.*, 2020a, 2020b). Various statistical methods attempt to tease apart bias from genuine changes (e.g. classical rarefaction and residual modelling), though not without complications (e.g. classical rarefaction can flatten diversity patterns (Alroy, 2010c, 2020; Chao & Jost, 2012; Close *et al.*, 2018), while residual modelling is dependent on the sampling proxy used and generally unable to determine whether low diversity results from low sampling (Dunhill *et al.*, 2014, 2018). Recent years have seen the application of coverage-based methods of sampling standardisation, such as Shareholder Quorum Subsampling (SQS) and coverage-based rarefaction (Alroy, 2010a; Chao & Jost, 2012), to palaeobiological occurrence databases (Benson *et al.*, 2016; Close *et al.*, 2017, 2020a, 2020b; Cleary *et al.*, 2018, 2020; Dunne *et al.*, 2018; Allen *et al.*, 2020) as a means of deducing trends in palaeodiversity through time. As SQS subsamples intervals to equal levels of completeness it returns more accurate relative richness estimates between sampled intervals than size-based rarefaction (Close *et al.*, 2018), although is still susceptible to some biases (Upchurch *et al.*, 2011; Alroy, 2020). Principally, SQS estimates can have a significant evenness signal and reflect evenness distributions of the underlying data rather than any biological trend

(Upchurch *et al.*, 2011; Mitchell, 2015; Alroy, 2020), which may be particularly important for datasets that are biased in ways that skew the evenness of frequency distributions within sampled intervals. A recently developed richness estimator, squares (Alroy, 2018), estimates higher richness when there are numerous rare taxa (i.e. singletons) and when common taxa are especially frequent. Squares is more robust to uneven distributions than SQS, though falls short when the ratio of richness counts to total number of taxa within intervals is very high (Alroy, 2020).

Until recently, no comprehensive through-Palaeozoic occurrence database existed (Henderson *et al.*, 2021), with previously-published databases limited in scope or not updated (Sallan & Coates, 2010; Romano *et al.*, 2016). Here, we examine modern and palaeogeographic distribution of Palaeozoic actinopterygian occurrences alongside local richness to attempt to tease apart spatiotemporal sampling biases and biogeographic patterns. In addition, we apply coverage-based sampling standardisation and squares extrapolation to the newly-assembled occurrence database of Palaeozoic actinopterygians to scrutinise patterns of diversity through the Palaeozoic, the suitability of the dataset, and the likely extent and impact of sampling biases, allowing assessment of previous hypotheses surrounding Palaeozoic actinopterygian diversity.

3.2 Methods

3.2.1 Data preparation

Global occurrences of Palaeozoic Actinopterygii (Henderson *et al.*, 2021), incorporating information on stratigraphy, lithology, geography, age and taxonomy that were compiled from the literature, were screened for taxonomically indeterminate

occurrences. Scale- and teeth-based occurrences were also removed as it is often difficult to assign them definitively to a taxon. Well-preserved fossils are generally required to attribute osteichthyan fossils to a genus (Romano *et al.*, 2016), and it is difficult to assign isolated scales from the same deposits to different species rather than distinct morphotypes from different parts of the body of one taxon (Esin, 1990; Trinajstic, 1999b) unless the isolated scales are directly comparable with contemporaneous body fossils (e.g. Gneudna and Gogo [Trinajstic, 1999a]). ICS stratigraphic stages of each occurrence were replaced with intervals of roughly equal length (~9 Ma), determined by either combining shorter intervals (e.g. Kasimovian [3.3 Ma] and Gzhelian [4.8 Ma] = Kasimovian and Gzhelian [8.1 Ma]), or splitting longer intervals (e.g. Visean [15.8 Ma] = early Visean [Chadian-Holkerian; 8.7 Ma] and late Visean [Asbian-Brigantian; 7.1 Ma]; boundary based on the age of the Dunsapie basalt, see Monaghan *et al.* [2014]).

After removal of indeterminate occurrences and occurrences that could not be assigned to equal-length intervals, this resulted in a dataset of 1,611 occurrences of 473 species (belonging to 226 genera), from 512 unique geographic localities. Generally, unique geographic localities represent unique assemblages in time and space and can therefore be considered communities for the purposes of local richness. However, a limited number (usually the more productive and explored localities) may not be unique in space or time for one of two reasons. Firstly, multiple horizons may outcrop at a single geographic locality, for example at at Glencartholm, where different taxa are found in separate horizons (e.g. *Mesopoma*: Horizon K; *Rhadinichthys*: Horizon F). Here, we treat Glencartholm as a single locality due to the occurrence of most fossils at the Macconochie site which has uncertain stratigraphy (Schram, 1983).

Secondly, the same horizon may outcrop at multiple localities, for example at Bear Gulch, where multiple locations are known within a confined local area (Lund & Poplin, 1999). Here, we treat these separate outcrops as separate localities with consistent stratigraphic information.

The cleaned dataset was then used for local richness and diversity estimation. Local richness estimates included occurrences that could not be constrained to a single interval by using the midpoint of their range as their occurrence age, while only occurrences attributable to a single interval were used in diversity estimation. All analyses were conducted within R 4.1.0 (R Core Team, 2020).

3.2.2 Alpha diversity (local richness)

Species per locality were counted as a measure of alpha diversity (local richness [Close *et al.*, 2019]). Occurrences indeterminate at species level were retained in line with the taxonomic hierarchy of the Paleobiology Database. Modern coordinates for these localities were translated into palaeocoordinates using the R 'chronosphere' package (version 0.1.5 [Ádám T. Kocsis & Nussaïbah B. Raja, 2019]). Local richness was then subset by marine and freshwater environment (brackish environments were included in marine counts) and plotted against palaeolatitude. Additionally, palaeogeographic maps showing local richness were produced in 'chronosphere' (Ádám T. Kocsis & Nussaïbah B. Raja, 2019) for each interval. It is uncertain whether some Permian localities (Pastos Bons – Brazil; Deep Red Run, Dundee, McCann Quarry, Pond Creek, South Dakota State Cement Plant Quarry – USA; Sobernheim – Germany) are Artinskian or Kungurian in age, and these localities are therefore plotted in both palaeogeographic maps.

3.2.3 Sampling standardisation and diversity estimation

Coverage-based sampling standardisation (Alroy, 2010a, 2010b, 2010c, 2014) was implemented to estimate global diversity patterns, first using coverage-based rarefaction, which is mathematically very similar to SQS, via the R package iNEXT (version 2.0.19 (Hsieh *et al.*, 2016)), following the procedure outlined in Dunne *et al.* (2018). The data were rarefied by geographic locality by analysing incidence-frequency matrices of the occurrence data. Extrapolated estimates were limited to no more than twice the observed sample size (Hsieh *et al.*, 2016). Coverage-rarefied richness was computed at genus level using roughly equal length bins, at quorum levels 0.3-0.7; higher quorums were unattainable and resulted in estimates exceeding double the reference sample size. Devonian bins were excluded due to the very small sample-sizes and low levels of coverage. Coverage in the early Visean and Kungurian is also extremely low, and estimates for these intervals will therefore be unreliable, particularly at higher quorums. Rank occurrence distributions and size- and coverage-based rarefaction curves were generated for each interval to investigate the reliability of coverage-rarefied richness estimates. A split-sum test was also conducted after dividing the data set into marine (including brackish) and freshwater occurrences, although the resultant low sample sizes meant that the highest attainable quorum was very low.

A second sampling standardisation method, squares, was also implemented (as in Allen *et al.* [2020]) due to the susceptibility of coverage-rarefied richness to unevenness in the underlying distribution of the data (Close *et al.*, 2018). Squares, unlike other extrapolators such as Chao 1, is designed to minimise underestimation resulting from unevenness (i.e. when there are lots of singletons and common taxa are

extremely frequent) (Alroy, 2018). Squares is also more accurate than other extrapolators (e.g. λ_5) and performs well in split-and-sum tests (Alroy, 2020). Squares extrapolated estimates of genus and species richness were conducted in R by applying Alroy's equation (Alroy, 2018), following the same procedure as Allen *et al.* (2020). In addition, we conducted split-and-sum tests after dividing the data set into marine (including brackish) and freshwater occurrences.

3.3 Results

3.3.1 Alpha diversity (local richness)

Local richness is generally low in the Devonian (Fig. 3.1), with only one locality containing more than three genera (Paddy's Valley, Gogo Formation, Frasnian, Australia). Levels of local richness are highest in the Carboniferous, particularly around the Serpukhovian-Bashkirian boundary (Fig. 3.1), before declining steadily in the latest Carboniferous (Kasimovian and Gzhelian) and early Permian (Cisuralian). Notable localities contributing to the mid-Carboniferous peak include Glencartholm (Scotland, late Visean, marine), Ardenrigg (Scotland, Bashkirian, freshwater), Longton (England, Bashkirian, marine) and the Bear Gulch localities (USA, Serpukhovian, marine) (Fig. 3.1a). With the exception of two notable localities (Kinney Brick Quarry, US, and Rio Negro, Uruguay) there are very few occurrences with marine and brackish palaeoenvironments in the latest Carboniferous (Kasimovian and Gzhelian) and earliest Permian (Asselian and Sakmarian). Instead, the vast majority of occurrences are freshwater in origin. However, few freshwater localities are present in the Artinskian and Kungurian, which yield very low richness, and occurrences and richness from marine settings also remain low. In the latest Permian (Wuchiapingian and

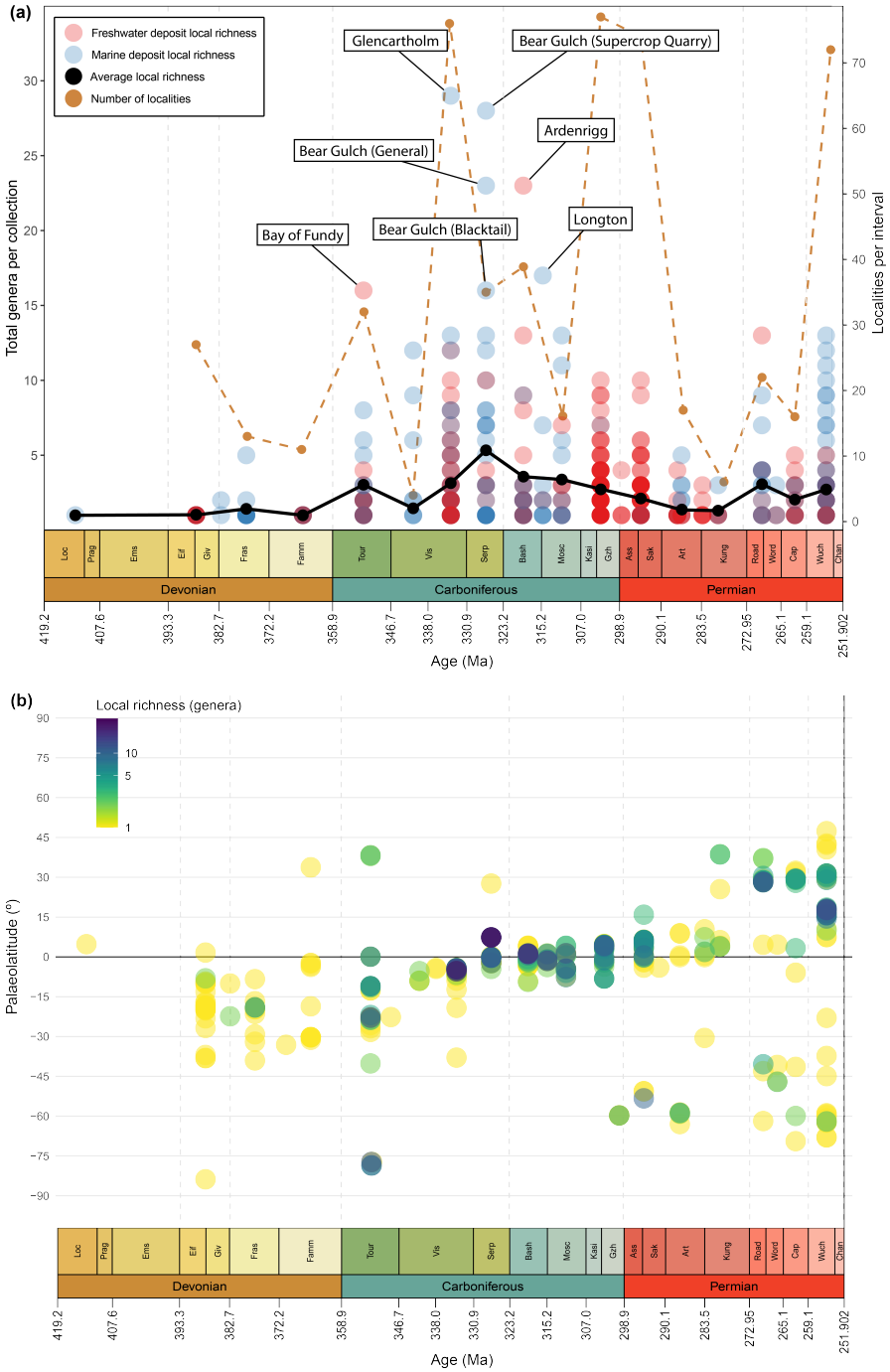


Figure 3.1: Local richness (number of species per fossil locality) of actinopterygians through the Palaeozoic. (a) Local richness plotted by environment, separated by freshwater (red) and marine (blue; incorporates brackish occurrences). Colour saturation (transparency) indicates density of localities, and the most species-rich localities are labelled. Note that purple indicates contemporary localities with similar diversity of marine and freshwater actinopterygians. (b) Palaeolatitude of localities through time, with local richness indicated by colour (yellow localities have low richness, progressing through green to the most diverse localities in indigo).

Changhsingian), marine localities generally have much higher genus counts than freshwater localities. Broadly, it is clear that sampling of different palaeoenvironments

throughout the Palaeozoic is highly heterogenous, with many intervals showing a clear dominance of either marine or freshwater occurrences (Fig. 3.1 and Appendix Fig. B.1).

3.3.2 Palaeomaps and geographical spread

3.3.2.1 Devonian

Despite their earliest occurrence being just north of the palaeoequator (*Meemannia*, Lochkovian, South China), actinopterygians are known almost exclusively from southern palaeolatitudes in the Devonian (Fig. 3.1b; Fig. 3.2a), likely reflecting the Devonian continental configuration in which nearly all landmasses are south of the palaeoquator. Only two other northern hemisphere occurrences are reported (*Cheirolepis*, Givetian, Svalbard [Newman *et al.*, 2021]; *Krasnoyarichthys*, Famennian, Russia [Prokofiev, 2002]). The majority of taxa occur at low palaeolatitudes (0° to -30°), with a small number just crossing into the mid-palaeolatitudinal band (-30° to -60°). A clear outlier, near the southern palaeopole (-83.81°), is the recently reported *Austelliscus ferox* from Brazil (Figueroa *et al.*, 2021).

Devonian actinopterygian occurrences mirror both continental configurations—the majority of landmasses and shallow seas were palaeoequatorial and in the southern hemisphere (Dowding & Ebach, 2019)—and the broader Devonian fossil record (Allison & Briggs, 1993; Powell, 2009; Close *et al.*, 2020b). Givetian and Eifelian occurrences are dominated by European (especially Scottish) deposits, with limited contributions from the USA, Australia, the Antarctic and Brazil (Fig. 3.2a). In contrast, Frasnian occurrences (Fig. 3.2b) are dominated by the Australian Gogo Formation,

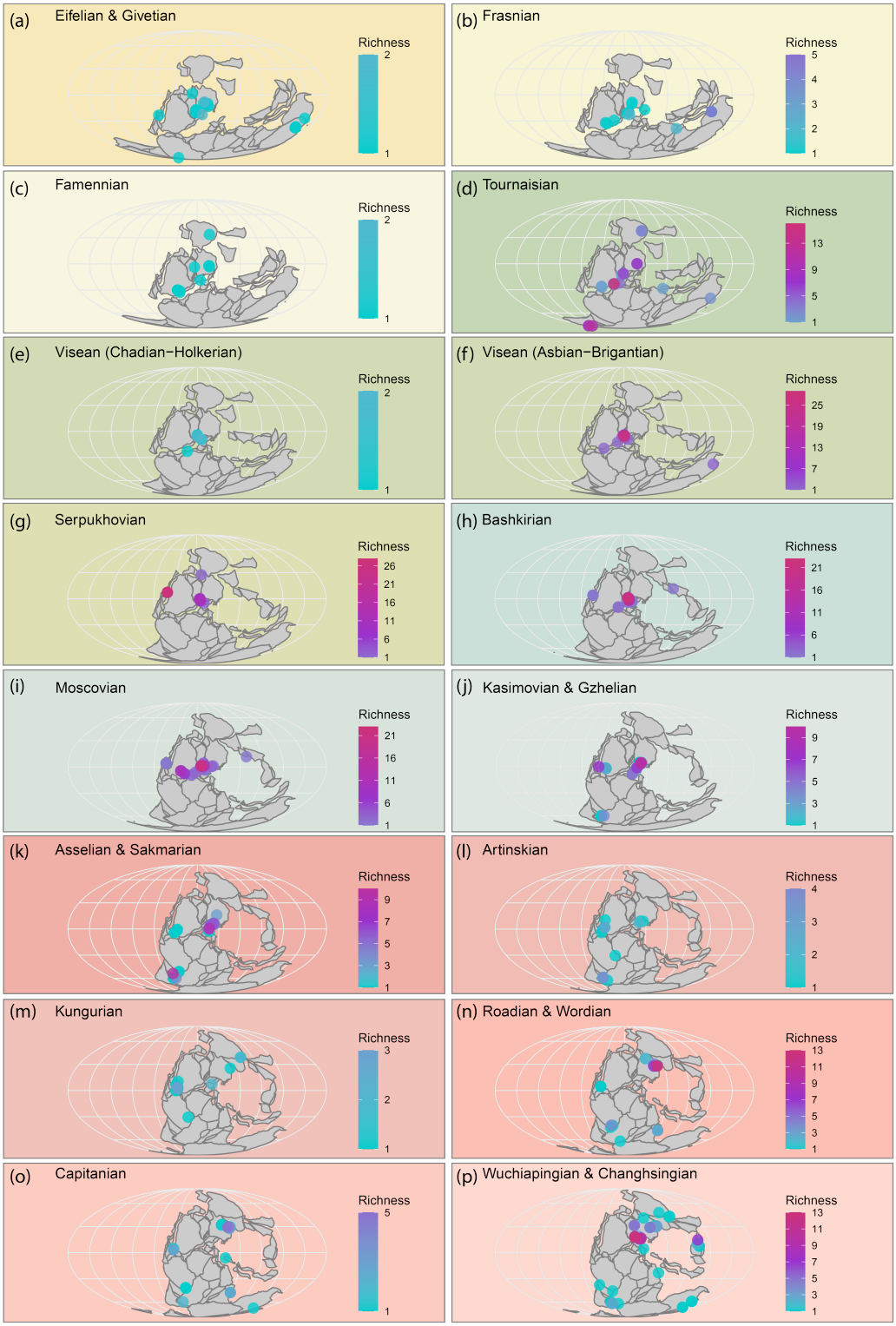


Figure 3.2: Palaeomaps showing palaeogeographic spread and local richness of individual localities through time plotted in roughly even-length intervals. Colour scales correspond to the richness of localities, ranging from low (light blue) to high (pink) richness.

with fewer occurrences from Europe and North America, and a single occurrence from Iran. The USA dominates Famennian occurrences (Fig. 3.2c), with additional

occurrences from Russia, Greenland and Belgium.

3.3.2.2 Carboniferous

In general, Carboniferous localities have both higher local richness and a broader palaeolatitudinal spread than in the Devonian, although are generally still restricted to low and southern palaeolatitudes (Fig. 3.1b). Most Tournaisian localities are clustered at low palaeolatitudes around the southern edge of Euramerica in regions that correspond to present-day Canada, USA, UK, and European Russia, although the Waaipoort Formation in South Africa (-78°) represents the richest high-palaeolatitude locality of the entire Palaeozoic. Localities with lower local richness are found in Australia, Turkey, and Siberia. In contrast, early Visean (Chadian-Holkerian) low-palaeolatitudes are few in number and extremely depauperate (Fig. 3.2e).

For much of the rest of the Carboniferous, local richness greatly increases while palaeolatitudinal spread decreases. Other than single occurrences from Australia and the USA, all late Visean actinopterygians are clustered in the UK and Ireland, including the highly diverse Glencartholm locality (figures 1b and 2f). Similarly, in the Serpukhovian (Fig. 3.2g), only a single occurrence is found outside a 20° palaeolatitudinal band centred around the palaeoequator encompassing UK localities, a single Belgian locality, and the speciose Bear Gulch localities. Geographic spread continues to decline in the Bashkirian (Fig. 3.2h) and Moscovian (Fig. 3.2i), with all but one occurrence within 10° of latitude of the palaeoequator. Again, localities are primarily known in Europe (Belgium, Czechia, France, Ireland, UK) and North America (Canada, USA), with a single Bashkirian taxon known from a low-latitude locality in the eastern Palaeotethys (China). The only latest Carboniferous (Kasimovian and Gzhelian; Fig. 3.2j) locality outside of this band is the -60° Gzhelian Ganigobis Shale,

which outcrops in South Africa and Namibia, albeit with low local richness. Broadly, Carboniferous actinopterygian palaeolatitudinal distribution matched other contemporaneous groups (Powell, 2009; Close *et al.*, 2020b).

3.3.2.3 Permian

Compared to the Carboniferous and Devonian, Permian occurrences generally display a broader geographic spread (reflecting increases in the broader fossil record [Powell, 2009; Close *et al.*, 2020b]) but lower local richness. The extent of palaeogeographic sampling in the Asselian and Sakmarian (Fig. 3.2k) is greater than the Kasimovian and Gzhelian, with more occurrences at higher palaeolatitudes, including the diverse Uruguayan fauna from Rio Negro (-53°). The Artinskian (Fig. 3.2l) is the most depauperate interval of the Permian, despite a comparatively high palaeogeographic spread: the locality with the highest local richness, Loeriesfontein, contains only four genera. Contrary to most other Palaeozoic intervals, there are very few European Artinskian localities.

From the Kungurian (Fig. 3.2m) onwards, localities occur across the broadest palaeolatitudinal spread of the entire Palaeozoic. This includes the first sampling of northern mid-palaeolatitudes since the Tournaisian. Roadian and Wordian localities (Fig. 3.2n) with the highest local richness are found in Russia, centred around 30° palaeolatitude, although less diverse occurrences are seen at high southern palaeolatitudes in Brazil, India, and Zimbabwe. In contrast to most other intervals, only two depauperate localities occur near the palaeoequator. This trend continues into the Capitanian (Fig. 3.2o), where localities yielding few genera are found across a wide range of palaeolatitudes, with very few at equatorial latitudes, and most diversity stems from Russia.

The Wuchiapingian and Changhsingian interval (Fig. 3.2p) has the broadest geographic spread in sampling of the Palaeozoic, possibly due to intensive research focus on the Permo-Triassic mass extinction event (Puttick *et al.*, 2017a; Vázquez & Clapham, 2017). Numerous localities are spread from southern mid- to high-palaeolatitudes, including opposing sides of the palaeopole (present-day South Africa and Australia). Notably, this interval contains the first Permian actinopterygians from the eastern Palaeotethys (present-day China). Northern low- to mid-palaeolatitudes have the highest local richness, stemming from assemblages in the UK and Germany, Russia, and Greenland.

3.3.3 Palaeodiversity estimates

3.3.3.1 Coverage-based rarefaction

Estimates of relative genus richness using coverage-based rarefaction (Fig. 3.3; for species level trends, see Appendix Fig. B.2) suggest an overall decline in diversity through the Carboniferous, with a sharp rise then subsequent fall in the Permian. Richness levels decrease rapidly from a peak in the Tournaisian to the early Visean with a small increase in the late Visean, before rising sharply in the Serpukhovian. The remainder of the Carboniferous is marked by a general decline, with the lowest observed values in the Kasimovian and Gzhelian, another intensely sampled interval. Richness estimates rise slightly across the Carboniferous-Permian boundary, with a drop in the Artinskian followed by a steady rise through the Kungurian to the Roadian

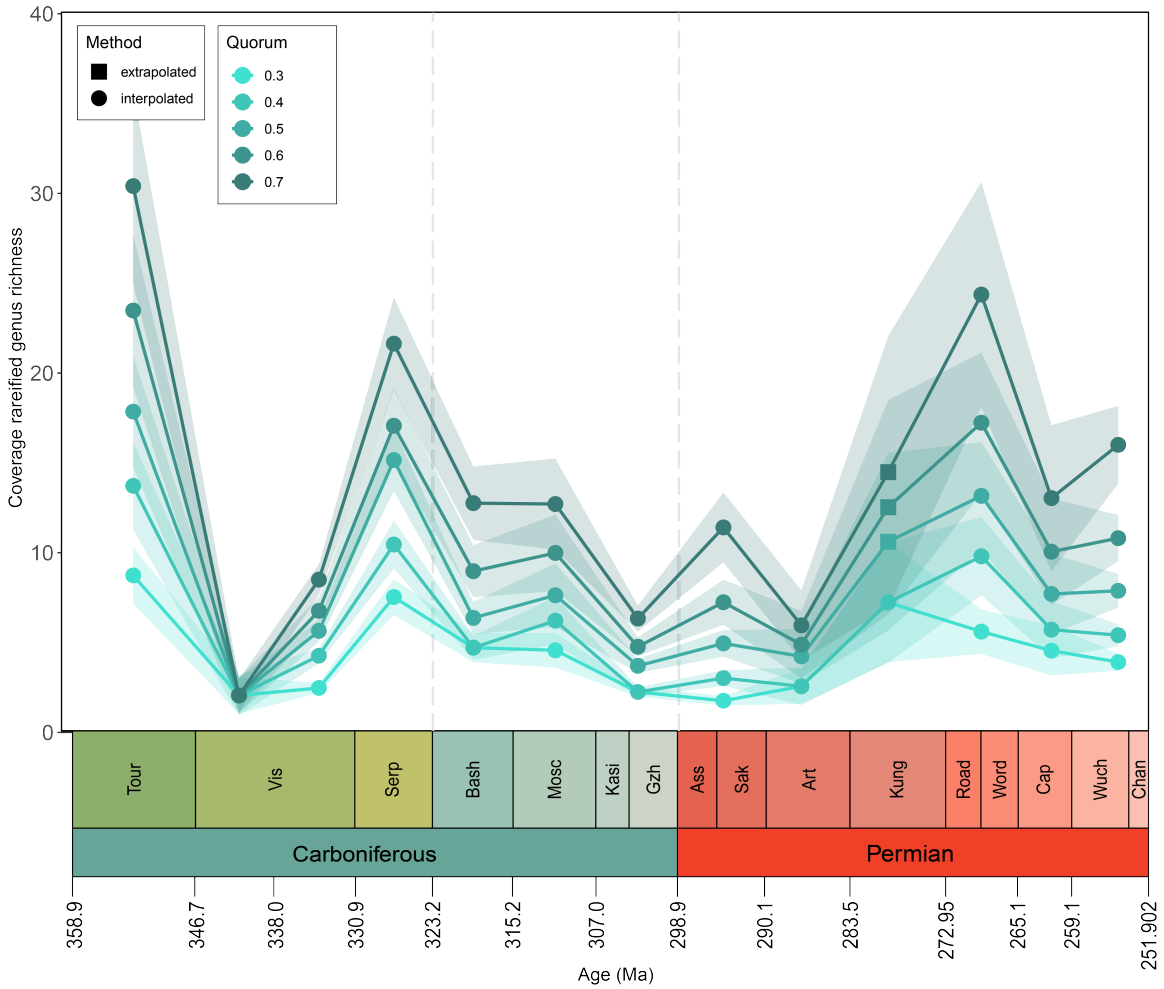


Figure 3.3: Coverage-based rarefaction estimates of Carboniferous and Permian actinopterygian diversity at genus level, showing estimates for different quorum levels in different colours from low quorums (0.3) in light blue to higher quorums (0.7) in darker blue. The shaded areas for each quorum are confidence intervals of estimates. Devonian intervals removed (see Methods). Estimates were either interpolated (circles) or extrapolated (squares) up to twice the reference sample size (Hsieh, Ma & Chao, 2016).

and Wordian. A decline marks the remainder of the Permian at low quorums, though there is a slight increase in the latest Permian at higher quorums.

3.3.3.2 Squares

Squares diversity estimates contrast with coverage-based rarefaction estimates: where coverage-based rarefaction returns low estimates, squares estimates are generally high. Squares-extrapolated genus richness estimates (Fig. 3.4;

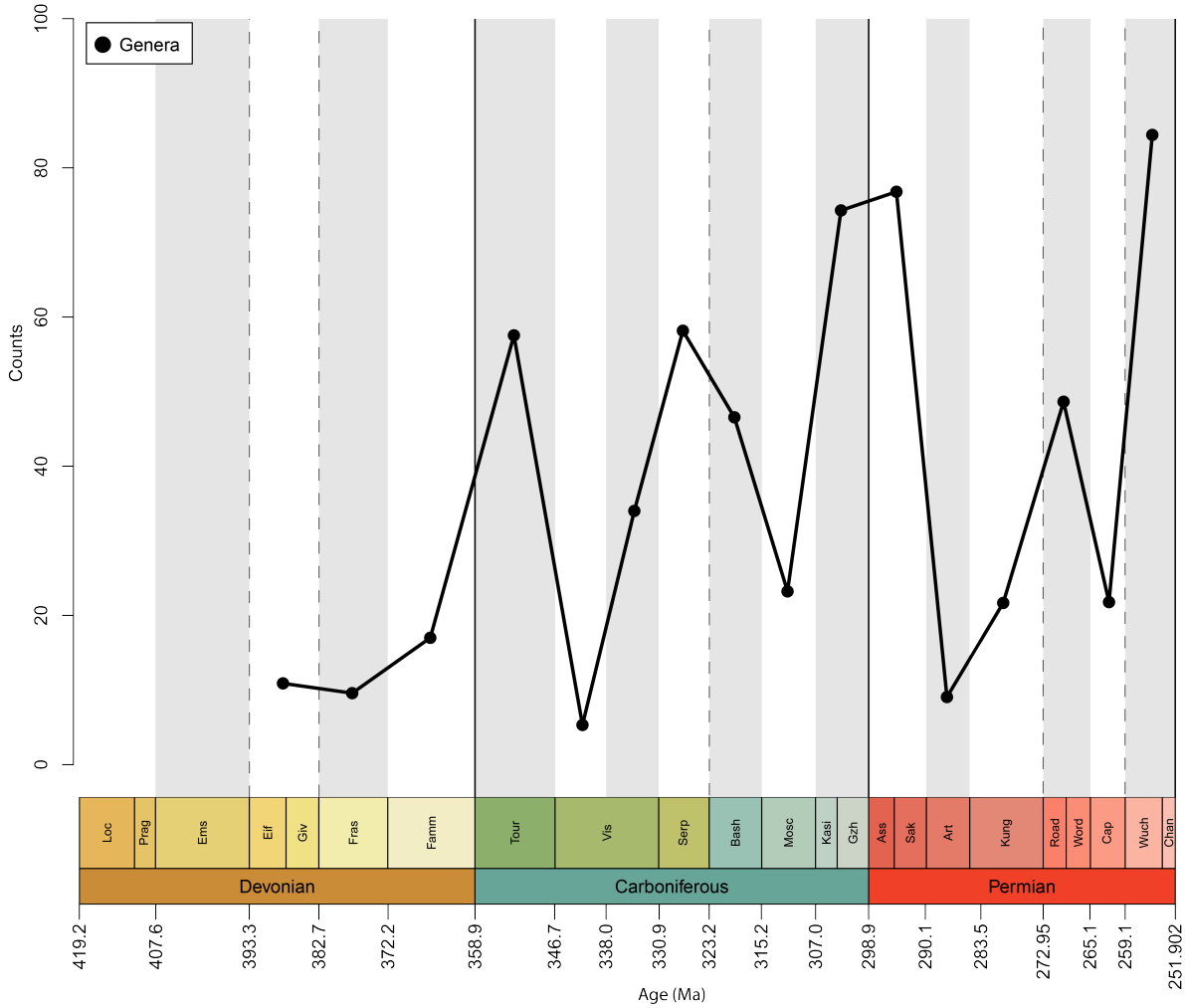


Figure 3.4: Squares diversity estimates of Devonian to Permian genus richness, plotted at the midpoints of equal-length intervals.

for species-level estimates see Appendix Fig. B.2) gradually increase throughout the Devonian and into the Tournaisian. Early Visean estimates drop sharply, before gradually rising in the late Visean to Serpukhovian. A slight decrease into the Bashkirian is followed by a steeper decline in the Moscovian. The highest estimates thus far are seen in the latest Carboniferous with a further increase into the Asselian and Sakmarian, followed by a precipitous drop in the Artinskian. Richness estimates rise in the Kungurian and marginally in the Roadian and Wordian before dropping in the Capitanian. The latest Permian (Wuchiapingian and Changhsingian) is the most diverse interval of the Palaeozoic.

3.3.3.3 Split-and-sum tests

Split-and-sum squares estimates for marine and freshwater subsets generally returned greater estimates than the whole dataset (Appendix Fig. B.3a), though there is no systematic trend related to the dominance of occurrences of a particular palaeoenvironment. Rather, estimates deviate more (i.e. are higher) from the total dataset when occurrences are dominated by either palaeoenvironment. This occurs because the squares equation estimates much higher diversity when there are more rare taxa, and therefore intervals dominated by marine occurrences tend to have much higher extrapolated estimates for freshwater diversity in the split datasets, and vice versa. Regardless, subsetting the dataset by palaeoenvironment leads to extremely poor sample sizes for either palaeoenvironment in most intervals. Average sampling probability in each interval was similar between environmental subsets (marine – 0.55, freshwater – 0.57) indicating no systematic bias in sampling of palaeoenvironments, however there is great variability in the sampling probability through time. Coverage-rarefaction split-and-sum tests resulted in very large deviations (Appendix Fig. B.3b) due to small samples and very low coverage, giving no meaningful information relative to the total dataset analysis.

3.4 Discussion

3.4.1 Biogeographic trends and biases

Palaeozoic actinopterygian occurrences are overwhelmingly geographically biased towards the northern hemisphere: fewer than 9% of known localities (52/586) are from the southern hemisphere (Henderson *et al.*, 2021). Certain regions are notably underrepresented throughout the Palaeozoic, such as the northern, eastern and

southern Palaeotethys (present-day Middle East, south and east Asia, north Africa) and the northern coastline of Laurussia (present-day Siberia, Kazakhstan and interior of Asia). Sampling through much of the Devonian and Carboniferous is limited to a narrow band around the palaeoequator, largely corresponding to present-day Europe and North America (Fig. 3.2), which also contain localities with the highest local richness (Henderson *et al.*, 2021). The most diverse localities trend from low- to mid-palaeolatitudes through the Palaeozoic, essentially tracking the migration of North America and Europe (Fig. 3.1b). Reporting new taxa from underrepresented regions (Figueroa *et al.*, 2021; Newman *et al.*, 2021) will have major implications for palaeogeographical spread, patterns of diversity, and interpretations of ray-finned fish evolution, especially in the face of taxonomic revisions invalidating many existing generic referrals (Coates & Tietjen, 2018; Schindler, 2018).

Ideally, rarefaction curves for sampled intervals should be close to asymptote before performing diversity estimation techniques to ensure that future sampling will not drastically alter face-value counts of richness. Inspection of the Palaeozoic ray-finned fish record suggests this condition has not yet been reached (Appendix Fig. B.4). In the short term, increased sampling of the most undersampled intervals will improve comparability. However, research focus on taxa from well-sampled regions that remain undescribed in museum collections (Allmon *et al.*, 2018; Marshall *et al.*, 2018) is also vital for attaining accurate estimates of actinopterygian diversity in the Palaeozoic, particularly at local scales. For example, indeterminate actinopterygians currently account for over 50% of fish fossils at the Kinney Brick Quarry locality (Williams & Lucas, 2013).

Both marine and freshwater deposits are recorded throughout the Palaeozoic, with the number of sampled marine and freshwater deposits roughly tracking each other through much of the Carboniferous. However, marine palaeoenvironments are scarce in the later Palaeozoic. This long-recognised Permian scarcity (Hurley *et al.*, 2007; McGowan & Smith, 2008; Friedman & Sallan, 2012) also extends back into the late Carboniferous (Fig. 3.1a; Appendix Fig. B.1). The near-complete lack of marine deposits bearing actinopterygians and the prevalence of freshwater deposits is also reflected in PBDB-derived gnathostome occurrences (Appendix Fig. B.5), and likely track the relative absence of marine deposits in western Europe (Smith & McGowan, 2007). Marine global rock volume reduces from the Carboniferous into the Permian, though marine rock volume still outnumbers non-marine (Muscente *et al.*, 2017). Indeed, marine deposits are common outside of Europe (e.g. North America [Peters & Heim, 2010]), and geographic plots of marine gnathostome occurrences from the PBDB (Appendix Fig. B.6) show significant Permian diversity outside of Europe.

Considered together, this may indicate that a regional decrease in the availability of deposits is partially responsible for the apparent reduction in actinopterygian diversity in the early Permian, but that there is a genuine global decline relative to other gnathostomes. However, close inspection of marine gnathostome occurrence records show them to comprise taxa which are far more readily identifiable on the basis of limited material (e.g. sharks [Hodnett *et al.*, 2012]). This suggests that there is a taphonomic bias whereby deposits do preserve vertebrate remains, yet they do not preserve body fossils sufficiently to recover identifiable actinopterygians. The dominance of European occurrences in the actinopterygian dataset suggests that low marine diversity in this period is linked to a sampling bias and regional absence of

these rocks rather than a true biological signal. There is certainly a change in the sampling of terrestrial vertebrates from aquatic to dryland terrestrial environments across the Carboniferous-Permian (Pardo *et al.*, 2019), and a similar change may explain the drop in sampling of Permian actinopterygians. Concurrent with this environmental shift is a noticeable palaeogeographical expansion: rather than being restricted to palaeoequatorial regions, Permian occurrences are reported further from the palaeoequator, reflecting the distribution of exceptional localities in the fossil record (Muscente *et al.*, 2017). It is unclear to what extent this represents a shift in sampling regime rather than an ecological expansion, though it may mirror the reduction in sampling of Euamerican deposits (Pardo *et al.*, 2019).

3.4.2 Palaeozoic actinopterygian diversity patterns

Broadly, it appears that the actinopterygian fossil record is too poor to deduce accurate diversity patterns through most of the Palaeozoic, and we caution against interpreting face-value patterns. Past works have interpreted the actinopterygian record as a general post-extinction recovery curve, with moderate diversification in the early Tournaisian, a peak in the mid-late Visean, and stability in the late Mississippian onwards (Sallan & Coates, 2010; Sallan & Friedman, 2012; Friedman & Sallan, 2012). In contrast, both our analyses recover an initial peak in the Tournaisian, perhaps reflecting high initial diversification as actinopterygians replaced other extinct gnathostomes (Sallan & Coates, 2010; Friedman & Sallan, 2012; Friedman, 2015). The sharp drop into the Visean results from the use of equal-length bins: the early Visean is extremely poorly sampled, and although the late Visean is the most intensely sampled interval of the Carboniferous, diversity estimates remain comparatively low. No prior study has investigated the Pennsylvanian below epoch level, but trends in the

Permian broadly agree with past study (Romano *et al.*, 2016). Heightened sampling may be responsible for the apparent early Permian peak in face-value actinopterygian richness.

Changes in mean local richness largely track changes in 'global' (gamma) raw diversity (Henderson *et al.*, 2021), with the exception of the latest Carboniferous and earliest Permian (Fig. 3.1). In the late Carboniferous and early Permian, high levels of sampling (localities and equal-area grid cells [Henderson *et al.*, 2021]) of isolated localities with low alpha diversity drives high 'global' diversity, with few contributions from diverse assemblages (Fig. 3.1). These richness patterns are drastically different to those reported for Palaeozoic tetrapods (Dunne *et al.*, 2018), and the overall decrease from the Carboniferous to Permian contrasts the biodiversification of invertebrates over the same period (Fan *et al.*, 2020).

In contrast to coverage-rarefied richness estimates, extrapolated estimates from squares analysis return very similar trends to face-value counts of richness (Sallan & Coates, 2010; Romano *et al.*, 2016; Henderson *et al.*, 2021). These differences persist regardless of whether sampling is via equal length intervals or geological stages and are likely due to taxonomic biases (see below). This recalls recent work on Palaeozoic tetrapods, which found that diversity patterns among reptiles and synapsids changed significantly depending on the quorum levels or use of squares (Brocklehurst, 2021). For example, coverage-rarefied actinopterygian richness decreases from the Tournaisian peak to the late Visean in contrast with previous hypotheses (Thomson, 1977; Sallan & Coates, 2010; Henderson *et al.*, 2021), yet both the face-value counts and squares estimates of species increase significantly from the Tournaisian to late Visean. There is consensus however, in the high diversity

of the Serpukhovian (Sallan & Coates, 2010; Henderson *et al.*, 2021), indicating genuine diversity, though the vast majority of this is driven by the diverse Bear Gulch fauna.

Trends into the Pennsylvanian also differ, with the greatest difference in the diametrically opposed estimates for the Kasimovian and Gzhelian, which is attributable to how the methods estimate diversity. The same is also true for the Asselian and Sakmarian and late Permian. Coverage-rarefied richness estimates depend on the attainable level of coverage, and examination of occurrence distributions (Appendix Fig. B.7) and rarefaction curves (Appendix Figs. B.8 and B.9) reveals that at higher coverage, the Kasimovian and Gzhelian would most likely represent one of the most diverse intervals. Squares, however, estimates higher richness when there are many singletons and when common taxa are especially common (Alroy, 2020), and these intervals fulfil both of these criteria. The combined presence of high-frequency taxa and numerous singletons results in these conflicting estimations for some intervals.

Taxonomy also plays a key role. The observed rise in early Permian species-level diversity estimates in both analyses and face value readings (Henderson *et al.*, 2021) reflects the presence of numerous species of few genera (namely *Amblypterus* and *Paramblypterus*). The problem of high-frequency genera is not unique to actinopterygians; such genera are known to bias other osteichthyan groups (Gardner *et al.*, 2019). In contrast, Kungurian estimates are based on very few occurrences of monospecific genera, and sampling of a high number of genera at low quorums results in high—yet unreliable—genus-level coverage-rarefied richness estimates. The extremely high Roadian and Wordian estimates in the analyses can also be explained by high numbers of singletons and relative absence of common genera.

3.4.3 Unevenness in the actinopterygian fossil record

Coverage-based rarefaction techniques produce the most reliable richness estimates when rank occurrence does not differ considerably between samples, even when samples have comparable face-value richness (Alroy, 2010a, 2010b, 2010c, 2020; Chao & Jost, 2012; Mitchell, 2015; Close *et al.*, 2018). Unevenness in occurrence distributions can therefore heavily influence the reliability of diversity estimates. Rank occurrence distribution plots for Palaeozoic actinopterygian genera and species indicate extreme unevenness within intervals and variation in evenness between intervals (Appendix Fig. B.7). Some intervals (e.g. Kasimovian and Gzhelian) contain one or two taxa with more than 60 occurrences, a handful with between 30 and ten occurrences, and a long tail of singletons or doubletons; others (e.g. Tournaisian) have a more even distribution. Differences can even arise between the genus- and species-level occurrence distributions in the same interval: in the Asselian and Sakmarian most species-level diversity stems from multiple species of two genera, resulting in low genus estimates at lower quorums, but higher species-level estimates due to the more even occurrence distributions (compare Appendix Figs. B.3a and B.3b; B.4c and B.4c).

Much of this imbalance is driven by ‘waste-basket’ genera erected by monographic descriptions (Agassiz, 1833-1844; Traquair, 1877b; Moy-Thomas & Dyne, 1938; Gardiner, 1969), despite a wide range of varied morphologies and extensive temporal and geographic ranges within genera (Sallan, 2014; Mickle, 2017; Henderson *et al.*, 2021). Palaeozoic taxa typically lack characters that can be easily attributed from isolated remains, and rely on well-preserved material in order to be confidently identified. Historical practice often relied on generalised characters (for example, as a fusiform actinopterygian) and attribution of specimens to ‘waste-basket’

genera, which masks true diversity. Six Palaeozoic actinopterygian genera (*Acrolepis*, *Amblypterus*, *Elonichthys*, *Palaeoniscum*, *Platysomus*, and *Rhadinichthys*) exhibit key characteristics of 'waste-baskets' (Plotnick & Wagner, 2006; Henderson *et al.*, 2021). They comprise significant proportions of occurrences (averaging more than 30% of occurrences in post-Devonian intervals: S10), and occur in contemporaneous freshwater and marine deposits (Appendix Fig. B.1), providing further indication that they represent multiple taxa. These 'waste-baskets' have the highest mean rank in occurrence distributions (Appendix Fig. B.11) and serve to concentrate frequency counts of the most common genera, contributing to unevenness in the occurrence distribution and distortion of coverage-based rarefaction estimates (Alroy, 2010c; Close *et al.*, 2018). The intervals most heavily biased towards frequent taxa (which also tend to contain 'waste-basket' taxa; Appendix Fig. B.11) are the late Visean (*Elonichthys*: 54/266 occurrences; *Rhadinichthys*: 54/266 occurrences), Kasimovian and Gzhelian (*Elonichthys*: 65/230; *Sphaerolepis*: 60/230), Asselian and Sakmarian (*Paramblypterus*: 53/154 occurrences; *Amblypterus*: 30/154 occurrences), and Wuchiapingian and Changhsingian (*Palaeoniscum*: 66/225 occurrences; *Platysomus*: 26/225 occurrences). Compounding the issue caused by high-frequency is the fact that these intervals tend to also have very long-tailed occurrence distributions, with many doubletons or singletons (Appendix Fig. B.7). One explanation for these long-tails is the fact that the literature is biased towards descriptions of new taxa rather than occurrences of already-known taxa (Alroy, 2010b), resulting in an increase of doubletons and singletons. Given that the rate at which new Palaeozoic actinopterygians are being described continues to rise (Henderson *et al.*, 2021), it is

unlikely that this trend will change (also meaning that rarefaction curves will not asymptote soon, causing problems for diversity estimation; Appendix Fig. B.4).

In the late Carboniferous and early Permian, however, high frequency of taxa results from a combination of 'waste-basket' occurrences, intensive sampling, and potentially palaeoenvironment, with many separate freshwater localities from Central European deposits yielding thousands of specimens of common genera (e.g. *Elonichthys*, *Sphaerolepis* and *Paramblypterus* [Štamberg & Zajíc, 2008; Zajíc, 2014]). Diversity in these intervals is principally derived from fluvio-lacustrine deposits designated as Lagerstätten (Romano *et al.*, 2016). As fossil fish tend to be better preserved in freshwater environments than marine (Schnetz *et al.*, 2022), this may translate to easier identification of taxa in freshwater environments, potentially biasing richness measures. While there is no relationship between palaeoenvironment and rank occurrence in the Palaeozoic overall (Appendix Fig. B.1), the intervals with the highest counts of occurrences of individual taxa are those that heavily sample freshwater deposits. Whether this phenomenon principally derives from a taphonomic bias or intensive research effort (Štamberg, 1991, 2007, 2016a; Štamberg & Zajíc, 2008; Zajíc, 2014) is difficult to ascertain. As coverage-based rarefaction produces lower estimates when evenness is low (Close *et al.*, 2018), these highly uneven intervals have low richness estimates at lower quorum levels (Fig. 3.3; Appendix Figs. B.3, B.4 and B.5). In contrast, at high quorums, where more taxa in the occurrence distribution can be sampled, uneven intervals receive much higher richness estimates (see exponential rise in the rarefaction curves of uneven intervals at high coverage; Appendix Figs. B.4 and B.5). These large changes at higher quorums in uneven intervals, potentially as a result of preservation bias and research effort, point towards

a significant impact of taphonomic filters and anthropogenic bias on diversity estimation. Localised investigations of specimen-level occurrences, sampling and rock records, alongside comparison between analogous regions, are necessary to tease apart the variable impact of these biases. In particular, investigating turnover and nestedness (components of beta diversity) will allow for the teasing apart of the impact that uneven sampling can have on evenness from biases caused by taxonomy.

'Waste-basket' taxa may also mask true diversity: the dominance of highly frequent taxa means that a high proportion of sampled taxa consists of these few taxa, likely contributing to lower diversity estimates. Revisionary taxonomic work, such as recognising new genera among previously congeneric actinopterygians (Coates & Tietjen, 2018), and restriction of *Elonichthys* to just three species (Schindler, 2018) rather than its previous 37, will alleviate this issue and mitigate the dominance of highly-frequent forms. These revisions, however, have the potential to increase unevenness in the other direction, as new taxa may end up as singletons or doubletons. Concurrently, oversplitting of taxa, a prevalent issue when taxa are biostratigraphically important (such as in the marine invertebrate fossil record [Close *et al.*, 2018]), may be a potential problem where actinopterygians are significant biostratigraphic markers (Tverdokhlebov *et al.*, 2005; Minikh & Minikh, 2009; Nurgaliev *et al.*, 2015).

Major variation in evenness between intervals is highlighted in the different trajectories of coverage-based rarefaction curves (Appendix Figs. B.8 and B.9). Taxonomic and geographic biases are exacerbated by small sample sizes and low coverage, with rarefaction curves crossing multiple times. Higher (more reliable) quorum levels are unobtainable for Palaeozoic actinopterygians due to the high

number of singleton taxa (Appendix Fig. B.7) controlling Good's *u* (Good, 1953). As a result, coverage is generally low (Appendix Figs. B.7 and B.8) and only low quorums—at which evenness signals are more pronounced (Alroy, 2020)—can be used. When evenness varies at low levels of sampling, size-based rarefaction can in fact be less biased than coverage-based rarefaction, especially at low levels of coverage (Close *et al.*, 2018). Trends between coverage- and size-based rarefaction estimates generally agree (Appendix Fig. B.12), although size-based rarefaction estimates higher diversity in some highly uneven intervals (e.g. late Visean; Wuchiapingian and Changhsingian). Small sample sizes (<200 occurrences) also have an effect on the accuracy of coverage estimates using Good's *u* (Close *et al.*, 2018): only four of the sampled Palaeozoic intervals have more than 200 occurrences (late Visean: 266; Serpukhovian: 204; Kasimovian and Gzhelian: 230; Wuchiapingian and Changhsingian: 232). Coverage-based rarefaction curves (Appendix Figs. B.4 and B.5) show these intervals to have among the highest coverage, along with the Bashkirian and Moscovian, highlighting the greater sampling of the Carboniferous than the Permian. Consequently, variation in evenness between intervals is having an overriding effect on sampling-standardised diversity estimates through time, with diversity estimates mostly tracking evenness and reflecting biases in the underlying data (Hannisdal *et al.*, 2017; Close *et al.*, 2018).

3.5 Conclusion and future directions

We present here the first local richness and palaeogeographic trends in Palaeozoic ray-finned fishes. Sampling of the Palaeozoic actinopterygian fossil record is heavily biased towards western Europe (especially the UK) and North America, which translates to a very restricted palaeogeographic spread for most of the Palaeozoic. A

suite of compounding problems plagues the actinopterygian fossil record and results in bias towards occurrences of both highly-frequent and singleton taxa, variation and unevenness in and between sampled intervals, and distortion of relative richness estimates. This confounds attempts to accurately estimate relative richness between intervals. Meanwhile, sampling is poor for regions other than Europe and North America for all but a few Carboniferous and Permian intervals. The result of this poor sampling is the inability to reach the high levels of coverage that allow statistical methods of sampling standardisation to generate meaningful diversity estimates.

Identifying the underlying issues with Palaeozoic actinopterygian data and the interweaving biases that are impacting the fossil record is crucial, and improving sample sizes and coverage will help to mitigate the sensitivity to evenness (Chao & Jost, 2012). Documenting and including existing 'dark data' (Allmon *et al.*, 2018; Marshall *et al.*, 2018) in museum collections, as well as focus on new material from under sampled regions, represent key first steps. As a result, size-based rarefaction curves for Palaeozoic intervals will likely not reach asymptote soon (Appendix Fig. B.4). More complete sampling of well-known regions (Lloyd & Friedman, 2013) may facilitate deduction of accurate local richness patterns (Close *et al.*, 2019). This strategy also goes some way towards accounting for the significant spatial structuring of 'global' fossil records (Benson *et al.*, 2016; Close *et al.*, 2017, 2020a, 2020b). Spatial standardisation, perhaps by restricting analyses to well-sampled localised regions spanning shorter intervals for which specimen- and outcrop-level data is available, represents a key avenue for research. Additionally, examining hierarchical patterns of diversity and patterns of beta diversity (Benson *et al.*, 2021) will allow for detailed investigation of the interwoven effects of uneven sampling, taxonomic bias and

taphonomy. Key candidate regions for such analyses include the late Visean-Moscovian of the UK and the latest Carboniferous-early Permian of Central Europe.

Other recently proposed methods, such as extrapolation of coverage-rarefied samples (Close *et al.*, 2018; Alroy, 2020) represent prospective avenues of research, both at local and global scales. However, existing global occurrence data for Palaeozoic actinopterygians is as yet inadequate for such combinations of extrapolation and rarefaction: sample sizes vary widely between intervals, which may result in inaccurate extrapolated richness trends (Colwell *et al.*, 1994; Chao *et al.*, 2009; Close *et al.*, 2018); sample sizes in all intervals are too low for size-based rarefaction curves to asymptote (Appendix Fig. B.4), meaning sample size has an overwhelming effect on diversity estimates (Close *et al.*, 2018); and occurrence distributions are also highly uneven, which biases extrapolators (though to a lesser extent than coverage-based rarefaction; Close *et al*. 2020a).

Overall, the occurrence data recorded in the literature is heavily impacted by sampling and likely results in inaccurate estimated and reported diversity trends at present. Differentiation of the freshwater and marine fossil records and localised diversity estimates for well-sampled regions present feasible avenues of research for reconstructing regional diversity. In addition, research efforts to fix problematic taxonomy of ‘waste-basket’ taxa, in hand with a general increase in sampling, open the possibility of estimating diversity in a spatially-standardised framework, so that we can truly begin to understand the origin, rise and establishment of the largest vertebrate clade.

4 A reinvestigation of the cranial anatomy and taxonomy of *Phanerosteon* (=*Carboveles*) *ovensi*, from the Lower Carboniferous (Tournasian) of Scotland, using computed tomography

My contribution to this chapter involved segmenting CT data, visiting specimens in museums, preparing the figures, interpreting the results, and writing the manuscript. S. Giles CT scanned the specimen and provided feedback on the interpretation of results and drafts of the manuscript. This chapter is in the process of being turned into a manuscript for publication. The editorial 'we' is used throughout the text to reflect these contributions.

4.1 Introduction

Following the End-Devonian Mass Extinction (EDME), global aquatic faunas underwent a major restructuring, with actinopterygians and chondrichthyans replacing 'placoderms' and sarcopterygians to become the dominant vertebrate groups. In addition to an increase in taxonomic diversity (Henderson *et al.*, 2023), new morphologies proliferate in the Carboniferous: the emergence of deep-bodied forms (Sallan & Coates, 2013) and diverse dentitions (Friedman *et al.*, 2018) showcase a

considerable rise in morphological diversity as actinopterygians occupied new niches recently vacated by other extinct vertebrates (Friedman & Sallan, 2012).

However, whether this diversification reflects classic examples of ecological release, as hypothesised for the diversification of birds (Ksepka *et al.*, 2017; Houde *et al.*, 2020) and mammals (Halliday *et al.*, 2016; Grossnickle *et al.*, 2019; Brocklehurst *et al.*, 2021) following the Cretaceous-Paleogene mass extinction, remains uncertain. Other critical aspects of early actinopterygian evolution during this period, such as the number of lineages crossing the Devonian-Carboniferous boundary and their recovery in the Tournaisian, are also far from clear. Until recently, most phylogenetic hypotheses suggested the survival of as little as one lineage through the EDME (Gardiner & Schaeffer, 1989; Coates, 1999; Giles *et al.*, 2017), with both taxonomic and morphological diversification taking place after the extinction event, mirroring similar trends in the chondrichthyan and sarcopterygian records (Sallan & Coates, 2010; Smithson *et al.*, 2012; Smithson *et al.*, 2016; Friedman & Sallan, 2012; Anderson *et al.*, 2015). A contrasting viewpoint suggests that an order of magnitude more lineages crossed the Devonian-Carboniferous boundary, seeding morphological diversification in the early Carboniferous (Cloutier & Arratia, 2004; Giles *et al.*, 2023).

Understanding the structure of actinopterygian diversity in the early Carboniferous is vital to teasing apart these patterns. Despite the importance of this interval, many classic Tournaisian actinopterygians have received little attention in the literature since the late 19th and early 20th centuries (Agassiz, 1833-1844; Traquair, 1881; White, 1927; Moy-Thomas, 1938), and grasp of both their anatomy and taxonomy remains rudimentary. New data can aid phylogenetic analyses seeking to clarify the relationships between Palaeozoic taxa and extant clades. While recent

efforts have greatly expanded the sampling of early actinopterygians (Choo, 2015; Giles *et al.*, 2015b, 2021; Mickle, 2017, 2018; Figueroa *et al.*, 2021; Newman *et al.*, 2021) the morphology of the overwhelming majority of Tournaisian taxa remains unclear. Revisiting long-known taxa is therefore necessary to generate robust hypotheses regarding morphological evolution across the Devonian-Carboniferous boundary, in turn allowing examination of timings of diversification, extinction selectivity and recovery, and ecological release.

Phanerosteon ovensi was originally erected and described as *Carboveles ovensi* by White (1927) from specimens collected at the Tournaisian locality of Foulden in Berwickshire, Scotland (Fig. 4.1a-c). These specimens were part of the collection of an “enthusiastic young local geologist” (White, 1927, p. 255), Thomas Middlemass Ovens, and following his unfortunate death at 19 years of age were donated to the Natural History Museum (then the British Museum of Natural History) by his parents. Although noting similarities with the later Viséan taxon *Phanerosteon mirabile* (Fig. 4.1f, 1g; Traquair, 1881) from Glencartholm, White (1927) justified the erection of a new genus on the basis of differences in squamation and the shape of the caudal fin. New material consisting of six specimens was reported by Moy-Thomas (1938), who produced cranial reconstructions based on these specimens (Fig. 4.1d) though without describing, figuring or providing specimen numbers for the material. *Carboveles* and *Phanerosteon* were subsequently united in the family Carbovelidae by Romer (1945b) in his compendium on vertebrate palaeontology.

Gardiner (1985) later used new material, also from Foulden, to revise White’s (1927) original account, noting the similarity of the tail, the number of lepidotrichia, and the absence of scales across much of the body (Fig. 4.1e). Gardiner (1985) concluded

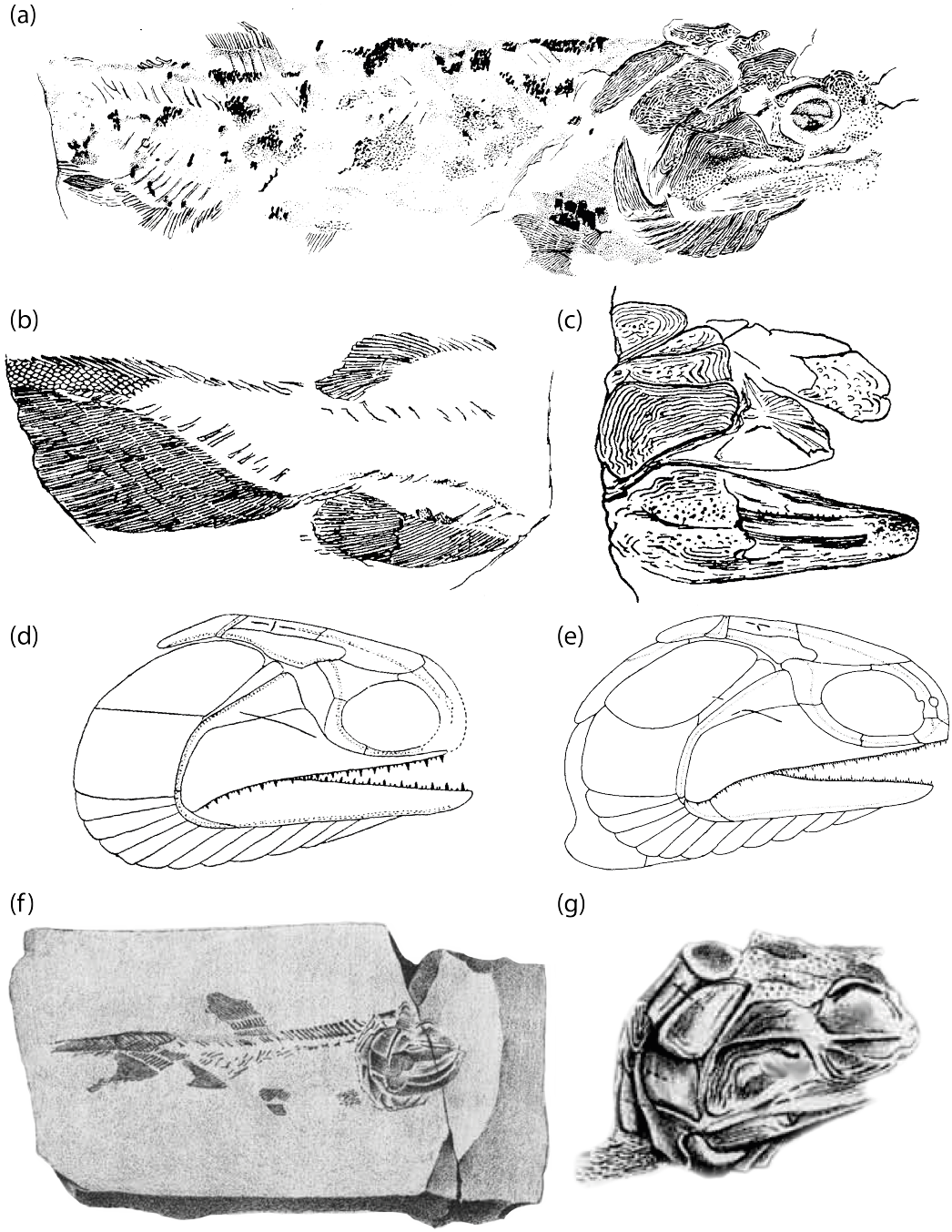


Figure 4.1: Specimens of *Phanerosteon ovensi* (a-e) and *Phanerosteon mirabile* (f & g) from the literature. (a) NHMUK P.13120 - *Phanerosteon ovensi* (holotype; White, 1927: fig. 14); (b) NHMUK P.13121 - *Phanerosteon ovensi* (White, 1927: fig. 16); (c) NHMUK P.13184 (White, 1927: fig. 15); (d) reconstruction of *Phanerosteon ovensi*, modified from Moy-Thomas (1938); (e) reconstruction of *Phanerosteon ovensi*, modified from Gardiner (1985); (f) drawing of *Phanerosteon mirabile* modified from Traquair (1912: pl. 37, fig. 5); (g) drawing of *Phanerosteon mirabile* modified from Traquair (1912: pl. 37, fig. 6).

that differences between *Carboveles ovensi* and *Phanerosteon mirabile* (Fig. 4.1f, 1g) were not significant enough to warrant separation into two genera, and synonymised

Carboveles with *Phanerosteon*. The axial skeleton was also described in detail by Sallan (2012) in a study examining axial regionalisation in early actinopterygians, which also described numerous other anatomical features shared between *Phanerosteon* and the contemporary genus *Tarrasius* as evidence for a potential relationship between the two genera. Most recently, a study investigating the various radiations of deep-bodied actinopterygians in the early Carboniferous referred to the anatomy of *Phanerosteon*, noting similarities with the contemporaneous taxa *Aetheretmon*, *Fouldenia* and *Styracopterus* (Sallan & Coates, 2013).

Here, we use µCT scanning and traditional descriptive techniques to investigate specimens referred to *Phanerosteon ovensi* and *Carboveles ovensi*. Redescription of *Phanerosteon ovensi* will also contribute critical morphological data allowing for future inclusion in phylogenetic analyses, which represents another step towards better understanding the evolution of Actinopterygii in the critical Tournaisian interval following the EDME.

4.2 Materials and Methods

4.2.1 Specimens

One specimen of *Phanerosteon ovensi* (Natural History Museum, London [NHMUK] PV P.13184) was identified for CT scanning. The specimen was figured by White (1927: fig. 15) and shows the right side of the cranium in lateral view; it has previously undergone mechanical preparation.

4.2.2 Geological context

The holotype (NHMUK P.13120) and most specimens (see below) of *Phanerosteon ovensi* are from Crooked Burn, Foulden, in Berwickshire, Scotland. Other specimens are known from Willie's Hole (UMZC 2011.7.11; NMS 2012.39.15). Deposits from Crooked Burn and Willie's Hole are part of the Calciferous Sandstone Series, Cementstone Group, now assigned to the Ballagan Formation (Greig, 1988), of the Dinantian regional stage, late Tournaisian. Smithson *et al.* (2012) note the Ballagan Formation at Willie's Hole (Chirnside) to be part of the CM (*Schopfites claviger-Auroraspor macra*) miospore biozone (Waters *et al.*, 2011a), from 348-347.6 Ma (Gradstein *et al.*, 2020). These localities are thought to represent euryhaline (brackish alluvial, lacustrine or lagoonal) environments (Waters *et al.*, 2011a).

Specimens of *Phanerosteon mirabile* come from Glencartholm, Eskdale, and Mumbie Quarry in Dumfriesshire, Scotland. Specimens of *Phanerosteon mirabile* occur in beds within the Glencartholm Volcanic Member of the Tyne Limestone Formation (Yoredale Group), which is mid-Visean in age (Stone *et al.*, 2012; Wood, 2017). The Glencartholm Volcanic Member is within the B1 ammonoid zone and the TC miospore zone (Neves *et al.*, 1973; Waters *et al.*, 2011b), corresponding with roughly 337.4 – 335.2 Ma (Gradstein *et al.*, 2020). The Glencartholm fish fauna contains more than 30 vertebrate taxa which are associated with marine invertebrates, thus likely representing a shallow marine environment (Schram, 1983; Wood, 2017). *Phanerosteon mirabile* accounts for around 1% of all fossil specimens from the locality, and 4% of actinopterygians (Schram, 1983).

4.2.3 CT scanning

CT scanning was carried out at the Department of Life Sciences, University of Bristol, using a Nikon XT H 225 ST with the scanning parameters: 210 kV, 68 uA, 12.16 um, with a 708 ms exposure, 2 frames per projection, and a 1 mm CU filter. The CT data were then segmented in MIMICS® Research v19.0 (biomedical.materialise.com/mimics, Materialise NV, Leuven, Belgium), to generate three-dimensional images of the specimen including previously unobserved elements within the matrix. 3D objects were then exported from MIMICS and processed in Blender 2.79 (blender.org) to create the final images. Interpretive drawings were made from these digital renders in Adobe Illustrator 2020.

4.2.4 Institutional abbreviations

GLAHM – Hunterian Museum, University of Glasgow, Glasgow; NHMUK – Natural History Museum, London; NMS – National Museum of Scotland, Edinburgh; UMZC – University Museum of Zoology, Cambridge.

4.2.5 Comparative material

Additional specimens of both *Phanerosteon/Carboveles ovensi* were also examined: for comparison NHMUK PV P.14553, P.14555, P.14559, P.16001, P. 16002, P. 61540a, b; NMS G.1980.40.20-25, 1984.67.56-60, 2012.39.15; GLAHM V8323-6; UMZC 2011.7.11) and *Phanerosteon mirabile* (NHMUK P.5984a, P.20205, P.20206, P.20208, P.20235, P.20236, P.20237, P.20296, P.22966; NMS 1891.53.13-16, 1970.26.27. However, the holotypes and key specimens are currently on loan, and although due to be returned in 2020, the ongoing impact of COVID-19 means that this

has not yet happened. Although we have attempted to obtain photographs of these specimens to examine in the meantime, this has not been successful.

4.2.6 Anatomical abbreviations

acc.vom – accessory vomer; an – angular; asc – ascending process of parasphenoid; bhc – buccohypophysial foramen; bpf – basipterygoid fenestra; bpt – basipterygoid process; clav – clavicle; cle – cleithrum; cor – coronoid; dent – dentary; dpal – dermopalatine; dpt – dermopterotic; dsph – dermosphenotic; ecpt – ectopterygoid; enpt – entopterygoid; fr – frontal; fr.ov – overlap for frontal; g.ic – groove for internal carotid; gul – gular; inc – infraorbital sensory canal; jug – jugal; la – lacrimal; mx – maxilla; mx.ram – suborbital ramus of maxilla; mnc – mandibular sensory canal; na – nasal; pa – parietal; par – prearticular; parc – parabasal canal; pin – pineal foramen; pmx – premaxilla; pop – preopercular; psph – parasphenoid; r.br – branchiostegal ray; spig – spiracular groove; suc – supraorbital sensory canal; te.in – inner tooth row, te.ou – outer tooth row; vom – vomer.

4.2.7 Anatomical terminology

We use conventional actinopterygian terminology for the description of the cranial bones whereby actinopterygian frontals and parietals are, respectively, homologous with sarcopterygian parietals and postparietals, following Gardiner (1984) and Gardiner & Schaeffer (1989).

4.3 Systematic palaeontology

Osteichthyes Huxley 1880

Actinopterygii Cope 1887

Genus *Phanerosteon* Traquair 1881

Species *Phanerosteon ovensi* (White 1927)

1927 *Carboveles ovensi* White, Trans. Roy. Soc. of Ed., p. 264, figs. 14-17.

1938 *Carboveles ovensi* Moy-Thomas, Geol. Mag., p. 315, fig. 7.

1985 *Phanerosteon ovensi* Gardiner, Trans. Roy. Soc. of Ed., p. 61, fig. 1a.

2012 *Phanerosteon ovensi* Sallan, Proc. Roy. Soc. B, ESM p. 8.

2012 *Phanerosteon ovensi* Smithson *et al*., Proc. Nat. Aca. Sci., fig. 3.

2013 *Phanerosteon ovensi* Sallan & Coates, Zoo. Jou. Lin. Soc., p. 162, 180, 192, fig. 18.

Etymology. Specific epithet in honour of Thomas Ovens.

Emended Diagnosis. Actinopterygian characterised by the following combination of characters: scales absent, with the exception of tube-like scales along the lateral line, some scales behind the pectoral girdle and on the axial portion of the tail; dorsal and anal fins long-based and placed posteriorly; tail lacking a distinct peduncle, and caudal fin is unforked and unevenly rounded; triangular dermosphenotic; crescent-shaped jugal containing multiple rami of the infraorbital canal; very thin lacrimal encasing the infraorbital canal; mandibular canal arches dorsally in the anterior half of the dentary; palate extensively covered with conical teeth; separate dermal palatal ossifications; blade-like accessory vomers; ornamentation on dermal skull bones primarily comprised of stout ridges; large dorsal ridges scales anterior to the caudal fin.

Holotype. NHMUK P.13120.

Other material. NHMUK P.14553, P.14555, P.14559, P.16001, P. 16002, P. 61540a, b; NMS G.1980.40.20-25, 1984.67.56-60, 2012.39.15; GLAHM V8323-6; UMZC 2011.7.11.

Locality and horizon. Crooked Burn (Foulden) and Chirnside, Berwickshire, Scotland. Calciferous Sandstone Series, Cementstone Group, Ballagan Formation, Dinantian regional stage, late Tournaisian. *Schopfites claviger-Auroraspor macra* miospore biozone, 348-347.6 Ma.

Synonyms. *Carboveles ovensi* White 1927.

Remarks. It was our intention to conduct a full taxonomic assessment of the genus *Phanerosteon* to determine whether White's (1927) original erection of *Carboveles ovensi* might be accurate, and reverse Gardiner's (1985) synonymisation of *Carboveles* and *Phanerosteon*. However, the holotypes and key specimens preserving the clearest morphological information of both *Phanerosteon ovensi* and *P. mirabile* are on loan. Specimens were due to be returned to the NHM and NMS in 2020, yet as a knock-on impact of the COVID-19 pandemic will not be returned until July 2023. We contacted the loanee to enquire about examining photographs of the specimens in the meantime but received no response. This has prevented a full taxonomic assessment and so we maintain the latest taxonomic act here (Gardiner, 1985).

Osteichthyes Huxley 1880

Actinopterygii Cope 1887

Genus *Phanerosteon* Traquair 1881

Species *Phanerosteon mirabile* Traquair 1881

Etymology. Traqauir (1881) did not provide etymological details, however *mirabile* is Latin for ‘wonderful’ or ‘miraculous’. *Phanerosteon* likely derives from the Greek, *phaneros*, meaning ‘visible’ or ‘evident’ and *osteon* meaning ‘bone’, in reference to the exposed axial skeleton.

Emended Diagnosis. Actinopterygian characterised by the following combination of characters: scales absent on majority of body, except for on the caudal fin, behind the pectoral fin and along the lateral line; tail heterocercal, with forked caudal fin that has a long axial lobe, and a distinct peduncle; absence of fringing fulcra; dorsal and ventral ridge scales present anterior to the caudal fin, and dorsal ridge scales anterior to the dorsal fin; dorsal fin anterior to the anal fin; absence of fringing fulcra; ornament largely pustular, with some ridges; subopercular with anteroventral process; tall neural spines, flaring slightly distally; long haemal spines supporting caudal fin rays; elongate axonosts and baseosts of dorsal fin.

Holotype. Traquair (1881) did not specify a type specimen, though Woodward 1891 defines the type as an “Imperfectly preserved fish” from the Geological Survey of Scotland. It is likely that the type specimen is NMS 1885.54.24 based on the descriptions.

Other material. NHMUK PV P.4703, P.5984, P.5984a, P.75249-75251; GSE 5697 (syntype), 4706, 4707; NMS 1891.53.13-16, 1970.26.27.

Locality and horizon. Glencartholm, Eskdale, and Mumbie Quarry, Dumfriesshire, Scotland. Glencartholm Volcanic Member, Tyne Limestone Formation (Yoredale Group), mid-Visean, B1 ammonoid zone, TC miospore zone, ~337.4 – 335.2 Ma.

Synonyms. None.

4.4 Description

The left side of specimen NHMUK P.13120 (preserved within the matrix) has sheared and been pushed dorsally relative to the right hand side, such that the toothed, medial face of the left prearticular directly faces the toothed, medial face of the right entopterygoid, and the left entopterygoid is opposite the right accessory vomer.

4.4.1 Skull roof

Very little new information on the skull roof of *Phanerosteon ovensi* can be gleaned from the CT scan data. The only elements present are a nasal and frontal, and possible fragments of a dermopterotic and a parietal (Figs. 4.2 and 4.3, na, fr, dpt?, pa). Anteriorly, the left nasal and frontal are displaced, such that their ventral face contacts the left lateral side of the specimen. As a result of this, the left nasal and frontal sit roughly parallel to one another. The nasal is covered with interrupted, vermiform ridges and carries a portion of the supraorbital sensory canal (Fig. 4.2, suc). The posterior margin of the nasal has an embayment that may be for the posterior nostril. Alternatively, two excavations on the ventral edge straddling the supraorbital sensory canal may be for the anterior and posterior nostrils, though this identification is uncertain. The frontal is also ornamented with interrupted, vermiform ridges and carries part of the supraorbital sensory canal (Figs. 4.2 and 4.3, suc). An excavation on the medial edge of the frontal may represent the pineal foramen (Fig. 4.2, pin?), though damage renders this determination difficult. Posterior to the frontal lies a small fragment of a dermal skull bone that is hard to identify, but is most likely a fragment of dermopterotic or parietal (Figs. 4.2 and 4.3, dpt?, pa?). A dermal bone medial to the orbit and dermosphenotic may represent a displaced left dermopterotic, although it is

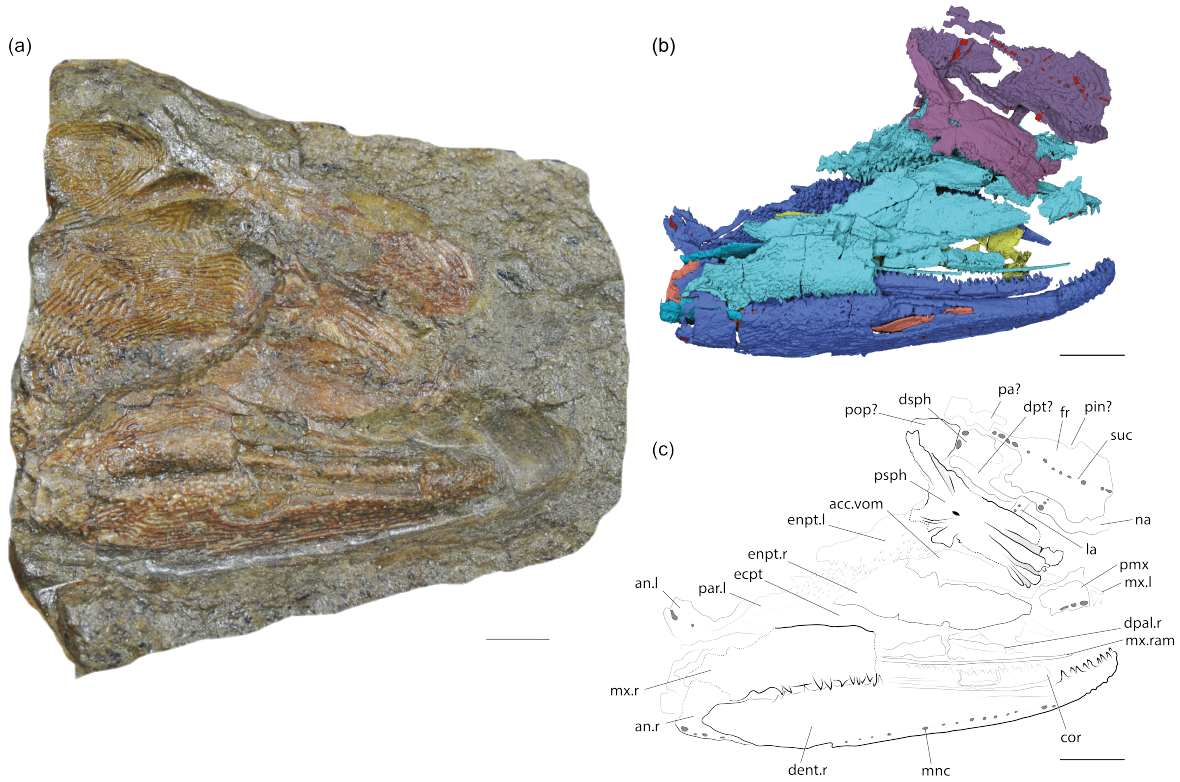


Figure 4.2: Lateral view of specimen and 3D render. (a) NHMUK PV P.13184. Skull of *Phanerosteon ovensi* NHMUK PV P.13184 in right lateral view. (b) three-dimensional render of the skull roof bones and infraorbitals (purple), parasphenoid (mauve), upper jaws (turquoise), lower jaws (dark blue), shoulder girdle (light blue), operculogular elements (red), gill skeleton (yellow) and sensory canals (maroon). (c) interpretive drawing of (b) with dashed lines indicating uncertain margins, dotted lines the internal course of sensory canals and grey fill the opening of sensory canals to the dermal surface. Abbreviations: acc.vomer, accessory vomer; an.l, left angular; an.r, right angular; cor, coronoid; dent.r, right dentary; dpal.r, right dermopalatine; dsph, dermosphenotic; ecpt, ectopterygoid; enpt.l, left entopterygoid; enpt.r, right entopterygoid; fr, frontal; inc, infraorbital sensory canal; it?, intertermporal; jug, jugal; la, lacrimal; mnc, mandibular sensory canal; mx.l, left maxilla; mx.r, right maxilla; mx.ram, suborbital ramus of maxilla; na, nasal; pa?, parietal; par.l, left prearticular; par.r, right prearticular; pmx, premaxilla; pop?, preopercular; psph, parasphenoid; r.br, branchiostegal ray; suc, supraorbital sensory canal. Scale bars = 3 mm.

difficult to determine how much of the bone is preserved (Figs. 4.2 and 4.3, dpt). It is elongate, with ridged ornamentation running antero-posteriorly along its length, and carries a canal across its width in the posterior half.

4.4.2 Infraorbitals

The orbit is partially enclosed by the dermosphenotic, jugal and lacrimal (Figs. 4.3 and 4.4, dsph, jug, la), though the anterior end of the lacrimal has rotated dorsally. The

lacrimal is thin and essentially a bony sheath surrounding the infraorbital sensory canal (Fig. 4.4, la), which continues posteriorly into the jugal. The jugal is crescent-shaped and possesses similar ridged ornamentation to the frontals. It is relatively shallow, with a curved dorsal edge, and lacks a notch on the orbital margin of the jugal. The infraorbital sensory canal extends through the jugal, tracking the curve of the bone, with small canals emerging from the posterior margin of the main canal and opening into pores on the dermal surface (Fig. 4.4, inc). Dorsal to the jugal, the triangular dermosphenotic receives the infraorbital canal from the jugal (Fig. 4.4, dsph). There is a modest expansion in the postero-dorsal corner of the dermosphenotic rather than a distinct posterior ramus. A smooth overlap area on the anterior extension of the dermosphenotic likely accommodated the nasal or frontal. The main trunk of the infraorbital canal exits through the dorsal margin of the dermosphenotic with small branches issuing anteriorly.

Slightly posterior and medial to the dermosphenotic may be part of the anterior portion of the dermopterotic (Figs. 4.2 and 4.3, dpt?). The fragment has a smooth anterior half where it was overlapped by the dermosphenotic and a posterior half ornamented with tubercles.

4.4.3 Upper jaws and palate

The upper jaw complex comprises the maxilla, premaxilla, dermopalatines, entopterygoid, ectopterygoid, accessory vomer, parasphenoid and possibly a paired

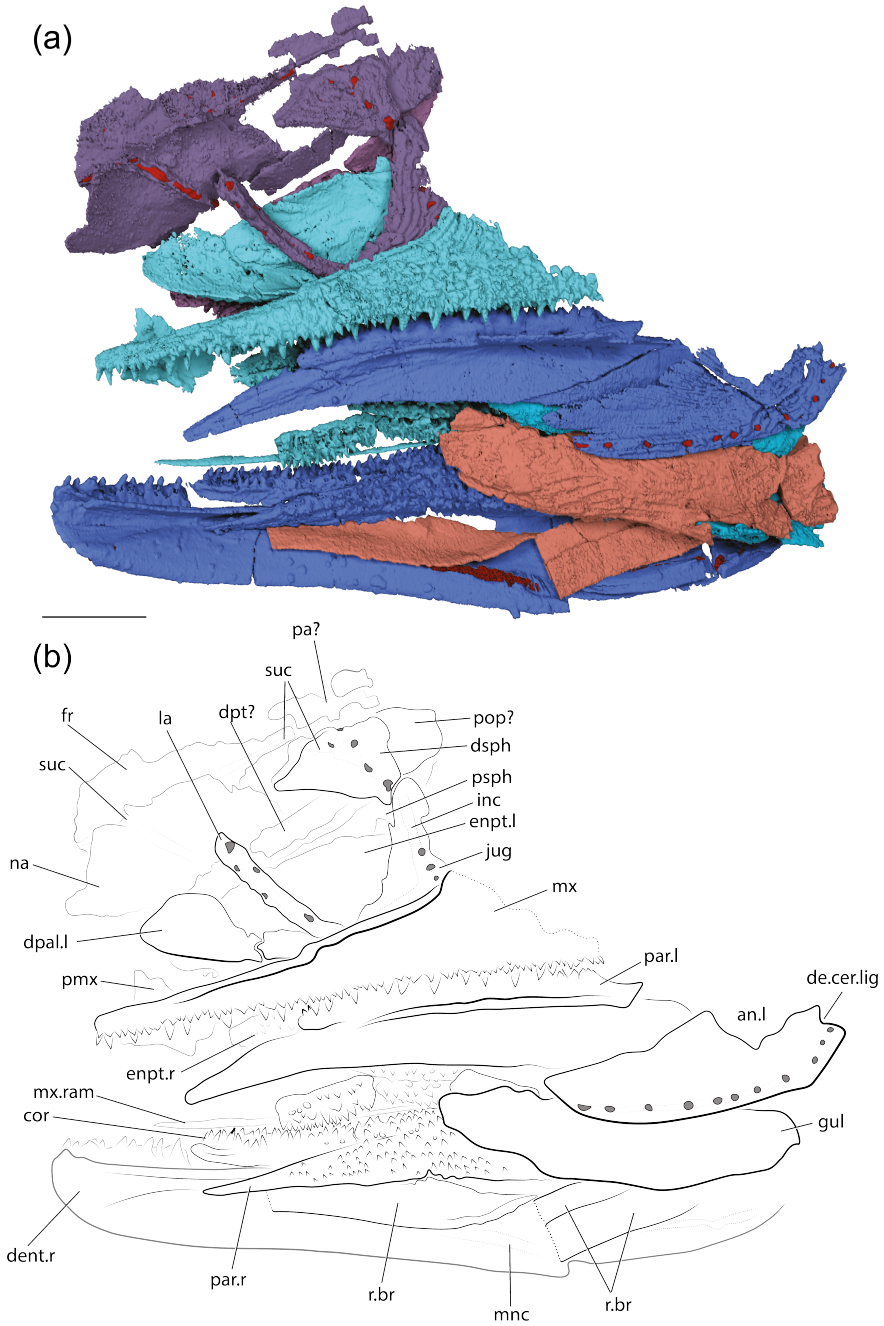


Figure 4.3: Skull of *Phanerosteon ovensi* NHMUK PV P.13184 in left lateral view. (a) three-dimensional render of the skull roof bones and infraorbitals (purple), parasphenoid (mauve), upper jaws (turquoise), lower jaws (dark blue), shoulder girdle (light blue), operculogular elements (red) and sensory canals (maroon). (b) interpretive drawing of (a) with dashed lines indicating uncertain margins, dotted lines the internal course of sensory canals and grey fill the opening of sensory canals to the dermal surface. Abbreviations: an.l, left angular; cor, coronoid; dent.r, right dentary; dpal.l, left dermopalatine; dsph, dermosphenotic; enpt.l, left entopterygoid; enpt.r, right entopterygoid; fr, frontal; inc, infraorbital sensory canal; it?, intertermporal; jug, jugal; la, lacrimal; mnc, mandibular sensory canal; mx, maxilla; mx.ram, suborbital ramus of maxilla; na, nasal; pa?, parietal; par.l, left prearticular; par.r, right prearticular; pmx, premaxilla; pop?, preopercular; psph, parasphenoid; r.br, branchiostegal ray; suc, supraorbital sensory canal. Scale bar = 3 mm.

vomer (Figs. 4.5 and 4.6, mx, pmx, dpal, enpt, ecpt, acc.vom, psph, vom?). A fragment

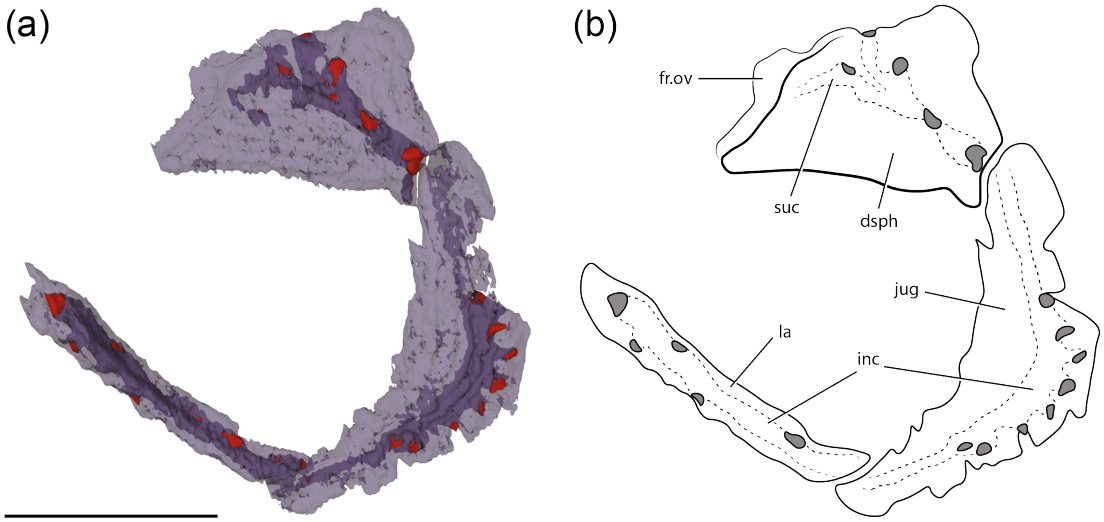


Figure 4.4: Infraorbitals of *Phanerosteon ovensi* NHMUK PV P.13184. (a) semi-transparent three-dimensional render of the dermosphenotic, jugal and lacrimal (purple) in lateral view, showing the internal course of the sensory canals (maroon). (b) interpretive drawing of (a) with dotted line indicating course of the sensory canals and grey fill indicating dermal opening of sensory canals. Abbreviations: dsph, dermosphenotic; fr.ov, overlap for frontal; inc, infraorbital sensory canal; jug, jugal; la, lacrimal; suc, supraorbital sensory canal. Scale bar = 3 mm.

of the premaxilla can be identified due to the presence of a sensory canal (Fig. 4.6, pmx). The margins of the premaxilla are incomplete, so teeth are lacking, a dorsal lamina is clearly present. Both maxillae are incompletely preserved, although most of the bone can be reconstructed using the principle of symmetry. Ornamentation consists of anteroposterior ridges, grading into pustular ornament posteroventrally. Two rows of teeth are borne on the maxilla: one of large teeth lingually, and one of smaller teeth, which grade into the dermal ornament, labially (Fig. 4.5 and 4.6, mx, te). The narrow suborbital ramus bears teeth along its full length (Fig. 4.6, mx.ram). A shelf runs along the medial surface of the maxilla, which contacts the endoskeletal palate and dermopalatines. The posterior part of the maxilla is only partially preserved. Teeth

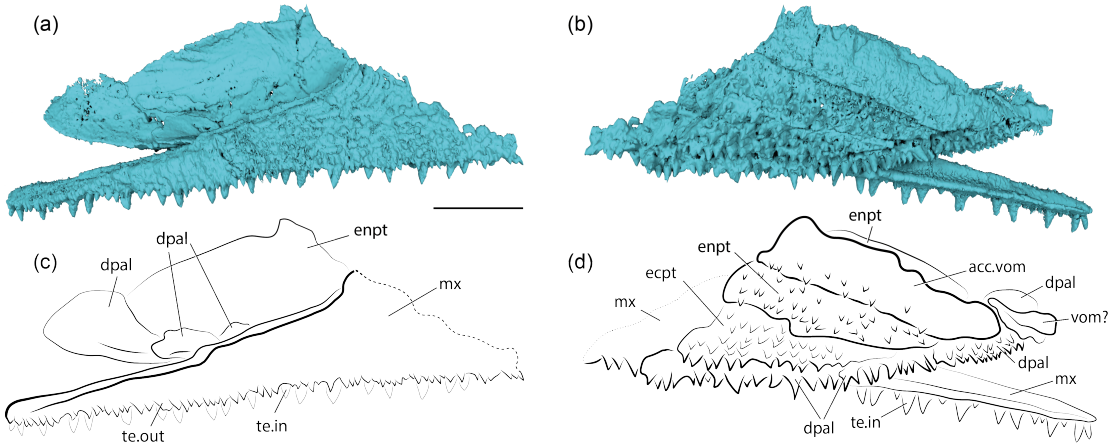


Figure 4.5: Upper jaw of *Phanerosteon ovensi* NHMUK PV P.13184. (a) three-dimensional render of the left upper jaw in lateral view. (b) three-dimensional render of the left upper jaw in medial view. (c) interpretive drawing of (a). (d) interpretive drawing of (b). Abbreviations: dpal, dermopalatine; ecpt, ectopterygoid; enpt, entopterygoid; mx, maxilla; te.in, inner tooth row; te.ou, outer tooth row; vom?, vomer. Scale bar = 3 mm.

protrude from the ventral margin and an expanded lamina is present dorsally, although the full extent is unknown.

Three distinct dermopalatines are preserved on the left side of the specimen (Fig. 4.5, dpal), as well as a possible paired vomer. Three dermopalatines are also preserved on the right side of the specimen (Fig. 4.6, dpal); anterior to these, the specimen has been prepared away dorsal to the maxilla. The dermopalatines are largely in contact with one another and are of similar lengths, though the posterior dermopalatine is marginally longer. Each dermopalatine possesses numerous large teeth along with similarly large empty tooth sockets. This indicates that up to four dermopalatines were present in total. This observation is corroborated by an extension of the medial suborbital shelf of the right maxilla, anterior to the preserved dermopalatines. The anteriormost dermopalatine has both a laterally directed articulating shelf (contacting the maxilla) and an expanded medial lamina (Fig. 4.5, dpal).

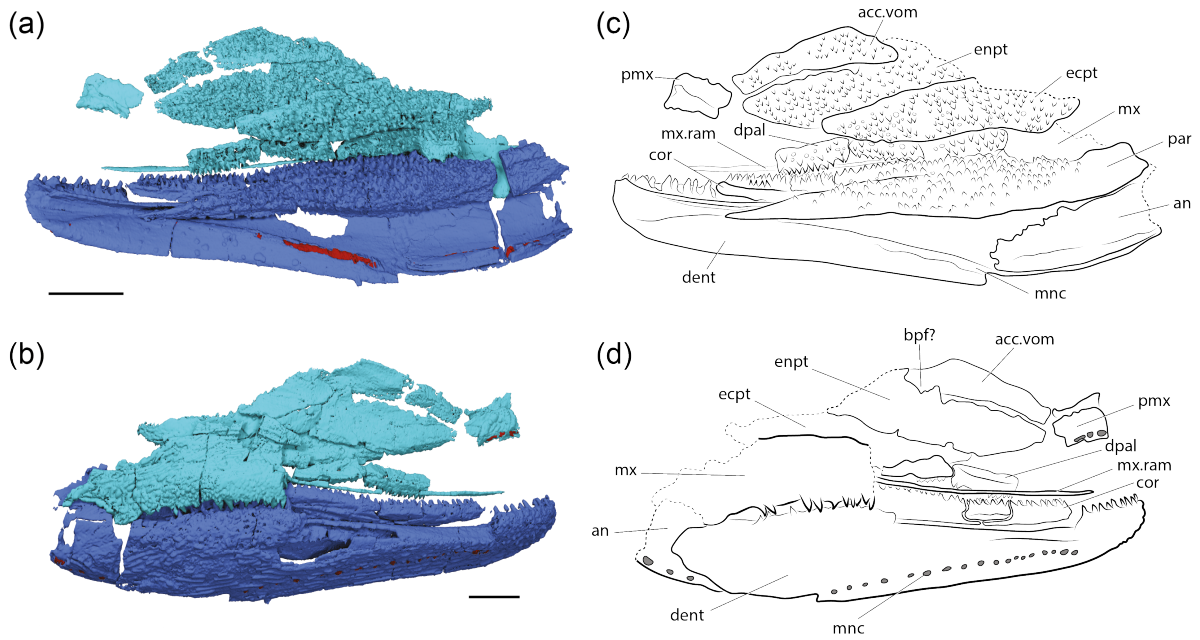


Figure 4.6: Right upper and lower jaw of *Phanerosteon ovensi* NHMUK PV P.13184. (a) three-dimensional render of the right upper jaw (turquoise), lower jaw (dark blue) and mandibular sensory canal (maroon) in medial view. (b) three-dimensional render of the right upper jaw (turquoise), lower jaw (dark blue) and mandibular sensory canal (maroon) in lateral view. (c) interpretive drawing of (a). (d) interpretive drawing of (b). Abbreviations: acc.vom, accessory vomer; an, angular; bpf?, basipterygoid fenestra; cor, coronoids; dent, dentary; dpal, dermopalatines; ecpt, ectopterygoid; enpt, entopterygoid; mnc, mandibular sensory canal; mx, maxilla; mx.ram, suborbital ramus of maxilla; par, prearticular; pmx, premaxilla. Scale bars = 3 mm.

Dorsal to the posterior dermopalatine, the anterior portion of the left ectopterygoid is preserved (Fig. 4.5, ecpt). This makes contact with the suborbital ramus of the maxilla and can be differentiated posterodorsally from a separate entopterygoid ossification (Fig. 4.5, enpt). Both of these bones possess teeth, which decrease in size dorsally. Only a narrow strip along the dorsal margin of the entopterygoid lacks teeth. A small process at the posterior end of this edentulous strip may correspond with the endoskeletal basipterygoid fenestra (Fig. 4.6, bpf). The ossification centre of the entopterygoid is in the middle of the posterior half of the bone. Anteriorly, the posterior margin of the accessory vomer (Figs. 4.5 and 4.6, acc.vom)

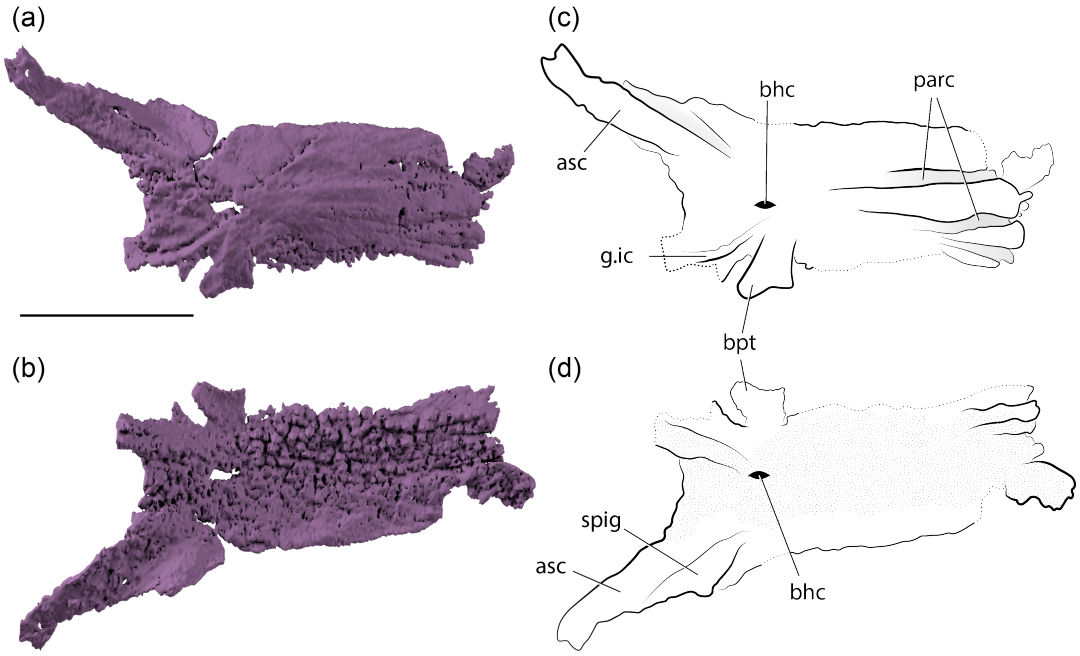


Figure 4.7: Parasphenoid of *Phanerosteon ovensi* NHMUK PV P.13184. (a) three-dimensional render of the parasphenoid in dorsal view. (b) three-dimensional render of the parasphenoid in ventral view. (c) interpretive drawing of (a). (d) interpretive drawing of (b) with faint stippling representing extent of denticles on ventral surface. Abbreviations: asc, ascending process of parasphenoid; bhc, buccohypophysial foramen; bpt, basipterygoid process; g.ic, groove for internal carotid; parc, parabasal canal; spig, spiracular groove. Scale bar = 3 mm. Anterior to the right.

overlaps the non-tooth bearing region of the entopterygoid. The accessory vomer is blade-like and possesses small teeth across its entire surface. Anterior to the left accessory vomer is a portion of a bone that may represent a posterior fragment of the left vomer (Fig. 4.5, vom).

The parasphenoid is largely complete, although squashed against the left palate (Figs. 4.2 and 4.7, psph). It extends the full length of the dermal jaws, and its ventral surface is covered with large, blunt teeth, with the exception of overlap areas along its lateral margins. The anterior margin of the parasphenoid is slightly damaged, although appears to have been multifid. Paired grooves for the parabasal canals on the dorsal surface of the parasphenoid flank a thick central ridge (Fig. 4.7, parc). These grooves

terminate just anterior to the large buccohypophysial foramen (Fig. 4.7, bhc). Stout basipterygoid processes (Fig. 4.7, bpt) are present lateral to the buccohypophysial foramen. A groove for the internal carotid extends posterolaterally from the buccohypophysial foramen to the posterior margin of the parasphenoid (Fig. 4.7, g.ic). A moderately large ascending process is preserved on the left side of the specimen, with a spiracular groove and denticles on its ventral surface (Fig. 4.7, asc, spig). The parasphenoid does not appear to have a posterior stalk. As the braincase is unmineralised, the positional relationship of the parasphenoid cannot be determined, but it is unlikely to have extended posterior to the ventral otic fissure.

4.4.4 Lower jaws

A dentary, angular, surangular, prearticular and coronoids are present in the lower jaw of *Phanerosteon ovensi* (Figs. 4.2, 4.3 and 4.6, dent, an, sur, par, cor). Only the right dentary is present, part of the dorsal margin and lateral portion of which has been prepared away revealing the gular internally, but a single row of conical, pointed teeth are present anteriorly and posteriorly. The ornamentation on the dentary largely consists of short, anteroposteriorly oriented ridges, but the ornament is pustular near the tooth row in the posterior half and symphysial region. The dentary does not taper at the rostral end. Posteriorly, however, the dentary narrows to accommodate the posterior part of the maxilla. The mandibular canal is transmitted from the angular into the dentary and arches in the anterior third of the bone before terminating at the anterior margin of the dentary (Fig. 4.6, mnc). It is open to the surface via a series of pores.

The suture between the dentary and angular is faint. The angular is ornamented by a series of ridges, except dorsally where it is unornamented for overlap by the

surangular and maxilla. A depression on the posterior face of the left angular was likely for the ceratohyal ligament (Fig. 4.3, de.cer.lig; Gardiner 1984: p. 327, fig. 90). The surangular is a thin, blade-like lamina medial to the posterior portion of the maxilla. Damage in this region of the lower jaw makes interpretation of the position of the suture between the surangular and angular difficult.

A horizontal shelf extends along much of the medial surface of the dentary, terminating just anterior to the surangular, and corresponds to a groove on the lateral face of the prearticular (Fig. 4.3 and 4.6, par). The prearticular extends almost the entire length of the lower jaws, and has a rounded posterior margin. A depression on the lateral surface of the posterior end of the prearticular accommodates the surangular. Anteriorly, a division into dorsal and ventral tooth-bearing bones makes the distinction between the anterior-most preserved coronoid and prearticular clear. Posteriorly, however, the coronoids and prearticular blend into one another, with the dense covering of teeth making distinction between them difficult. This apparent anterior-most coronoid may actually represent the second coronoid (with the anterior coronoid not preserved) and is distinct from the next coronoid in sequence posteriorly (Figs. 4.2, 4.3 and 4.6, cor). This coronoid also has a posterior process that underlies the succeeding coronoid. The distinction is more obscure posteriorly, however, as a continuous sheet of pointed teeth with no clear sutures is presented medially. In lateral view, dorsal to the groove accommodating the dorsal shelf of the dentary, there is a topographic differentiation between the rounded, ‘coronoid-like’ region of the bone and the ventral, plate-like prearticular region though no sutures are present. A difference

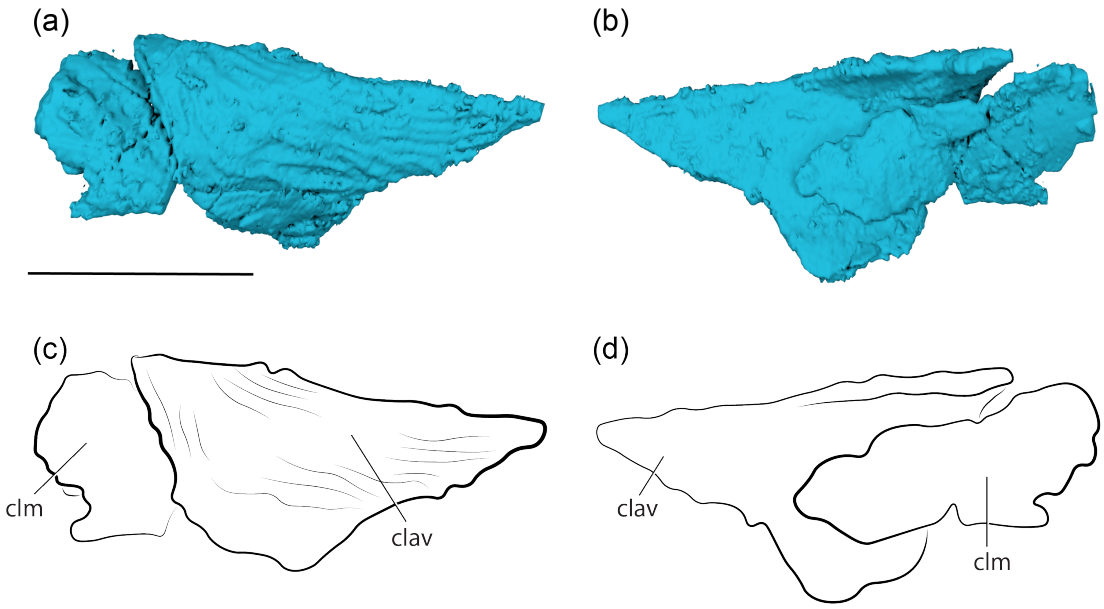


Figure 4.8: Clavicle and cleithrum of *Phanerosteon ovensi* NHMUK PV P.13184. (a) three-dimensional render of the clavicle and cleithrum in lateral view. (b) three-dimensional render of the clavicle and cleithrum in medial view. (c) interpretive drawing of (a). (d) interpretive drawing of (b). Abbreviations: clav, clavicle; clm, cleithrum. Scale bar = 3 mm.

between the left and right prearticulars is the curvature of the anterior left prearticular ventrally, whereas the right prearticular is broadly straight anteriorly.

4.4.5 Shoulder girdle, operculogular system and gill skeleton

The elements of the shoulder girdle, due to disarticulation of the fossil, have shifted so that they are medial to the posterior half of the right mandible. The cleithrum is incomplete, though it is clear that the clavicle overlaps the anterior projection (Fig. 4.8, cle). Most of the cleithrum is missing, including the broad posterior section and dorsal limb. The right clavicle is triangular in lateral view, strongly curved, and ridged with anteroposterior ornament (Fig. 4.8, clav). Posteriorly, the clavicle curves medially around the cleithrum, with the ventral margin extending further medially than the

dorsal. The dorsal margin of the clavicle is damaged and so it is unclear whether the clavicle had a prominent dorsal extension.

At least four branchiostegal rays sit medial to the angular and dentary, and lateral to the clavicle (Fig. 4.3, r.br). The branchiostegal rays taper posteriorly, have stout ridged ornament running parallel with the ventral margin of the bone ventrally, an unornamented dorsal portion where they overlap. Another slightly damaged element, which may be a lateral gular (Fig. 4.3, gul), lies alongside the branchiostegal rays. It is double the width of the branchiostegal rays, roughly half the length of the dentary and also bears stout ridges of ornament.

Numerous, small ossifications of the gill skeleton are present between the jaw complexes though are too fragmented to allow identification.

4.5 Discussion

4.5.1 Updates to previous descriptions

Investigation of *Phanerosteon ovensi* using µCT scanning reveals undescribed internal anatomy and allows for revision and supplementation of previous descriptions (White, 1927; Moy-Thomas, 1938; Gardiner, 1985; Sallan, 2012). Both Moy-Thomas (1938) and Gardiner (1985) depict the dermosphenotic as having a prominent posteriorly directed ramus, while Sallan (2012) describes a t-shaped dermosphenotic, rather than the small extension in the postero-dorsal corner that is present in this specimen. The dermosphenotic is also small relative to the rest of the skull in this specimen (*contra* Moy-Thomas, 1938), though the extent of damage is unclear. In addition, the shape of the jugal conforms more to the reconstruction of Moy-Thomas (1938) than that of Gardiner (1985) in being strongly curved rather than mostly straight. Here we show

previously unknown features of the infraorbital sensory canal: multiple rami branching off the infraorbital canal in the jugal; and an anteriorly directed branch of the sensory canal in the dermosphenotic.

In the initial description of *Phanerosteon ovensi* the teeth were referred to as “rather feeble” (White, 1927, p. 266), with two rows of small teeth, the more labial grading into the ornament. While two rows of teeth are present on the maxilla, we only identify one row on the dentary. We also do not consider the teeth of the primary tooth row to be small, but rather large as described in *Phanerosteon mirabile* (Moy-Thomas & Dyne, 1938). Furthermore, the primary tooth row is lingual, with the smaller teeth more labial and grading into the ornament. This contrasts with White's (1927) account, which describes smaller teeth inside the principal tooth row (possibly misidentifying the coronoid dentition) as well as denticles grading into the ornament

Greater detail of the morphology of the lower jaw than that given in previous descriptions is now available. Notably, the course of the mandibular sensory canal differs from the reconstructions of White (1927) and Gardiner (1985) in arching in the anterior half of the dentary and exiting via the anterior margin of the dentary rather than via the dorsal margin. We also show the medial surface of the dentary and clarify the morphology of the postdentary bones, including the presence of a surangular.

The most substantial additions to previous descriptions concern the prearticular, coronoids, dermopalatines and palatal ossifications. Of these, only the palate is mentioned previously as “too fragmentary for description” (White, 1927, p. 265). Most notable is the complete coverage of the palate in large teeth, with several empty tooth sockets, as well as four dermopalatines. The parasphenoid and long accessory vomers

are also denticulated. As such, the dermal bones of the oral cavity of *Phanerosteon ovensi* are now fully described and can be shown to be almost entirely covered in robust teeth.

While *Phanerosteon mirabile* and *P. ovensi* share some notable characteristics, such as the general absence of body scales, presence of ridge scales and absence of fringing fulcra, there are a number of key differences. The most notable concern tail and fin morphologies (Fig. 4.9). *P. mirabile* has a forked tail and a distinct caudal peduncle, while in *P. ovensi* the tail is unforked, rounded and lacks a distinct peduncle (Sallan, 2012), resembling the depiction in White's original description (White, 1927) more than Gardiner's revision stating that the tails are similar (Gardiner, 1985). *P. ovensi* displays a small gap between the posterior base of the dorsal and anal fins and the start of the caudal fin, whereas the median fins in *P. mirabile* are more placed more anteriorly; the dorsal fin base in *P. ovensi* is also longer than that of *P. mirabile*. *P. mirabile* also has roughly evenly segmented fin rays on the entirety of the pectoral fin, while in *P. ovensi* the proximal segments are elongated and distally segmented. Finally, the dermal ornamentation of the skull roof differs, with tubercles dominating in *P. mirabile* in contrast to stout ridges in *P. ovensi*.

The possession of a tail that was less forked than that of *Phanerosteon* was one of White's initial reasons for erection of the new genus *Carboveles* (White, 1927), despite other similarities. However, when Gardiner (1985) later revisited the genus and examined new material, he did not uphold this assignment, and synonymised the

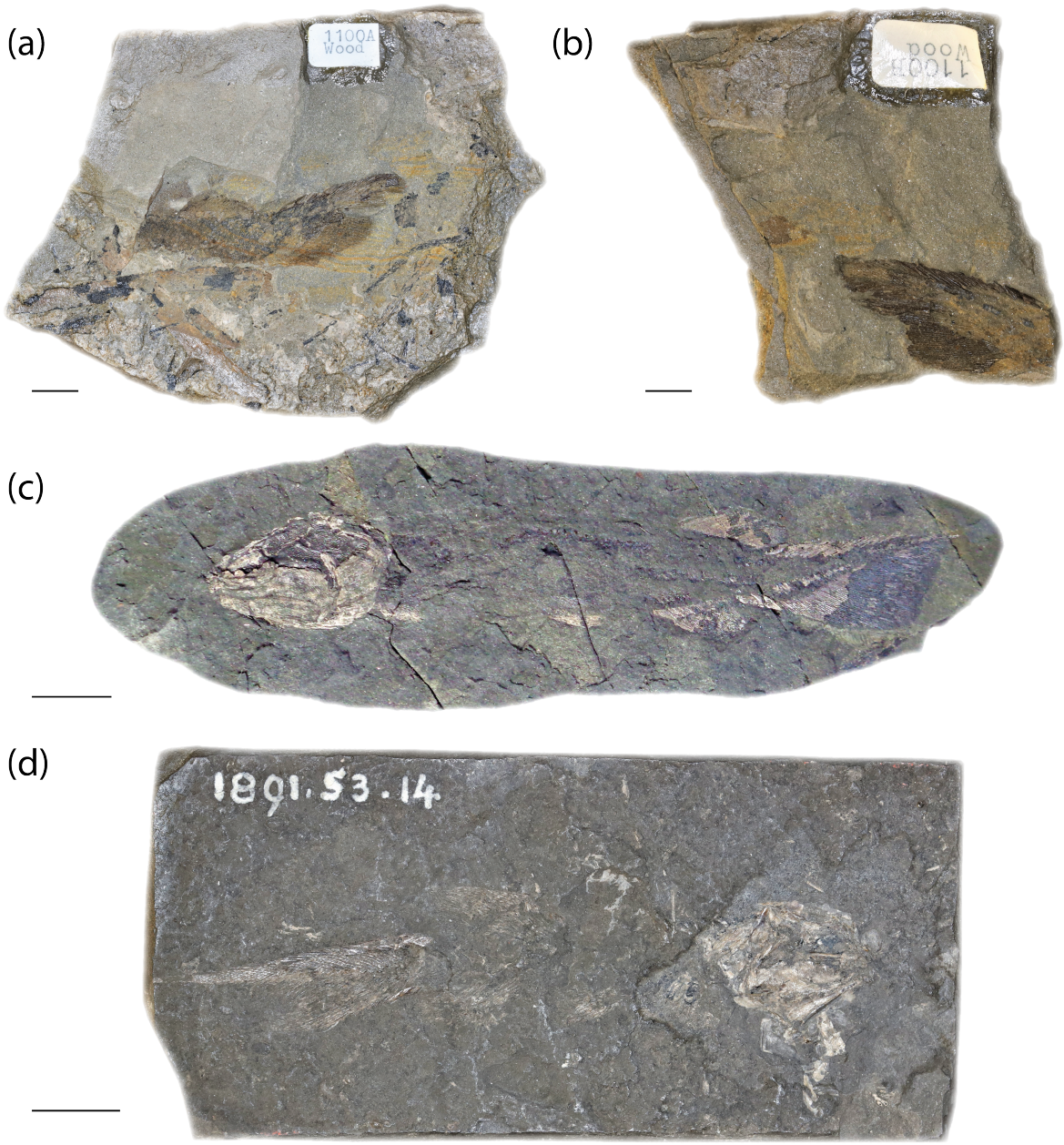


Figure 4.9: Selected fossil specimens of *Phanerosteon ovensi* (a-c) and *Phanerosteon mirabile* (d) showing the differences in tail morphology. (a) and (b) part and counterpart of NMS 1980.40.20 (*Phanerosteon ovensi*); (c) UMZC 20111.7.11 (*Phanerosteon ovensi*); (f) NMS G.1891.53.14 (*Phanerosteon mirabile*). Scale bars = 10 mm.

genera. With the caveat that we have not been able to examine the type and other key specimens, we uphold these taxonomic acts to synonymise *Carboveles* with *Phanerosteon* but distinguish between two species within *Phanerosteon*.

4.5.2 Morphological changes in the Carboniferous

Devonian and Carboniferous actinopterygians have been long recognised to possess broadly different morphological character sets, and these have been used to support a model of low lineage survival across—and high diversification after—the EDME (Giles *et al.*, 2023). Devonian actinopterygians tend to be morphologically conservative, with limited disparity in body shape, feeding morphology or locomotor mode. However a clearcut distinction between Devonian and Carboniferous morphologies is likely erroneous, and *Phanerosteon ovensi* further bridges gaps between Devonian and later Carboniferous forms.

Previous accounts of *Phanerosteon ovensi* describe or depict a dermosphenotic with a posterior ramus, however the specimen here lacks this ramus, instead having a triangular dermosphenotic (N.B. the only other specimens available to us and not on loan do not have the dermosphenotic clearly preserved). This contrasts all Devonian actinopterygians, which possess either a short (e.g. Mimiidae and *Osorioichthys*, Gardiner, 1985; Taverne, 1997; Choo *et al.*, 2009; Choo, 2012) or very long (all other Devonian actinopterygians, Gross, 1953; Jessen, 1968; Dunkle and Schaeffer, 1973; Long, 1988; Arratia & Cloutier, 1996; Daeschler, 2000; Cloutier & Arratia, 2004; Long, Choo and Young, 2008; Choo, 2015; Giles *et al.*, 2015; Choo *et al.*, 2019) posterior ramus of the dermosphenotic. After the end-Devonian however, two new dermosphenotic morphologies appear: 1) a reduced posterior ramus resulting in a triangular dermosphenotic (Long, 1988); 2) a reduced posterior ramus and increased curvature around the orbit to form a crescent-shaped dermosphenotic (Gardiner, 1963; Gardiner & Schaeffer, 1989; Sallan & Coates, 2013).

Phanerosteon ovensi shares possession of accessory vomers with a select few actinopterygians; no extant taxa possess these bones. The majority of the taxa in which accessory vomers are present have been investigated using cross sectioning methods: either grinding and serial sectioning (*Australosomus kochi, Mimipiscis toombsi* and *Pteronisculus stensioi*, Nielsen, 1942, 1949; Gardiner, 1984); or CT-scanning (*Brazilichthys macrognathus, Eurynotus crenatus, Fukangichthys longidorsalis, Palaeoneiros clackorum*, *Phanerosteon ovensi,* and *Raynerius splendens*, Giles *et al.*, 2015, 2017, 2023; Friedman *et al.*, 2018; Figueroa *et al.*, 2019). The occurrence in other taxa occurs either when a mostly articulated palate is present and exposed (*Elonichthys binneyi,* Watson, 1925; *Woodichthys bearsdeni,* Coates, 1998) or uncrushed and able to be fully prepared (*Moythomasia durgaringa,* Gardiner, 1984). Confirmation of accessory vomers was rare prior to CT-based investigations, highlighting that renewed study of internal anatomy can alter character distributions and ultimately sequences of morphological evolution. In many instances where the fossil and method of investigation permit observation of the articulated palate in stem-actinopterygians (and *Fukangichthys*) there is an accessory vomer, suggesting that this bone is primitively present and then lost in derived cladistians and actinopterans.

Phanerosteon ovensi is also one of the first actinopterygians (alongside *Novogonatodus kasantsevae*, *Lambeia pectinatus* and *Palaeoneiros clackorum*) to possess multiple branches emanating from the infraorbital sensory canal in the jugal, a feature uncommon prior to the Tournaisian (Jessen, 1968; Giles *et al.*, 2023). Several factors may affect the observation of this character, however. Again, without CT-scanning allowing the segmentation of the infraorbital canal in *Phanerosteon ovensi* this feature would not have been observed, as the canal is hidden externally by

ornamentation. It may be that this feature, like presence of accessory vomers, is more likely to be observed when examining using tomographic methods. Investigation of taxa previously thought to lack this trait may result in wider observation among actinopterygians, with the potential to alter patterns of character evolution. For example, CT-based description of a Late Devonian actinopterygian (*Palaeoneiros clackorum*; Giles *et al*., 2023) shows the presence of this typically Carboniferous feature (and others: dermal basipterygoid process and perforated dorsal aortic canal), in the Devonian, indicating that the distinction between traditionally Devonian and Carboniferous morphologies will be blurred as new material is described.

4.5.3 Ecological expansions

The dentary morphology of Devonian actinopterygians is highly morphologically conservative and displays low functional disparity (Anderson *et al.*, 2011). Stabilisation of mandibular morphology in the Palaeozoic was suggested by Hill *et al.* (2018) to represent an optimal morphology for the feeding ecology of taxa, which may be the case with these small, fusiform actinopterygians. *Tegeolepis clarki* (Famennian; Dunkle & Schaeffer, 1973) and *Austelliscus ferox* (Pragian-Eifelian; Figueroa *et al.*, 2021), both large, predatory taxa, represent obvious morphological outliers. On the surface, *Phanerosteon ovensi* exemplifies the continuation of orthodox dentary morphology into the Tournaisian.

Implications of this conservatism in an ecological sense are unclear. It is tempting to conclude that such low morphological disparity correlates with low ecological disparity and that small, predatory, fusiform fishes were occupying similar ecosystem roles. In reality, the picture is more nuanced, with dentition and three-

dimensional morphology, rather than just aspects of two-dimensional mandibular shape (such as relative length, width and curvature), likely differentiating taxa and more clearly indicating ecological role. Other small, fusiform Tournaisian taxa from the same locality as *P. ovensi*, such as *Fouldenia ischiptera* (Traquair, 1881; Sallan & Coates, 2013) are only superficially similar. Despite some resemblance of external dentary shape the two taxa clearly occupied different niches, with *Fouldenia* lacking dentary dentition and hypothesised to have a durophagous diet (Sallan & Coates, 2013).

Furthermore, aspects of dentary morphology other than shape appear to be more important indicators of diet and ecology. For example, the perpendicular angle of the insertion of the adductor fossa on the mandible is an important determinant of bite force (Bellwood, 2003), as exemplified by the Viséan *Eurynotus crenatus* (Friedman *et al.*, 2018), a taxon which also has substantially modified dentition. While *Phanerosteon ovensi* initially seems to represent a continuation of the typical Devonian actinopterygian dentary morphology, the presence of extensive dentition in the mouth may hint at subtler changes to functional morphology and/or ecology, which will not be detected by analyses excluding this information (e.g. Hill *et al.*, 2018). There is an explosion in cranial morphospace occupation following the end-Devonian extinction (Sallan & Friedman, 2012) and the subtle morphological changes in *Phanerosteon ovensi* echo this increased overall cranial disparity. These changes in the dentition may lend credit to the ‘feeding first’ hypothesis of diversification of actinopterygians in the earliest Carboniferous (Sallan *et al.*, 2011).

Other notable features of the jaw apparatus of *Phanerosteon ovensi* that are not apparent externally and typically not observable via traditional descriptive techniques

include the coverage of the entire oral surface in large, conical dentition. The apparent novelty of this feature in *P. ovensi* comes with the caveat this it might be widespread, but unknown, in a much broader sample of Palaeozoic actinopterygians. *P. ovensi* is, in fact, the perfect representation of this problem, the taxon being originally described by White (1927, p. 266) as having “rather feeble” dentition. This study therefore provides another piece of evidence of the utility of CT scanning for revisiting long-known—yet little understood—Palaeozoic ray-finned fishes.

Tournaisian aquatic faunas also show a distinct rise in the proportion of actinopterygians relative to the very low levels throughout the Devonian (Sallan & Coates, 2010; Friedman, 2015, 2022). Barring some fossil faunas with very low relative richness of actinopterygians (e.g. Niddrie, Dora, Ducabrook, Burnmouth; Sallan & Coates, 2010; Friedman, 2015; Otoo *et al.*, 2019) these higher proportions continue, with actinopterygians making up close to half of all fishes in faunas throughout the Carboniferous. Morphological disparity (particularly in cranial morphology) continues to rise throughout the Carboniferous at higher levels than seen in the Tournaisian (Sallan & Friedman, 2012; Friedman, 2015), the most notable examples being the multiple convergent evolutions of durophagy. The eurynotiforms *Fouldenia ischiptera* (Tournaisian), *Styracopterus fulcratus* and *Eurynotus crenatus* (Viséan) exhibit the first strictly durophagous feeding in actinopterygians (Sallan & Coates, 2013; Friedman *et al.*, 2018), and this feeding strategy recurs in other Palaeozoic groups (e.g. amphicentrids [*sensu* Friedman *et al.,* 2018] and platysomids/bobasatraniids).

4.6 Conclusions

CT scanning has revealed new morphological details of the Tournaisian actinopterygian *Phanerosteon ovensi*. Comparison with the type species of *Phanerosteon* (*P. mirabile*) confirms that while they share some features, such as a naked trunk, the morphology of the fins differs significantly. *Phanerosteon ovensi* also has unique features uncovered by CT scanning, such as the extensive palatal dentition. These new morphological details in *Phanerosteon ovensi* add to mounting evidence of key innovations and morphological changes in Carboniferous actinopterygians, which occurred in tandem with their increasing relative diversity. Importantly, this may parallel the diversification and expansion of actinopterygians into new niche space as other groups of fishes went extinct. Continued descriptions of fishes from this key period will be critical in determining the impact on actinopterygians of the end-Devonian mass extinction, and their response to it.

5 A new genus and species of actinopterygian from the Upper Carboniferous (Bashkirian) of Northern England

My contribution to this chapter involved segmentation of CT data, visiting museum collections, describing specimens, conducting phylogenetic analyses, preparing the figures, interpreting the results, and writing the manuscript. S. Giles CT scanned the specimen, segmented CT data and provided feedback on the interpretation of results and drafts of the manuscript. This chapter is in the process of being turned into a manuscript for publication. The editorial 'we' is used throughout the text to reflect these contributions.

5.1 Introduction

The British Isles are among the most intensely sampled regions of the Palaeozoic fish fossil record (Lloyd & Friedman, 2013) and yield substantial numbers of problematic genera that require reinvestigation and taxonomic revision (Henderson *et al.*, 2023). One approach to addressing geographic biases in the fossil record is to focus on regional trends in order to understand local diversity dynamics (Benson *et al.*, 2016; Close *et al.*, 2019, 2020a, 2020b). Reinvestigating actinopterygians from the British Isles therefore represents an opportunity to refine taxonomy for more accurate hypotheses of local diversity dynamics and reveal hidden morphological diversity in traditionally overlooked material. Masked diversity and bias in the record are not only

a problem for understanding trends in richness through time, but for developing accurate phylogenetic hypotheses. Recent research programs have uncovered numerous new Palaeozoic actinopterygians (Giles *et al.*, 2015b, 2023; Elliott, 2016; Štamberg, 2016b; Mickle, 2017, 2018; Wilson *et al.*, 2018; Choo *et al.*, 2019; Bakaev & Kogan, 2020; Figueroa *et al.*, 2021; Newman *et al.*, 2021; Stack & Gottfried, 2021) and redescribed or revised existing taxa (Choo, 2012, 2015; Sallan & Coates, 2013; Coates & Tietjen, 2018; Stack *et al.*, 2021; Argyriou *et al.*, 2022), increasingly populating the actinopterygian stem and recognising cryptic patterns of diversification outside of the crown group.

Regional museum collections in the United Kingdom represent a key resource for solving taxonomic issues, identifying new actinopterygians and adding data to phylogenies and occurrence databases. Much of the collection and description of specimens occurred in the mid to late 19th and early 20th centuries as a by-product of coal mining during heavily industrial periods of British history, with fossils often amassed in private collections and later donated to museums. While many specimens ended up in large national museum collections (e.g. Natural History Museum, London; National Museums Scotland, Edinburgh), significant numbers also accrued in regional museums. Naturally, a consequence of such intense sampling was that some specimens were overlooked by the relatively few pioneering palaeontologists working on fossil fishes during this period, giving rise to the ‘dark data’ phenomenon (Allmon *et al.*, 2018; Marshall *et al.*, 2018), but also presenting a ripe opportunity for contemporary reinvestigations.

A perfect example of this is MM L.1696, held in the Manchester Museum (Fig. 5.1). This specimen, a nodule containing the anterior two thirds of a near-perfectly

articulated fish, was figured and assigned to *Elonichthys aitkeni* over 125 years ago, although without any accompanying taxonomic justification or description (Bolton, 1895, fig. 14, pl. 3), and has not been re-examined since. Traquair (1886) had earlier erected *E. aitkeni* from roughly contemporary deposits in Lancashire, Derbyshire and Cheshire, though without figuring any specimens or specifying a type. Woodward (1891) subsequently recorded additional specimens of *E. aitkeni* present in the British Museum of Natural History (Natural History Museum), including material from Devon, and designated the lectotype to be a specimen in the private collection of J. Aitken (Woodward, 1891).

The taxonomic history of both the genus and species is turbulent, with the lectotype having been lost since before the start of the 20th century (Gardiner 1963). *Elonichthys* has long been recognised as a wastebasket taxon (Mickle, 2017; Henderson *et al.*, 2023), and the species was moved to a new genus, *Mesonichthys*, by Gardiner (1963). However, Gardiner chose as the neotype for *Mesonichthys aitkeni* a specimen from Devon (see 5.3 Systematic Palaeontology, Remarks), which was noted even by Traquair (1901) as potentially a different taxon to the original '*aitkeni*' species. Despite a series of publications commenting on the anatomy and taxonomy of *E. aitkeni* over the next three quarters of a century (Traquair, 1901; Watson, 1925; Aldinger, 1937; Gardiner, 1963), L.1696 appears to be absent from the Palaeozoic actinopterygian literature until works by Coates (1999) and Figueroa *et al.* (2023), both of which merely note the existence of the specimen in the collections of the Manchester Museum.

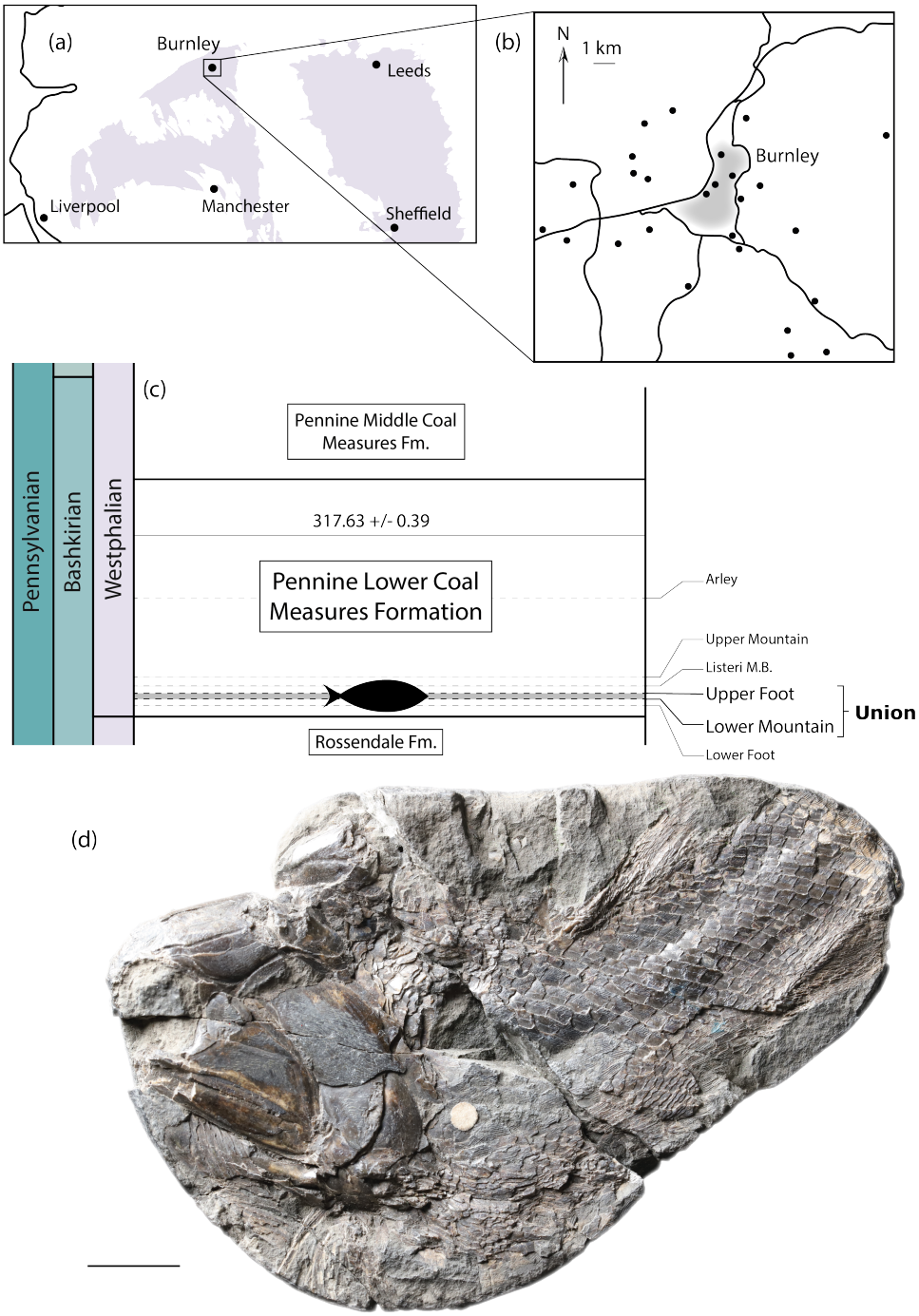


Figure 5.1: Possible localities and stratigraphic horizon of 'new taxon' MM L.1696: (a) Map of the north-west of England showing the geographic distribution of Westphalian coal deposits (shaded regions; adapted from Waters et al. [2013]); (b) map of collieries of the Burnley coalfield (urban area of present-day Burnley shaded; adapted from Williamson [1999]); (c) simplified geological column showing the provenance of the specimen in the Lower Mountain and Upper Foot coal seams (which join to form the Union coal seam in Burnley; shaded region) in the Pennine Lower Coal Measures Formation; (d) MM L.1696. Scale bar = 10 mm.

CT scanning has facilitated the recognition of new taxonomic and morphological diversity in Palaeozoic actinopterygians by revealing otherwise hidden features of

internal anatomy (Giles & Friedman, 2014). L.1696 represents a key opportunity for CT investigation for three reasons: 1) the specimen possesses a substantial amount of the dermal skeleton (Fig. 5.1; Appendix Fig. C.1); 2) the specimen is preserved in a nodule, with preparation showing 3D preservation of the braincase, indicating the preservation of additional internal endoskeletal ossifications; 3) the specimen has never been formally described, despite being known since the 19th century, and so represents a potential instance of taxonomic and morphological diversity hiding in plain sight.

Here, we recognise L.1696 as a new genus and species of Carboniferous actinopterygian, describe its anatomy and add it to an updated phylogenetic analysis. We also discuss sequences of character evolution arising from similarities between L.1696 and other actinopterygians, problems this has raised for phylogenetic analyses and conduct an exploratory analysis of phylogenetic methodologies in the context of early actinopterygian evolution. Lastly, we underscore the importance of revisiting regional museums as a vital component of bringing ‘dark data’ into the light.

5.2 Materials and Methods

5.2.1 Specimens

MM L.1696 is curated in the Manchester Museum (Appendix Fig. C.1). Information in the accession register of the Manchester Museum notes that the specimen is from the “Burnly (*sic*) Coalfield” and was donated, along with a number of other specimens, by Sir. Ughtred Kay-Shuttleworth. This donation appears to have taken place in 1893 (Page, 1977). Comparison of the specimen with the corresponding plate in Bolton (1895: fig 14, pl.3) indicates that it has been mechanically prepared around the skull

region between originally being figured and being borrowed in the early 2010s, although it is not clear when or by whom.

5.2.2 Geological context

Bolton (1904) identifies the nodule as coming from above the “Mountain Mine ‘Four Foot’, where the Upper Foot and Lower Mountain seams had joined” – the joining of these seams in Burnley is called the Union Coal (Williamson, 1999), and the layer is also called the Soapstone Bed (Coates, 1999; Coates & Tietjen, 2018). These coal seams all occur in the lower half of the Pennine Lower Coal Measures Formation, corresponding with the early Langsettian regional substage, and late Bashkirian stage (Waters *et al.*, 2011c). It is not possible to identify the specific colliery the specimen was found in, as this information was not recorded by Bolton (1895); there were numerous collieries surrounding Burnley (Fig. 5.1; Williamson, 1999) which belonged to the Kay-Shuttleworth estate. Coeval ammonoids (*Gastrioceras*, Bolton, 1904) and precise U-Pb dates provide an age range of 318.60 – 317.63 Ma (Pointon *et al.*, 2012; Gradstein *et al.*, 2020).

5.2.3 CT scanning

L.1696 was CT scanned at the CTEES facility in the Department of Earth and Environmental Sciences, University of Michigan, using a Nikon XT H 225 ST Industrial CT scanner with the scanning parameters: 155 kV, 185 uA, 28.74 um, with 6.96 optical magnification, a 2.83s exposure, 4 frames per projections, a 1.6 mm Cu filter, and a tungsten target. The CT data were segmented in MIMICS® Research v. 23.0 (biomedical.materialise.com/mimics, Materialise NV, Leuven, Belgium), to generate three-dimensional images of the specimen including elements within the matrix. 3D

objects were then exported from MIMICS and processed in Blender 3.3.1 (blender.org) to create the final renders, with figures composed in Adobe Illustrator 2022.

5.2.4 Institutional abbreviations

BGS – British Geological Survey, Keyworth; CASM – Sedgwick Museum of Earth Sciences, Cambridge; GLAHM – Glasgow Hunterian Museum, Glasgow; MM – Manchester Museum, Manchester; NHMUK – Natural History Museum, London; NMS – National Museums Scotland, Edinburgh.

5.2.5 Comparative material

Specimens of *Mesonichthys aitkeni* were examined by eye, under microscope and using high-resolution photographs (BGS GSM 4520; MM W.1013, W.1014, L.2358, L.11615, LL.13383; NHMUK PV OR 30575, PV OR 30576, PV OR 30577, PV OR 30578, PV OR 30579, PV OR 30580, P.24816, P.24817, P.10475, P.11617, P.21006, P.21007, P.24598, P.26817, P.26818, P.31250, P.31251, P.36246, P.36247, P.50119, P.56950, P.56951, P.57021, P.57023, P.57961, P.57962, P.6100, P.6102, P.61520, P.61525a, P.61525b, P.61525c, P.61525d, P.7960, P.851, P.9880; NMS 1898.176.74, 1957.1.5668, 1896.115.55; GLAHM V3206, V3194, V3409; CASM E4889, E4890).

5.2.6 Phylogenetic analyses

Analyses were conducted in TNT v.1.6 (Goloboff & Morales, 2023) and MrBayes v.3.2.6 (Ronquist *et al.*, 2012) using a character matrix that was modified from Giles *et al.* (2023) and Argyriou *et al.* (2022). Various characters (c.110, c. 170, c.182, c.223, c.224, c.273 of this analysis) and taxa (*Birgeria stensioei, Brachydegma caelatum, Brazilichthys macrognathus, Neoproscinetes penalvai, Polyodon spathula, Saurichthys ornatus, Yelangichthys macrocephalus*) from Argyriou *et al.* (2022) were

integrated into the matrix of Giles *et al.* (2023). The codings for *Trawdenia planti* were modified based on recent re-descriptions (Coates & Tietjen, 2018). In addition, some characters (e.g. c.99, c.233, c.246) and taxa from Giles *et al.* (2023) were modified, 11 new characters were added (c.100, c.111, c.112, c.138, c.219, c.229, c.231, c.232, c.234, c.247, c.248), and four new taxa were added (*Boreosomus reuterskioldi*, *Mesonichthys aitkeni*, *Ptycholepis bollensis,* new taxon). The total dataset comprises 132 taxa and 307 characters. See Appendices C.2 and C.3 for full taxon and character lists.

In both parsimony and Bayesian analyses an outgroup constraint of [*Dicksonosteus arcticus* [*Entelognathus primordialis* [[*Acanthodes bronni* [*Cladodoides wildungensis*, *Ozarcus mapesae*]][ingroup]]]] was enforced to ensure Osteichthyes were monophyletic and establish character polarities. The function *createMrBayesConstraints* from the R package '*paleotree*' (Bapst, 2012) was used to generate constraints for MrBayes.

Parsimony analyses consisted of an initial tree search using the 'New Technology search' function (employing Sectorial Search, Ratchet, Drift and Tree Fusing with the default parameters), starting with 10 initial addition sequences until the minimum length tree was found 100 times. The resulting trees were then subjected to a round of Tree Bisection Reconnection (TBR), holding up to 100,000 trees. This step was repeated, with suboptimal trees retained to calculate Bremer Decay Indices, and bootstrap values (absolute frequencies) were calculated from 1,000 replicates. The equal weights parsimony analysis was repeated utilising implied weights (k = 1, k = 3, k = 12, k = 100) to examine the effect of increasingly weighting against homoplasy, as evidence suggests implied weights may be useful in phylogenetic analyses (Goloboff

et al., 2018; Smith, 2019). Implied weighting with a soft concavity (i.e. high value of k) which only softly penalises homoplasy may be more appropriate than Bayesian and equal weights when dealing with discrete morphological data (Goloboff *et al.*, 2018, 2019; Sansom *et al.*, 2018; Sookias, 2020). Though Bayesian inference may return more accurate trees under simulated data (albeit at the cost of resolution [Puttick *et al.*, 2019]), trees generated under implied weights contain useful information (Smith, 2019). Equal weights, on the other hand, returns less accurate and less resolved trees than both implied weights and Bayesian methods (Smith, 2019). Additionally, parsimony analyses implementing a negative constraint preventing polypterids and chondrosteans from forming a clade were also conducted to examine any resultant changes in tree topologies. This constraint is justified on the basis of both molecular and morphological data (Near *et al.*, 2012; Broughton *et al.*, 2013; Giles *et al.*, 2017; Hughes *et al.*, 2018; Dornburg & Near, 2021).

The Bayesian analyses implemented the Markov (Mk) model (Lewis, 2001; Wright & Hillis, 2014), modelling character change in two different ways. The ‘maximise information’ and ‘minimise assumptions’ methods of Bapst, Schreiber & Carlson (2018) were used, following Pates *et al.* (2022). The ‘minimise assumptions’ method was used as it allows rate variation among characters and relaxes assumptions about character transitions, which in turn may result in a better fit of the model to the data (Wright *et al.*, 2016; Pates *et al.*, 2022). Four independent runs of four chains were run, sampling trees every 1000 generations until runs converged. Convergence was checked in Tracer 1.7 (Rambaut *et al.*, 2018), and 25% of each run was discarded as burn-in.

We also visualise trees that were recovered by phylogenetic analyses as a multi-dimensional treespace representing Robinson-Foulds (RF) distances between

sampled trees, following the methodology outlined in Pates *et al.* (2022). Under this method, pairwise unweighted RF distances (Robinson & Foulds, 1981) are calculated for the tree sample with classical multidimensional scaling conducted on the resulting RF distances (negative eigenvalues are corrected for using a constant; Cailliez, 1983). Calculations and visualisations were generated in R v.4.1.0 (R Core Team, 2020) using the '*ape'* (Paradis *et al.*, 2004) and '*phangorn'* (Schliep, 2011) packages. Tree samples were reduced to 10,000 trees when necessary for computation purposes.

5.2.7 Anatomical abbreviations

II - optic nerve; III - oculomotor nerve; IV - troclear nerve; V+VII lat - trigeminal and lateral branch of facial nerve; VO - profundus nerve; VI - abducens nerve; VII - facial nerve; VIIfhm - hyomandibular branch of facial nerve; IX - glossopharyngeal nerve; X - vagus nerve; a.fb - anterior fossa bridgei; acv - anterior cerebral vein; adf - anterior dorsal fontanelle; ahy - groove for the afferent hyoid artery; an - angular; ant.amp - ampulla of the anterior semicircular canal; aop - accessory opercular; apr - anterior process of scapulocoracoid; apr.pv - anterior process of pelvic plate; art.1.i - articulation of infrapharyngobranchial I; art.1.s - articulation of suprapharyngobranchial I; asc - anterior semicircular canal; asc.p - ascending process; aur - cerebellar auricules; av - accessory vomer; bb.1-3 - basibranchial I-III; bhc - buccohypophyseal canal; bpf - basipterygoid foramen; bpt - basipterygoid process; br - branchiostegal rays; br.l – enlarged dorsal-most branchiostegal ray; bsph - basisphenoid; bv - basiventral; cao - canal for the dorsal aorta; cb.1-5 - ceratobranchial I-V; c.c - crus commune; chy.a - anterior ceratohyal; chy.p - posterior ceratohyal; clav - clavicle; cle - cleithrum; con - articulatory condyles; cot - articulatory cotyles; cp - coronoid process; crsp - craniospinal process; den - dentary; df - dorsal fin endoskeletal elements; dhy -

dermohyal; di - diencephalon; dmc - dorsal muscle canal; dp - dorsal process of clavicle; dpt - dermopterotic; dr - distal radials; dsph - dermosphenotic; epi.1-4 - epibranchials I-IV; epi.a - epibranchial artery; epsa - efferent pseudobranchial artery; exl - external lamina of cleithrum; f.ram.dors - foramina for branches of the ramus ophthalmicus; fm - foramen magnum; foa - foramen for orbital artery; fr - frontal; g.o.a - groove for the orbital artery; ha - haemal arches; hb.1-3 - hypobranchial I-III; hh - hypohyal; hm.vp - ventral process of hyomandibular; hmd - hyomandibular; hmf - hyomandibular facet; hy.o.a - hyo-opercular artery; ica - internal carotid artery; iclav - interclavicle; id - interdorsal; ih - interhyal; ios - interorbital septum; ip.1-3 - infrapharnygobranchial I-III; jc - jugular canal; jug - jugal; l.c.c - lateral cranial canal; lat.amp - ampulla of the lateral semicircular canal; lda - lateral dorsal aorta; lsc - lateral semicircular canal; mc - mandibular canal; mcp - mesocoracoid process; Men - Mentomeckelian; Mk - Meckelian; mr - fin rays; mx - maxilla; my - myodome; na - neural arch; not - notochord; o.a - orbital artery; o.rec.m - superior, inferior, internal recti muscles; oc.a - occipital artery; olf.b - olfactory bulb; olf.t - olfactory tract; oof - otoccipital fissure; op - opercular; op.pr - posterior opercular process; opc - opercular process; opt.l - optic lobes; opth - ophthalmic artery; p.epi - epineural process; p.fb - posterior fossa bridgei; pa - parietal; part - prearticular; pbl - postbranchial lamina of cleithrum; pdf - posterior dorsal fontanelle; pelv - pelvic plate; pn - pectoral notch; pop - preopercular; por - postorbital process; pos.amp - ampulla of the posterior semicircular canal; ppt(i/ii) - radials I and II of the propteryigum; pq - palatoquadrate; pq.do - dermal ossifications on palatoquadrate; pr - proximal radials; pr.b - prootic bridge; prscl - presupracleithrum; ps - posterior scute; psc - posterior semicircular canal; psp - parasphenoid; qu - quadrate; r - radials; r.gass.g - recess for the gasserian

ganglia; r.lat.g - recess for the lateralis ganglia; s.su - sinus superior; sac - sacculus; scap - scapulocoracoid; scf - supracoracoid foramina; scl - supracleithrum; sn – supraneural; sop - subopercular; sp.1-2 - suprapharyngobranchial I-II; spi.g - spiracular groove of parasphenoid; spib - spirabular bar; spig - spiracular groove; spig.pq - spiracular groove of palatoquadrate; spio - spinooccipital nerve; sub - suborbital; suc - supraorbital sensory canal; sur - surangular; sy – symplectic; te – teeth; tel - telencephalon; utr - utriculus; v.fon - vestibular fontanelle; vf - ventral fissure; vmc - ventral muscle canal; zy - zygal plates.

5.2.8 Anatomical terminology

We use the conventional actinopterygian terminology for the description of the cranial bones whereby actinopterygian frontals and parietals are, respectively, homologous with sarcopterygian parietals and postparietals, following Gardiner (1984) and Gardiner & Schaeffer (1989).

5.3 Systematic palaeontology

Osteichthyes Huxley 1880

Actinopterygii Cope 1887

Genus gen. nov.

Type species spec. nov.

Etymology.

Generic diagnosis. As for species.

Species diagnosis. Actinopterygian characterised by the following combination of characters: sensory canals of skull roof running in broad canals; broad, straight ridges of ornament on the skull roof; posteroventral process of maxilla with rectangular ventral portion; ornament of maxilla consisting of ridges extending parallel to dorsal margin of maxilla; accessory operculum; distinct, tear-shaped posteroventral process of operculum; spiracular groove with spiracular bar demarcating the dorsal margin; small, circular vestibular fontanelles not connected to the otico-occipital fissure; single perforation piercing midline of dorsal aorta; lozenge-shaped basipterygoid fenestra of palatoquadrate; coronoid process solely contributed to by surangular; hyomandibula with distinct opercular process; thin, ventral process (anterior lamella) extending from anterior margin of hyomandibula; two ossified accessory hyoid elements; anterior and posterior ceratohyals; three ossified basibranchials; anterior hook-like ventral processes on ceratobranchials III and IV; posteriorly-bifurcating process on ceratobranchial V; interdorsals between neural arches.

Holotype. MM L.1696, a specimen encased in a split nodule showing the anterior two-thirds of a fish in part and counterpart. The specimen is missing the snout, anterior portion of the skull roof and lower jaw, part of the anal fin and the entire caudal fin.

Locality and horizon. Burnley, Lancashire. Precise locality unclear; one of the collieries within the Kay-Shuttleworth estate. Soapstone Bed of the Mountain Mine ‘Four Foot’ coal (also called the Union Coal in Burnley), Pennine Lower Coal Measures Formation, late Bashkirian (Langsettian substage), 318.6-317.63 Ma.

Synonyms. *Elonichthys aitkeni* – Bolton, 1895. The animal life of the Lancashire Coal Measures. *Transactions of the Manchester Microscopical Society*. p. 123-135, pl. 3, fig. 14.

Elonichthys aitkeni – Bolton, 1904. The palaeontology of the Lancashire Coal Measures. *Transactions of the Manchester Geological Society*. p. 405.

Elonichthys aitkeni – Coates, 1999. Endocranial preservation of a Carboniferous actinopterygian from Lancashire, UK, and the interrelationships of primitive actinopterygians. *Phil. Trans. R. Soc. Lond. B*. p. 438. (erroneously referred to as specimen MM L.1296.)

Mesonichthys aitkeni – Figueroa *et al.*, 2023. Exceptional fossil preservation and evolution of the ray-finned fish brain. *Nature*. p. 492.

Remarks. Since inception the taxon *Elonichthys aitkeni* was poorly defined and lacked a specified type (Traquair, 1886). A subsequent record of specimens (Woodward, 1891), which did not mention L.1696, referred additional material from a new locality in Devon, and designated one of Traquair's original specimens as the lectotype. Traquair (1901) expanded the description of the taxon—cautioning of some dissimilarly between the Devon material and the original specimens—also without reference to L.1696. The taxon was formally revised in the latter half of the 20th century, when Gardiner (1963) erected a new taxon, *Mesonichthys aitkeni*, for all of the material previously contained within *Elonichthys aitkeni*—apparently without examining any specimens outside of London (the British Museum and Geological Survey Museum, today the Natural History Museum)—and designated a specimen from Devon as the neotype. L.1696 appears to have never been formally described or included in any

systematic description of *Elonichthys* or *Mesonichthys aitkeni*. Although the genus and species diagnosis of *Mesonichthys aitkeni* is imprecise (Appendix C.4), L.1696 falls outside the genus diagnosis of *Mesonichthys* in possessing an accessory opercular and posterior process of the operculum and lacking broad ventral ridges of the scales. It also displays numerous other anatomical differences when compared with both the neotype and associated material of *Mesonichthys aitkeni*, warranting the erection of a new genus and species.

5.4 Description

5.4.1 Dermal cranial elements

Anteriorly, the specimen is damaged, preventing description of any dermal rostral bones. The skull roof and braincase are slightly dorsally displaced relative to the rest of the skull; the right side of the skull in particular has rotated dorsally. As a result, there is a gap between the skull roof elements (frontals, parietals, dermopterotic) and braincase and the other skull bones (the preopercular, opercular, dermohyal, suborbitals, maxilla, etc.) (Fig. 5.2). The frontals are rectangular with a roughly straight suture between them (fr, Fig. 5.3). Posteriorly, the suture with the parietals is also straight, although the parietals themselves have been prepared away and endochondral bone is exposed in this region of the specimen. Skull roof ornamentation consists of broad straight ridges that run antero-posteriorly. The skull roof bears a large canal for the supraorbital sensory canal (suc, Fig. 5.3), which runs largely parallel with the lateral margin of the frontal, before passing into the parietal (pa, Fig. 5.3). The dermopterotic (dpt, Fig. 5.3) is long, extending nearly the entire length of the parietals and frontals. The ornament consists of broad, singular, wavy ridges running antero-

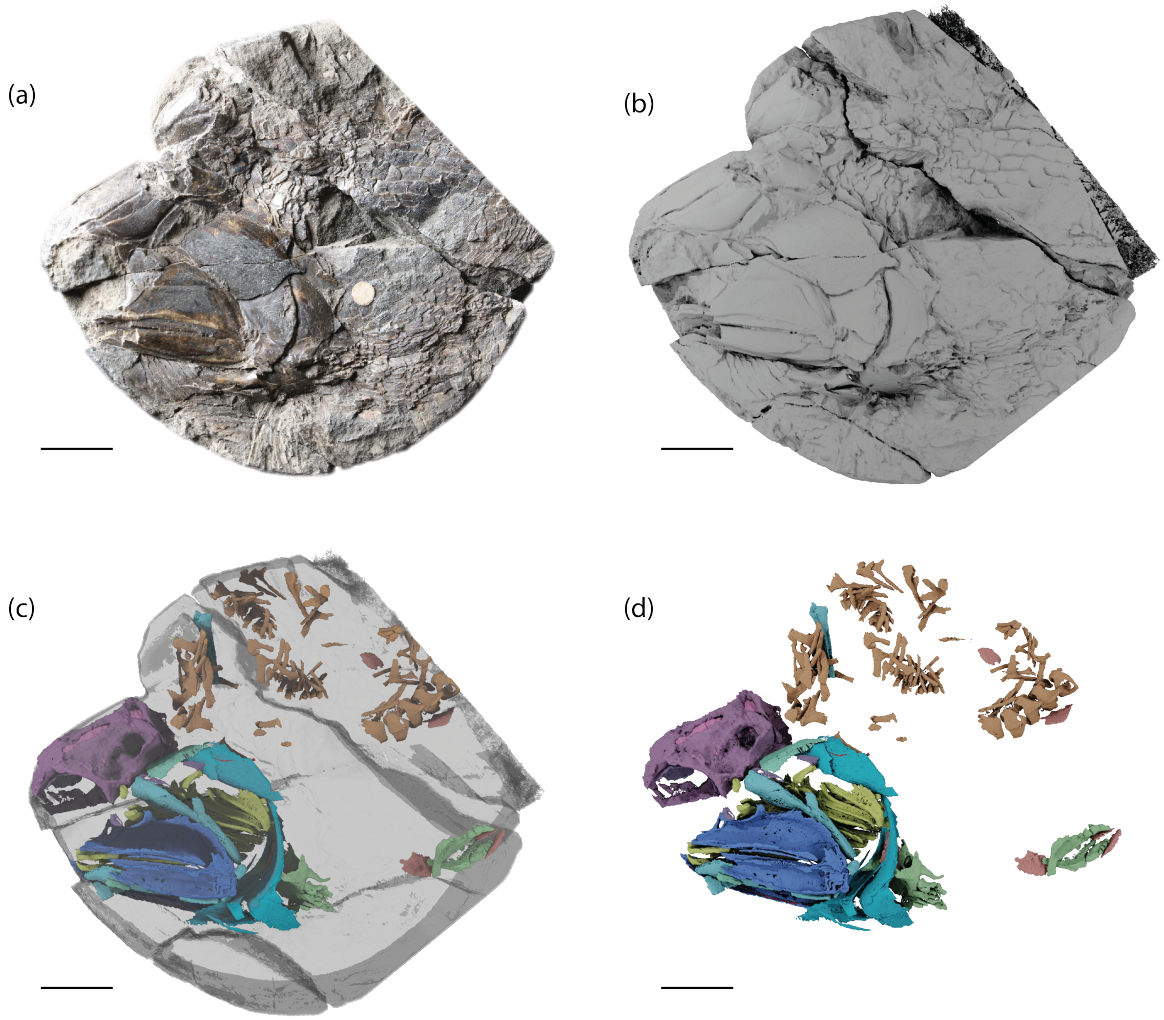


Figure 5.2: Anatomy of 'new taxon' MM L.1696: (a) Photograph of part in left lateral view, (b) 3D render of exterior in left lateral view, (c) 3D render in left lateral view with transparency enabled to show internal anatomy, (d) 3D render of internal anatomy in left lateral view. Scale bar = 10 mm. Axial skeleton – orange; braincase – lilac; endocast – pink; gill skeleton – yellow; hyoid arch – pastel light blue; jaws – dark blue; paired fin endoskeleton – green; dermal pectoral girdle – cyan; scales – brown; sensory canals – red.

posteriorly. The dermopterotic has a somewhat undulating contact with the frontal and parietal and a convex ventral margin, and would have contacted the opercular posteriorly. The otic portion of the lateral line canal is visible externally as a deep groove in the part, with the roof of the canal visible in the counterpart. Fragments of the dermosphenotic (dsph?, Fig. 5.3) are present both *in situ* just anterior to the

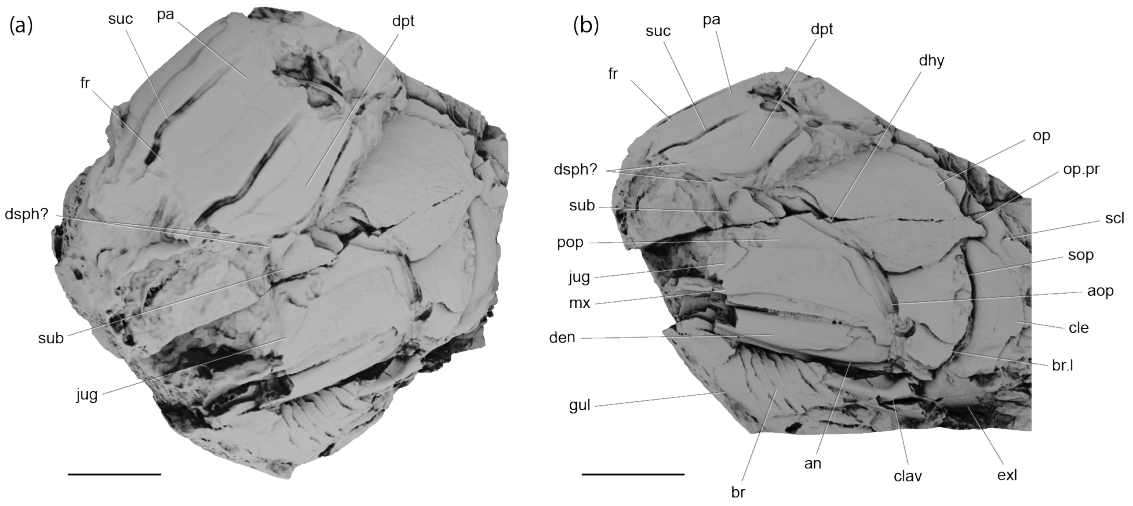


Figure 5.3: Cranium of 'new taxon' MM L.1696: (a) Skull in left anterolateral view, showing skull roof. (b) Skull in left lateral view. an - angular; aop - accessory opercular; br - branchiostegal rays; br.l – enlarged dorsal-most branchiostegal ray; clav - clavicle; cle - cleithrum; den - dentary; dhy - dermohyal; dpt - dermopterotic; dsph - dermosphenotic; exl - external lamina of cleithrum; fr - frontal; jug - jugal; mx - maxilla; op - opercular; op.pr - posterior opercular process; pa - parietal; pop - preopercular; br - branchiostegal rays; scl - supracleithrum; sop - subopercular; sub - suborbital; suc - supraorbital sensory canal. Scale bars = 10 mm.

dermopterotic, and slightly separated and anteroventral to the dermopterotic. Rounded suborbitals (sub, Fig. 5.3) are present posterior to the dermosphenotic; two appear to be present, though the exact number is difficult to ascertain due to damage. The posterior part of the jugal (jug, Fig. 5.3) is present ventral to the dermosphenotic and suborbitals. It has a slender dorsal process and a broader posterior process, which together form an embayment along the posterior edge of the jugal in which the suborbitals sit.

The preoperculum is slender and has two distinct limbs (pop, Fig. 5.3), curving around the posterodorsal corner of the maxilla. The dorsal limb widens towards the anterior tip and extends nearly all the way along the dorsal margin of the postorbital lamina of the maxilla. The ventral limb extends down the posterior margin of the maxilla. A small thin accessory operculum (aop, Fig. 5.3) is present posterior to the

ventral limb of the preoperculum, spanning the anterior junction of the operculum and suboperculum. The dermohyal (dhy, Fig. 5.3) sits between the preoperculum and operculum, with the anterior margin bounded by the suborbitals. A fragment of the dermohyal is also closely applied to the upper portion of the hyomandibular. The operculum is rhomboidal (op, Fig. 5.3b), with a distinct, tear-shaped process at the posteroventral corner (op.pr, Fig. 5.3b). The ornamentation on the opercular runs anteroposteriorly in thick, sub-parallel ridges. A crack running antero-posteriorly through the fossil has split the dermohyal and opercular in two, resulting in dorsal and ventral pieces. The dermal shoulder girdle has also pushed anteriorly into the operculogular series, and now overlies several branchiostegals ventrally, and underlays the opercular dorsally. The suboperculum (sop, Fig. 5.3), which is smaller than the operculum and is also ornamented in sub-parallel, sometimes wavy ridges, has sustained some damage posteriorly. At the anteroventral margin of the suboperculum is an enlarged branchiostegal ray, approximately a quarter of the depth of the suboperculum and more than twice the depth of any other branchiostegal (br.l, Fig. 5.3). A series of branchiostegal rays (br, Fig. 5.3) are present in MM L.1696, though are interrupted just ventral to the posterior region of the lower jaw by the clavicle, which has been pushed slightly anteriorly and externally. The series of branchiostegal rays anterior to the clavicle are all long, thin, overlapping bones, whereas posterior and dorsal to the interrupting clavicle, the branchiostegal rays are shorter. Anterior to the branchiostegal rays there may be a long lateral gular (gul, Fig. 5.3), an impression of which is present in the counterpart.

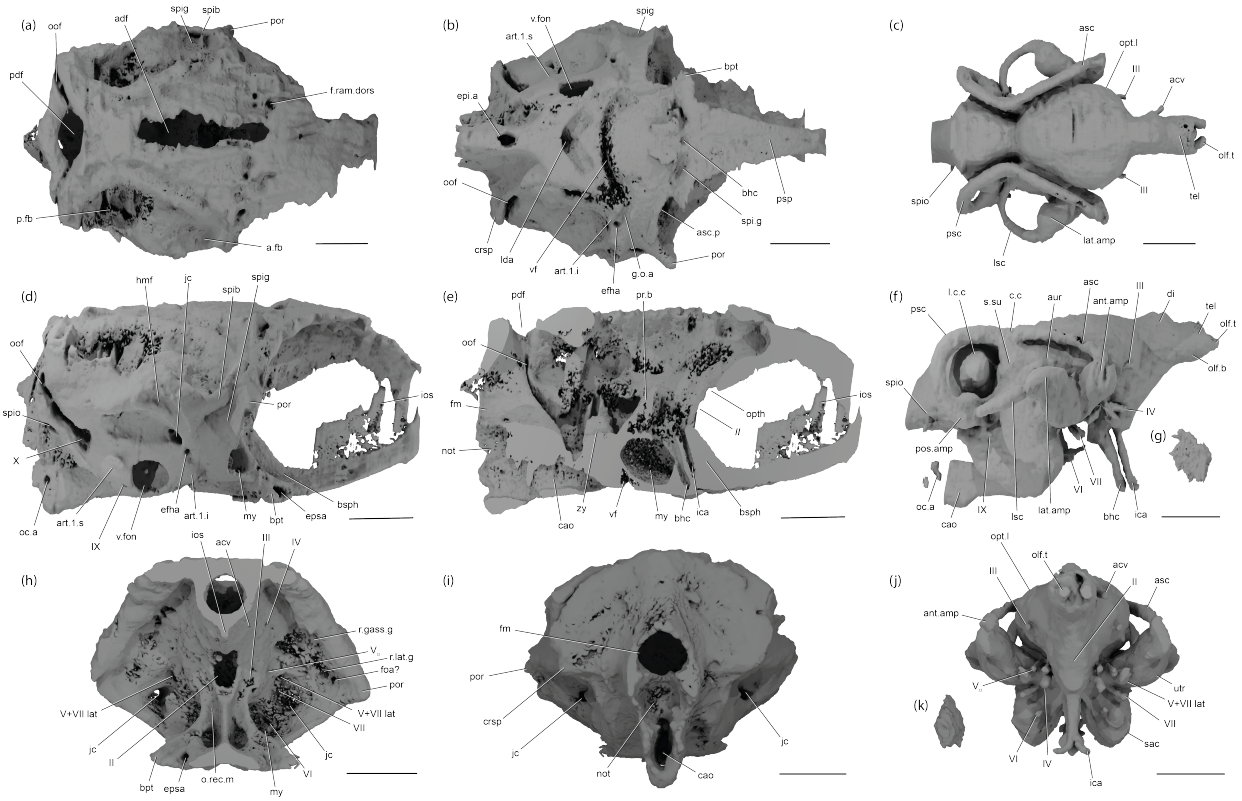


Figure 5.4: Braincase of ‘new taxon’ MM L.1696: (a) dorsal, (b) ventral, (d) right lateral, (e) sagittal, (h), anterior, and (i) posterior view. Endocast: (c) dorsal, (f) right lateral, and (j) anterior view. Otolith removed from within the utriculus: (g) lateral and (k) anterior view. II - optic nerve; III - oculomotor nerve; IV - trochlear nerve; V+VII lat - trigeminal and lateral branch of facial nerve; VO - profundus nerve; VI - abducens nerve; VII - facial nerve; IX - glossopharyngeal nerve; X - vagus nerve; a.fb - anterior fossa bridgei; acv - anterior cerebral vein; adf - anterior dorsal fontanelle; ant.amp - ampulla of the anterior semicircular canal; art.1.i - articulation of infrapharyngobranchial I; art.1.s - articulation of suprapharyngobranchial I; asc - anterior semicircular canal; asc.p - ascending process; aur - cerebellar auricles; bhc - buccohypophyseal canal; bpt - basipterygoid process; bsph - basisphenoid; c.c - crus commune; cao - canal for the dorsal aorta; crsp - craniospinal process; di - diencephalon; epi.a - epibranchial artery; epsa - efferent pseudobranchial artery; f.ram.dors - foramina for branches of the ramus ophthalmicus; fm - foramen magnum; foa - foramen for orbital artery; g.o.a - groove for the orbital artery; hmf - hyomandibular facet; hy.o.a - hyo-opercular artery; ica - internal carotid artery; ios - interorbital septum; jc - jugular canal; l.c.c - lateral cranial canal; lat.amp - ampulla of the lateral semicircular canal; lda - lateral dorsal aorta; lsc - lateral semicircular canal; my - myodome; not - notochord; o.a - orbital artery; o.rec.m - superior, inferior, internal recti muscles; oc.a - occipital artery; olf.b - olfactory bulb; olf.t - olfactory tract; oof - otoccipital fissure; opt.l - optic lobes; opth - ophthalmic artery; p.fb - posterior fossa bridgei; pdf - posterior dorsal fontanelle; por - postorbital process; pos.amp - ampulla of the posterior semicircular canal; pr.b - prootic bridge; psc - posterior semicircular canal; psp - parasphenoid; r.gass.g - recess for the gasserian ganglia; r.lat.g - recess for the lateralis ganglia; s.su - sinus superior; sac - sacculus; spi.g - spiracular groove of parasphenoid; spib - spiracular bar; spig - spiracular groove; spio - spinooccipital nerve; tel - telencephalon; utr - utriculus; v.fon - vestibular fontanelle; vf - ventral fissure; zy - zygal plates. Scale bar = 3 mm.

5.4.2 Braincase

The braincase of L.1696 is ossified as a single unit that is almost completely mineralised. The occipital region can be distinguished from the otic region by a partial otico-occipital fissure (oof, Fig. 5.4a, 5.4b, 5.4d, 5.4e), but the fissure is incomplete ventrally so that the regions are co-ossified. Similarly, the ventral fissure only partially separates the otic region from the basisphenoid and orbitotemporal regions (vf, Fig. 5.4b, 5.4d). The ethmoid region of the braincase is unmineralised.

The orbital region is generally well ossified. The interorbital septum (ios, Fig. 5.4d, 5.4e, 5.4h) has only a short dorsal component and thin ventral component, resulting in a large unossified area between the orbits. Dorsally, the portion of the braincase anterior to the pineal opening has been manually prepared, so the extent of the supraorbital shelves, and whether they were pierced by any canals, cannot be determined. A single large, oval opening piercing the interorbital septum transmitted the optic nerves (nerve II; II, Fig. 5.4e, 5.4h). The dorsal portion of this opening is developed as a broad notch, and the ophthalmic arteries (opth; Fig. 5.4e) likely entered the orbit here. Immediately lateral to the opening for the optic nerves are two foramina for the branches of the oculomotor nerve (nerve III; III, Fig. 5.4h). The trochlear nerve (nerve IV; IV, Fig. 5.4h) opens high on the orbital wall, some way dorsal to the oculomotor nerve, as does the anterior cerebral vein (acv, Fig. 5.4h).

The posterior orbital wall is fairly flat, rather than deeply concave, and is framed by the postorbital processes (por, Fig. 5.4a, 5.4b, 5.4d, 5.4h, 5.4i). The posteromedial corner of the orbit houses the posterior myodome (my, Fig. 5.4d, 5.4e, 5.4h), which contained the external recti muscles, and is developed as a single cavity that extends

across the midline. The prootic bridge extends dorsally, partially enclosing the saccus vasculosus and forming the posterior wall of the pituitary (pr.b, Fig. 5.4e). The posterodorsal wall of the posterior myodome bears a small foramen for the abducens nerve (nerve VI; VI, Fig. 5.4e); the ventral surface has no foramina. Lateral to the posterior myodome is the anterior opening of the enclosed jugular canal (jc, Fig. 5.4h). Several smaller foramina are also present for the profundus nerve (V_o; V_o, Fig. 5.4h), the middle cerebral vein (mcv; Fig. 5.4h), the trigeminal and lateral branch of the facial nerve (nerve V+VII lat; V+VII lat, Fig. 5.4h) and the facial nerve (nerve VII; VII, Fig. 5.4h). The facial nerve opens into the medial wall of the jugular canal. The trigeminal nerve and lateral branch of the facial nerve enter the orbit together in a small depression (the trigeminofacialis chamber) dorsomedial to the jugular canal, and the middle cerebral vein opens just above this, but only on the left side of the orbit. A third canal, medial to both of these, transmits the profundus.

Dorsal and lateral to the anterior opening of the jugular canal are two shallow recesses, likely for the gasserian (r.gass.g, Fig. 5.4h) and lateralis ganglia (r.lat.g, Fig. 5.4h; cf. *Lawrenciella*; Pradel *et al.*, 2016: fig. 4). No depression is present ventral to the jugular canal for the geniculate ganglion, likely due to the proximity of the jugular to the posterior myodome. The lateral depression may also contain a foramen for the orbital artery (foa?; Fig. 5.4h).

Although co-ossified with the rest of the braincase, the basisphenoid (bsph, Fig. 5.4d, 5.4e) can be clearly differentiated. Stout anterolaterally-directed struts extend from the pars basiphenoid to the lateral margin of the braincase and mark the anterior boundary of the posterior myodome. A depression for the superior, inferior and internal recti muscles lies between the strut and pars basisphenoid (o.rec.m, Fig. 5.4d, 5.4h),

and is continuous with the posterior myodome. Its medial wall is also pierced by a branch of the internal carotid artery. The endoskeletal basipterygoid processes are short (bpt, Fig. 5.4b, 5.4d, 5.4h). A foramen for the efferent pseudobranchial arteries (epsa, Fig. 5.4d, 5.4h), which connects to the internal carotid, is present anteromedial to the basipterygoid process.

Much of the dorsal face of the braincase is occupied by the anterior and posterior dorsal fontanelles and the anterior and posterior fossa bridgei, but is generally complete and well mineralised. The anterior dorsal fontanelle (adf, Fig. 5.4a, extends from the orbits to the anterior margin of the posterior fossa bridgei. The epiphysial part of the fontanelle is marked by a constriction in its anterior third. There is no clear median ridge anterior to the fontanelle, though there is a shallow depression and a multiple foramina lateral to the epiphysis, likely for branches of the ramus ophthalmicus superficialis trigemini, the ramus ophthalmicus lateralis and vessels (f.ram.dors, Fig. 5.4a). A shallow anterior fossa bridgei (a.fb; Fig. 5.4a) is developed posteromedial to the postorbital process on the dorsal face of the braincase. There is no pre-spiracular fossa. A faint ridge forms a broad semicircle on the dorsal surface lateral to the anterior fontanelle, extending from the posterior margin of the orbit to the otico-occipital fissure (Fig. 5.4a, 5.4d). This ridge runs roughly parallel and medial to the posterior and anterior semicircular canals. Another, more lateral ridge follows the lateral margin of the semicircular canals from the anterior fossa bridgei (a.fb, Fig. 5.4a) to the posterior fossa bridgei (p.fb, Fig. 5.4a). The posterior fossa bridgei is developed as a single, circular depression and large and deep. Its posteromedial walls are thin, but the fossa bridgei does not connect to cranial cavity.

The otic region of the braincase extends from the postorbital process to the otico-ocippital fissure and ventrally to the vestibular fontanelles. The lateral face of the postorbital process bears the spiracular groove (spig, Fig. 5.4a, 5.4b, 5.4d). Rather than an enclosed spiracular canal, a thick posteroventrally directed bar (spib; Fig. 5.4a, 5.4d) demarcates the top of the spiracular groove. A facet for articulation of the hyomandibula lies at the posterior margin of this bar, on the back of the postorbital process (hmf, Fig. 5.4d). Beneath the facet for the hyomandibula is a large groove for the jugular vein which becomes an enclosed canal anteriorly (jc, Fig. 5.4d). Ventral to the jugular vein canal is a small foramen for the efferent hyoid artery (efha, Fig. 5.4b, 5.4d). The external groove for the efferent hyoid artery (efha, Fig. 5.4b, 5.4d) curves around a small lateral extension for the articulation of the first infrapharyngobranchial (art.1.i, Fig. 5.4b, 5.4d) to reach the ventral fissure (vf, Fig. 5.4b, 5.4e). A lateral extension of the braincase which generally conforms to the shape of the posterior and lateral semicircular canals of the endoskeletal labyrinth overhangs the groove for the jugular. The vestibular fontanelles (v.fon, Fig. 5.4b, 5.4d) are small and almost circular, opening laterally from the braincase separate from the ventral fissure and (externally separate) from the otico-occipital fissure. A foramen for the exit of the glossopharyngeal nerve (nerve IX; IX, Fig. 5.4d) is present on the right side of the braincase, posterior to the jugular groove. Two articulatory facets for the first suprapharyngobranchial are present on the lateral surface of the braincase (art.1.s, Fig. 5.4b, 5.4d), posterodorsal to the vestibular fontanelle. The dorsal facet is horizontal and slightly crescentic, while the ventral one is simply round.

The posterior dorsal fontanelle and otico-occipital fissure separate the otic and occipital regions of the braincase. The fontanelle is small and ovoid (pdf, Fig. 5.4a,

5.4e). The otico-occipital fissure runs from the lateral margins of the posterior dorsal fontanelle anteroventrally, however the fissure is only continuous internally (oof, Fig. 5.4e). An opening for the vagus nerve (nerve X; X, Fig. 5.4d) exits the braincase in the occipital fissure posteroventrally roughly halfway down between the dorsal and ventral margin of the braincase. The opening for the vagus nerve is much clearer externally on the right side of the braincase, and this is also where the fissure terminates externally.

The foramen magnum is marginally taller than wide, and is larger than the circular entrance for the notochord (fm, Fig. 5.4e, 5.4i). A subtle median crest extends dorsally from the foramen magnum. The notochordal canal is conical and short, terminating within the occipital region level to the posterior dorsal fontanelle (not, Fig. 5.4e, 5.4i). Both the floor and ceiling of the notochordal canal are incomplete on the midline, so the foramen magnum, notochord and dorsal aorta are all continuous posteriorly. A small foramen lateral to the foramen magnum marks the exit of the spino-occipital nerve (spio, Fig. 5.4d). The posterior opening for the dorsal aorta is much taller than wide, though constricts to a rounded, enclosed canal (cao, Fig. 5.4e, 5.4i). A foramen for the occipital artery exits the lateral wall of the dorsal aorta near its posterior margin (oc.a, Fig. 5.4d). A single midline opening for the epibranchial arteries perforates the aortic canal about halfway along its length (epi.a, Fig. 5.4b). Anteriorly, the dorsal aorta bifurcates into the lateral dorsal aortae just posterior to the ventral fissure (lda, Fig. 5.4b), and the grooves for the lateral aortae are very short. The v-shaped median zygal plates are present within the neurocranium above the bifurcation of the dorsal aorta (zy, Fig. 5.4e). Lateral to the midline openings, the posterior face of the occiput is broadly concave, developed into shallow depressions for the trunk

musculature. Modest craniospinal processes form the lateral limit of these depressions (crsp, Fig. 5.4b, 5.4i).

5.4.3 Parasphenoid

The parasphenoid (psp; Fig. 5.4b) is thin anteriorly, edentulous and tightly bound to the neurocranium. The bucco-hypophyseal canal (bhc; Fig. 5.4b) pierces the ventral surface of the parasphenoid, in between the (parasphenoid) spiracular grooves (spi.g, Fig. 5.4b) which run dorsally along long, broad ascending processes (asc.p; Fig. 5.4b). The ascending processes extend around the posterior margin of the orbit. Posterior to the ascending processes is a posterior projection that is narrower than the main body of the parasphenoid, which ends as two short paired posteriorly-directed processes separated by a shallow groove across the midline. No toothplates are present posterior to the parasphenoid.

5.4.4 Endocast

The forebrain region of the endocast of L.1696 is narrow and lacks distinctive olfactory bulbs, though the telencephalon (tel, Fig. 5.4f) has a very slight dorsal bulge which may represent the olfactory bulbs (olf.b, Fig. 5.4c, 5.4f, 5.4j). The posterior-most section of very narrow paired olfactory tracts (where they join the telencephalon) are present (olf.t, Fig. 5.4c, 5.4f, 5.4j), emanating anteriorly from the forebrain region. Another small dorsal bulge in the forebrain region may differentiate the diencephalon (di, Fig. 5.4f) from the telencephalon (though this is where the neurocranium is open through the anterior-most/epiphysial region of the anterior dorsal fontanelle). The unpaired anterior cerebral vein emerges from the lateral margin of the left side of the endocast (acv, Fig. 5.4c, 5.4j), exiting through the dorsal interorbital septum.

The endocast expands significantly, both laterally and ventrally, posterior to the telencephalon. The ventral expansion is the beginning of the hypophyseal region and opens into the orbit through the optic nerve foramen anteriorly (II, Fig. 5.4j). The oculomotor nerve (nerve III; III, Fig. 5.4c, 5.4j) leaves the middle of the lateral wall of the endocast to exit through the postorbital wall. Posterior to the optic nerve foramen and ventral to the oculomotor nerve, the trochlear nerve (IV, Fig. 5.4j) emerges laterally from the hypophyseal recess. Only a single canal exits the right side of the endocast, which subsequently bifurcates before reaching the postorbital wall (Fig. 5.4f, 5.4j), whereas the left trochlear nerve has two roots exiting the endocast. Ventrally, the buccohypophysial canal (bhc, Fig. 5.4f) and internal carotid (ica, Fig. 5.4f) extend ventrally in parallel. The internal carotid bifurcates ventrally (Fig. 5.4j), though whether this bifurcation represents paired branches of the internal carotid prior to the splitting of this vessel into the efferent pseudobranchial artery and the palatine nerve is uncertain. Behind the internal carotid the buccohypophysial canal diverges from the pituitary region of the endocast, which also opens ventrally into the posterior myodome via the pituitary fontanelle. The buccohypophysial canal does not enter the posterior myodome anteriorly, instead, it only opens into the myodome through the pituitary fontanelle in the anterior roof of the posterior myodome (bhc, Fig. 5.4e).

The lateral expansion of the endocast is due to large, rounded optic lobes (opt.l, Fig. 5.4c) in the mesencephalon, which roughly double the width of the endocast relative to the forebrain. No groove separates the optic lobes. The dorsal margin of the mesencephalon opens into the anterior dorsal fontanelle, which runs approximately the length of the mesencephalon.

Posterior to the optic lobes, small cerebellar auricles (aur, Fig. 5.4f) project laterally occupying the space within the anterior semicircular canal (asc, Fig. 5.4c, 5.4f, 5.4j) posterior to the ampulla of the anterior SSC and roughly adjacent to the ampulla of the lateral SSC (lsc, Fig. 5.4c, 5.4f). The auricles are only slightly separated from the optic lobes and bear no ridges demarcating the location of the middle cerebral vein or longitudinal dorsal vein. The profundus (nerve V_0) projects from the endocast below the cerebellar auricles, and the trigeminal and lateralis (nerves V and VII lat) and facial (nerve VII) nerve canals extend lateral to the profundus (Fig. 5.4f, 5.4j).

All of the semicircular canals are separate from the main body of the endocast. The posterior (psc, Fig. 5.4c, 5.4f) and lateral semicircular canals (lsc, Fig. 5.4c, 5.4f) are both short and curved, whereas the anterior semicircular canal is flatter and less curved (asc, Fig. 5.4c, 5.4f, 5.4j). The anterior and posterior canals extend above the dorsal limit of a very constricted portion of the hindbrain region of the endocast, so that the crus commune is dorsal to the endocast roof. The ampulla of the anterior SSC (ant.amp, Fig. 5.4f) joins the antero-dorsal portion of the rounded utricular recess (utr, Fig. 5.4j), while the ampulla of the lateral SSC (lat.amp, Fig. 5.4c, 5.4f) joins the postero-dorsal region of the utriculus. The sinus superior (s.su, Fig. 5.4f) lies above a relatively large sacculus (sac, Fig. 5.4f, 5.4j), from which the abducens nerve (nerve VI; Fig. 5.4f, 5.4j) emanates anteriorly (entering the posterior myodome) and the glossopharyngeal nerve (nerve IX; Fig. 5.4f) emanates laterally (in the posterior half of the sacculus). The sinus superior and cerebellar auricles are confluent. An otolith with a rounded medial margin and flat if not marginally concave lateral face, is present within the right sacculus (Fig. 5.4g & 5.4k). While the utriculus (utr, Fig. 5.4j) is

confluent with the sacculus (sac, Fig. 5.4j) posteriorly, there is a large groove separating the two pouches anteriorly.

Posterior to the crus commune (c.c, Fig. 5.4c, 5.4f), the endocast expands again following the constriction level with the crus commune, eventually opening dorsally into the posterior dorsal fontanelle and laterally into the lateral cranial canal (l.c.c, Fig. 5.4f). The lateral cranial canal projects within the curve of the posterior SSC above the ampulla of the posterior SSC (pos.amp, Fig. 5.4f). The endocast then sharply constricts towards the foramen magnum. In this region, the spino-occipital nerve (spio, Fig. 5.4c, 5.4f) emerges from the ventrolateral region of the endocast exiting through the walls of the foramen magnum. Ventral to the foramen magnum, the insertion of the notochord into the braincase is very short, terminating just ventral to the spino-occipital nerves. Ventral to the notochord, two canals for the occipital arteries (oc.a, Fig. 5.4f) branch off from the lateral walls of the dorsal aorta (cao, Fig. 5.4f) and exit the braincase walls.

5.4.5 Upper jaws and palate

The maxilla is cleaver-shaped, with a narrow suborbital portion and a broad postorbital lamina (mx, Fig. 5.2). The most anterior part of the maxilla is missing, however. The dorsal margin of the postorbital lamina is flat and straight, before curving steeply after the posterodorsal corner. A posteroventral extension of the maxilla, which has a rectangular ventral portion, slightly overlaps the lower jaw. This, plus a slight ventral flexion below the suborbitals, gives the ventral margin of the maxilla a slight S-shape. The ornamentation consists of fine antero-posterior striations and short ridges that curve in the posterior half of the maxilla.

The palatoquadrate is a single element extending the entire length of the upper jaw (pq, Fig. 5.5a, 5.5b). Although continuously ossified, the palatoquadrate is very thin (except in the quadrate region) and is hard to separate from the dermal ossifications that sheath its medial surface; these dermal bones seem to be formed from a single ossification extending along the ventral margin of the palatoquadrate (pq.do, Fig. 5.5b). Overall, the palatoquadrate has a broad postorbital region with a convex dorsal margin that broadly tracks that of the maxilla, while the ventral margin of the whole bone is slightly concave where it contacts the maxilla; it also has a concave lateral face. The ventral margin of the palatoquadrate has a distinct lateral shelf that reaches the maxilla. Anteriorly, the palatoquadrate curves distinctly towards the midline. The medial surface of the autopalatine region contacts the accessory vomers (av, Fig. 5.5b). There are two accessory vomers on each side, the more anterior is elongate and rectangular while the more posterior is shorter and ovoid.

The anterior half of the palatoquadrate has two processes separated by a curved embayment. A large dorsally and medially directed process frames a lozenge-shaped basipterygoid fenestra (bpf, Fig. 5.5a, 5.5b). Behind the basipterygoid fenestra, the embayment is long and bounded posteriorly by a thin, partially ossified region of the palatoquadrate. It is unclear, however, whether this is truly a process or whether the bone is incompletely ossified in the dorsal metapterygoid region. The latter may be indicated in this specimen by a gap between the anterior metapterygoid region of the

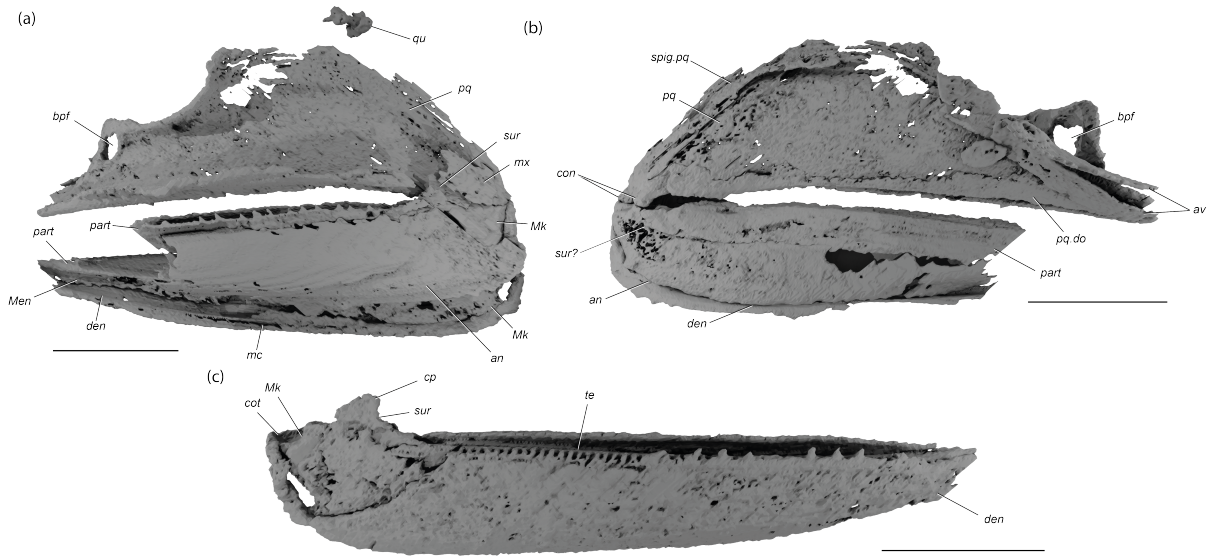


Figure 5.5: Jaws and palate of 'new taxon' MM L.1696: (a) all jaw and palatal bones (excluding maxilla) in left lateral view (b) left lower jaw and palate in medial view (c) right lower jaw in right lateral view. an - angular; av - accessory vomer; bpf - basipterygoid foramen; con - articulatory condyles; cot - articulatory cotyles; cp - coronoid process; den - dentary; Men - mentomeckelian; mc - mandibular canal; Mk - Meckelian; mx - maxilla; part - prearticular; pq - palatoquadrate; pq.do - dermal ossifications on palatoquadrate; qu - quadrate; spig.pq - spiracular groove of palatoquadrate; sur - surangular; te - teeth. Scale bar = 5 mm.

palatoquadrate and the anterior limb of the hyomandibular. The top of the palatoquadrate bears a distinct spiracular groove (spig.pq, Fig. 5.5b) that runs from the dorsal process right to the posteroventral edge. There is no extension of the metapterygoid region dorsal to the spiracular groove. It is unclear whether small concavities in the posterodorsal margin of the palatoquadrate are the result of preservation, incomplete ossification or represent canals for the internal mandibular branch of the facial nerve (cf. Gardiner, 1984: fig. 55, 56). Posteriorly, the palatoquadrate contacts the medial wall of the maxilla (mx, Fig. 5.5a), as well as the interhyal. Posteroventrally it contacts the articular region of the Meckel's cartilage of the lower jaw via two distinct condyles (con, Fig. 5.5b). Anterior to these condyles is

an opening for the adductor fossa. Denticles appear to be absent on the palatoquadrate and accessory vomers and other toothplates.

5.4.6 Lower jaws

The dentary comprises most of the lower jaw (den, Fig. 5.5), although the anterior portion of the left dentary is damaged. From the right dentary (Fig. 5.5c) it is clear that the dentary tapers slightly rostrally and that it bears small teeth (te, Fig. 5.5c) on the oral margin posteriorly, with larger teeth anteriorly. Ornament on the dentary consists of irregular longitudinal ridges. The mandibular canal tracks the ventral margin of the dentary along the entire length, before sharply turning dorsally at the posterior edge. A groove lies just above the mandibular canal on the internal surface of the dentary and there is a horizontal shelf on the medial face of the dentary in the anterior half of the bone. There is a single Meckelian ossification medial to the dentary (Mk, Fig. 5.5a) which extends anteriorly more than half the length of the dentary and is particularly robustly ossified posteriorly where it bears two cotyles for articulation with the condyles on the palatoquadrate (cot, Fig. 5.5c). Anterior to the Meckelian there is a large mentomeckelian ossification that reaches the anterior margin of the lower jaw (Men, Fig. 5.5a). The prearticular is long and blade-like, curving slightly medially and ventrally towards the anterior end. It overlies the mentomeckelian anteriorly and extends posteriorly to reach the articular region of the Meckelian. On the lateral face of the prearticular is a horizontal shelf where the bone articulates with the corresponding shelf of the dentary. The ventral margin of the posterior half of the prearticular abuts the dorsal margin of the Meckelian. The angular (an, Fig. 5.5) has a much longer ventral portion than dorsal and extends reasonably far along the ventral margin of the lower jaw (about halfway along what is preserved of the dentary – this is based on what

appears to be a suture on the exterior of the fossil, however no such suture is present on the right dentary within the rock matrix (possibly due to scan resolution not being high enough to detect the suture). Anteriorly, the angular forms an S-shaped suture with the dentary. Posteriorly, the angular is rounded, and the dorsal portion is overlain by the maxilla. A surangular is present and bears a coronoid process dorsally. At the posterior end of the lower jaw the small adductor fossa is bounded by the surangular and short coronoid process laterally (cp, Fig. 5.5c), the articular region of the Meckelian posteriorly, and the prearticular anteriorly and medially.

5.4.7 Hyoid and gill skeleton

The left hyomandibular is fully preserved roughly *in situ*, whereas the right hyomandibular is broken (with the dorsal part missing) and displaced dorsally. The hyomandibular has two distinct dorsal and ventral portions (hmd, Fig. 5.6a, 5.6c). The ventral limb is much more slender than the dorsal limb, which gradually splays out anterodorsally. A very distinct opercular process is much larger than in many other actinopterygians (opc, Fig. 5.6a, 5.6c). On the medial surface of the hyomandibular, a ridge with an associated groove runs from the opercular process to the ventral margin of the dorsal limb near to top of the bone. This groove likely held the hyomandibular trunk of the facial nerve (VIIfhm, Fig. 5.6b). A very thin splint of bone forms a ventral process extending ventrally from the ventral margin of the hyomandibula where the dorsal and ventral limbs meet (hm.vp; Fig. 5.6c). No perforations are apparent on the hyomandibular.

Two intermediate ossified elements link the hyomandibula (dorsal component) and the ceratohyal (ventral component) in the hyoid arch. These elements appear to

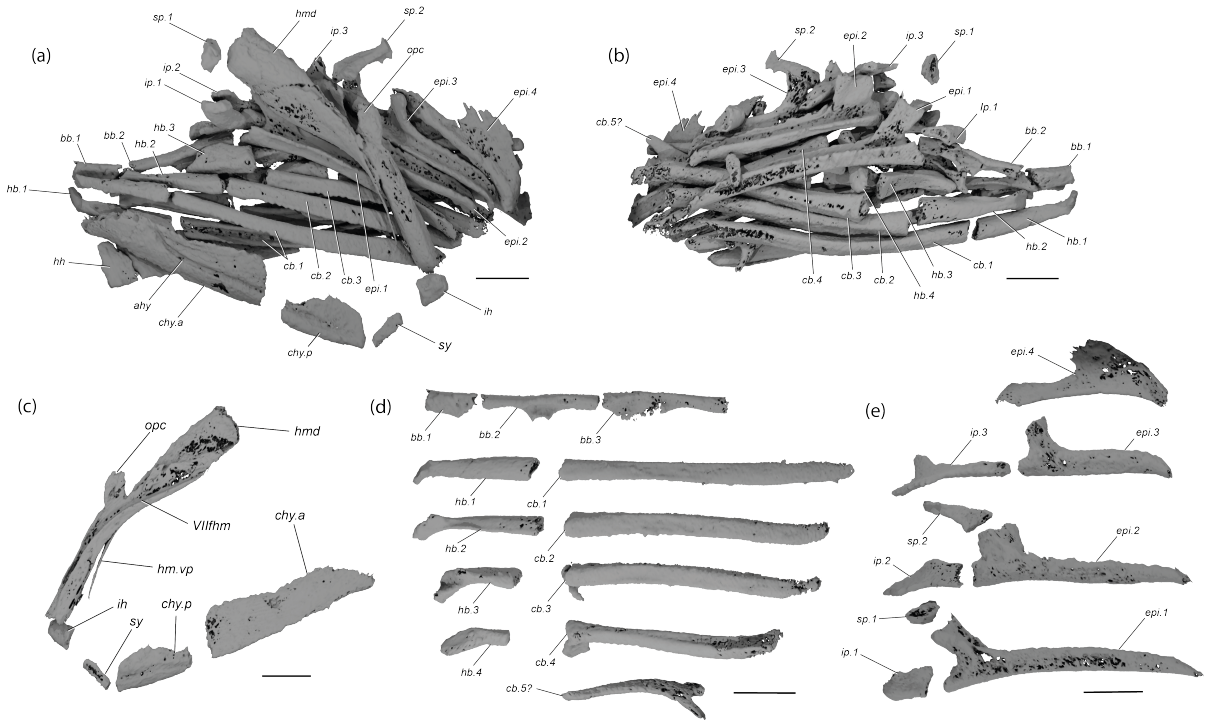


Figure 5.6: The hyoid and gill skeleton of ‘new taxon’ MM L.1696: (a) hyoid and gill together as preserved in left lateral view, (b) gill skeleton as preserved in right lateral view, (c) isolated hyoid arch in right lateral view, (d) basibranchials, hypobranchials and ceratobranchials separated in lateral view, (e) epibranchials, infrapharyngobranchials and suprapharyngobranchials separated in lateral view. VIIfhm - hyomandibular branch of facial nerve; ahy - groove for the afferent hyoid artery; bb.1-3 - basibranchial I-III; cb.1-5 - ceratobranchial I-V; chy.a - anterior ceratohyal; chy.p - posterior ceratohyal; epi.1-4 - epibranchials I-IV; hb.1-3 - hypobranchial I-III; hh - hypohyal; hm.vp - ventral process of hyomandibular; hmd - hyomandibula; ih - interhyal; ip.1-3 - infrapharyngobranchial I-III; opc - opercular process; sp.1-2 - suprapharyngobranchial I-II; sy - symplectic. Scale bar = 3 mm.

be arranged in a dorsoventral series rather than subparallel. We term the more dorsal of these elements (sitting just beneath the ventral limb of the hyomandibula) the interhyal (ih, Fig. 5.6a, 5.6c) and the ventral element (which lies medial to the posterior margin of the lower jaw) the symplectic (sy, Fig. 5.6a, 5.6c), while noting difficulties in assigning homologous names to accessory hyoid elements (Argyriou *et al*., 2022). The interhyal is stout and slightly cylindrical, albeit with a slight curvature, while the symplectic is thin and rod-like. The symplectic extends anteroventrally to almost

contact the posterior margin of the posterior ceratohyal. As preserved, the interhyal contacts the posterior tip of the palatoquadrate and the posterior-most part of the lower jaw separates the interhyal and the symplectic (Fig. 5.7).

Two ceratohyals are present, a posterior (chy.p, Fig. 5.6a, 5.6c) and anterior (chy.a, Fig. 5.6a, 5.6c) ceratohyal. Both ceratohyals are plate-like and have grooves running along the lateral surfaces for the afferent hyoid artery (ahy, Fig. 5.6a). The anterior ceratohyal is more than twice the length of the posterior and curves medially in the anterior half. The lateral groove of the posterior ceratohyal closely tracks the ventral margin of the bone, while that of the anterior ceratohyal arches anteriorly to reach the dorsal margin anteriorly. The anterior portion of the left anterior ceratohyal is missing, which also means that the left hypohyal is missing. Part of the right hypohyal is present immediately anterior to the anterior ceratohyal (hh, Fig. 5.6a), though appears to also be damaged anteriorly such that any bend in the bone to the contact the anterior basibranchial is missing.

Three ossified basibranchials are present. The anterior basibranchial (bb.1, Fig. 5.6d) is by far the shortest due to damage, being broken at the anterior end of the specimen in line with the break on the suborbital ramus of the maxilla; it is less than half the length of the second (bb.2, Fig. 5.6d) and third (bb.3, Fig. 5.6d). No clear articulatory facets are present on the anterior surface of basibranchial 1 due to damage. The two subsequent basibranchials are roughly equal in length. All three basibranchials have flat dorsal surfaces, but ventral extensions on the ventral surfaces. The anterior basibranchial has a very gradual ventral extension such that the bone is broadly triangular in cross-section, while on the second and third basibranchials the extension is much more of a distinct ridge. On basibranchial 2 this ridge protrudes

sharply in the middle (antero-posteriorly) of the bone and has a concave ventral margin forming a facet for articulation with hypobranchial 3. The ridge on basibranchial 3, in contrast, begins and extends furthest ventrally in the anterior part of the bone before gradually sloping back to meet the main body in the posterior half. In anterior view/transverse view, however, the ridge rises sharply, with concave embayments on either side for articulation with hypobranchial 4. In dorsal view the anterior basibranchial has parallel lateral margins. The second basibranchial, however, constricts in the anterior half before extending convexly again in the posterior half and finally constricting again posteriorly; this gives a vague S-shape to the lateral extent of this basibranchial. The third basibranchial has a simpler dorsal profile, simply tapering posteriorly in the anterior half and remaining of consistent width in the posterior half.

The first hypobranchials (hb.1, Fig. 5.6a, 5.6b, 5.6d) are slender, though gradually increase in width posteriorly until they reach the posterior margin, with is flat and serves at the point of articulation with ceratobranchial I (Fig. 5.7). Anteriorly, the bones narrow and deflect medially to curve around basibranchial I. The ventral surface of hypobranchial I is slightly concave. The second set of hypobranchials (hb.2, Fig. 5.6a, 5.6b, 5.6d) articulate with the basibranchials between the first and second basibranchials (Fig. 5.7). Their morphology is similar to hypobranchial I, though they are broader and have a more robust and less deflected anterior region with two clear articular processes at the anterior tip, as well as a small third process on the dorsal surface where the bone deflects medially. The ventral concavity of hypobranchial II results in two clear ridges along the length of the bone behind the anterior articulatory region. The posterior tip of hypobranchial II is also in nearly direct communication with ceratobranchial II by means of a flat articulatory surface. The third hypobranchials

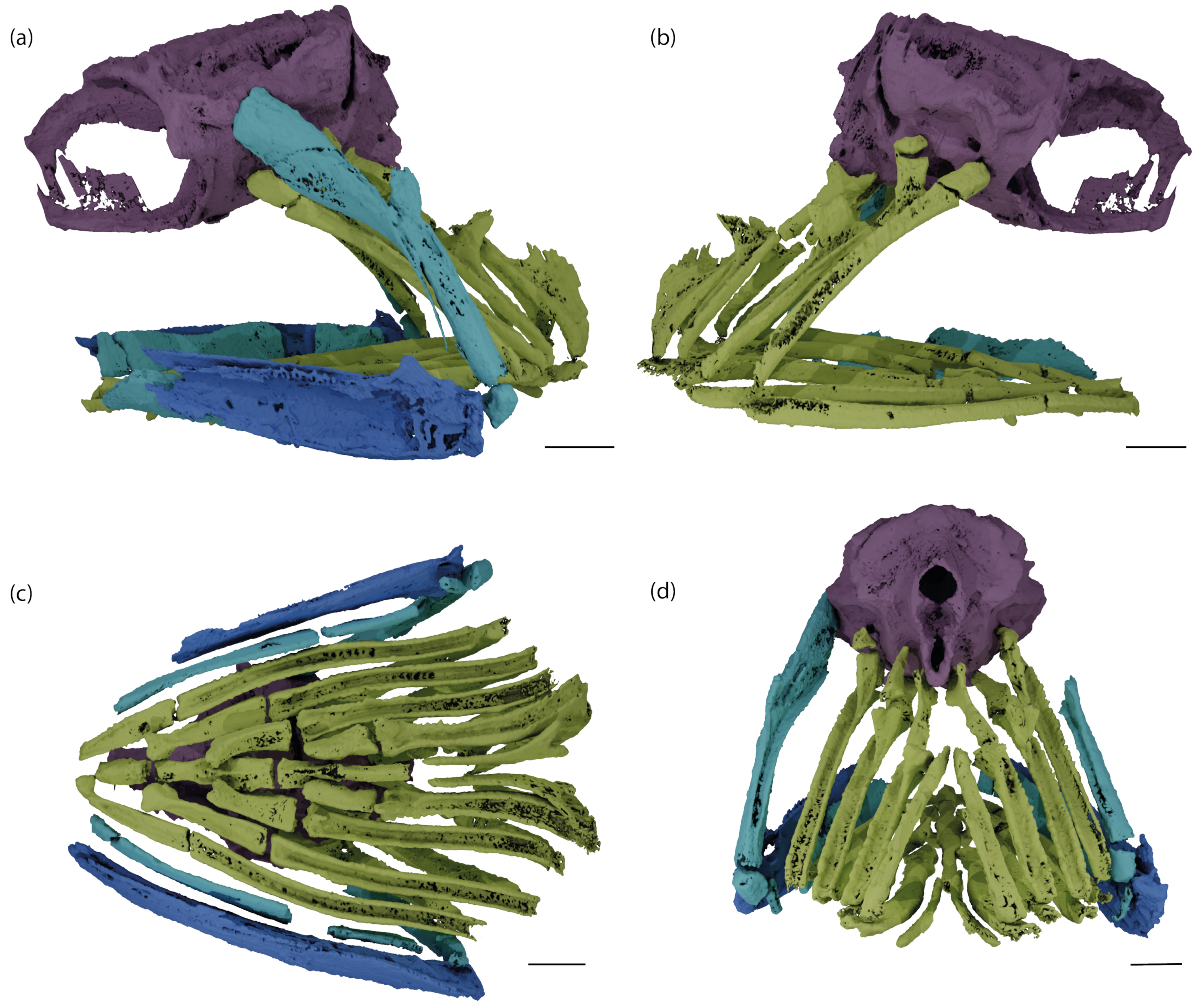


Figure 5.7: The rearticulated braincase, jaws, hyoid and gill skeleton of 'new taxon' MM L.1696: (a) left lateral view, (b) right lateral view, (c) ventral view, and (d) posterior view. Colours as in Figure 3. Scale bar = 3 mm.

(hb.3, Fig. 5.6a, 5.6b, 5.6d) are significantly different to the preceding two; they are shorter, stouter and much more curved, though they remain slightly concave on the ventral surface. Hypobranchial III almost has two distinct regions, a plate-like posterior section, and a twisted, more rounded anterior region. The right hypobranchial III of MM L.1696 has collapsed and rotated medially so that it is ventral to and upside down relative to the left hypobranchial III. Anteriorly, there are still two clear articular processes, the dorsal of which appears to fit into the concave ridge of basibranchial II. This dorsal process proceeds to form a ridge running posteriorly along the inner

surface gradually moving dorsally to the posterodorsal corner of the bone. The ventral process forms a ridge along the exterior which curves dorsally to form the dorsal margin of the tall plate-like region of the bone. Posteriorly, there is an articulatory region for ceratobranchial III. Hypobranchial IV (hb.4, Fig. 5.6a, 5.6b, 5.6d) has simpler morphology, it is short and is broad and flat posteriorly and more rounded anteriorly. A ridge runs from the posteromedial corner across the dorsal surface to the anterolateral corner. Posteriorly, there is a facet for the articulation with ceratobranchial IV. Hypobranchial IV articulated with the midline ventral ridge of basibranchial III. As with hypobranchial III, the right hypobranchial IV in this specimen has fallen underneath the left.

Five ceratobranchials are present. Ceratobranchial 1 is the longest, and is a slender bone which curves in the posterior half (cb.1, Fig. 5.6a, 5.6b, 5.6d). The ventral surface of ceratobranchial I is concave, bearing a deep groove along the entire length (for the afferent artery and branchial nerve; Gardiner, 1984). Anteriorly, ceratobranchial I articulates with hypobranchial I, and posteriorly with epibranchial I (Fig. 5.7). Ceratobranchial II is very similar morphologically to ceratobranchial I, although is slightly shorter (cb.2, Fig. 5.6a, 5.6b, 5.6d). Ceratobranchial III is also similar, but the anterior articulatory surface is broader (cb.3, Fig. 5.6a, 5.6b, 5.6d), corresponding with the broad posterior of hypobranchial III. Ceratobranchial III also appears to have a thin, curved ventral process at the anteroventral corner. On ceratobranchial IV, which is shorter but otherwise morphologically similar to the preceding ceratobranchials, this ventral process is much more robust and pronounced (cb.4, Fig. 5.6a, 5.6b, 5.6d). Small extensions on the lower edge of ceratobranchial IV may represent small teeth or

rakers. The posterior tip of ceratobranchial IV also splays out relative to the elongate body of the bone.

A pair of matching bones are tentatively interpreted as the fifth ceratobranchials. Ceratobranchial V is flat rather than grooved on the ventral surface like the other ceratobranchials (cb.5?, Fig. 5.6a, 5.6b, 5.6d), and also bifurcates posteriorly. As preserved, the left ceratobranchial V sits just above ceratobranchial IV with the anterior tip around a third of the way along ceratobranchial IV. Ceratobranchial V is short and so does not extend posterior to ceratobranchial IV. The right ceratobranchial V is displaced and appears to have fallen down between all of the other ceratobranchials. Another rod-like element about the length of ceratobranchial V (which is also morphologically very similar to the fifth ceratobranchial of many other Palaeozoic actinopterygians) is present running essentially parallel to what we have here determined the left ceratobranchial V, making identification of these bones dubious.

The four epibranchials present in L.1696 gradually shorten in series. The first three epibranchials are similar morphologically, the main difference being length – epibranchial I is the longest, and epibranchial III is the shortest (epi.1-3, Fig. 5.6a, 5.6b, 5.6e). Anteriorly, the first three epibranchials bifurcate into a flat anterodorsally directed process for the articulation with the suprapharyngobranchials, as well as an anterior portion for articulation with the infrapharyngobranchials. The anterodorsal processes have two articulatory heads. The anterodorsal process of epibranchial II is noticeably wide than that of epibranchial I and III. All of the first three epibranchials also bear a deep dorsal groove and an associated ridge on the lateral margins which both run most of the length of the bones. The fourth epibranchial (epi.4, Fig. 5.6a, 5.6b, 5.6e) however is significantly different to epibranchials I-III, with no processes anteriorly and a

significantly ventral curve. Instead, the anterior half of the bone is round and constricts slightly in the anterior half. Additionally, the posterior half of epibranchial IV bears a large dorsal crest.

Two sets of infrapharyngobranchials (ip, Fig. 5.6a, 5.6c) and suprapharyngobranchials (sp, Fig. 5.6a, 5.6b, 5.6e) are present. The first set lie at the anterior tip of epibranchial I. The first infrapharyngobranchials (ip.1, Fig. 5.6a, 5.6b, 5.6e) are stout and rounded, though have a small groove similar that on the epibranchial. The corresponding suprapharyngobranchials (sp.1, Fig. 5.6a, 5.6b, 5.6e) are very small, nodular bones that fill the space between the uncinate process of the epibranchial and the neurocranium. The second infrapharyngobranchials are flatter, have a slight bend and are concave posteriorly where they articulate with epibranchial II. The left suprapharyngobranchial II (the right is absent; sp.2, Fig. 5.6a, 5.6b, 5.6e) is broad where it meets the epibranchial and tapers dorsally where it articulates with the neurocranium (Fig. 5.7). The third infrapharyngobranchials (ip.3, Fig. 5.6a, 5.6b, 5.6e) are morphologically distinct from the preceding two in having a rod-like posterior section which expands out to a broad, flat head bearing a large concavity. This concavity is where the infrapharyngobranchials wrap around the occiput of the neurocranium (specifically the bone enclosing the dorsal aorta; Fig. 5.7).

5.4.8 Pectoral girdle

The dermal pectoral girdle of L.1696 consists of a presupracleithrum, supracleithrum, cleithrum, clavicle and a possible interclavicle. The reasonably large presupracleithrum (prscl, Fig. 5.8a) overlies the antero-dorsal region of the supracleithrum. The presupracleithrum is taller (dorso-ventrally) than it is long (antero-posteriorly), has a

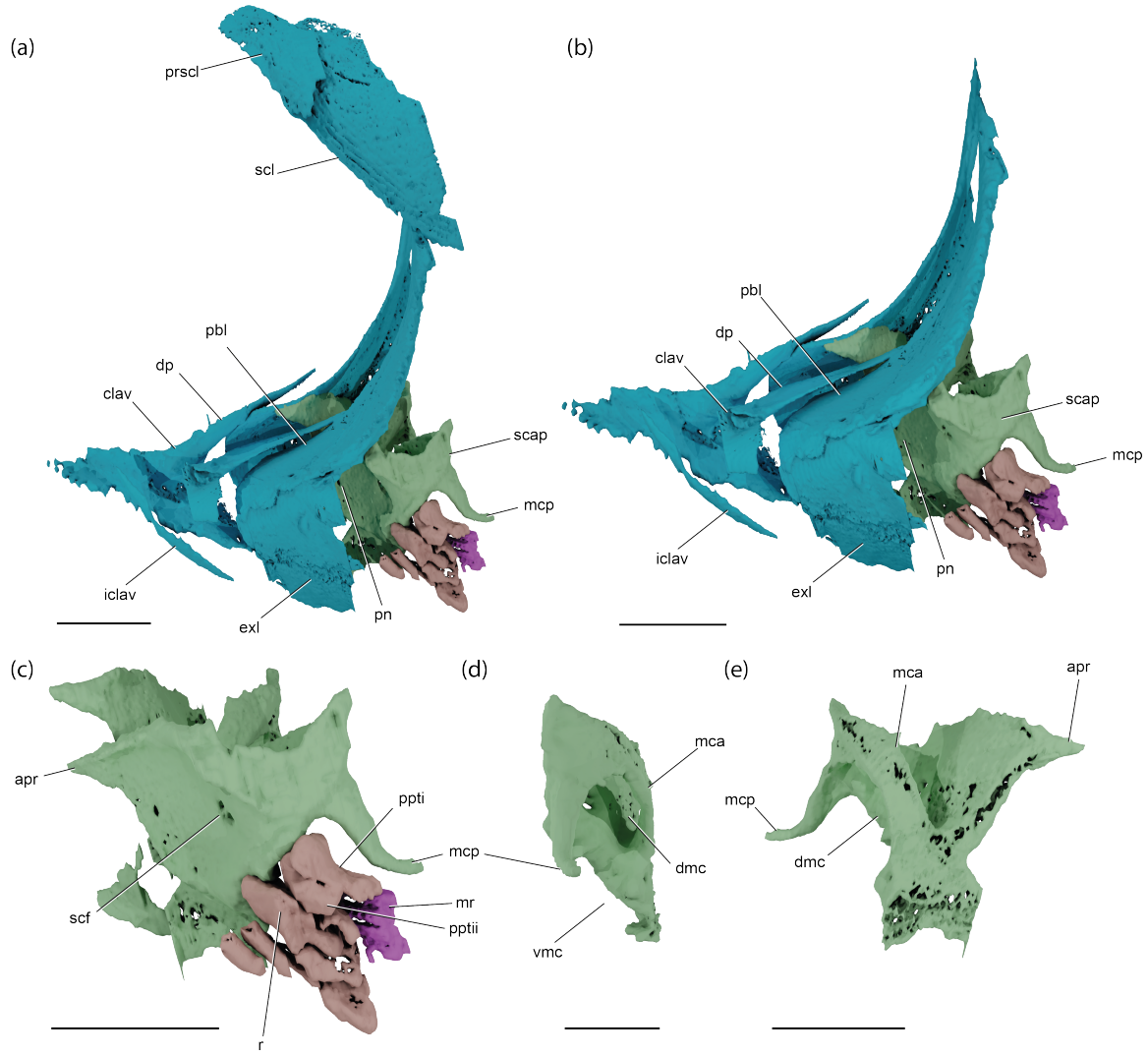


Figure 5.8: The dermal shoulder girdle (cyan) and pectoral skeleton (scapulocoracoid – green; radials – red; lepidotrichia – pink) of 'new taxon' MM L.1696: (a) left lateral view including supracleithrum and presupracleithrum, (b) left lateral view without the supracleithrum and presupracleithrum, (c) lateral view of pectoral endoskeleton, (d) posterior view of scapulocoracoid, (e) medial view of scapulocoracoid. apr - anterior process of scapulocoracoid; clav - clavicle; dp - dorsal process of clavicle; dmc - dorsal muscle canal; exl - external lamina of cleithrum; iclav - interclavicle; mcp - mesocoracoid process; mr - fin rays; pbl - postbranchial lamina of cleithrum; pn - pectoral notch; ppt(i/ii) - radials I and II of the propteryigum; prscl - presupracleithrum; r - radials; scap - scapulocoracoid; scf - supracoracoid foramina; scl - supracleithrum; vmc - ventral muscle canal. Scale bar = 4 mm.

marginally concave anterior margin, and a convex posterior margin. There are no posterior serrations. The presupracleithrum is displaced, and has shifted ventrally to sit beneath the dorsal region of the operculum. The supracleithrum however has

shifted anteriorly to also sit underneath the operculum. The supracleithrum (scl, Fig. 5.8a) is long, with a roughly straight anterior margin. The left supracleithrum of L.1696 appears to have a concavity in the antero-dorsal region, however this may in fact be a breakage of the bone. Nonetheless, the dorsal-most part of the bone that remains is smooth likely for overlap by the posttemporal. In medial view the lateral line canal runs from the antero-dorsal corner of the supracleithrum to the middle of the posterior margin. The ventral portion of the supracleithrum overlies the dorsal tip of the cleithrum. Linear ridges of ornamentation run parallel with the anterior margin of the supracleithrum.

The cleithrum (cle, Fig. 5.3b) has a broad external lamina (exl, Fig. 5.3b), visible on the left cleithrum on the exterior of the fossil. The dorsal portion of the cleithrum curves medially and the medial margin is concave. The anterior margin (the postbranchial lamina; pbl, Fig. 5.8a, 5.8b) of the cleithrum is also concave, curving down towards the anterior portion of the cleithrum, which forms the posterior margin of the branchial cavity. Close to the somewhat damaged posteroventral margin of the cleithrum there is an embayment for the pectoral fin (the pectoral notch; pn, Fig. 5.8a, 5.8b), which is relatively shallow and subtle. While no pre-pectoral spine-like outgrowth is present this may be an artefact of preservation. The large ventral portion of the cleithrum curves medially and is overlapped slightly by the clavicle, though there is no large anteroventral projection of the cleithrum medial to the clavicles. The clavicle (clav, Fig. 5.8a, 5.8b) has a long, slender dorsal process (dp, Fig. 5.8a, 5.8b), which extends roughly a third of the way up anterior margin of the cleithrum. The clavicle also has a long posteroventral extension extending around the ventral portion of the cleithrum and resulting in a highly concave posterior margin of the clavicle. This ventral

part of the clavicle also curves medially, such that no large flat ventral portion is present. A thin strip of bone between the clavicles is likely an elongated interclavicle (iclav, Fig. 5.8a, 5.8b).

Both the left and right scapulocoracoids (scap, Fig. 5.8) are present in L.1696 as single ossifications, while only some elements of the left fin endoskeleton are present. The dorsal margin of the endoskeletal pectoral girdle (the scapulocoracoid) contacts the cleithrum, suturing across the medial surface of the postbranchial lamina in a posterolateral direction. At the anterior tip of this contact is the anterior process (apr, Fig. 5.8c, 5.8e). The lateral wall of the scapulocoracoid is pierced by the two small supracoracoid foramina (scf, Fig. 5.8c), however the presence of any coracoid foramina is unclear. The mesocoracoid arch (mca, Fig. 5.8d, 5.8e) curves dorsally and posteriorly around a large dorsal muscle canal (Fig. 5.7c. 5.7d). The continuation of the mesocoracoid arch at the posterior end of the endoskeletal girdle leads to the mesocoracoid process ventrally (mcp, Fig. 5.8a, 5.8c, 5.8d, 5.8e), which protrudes ventro-posteriorly before deflecting posteriorly at the distal tip, and a smaller process dorsally. On the lateral face, a ridge separates the middle of the bone and the coracoid region. Ventral to this ridge, the coracoid region of the bone encloses the ventral muscle canal (vmc, Fig. 5.8d, 5.8e) medially (with the cleithrum forming the lateral boundary).

The endoskeletal pectoral fin elements preserved include the propterygium, radials and a possible metapterygium. Proximally, there is a two-part propterygium (a marginal and submarginal propterygium), two larger radials with spatulate heads, a smaller radial (though this may be simply the proximal fragment of the radial) and what may be the proximal fragment of the metapterygium, however only one fragmented

distal radial is present posterior to the propterygium. The propterygium is perforate and has two parts (ppti, pptii, Fig. 5.8c), each of which are short and broad. Both are much wider at the base than subsequent radials, and both have grooves accommodating the propterygial canal on the surface where they make contact. The proximal surface of both bones bears an embayed facet where they articulate with the scapulocoracoid. The other proximal radials follow in close sequence to the submarginal propterygium (r, Fig. 5.8c), all of these have slim bases with facets on the proximal surface for articulation with the scapulocoracoid, though only the one immediately ventral to the submarginal propterygium is actually in contact with the scapulocoracoid. Only two of the radials extend distally, flaring to form spatulate heads. The two others are very short, which may be due to damage to the distal portions, however these shorter elements could also be preaxial radials that articulated with a missing metapterygium. At least 9 fin rays are present (mr, Fig. 5.8c), with bases underlying the distal radial and propterygium medially. The rays are damaged distally, however, preventing determination of their relative lengths.

5.4.9 Pelvic girdle

Elements of both the left and right pelvic girdle are preserved in L.1696. The pelvic plate (pelv, Fig. 5.9) is curved and has a distinct anteromedial process (apr.pv, Fig. 5.9). The outer face is flat, but the inner surface has a clear ridge and thickening of the bone at the apex of the curve. No grooves or foramina are present on the pelvic plate. Four gradually posteriorly lengthening proximal radials (pr, Fig. 5.9) are present posterolateral to the left pelvic plate, with a small round bone also present just lateral to the third of these radials. Posterolateral to the right pelvic plate, however, there is a

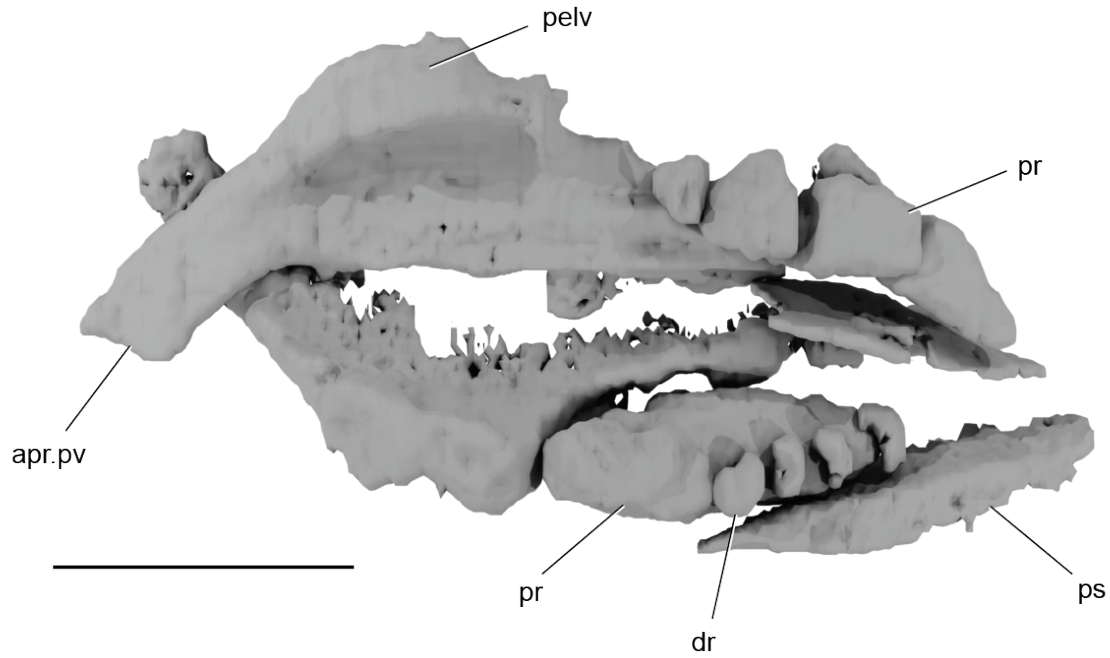


Figure 5.9: The pelvic girdle of ‘new taxon’ MM L.1696 in left lateral view. apr.pv - anterior process of pelvic plate; dr - distal radials; pelv - pelvic plate; pr - proximal radials; ps - posterior scute. Scale bar = 3 mm.

single larger ossification. Two elongated proximal radials (pr, Fig. 5.9) are present immediately posterior to the right pelvic plate, though one of these large elements posterolateral to the right pelvic plate may be a fragment of the pelvic plate itself. Four very small bones distal to the right pelvic plate and proximal radials may represent additional small distal radials (dr, Fig. 5.9). On the left side any distal radials are missing, and it is likely that some proximal radials are missing from both sides too, such as the longer posterior radials. Two blade-like posterior scutes (ps, Fig. 5.9) are present posterior to the pelvic girdles.

5.4.10 Fins

Parts of the pectoral, pelvic, dorsal and anal fins are present in L.1696 (Fig. 5.1); the caudal fin is missing. The left pectoral fin extends out from the body, though all details are not visible due to damage to the specimen and the distal extremity is missing. It

inserts low on the flank, with a thin base and wider distal portion. The segmented lepidotrichia elongate distally. While the pelvic fin endoskeleton is present within the matrix, the external pelvic fin is not visible on the specimen due to damage. The dorsal fin is short, roughly triangular and has a long base around double the length of the fin depth. The lepidotrichia are regularly segmented. The distal portion of the anal fin is missing, but the fin has a relatively long base with evenly segmented, short lepidotrichia. The anal fin inserts posterior to the dorsal fin. Small fringing fulcra are present near the base of the fin. Anterior to the anal fin are a set of anal basal fulcra bearing ridged ornamentation.

5.4.11 Axial skeleton

The axial elements, comprised of dorsal and ventral arches, and supraneurals, are arranged in four main concentrations, one immediately posterior to the braincase (group 1), one at the dorsal extremity of the fossil (group 2), one ventral to group 2 (group 3), and one posterior-most group dorsal to the pelvic girdle (group 4). The region of the specimen posterior to the pelvic girdle was not CT scanned, so the presence of any infrahaemals or specialised caudal axial elements is uncertain. No ossified centra or ribs are present. The dorsal neural arches consist of paired basidorsals and interdorsals. The neural arches (na, Fig. 5.10) have a slender neural spine extending dorsally which widens slightly at the distal tip, and a flat, laterally directed epineural

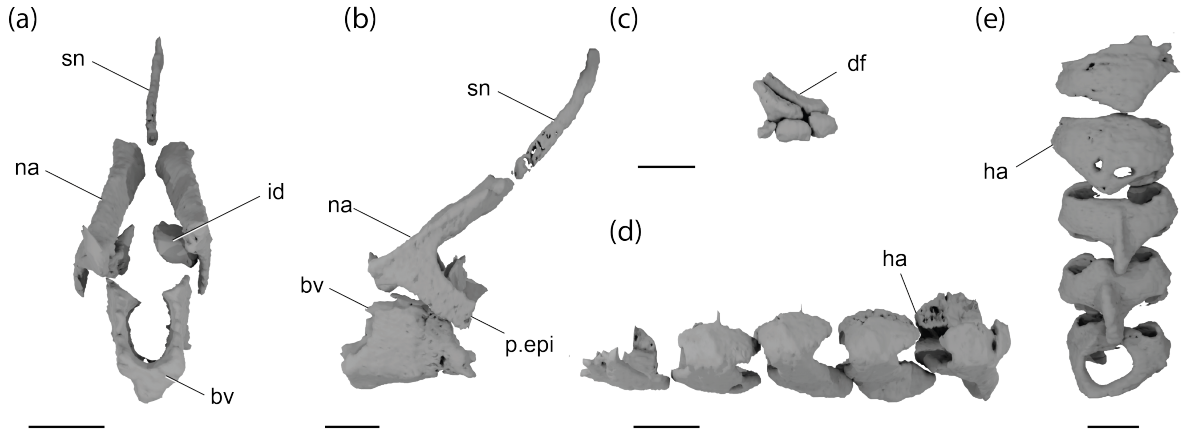


Figure 5.10: Axial elements of 'new taxon' MM L.1696: (a) anterior neural arch, supraneurals, interdorsals and anterior haemal arch in anterior view and (b) left lateral view. (c) Endoskeletal dorsal fin elements in left lateral view. Posterior haemal arches in left lateral view (d) and ventral view (e). bv - basiventral; df - dorsal fin endoskeletal elements; ha - haemal arches; id - interdorsal; na - neural arch; p.epi - epineural process; sn - supraneural. Scale bars = 2 mm.

process (p.epi, Fig. 5.10). The medial surface of the neural arch has a longitudinal ridge and the epineural processes are slightly concave medially where they wrap around the subsequent neural arch/notochord. Small nodular interdorsals (id, Fig. 5.10) are present between the neural arches in the group of axial bones behind the braincase (group 1) and the group ventral to the dorsal fin (group 3). Group 2 of axial elements has standard paired neural arches, but no ventral arches or interdorsals. In the two posterior concentrations of axial elements (groups 3 and 4), thin, rod-like supraneurals (sn, Fig. 5.10) are present alongside the neural arches (which are morphologically similar to the anterior arches). The haemal arches are generally fused at the midline, though there may be some paired basiventrals. The anterior-most preserved ventral arch (basiventral) (bv, Fig. 5.10) is in group 1, behind the braincase, and is extremely deeply curved internally to accommodate the notochord. Posteriorly, this anterior basiventral extends very slightly at the posteroventral region of the bone, forming a small median keel on the ventral surface. No other haemal arches are

preserved in group 1, or in group 2 or 3, but five haemal arches are present in group 4 in articulation with each other. These more posterior haemal arches (post.ha, Fig. 5.10) differ morphologically from the anterior-most haemal arch – the lateral/vertical component of the arch is shorter, but the horizontal portion is wider (i.e. the concavity for the notochord is shallower). Additionally, the lateral component is greatly curved rather than flat, so much so that dorsally it continues curving so that it is horizontal again. In transverse view, these haemal arches look like a squashed heart shape (albeit with a missing top). As with the anterior haemal arch, these arches have a posteroventral extension, which becomes gradually more distinct in the posterior arches. By the third haemal arch in the group 4 series, the posteroventral extension embraces the anterior margin of the next haemal arch in sequence, forms a distinct median keel and is flanked by paired concavities. The second haemal arch in this series appears to have paired foramina in the posterior region of the horizontal floor at the base of the posterior extension, while the last in sequence has a large whole (which may be a result of damage).

Elements just above group 4 of the axial skeleton may represent endoskeletal dorsal fin elements (df, Fig. 5.10c), comprised of two pairs of bones seemingly in sequence. There is a ventral spherical element sitting beneath and articulating with a dorsal bone that has a bulbous ventral region (where it articulates with the ventral bone) and a thinner rod-like dorsal extension. The morphology of these two pairs of bones is reminiscent of dorsal fin proximal and distal radials (cf. Nielsen, 1942: fig. 50, p.217 and fig. 77, p. 369), though appear to be inverted so that the distal radials are ventral to the proximal radials.

5.4.12 Squamation

The scales of MM L.1696 are rhomboid, and have ridged, unbranching ornamentation, peg and socket articulation and a small anterodorsal process. The lateral line scales bear a canal for the lateral line, while the scales low on the flank are flatter than those on the dorsal and lateral region which remain fairly uniform along the length of the body (until the specimen breaks posterior to the anal fin). No clearly distinct ridge scales are present.

5.5 Phylogenetic results

Equal weights parsimony analysis results in large polytomies for all Palaeozoic taxa (Fig. 5.11a) below the neopterygian crown node. Nearly all Palaeozoic and some Mesozoic actinopterygians collapse into a polytomy, with only some clades resolved (Styracopteridae – *Styracopterus* and *Fouldenia*; Mimiidae – *Gogosardina* and *Mimipiscis*). Some congeneric species (*Birgeria* spp. and *Saurichthys* spp.) are united, though others (*Boreosomus* spp., *Cheirolepis* spp. and *Moythomasia* spp.) are not. Polypterids and chondrosteans form distinct clades within the broader polytomy. Actinopterygian monophyly is also not upheld, indicating how unstable early actinopterygian phylogeny currently is. Notably, *Ptycholepis bollensis* and L.1696 are sister-taxon, corroborating morphological data evidencing their affinity (see below).

Implied weights analyses unsurprisingly return more resolved trees (Fig. 5.11b; Appendix Fig. C.2), even with very weak concavity that weights only very gently against homoplastic characters (k = 100, Fig. 5.11b). Under this scenario, tree topology of strict consensus trees closely resembles previous iterations of this matrix (Figueroa *et al.*, 2021; Argyriou *et al.*, 2022; Giles *et al.*, 2023), with minor differences. A polypterid and

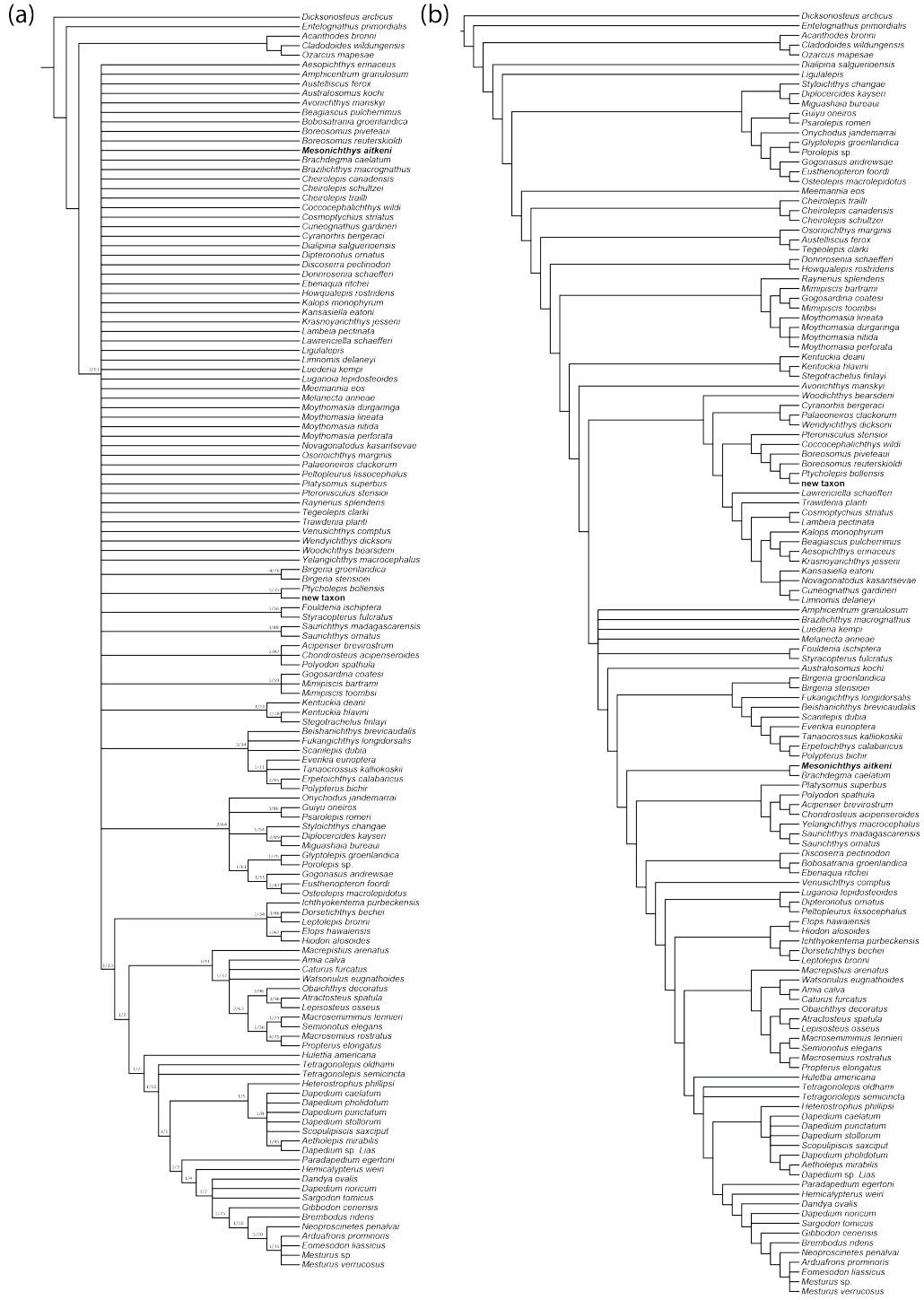


Figure 5.11: Results of parsimony analysis. Strict consensus trees obtained from (a) equal weights (tree length = 1865) and (b) implied weights (k = 100; tree length = 13.91707) with only outgroup constraint. New taxon and *Mesonichthys aitkeni* indicated in bold.

chondrostean clade is not recovered (Giles *et al.*, 2023), with topology of extant clades instead reflecting the molecular and morphological consensus (Near *et al.*, 2012;

Broughton *et al.*, 2013; Giles *et al.*, 2017; Hughes *et al.*, 2018; Dornburg & Near, 2021). *Birgeria* and *Saurichthys* are recovered as stem-polypterids and stem-chondrosteans, respectively (Argyriou *et al.*, 2022), while *Brachydegma caelatum* is placed as a stem actinopteran (alongside *Mesonichthys aitkeni*). L.1696, *Ptycholepis bollensis*, *Boreosomus reuterskioldi* and *Boreosomus piveteaui* form a monophyletic clade, with *Coccocephalus wildi* and *Pteronisculus stensioi* as successive sister-taxa. Notably, this clade is nested within a broader clade of Devonian and stratigraphically younger forms on the actinopterygian stem.

50% majority rule consensus trees of both Bayesian methods ('maximise information' and 'minimise assumptions') are slightly better resolved than strict consensus equal weights trees, though retain a large polytomy containing most Palaeozoic taxa, polypterids and chondrosteans (Fig. 5.12). Again, L.1696, *Ptycholepis bollensis*, *Boreosomus reuterskioldi* and *Boreosomus piveteaui* are monophyletic, with reasonable support (BPP = 0.88, 'maximum information'; BPP = 0.97, 'minimise assumptions'). *Brachydegma caelatum* is recovered as a stem-polypterid (Argyriou *et al.*, 2022) under the 'minimum assumptions' method, unlike in our parsimony analyses. Consensus trees showing all compatible clades (rather than collapsing nodes with lower than 50% posterior probability; Fig. 5.13) return tree topologies similar to that returned by implied weights with a weak concavity (Fig. 5.11b), though posterior probability of most nodes along the backbone of the tree are particularly low.

Conducting analyses with implied weights clearly improves resolution of actinopterygian phylogeny, although returns some strange clades at low values of k, such as the Carboniferous *Lambeia pectinata* forming the sister taxon to

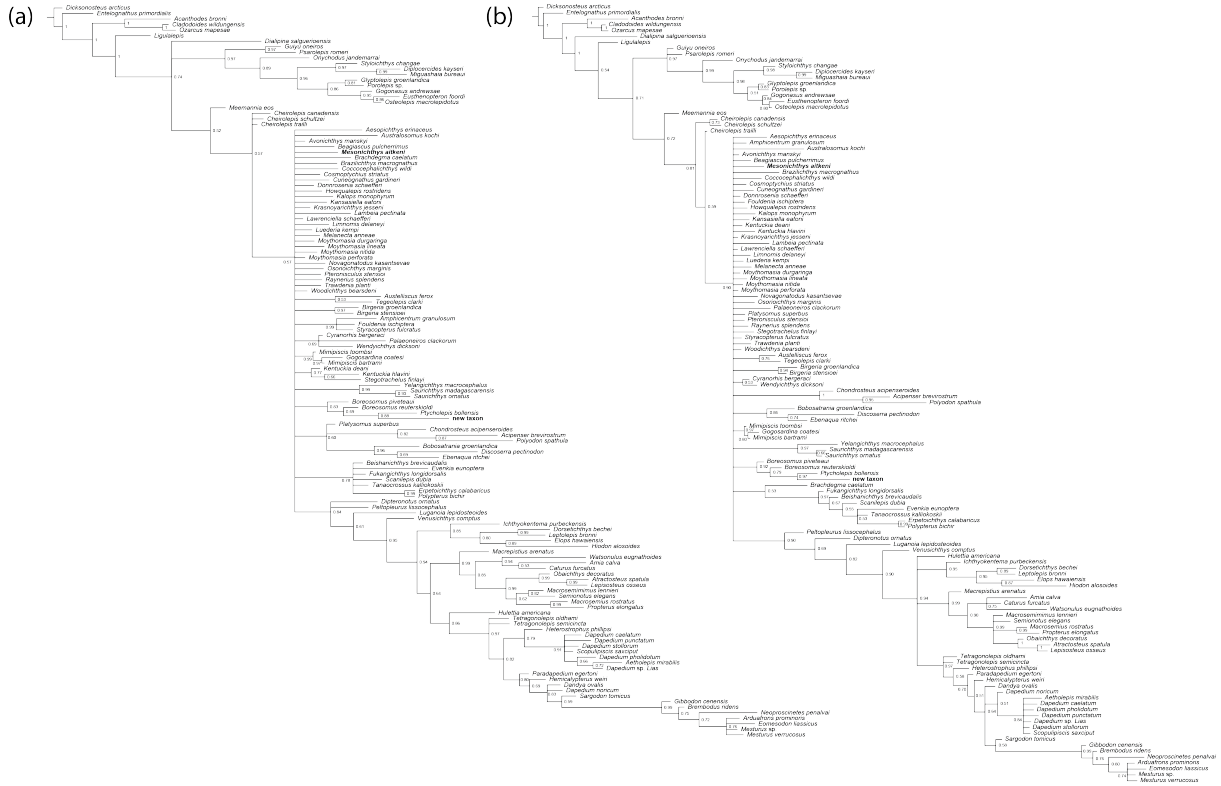


Figure 5.12: Results of Bayesian analysis. Consensus tree showing 50% majority rule consensus trees from (a) ‘maximum information’ and (b) ‘minimum assumptions’ methods. Digits at nodes also show posterior probability support. New taxon and *Mesonichthys aitkeni* indicated in bold.

sarcopterygians, Devonian ‘palaeopterygians’ nesting within crown-polypterids, and L.1696 forming a clade with a cladistian (Appendix Fig. C.2). These erroneous topologies are likely due to a combination of high levels of homoplasy and the high proportions of missing character data, and highlight the unsuitability of strong implied weights in this dataset.

Treespace visualisations show that different methods explore different areas of treespace (Fig. 5.14). Both the ‘maximum information’ and ‘minimum assumptions’ Bayesian methods explored similar topologies, with implied weights analyses that more heavily penalise homoplasy (k = 1, k = 3 and k = 12) also within this range. Equal weights analyses explored two separate islands of trees distinct from the Bayesian

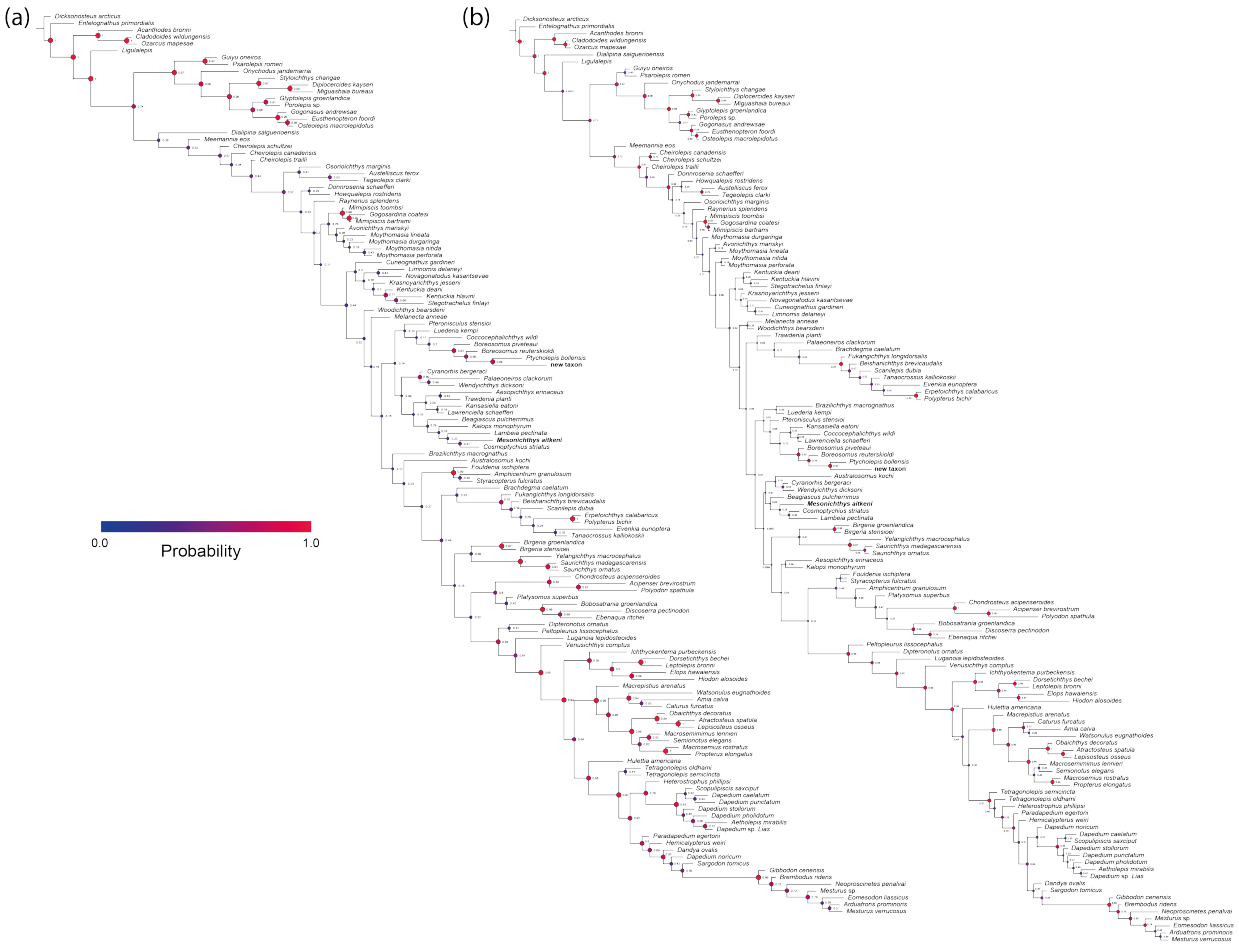


Figure 5.13: Results of Bayesian analysis. Consensus tree showing all compatible clades from (a) 'maximum information' and (b) 'minimum assumptions' methods. Nodes are sized and coloured by posterior probability support. Digits at nodes also show posterior probability support. New taxon and *Mesonichthys aitkeni* indicated in bold.

trees, with a much smaller group of trees closer to the Bayesian island. Implied weights analyses very softly weighting against homoplasy (k = 100) clustered around the smallest group of equal weights trees, intermediate to all three disparate islands of trees. This suggests benefits to applying multiple methods of inference, as each has different optimality criteria and recovers trees that settle in different areas of treespace.

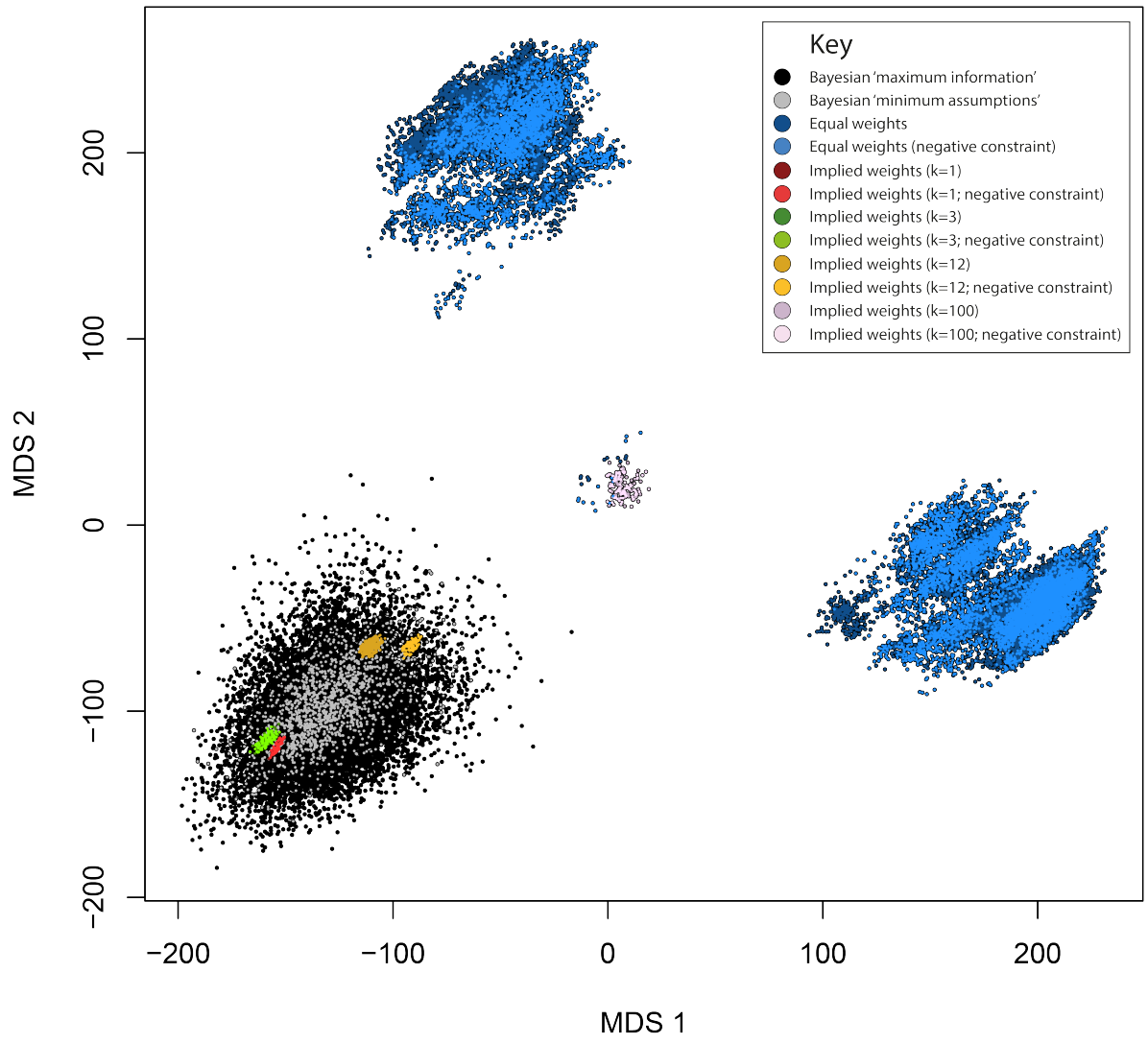


Figure 5.14: Treespace with sample of trees coloured by phylogenetic method (Bayesian – black and grey; equal weights parsimony – blue; implied weights, k = 1 – red; implied weights, k = 3 – green; implied weights, k = 12 – yellow; implied weights, k = 100 – purple).

5.6 Discussion

5.6.1 Taxonomic reassessment

While a complete revision of *Mesonichthys aitkeni* is outside of the scope of this contribution, comparison with other specimens referred to the genus (and species) shows anatomical differences that justify the removal of L.1696 to a new taxon.

The anatomy of *M. aitkeni* is best shown in specimens from the Culm Measures of Devon, including NHMUK PV P.6100, the neotype proposed by (Gardiner, 1963) (Fig. 5.15a, b). Differences are particularly noticeable in the shape and proportion of dermal bones. For example, the dermopterotic of L.1696 is significantly larger than the triangular dermopterotic of P.6100. L.1696 bears a stout, rectangular posteroventral extension of the maxilla, in contrast to the tapered posteroventral process of P.6100, and the angular of L.1696 is proportionately much longer than that of P.6100. Additionally, the opercular is rhomboid in L.1696, with a concave ventral margin, and bears a distinct, tear-shaped posteroventral process. This contrasts with the rectangular opercular in P.6100, which has a straight ventral margin and lacks a posteroventral process. The presence of an accessory opercular (absence of which was a primary reason given by Gardiner (1963) for erecting a new genus to contain *'Elonichthys' aitkeni*) further confirms the differences in cheek morphology that justify separation of L.1696 from P.6100 and other specimens within *Mesonichthys aitkeni*.

Pronounced differences are also present in dermal ornamentation pattern. Ornament across L.1696 generally comprises broad ridges whereas the dermal bones of P.6100 and other Culm Measures specimens are ornamented with narrower, closely spaced ridges (Fig. 5.15a, b). Ornamentation on the maxilla of L.1696 runs parallel with its dorsal margin, whereas in P.6100 the ridges exit the maxilla anterodorsally. The ornament on the preopercular in L.1696 is simple and straight, but complex and curved in P.6100. Lastly, L.1696 lacks the thick ventral ridges on the scales that are present in P.6100—and, indeed, included in the original species diagnosis for '*Elonichthys' aitkeni* (Traquair 1886). It is important to note that most details of the ornamentation are derived from the mouldic counterpart, and are missing from the part.

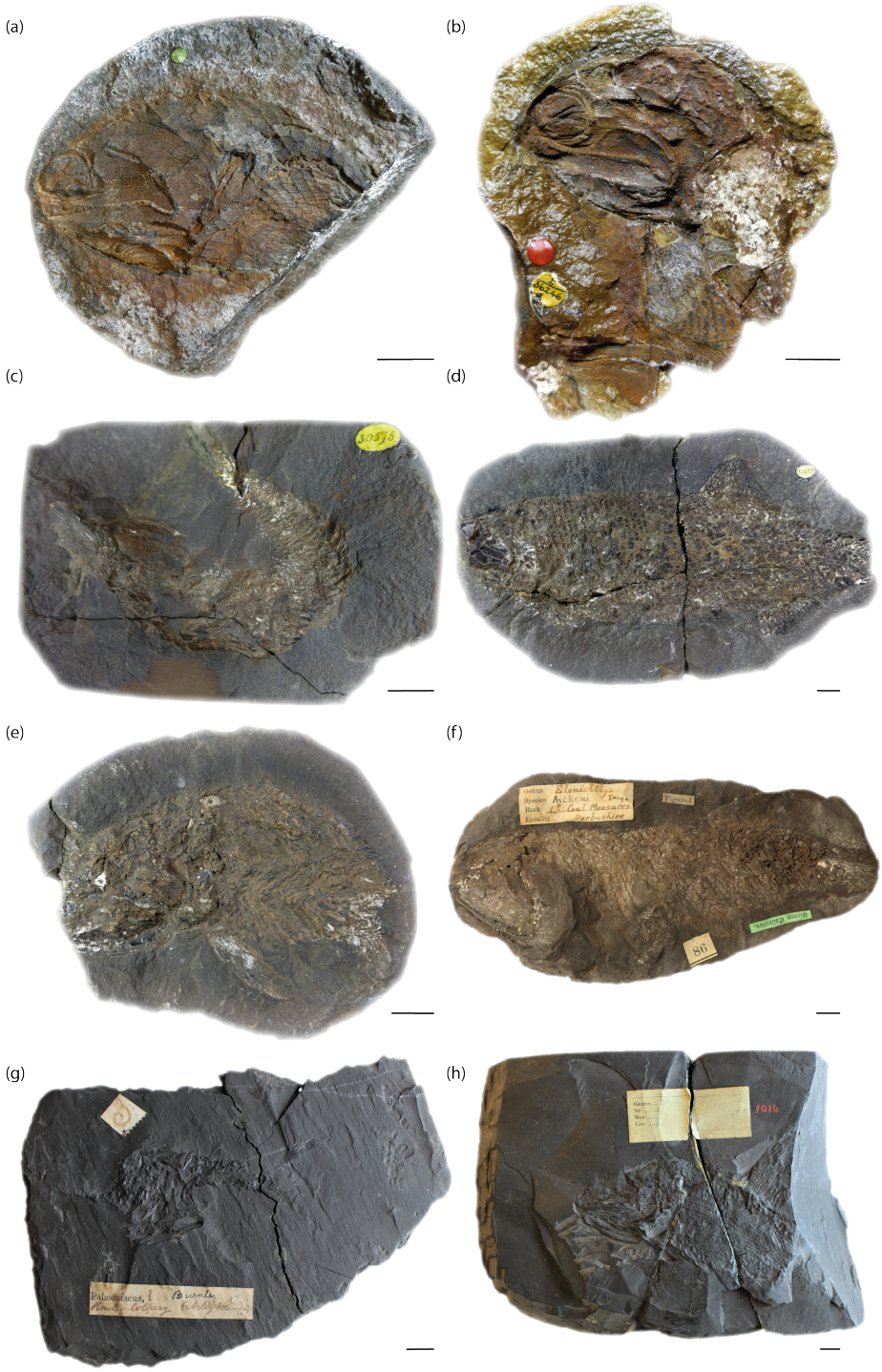


Figure 5.15: Comparative anatomy of *Mesonichthys aitkeni*. (a) NHMUK PV P.6100 (neotype – Instow, Devon), (b) NHMUK PV P.36246 (Instow, Devon), (c) NHMUK PV OR 30575 (Stanton-by-Dale, Derbyshire), (d) NHMUK PV OR 30577 (Stanton-by-Dale, Derbyshire), (e) NHMUK PV OR 30576 (Stanton-by-Dale, Derbyshire), (f) CASM E.4889 (Stanton-by-Dale, Derbyshire), (g) MM L.2358 (Arley Mine, Lancashire), (h) MM W.1013 and W.1014 (Arley Mine, Lancashire). Scale bars = 10 mm.

In contrast, some features clearly present in the part (such as the posterior process of the opercular) are absent in the mould. We would therefore suggest caution when

interpreting specimens which consist solely of mouldic impressions and comparing them with other taxa.

The internal anatomy of *Mesonichthys aitkeni* is only known from CASM E.4890, described from natural external moulds by Watson (1925); unfortunately the poor preservation of external dermal bones in this material (Fig. 5.15c-f), from Stanton-by-Dale in Derbyshire, makes comparison with the external anatomy of L.1696 difficult. Most notable are differences in the gill skeleton, with CASM E.4890 described by Watson (1925) as possessing a urohyal, four ceratobranchials, a single ceratohyal, and vastly different basibranchials to L.1696. L.1696 lacks a urohyal and has five ceraotobranchials and two ceratohyals. Furthermore, the third basibranchial of L.1696 is thin and similar to the anterior two basibranchials, while in CASM E.4890 there appear to be only two basibranchials, with the more posterior basibranchial large and flared posteriorly. Additional evidence that these specimens belong to different taxa are that the braincase of L.1696 is completely ossified as a single unit, while CASM E.4890 exhibits separate braincase ossifications, and that the opercular process of the hyomandibular is pronounced in L.1696 (Watson, 1925). Comparison with another other Cambridge specimen, CASM E.4889 (Fig. 5.15a; Traquair, 1901, pl. 17, fig. 1), and an additional Stanton-by-Dale specimen in the British Geological Survey collection (BGS 4520, BGS 4520A) shows differences in the opercular morphology and the absence of an enlarged dorsal-most branchiostegal. We would, however, caution that CASM E.4890 requires reinvestigation and reinterpretation.

5.6.2 Comparative morphology

L.1696 has several apparently unique anatomical features: a tear-shaped posteroventral process on the operculum, hook-like anteroventral processes on the third and fourth ceratobranchials, and posteriorly-bifurcating fifth ceratobranchials. L.1696 also possesses other characters that are unusual among late Carboniferous actinopterygians, including a pronounced hyomandibula opercular process, two accessory hyoid elements, and two ossified ceratohyals.

Operculum. The operculum of most generalised 'palaeopterygian' fishes tapers gradually to a posterior point (Gardiner, 1963, 1969; Sallan, 2014). *Coccocephalus* (Poplin & Véran, 1996) and *Mesonichthys* (Gardiner, 1963; Beltan, 1978), both contemporaries of L.1696, as well as *Wendyichthys* (Lund & Poplin, 1997) possess a small rounded extension in this region of the operculum, and some species of *Pteronisculus* (*P. stensioi*, *P. magnus*: Nielsen, 1942; *P. cicatrosis*: Lehman 1952) show a posterior constriction, though in none of these taxa does the opercular form a distinct process. In published line drawings of *Palaeoniscum freieslebeni*, the posterior margin of the operculum is depicted as either constricting posteriorly or with a small rounded extension (Aldinger, 1937; Haubold & Schaumberg, 1985); variable morphology is also depicted in *Nematoptychius greenocki* (Traquair, 1877b, 1909; Aldinger, 1937; Gardiner, 1963). Generally, the operculum is described extremely briefly and only in terms of its relative proportions. It may be that renewed investigation of museum specimens will reveal additional instances of this apparent apomorphy.

Ceratobranchials. A peculiar feature of L.1696 is the presence of hook-like ventral process at the anterior extent of the third and fourth ceratobranchials. In most

‘palaeopterygians’, ceratobranchials I–IV are elongate, grooved, rod-like ossifications that are broadly homogenous, differing only in their length and the thickness of the bone at their distal tip (e.g. *Boreosomus:* Nielsen, 1942; *Birgeria*: Stensiö, 1921; *Raynerius*: Giles *et al.*, 2015; *Coccocephalus*: Poplin and Véran, 1996, *Palaeoneiros*: Giles *et al.*, 2023; *Brazilichthys*: Figueroa, Friedman and Gallo, 2019*, Mimipiscis*: Gardiner, 1984). Variation is seen in *Australosomus kochi*, where ceratobranchial IV is developed as a broad plate (Nielsen, 1949). A ventral process is found on the first ceratobranchial of *Moythomasia durgaringa* (Gardiner, 1984: fig. 115), although this appears to be a broad flange rather than narrow recurved hook. As with the posteroventral process of the opercular, the failure to identify this feature in other early actinopterygians may be due to the difficulty of observing the ceratobranchials; they are typically buried within the rock matrix or partially obscured by more lateral ossifications (cf. *Acrorhabdus*, [Stensiö, 1921], *Boreosomus* [Nielsen, 1942]). Even where the gross morphology of the ceratobranchials can be described, delicate features at the proximal (and distal; see below) extremities are harder to observe using traditional descriptive techniques.

L.1696 also possesses an unusual feature at the distal end of ceratobranchial V. Most early actinopterygians have five ceratobranchials, with the fifth formed as a simple rod (e.g. *Mimispicis*, Gardiner, 1984; *Pteronisculus,* Nielsen, 1942). The ossification we interpret as ceratobranchial V of L.1696 differs in that it is laterally flattened and bifurcates posteriorly. Nothing in the published literature shares this morphology, though similar anatomy appears to be present in “*Perleidus*” *stoschiensis* from the Early Triassic of East Greenland (S. Giles, pers. obs. unpublished CT data). The morphology of ceratobranchial V fairly conservative in actinopterygians, but

variation is not unknown: it is plate-like and flares posteriorly in *Australosomus kochi* (Nielsen, 1949) and it is reduced (*Brachydegma*, Argyriou *et al.* 2022) or completely lost (*Birgeria*, Stensiö 1921; scanilepids, Giles *et al.*, 2017) in some taxa.

Hyoid arch. Recent CT-based work has highlighted new aspects of hyoid arch evolution in early actinopterygians, most notably the presence of two accessory hyoid elements and a double jaw joint—features previously thought restricted to neopterygians—in the probable stem actinopterygian *Brachydegma* (Argyriou *et al.*, 2022). Data from L.1696 adds to the complexity of these, and other, hyoid arch character distributions.

The presence of a distinct opercular process of the hyomandibula in L.1696 prompted a reinvestigation of this feature in early actinopterygians. Many Palaeozoic actinopterygians are described as having an opercular process. However, in the majority of taxa, this 'process' is in fact a small flange on the dorsal margin of the hyomandibula (e.g. *Palaeoneiros*, *Mesonichthys, Coccocephalus, Brazilichthys*; Fig. 5.16) rather than a distinct process that extends away from the ossification. L.1696 predates other taxa possessing this feature by more than 60 million years and represents the earliest occurrence of a distinct opercular process. Aside from extant taxa and their close Mesozoic and more recent relatives, well-developed opercular processes are otherwise reported only in the Triassic *Acrorhabdus bertili* and *Boreosomus* (*B. piveteaui*, *B. reuterskioldi*) and the Jurassic *Ptycholepis* (*P. bollensis*, *P. marshi*) (Stensiö, 1921; Nielsen, 1942; Wenz, 1959; Schaeffer, Dunkle & McDonald, 1975).

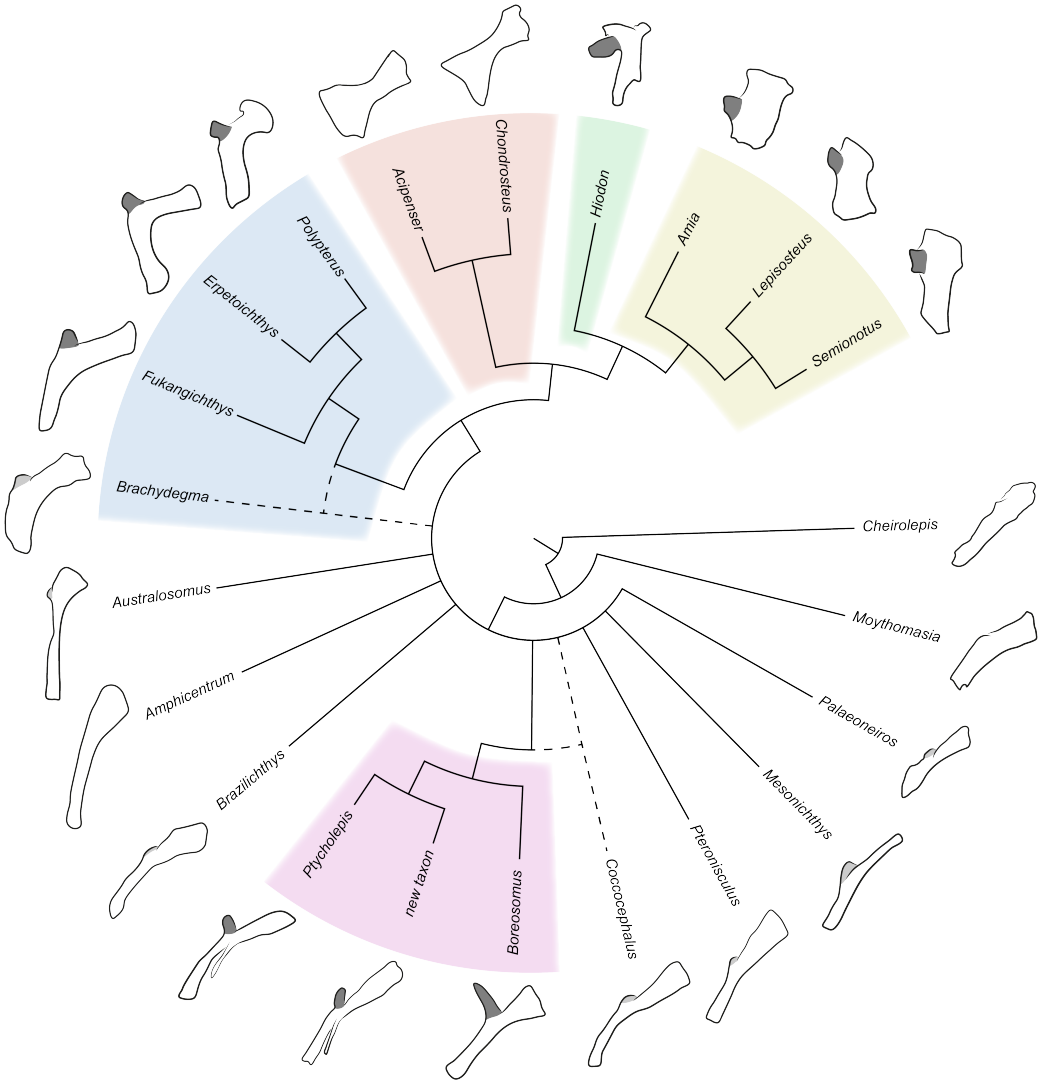


Figure 5.16: Hyomandibula morphology of selected actinopterygians. Hyomandibulae redrawn from the following sources: *Cheirolepis trailli* - Giles et al. (2015); *Moythomasia durgaringa* - Gardiner (1984); *Palaeoneiros clackorum* - Giles et al. (2023); *Mesonichthys aitkeni* - Watson (1925); *Pteronisculus stensioei* - Nielsen (1942); *Coccocephalus wildi* - Poplin and Véran (1996); *Boreosomus reuterskioldi* - Nielsen (1942); new taxon - this study; *Ptycholepis bollensis* - Wenz (1959); *Brazilichthys macrognathus* - Figueroa et al. (2019); *Amphicentrum granulosum* - Bradley-Dyne (1939); *Australosomus kochi* - Nielsen (1949); *Brachdegman caelatum* - Argyriou et al. (2022); *Fukangichthys longidorsalis* - Giles et al. (2017); *Erpetoichthys calabaricus* - Giles et al. (2017); *Polypterus bichir* - Allis (1922); *Acipenser brevirostrum* - Hilton et al. (2011); *Chondrosteus acipenseroides* - Hilton and Forey (2009); *Hiodon alosoides* - Hilton (2002); Amia calva - Grande and Bemis (1998); Lepisosteus osseus - Grande (2010); *Semionotus elegans* - Olsen and McCune (1991). Dark grey shading indicates distinct opercular process, light grey shading indicates structures previously described as an opercular process in early actinopterygians. Dashed lines show uncertain placement of specific taxa. Key clades are highlighted: ptycholepids - purple; total-group polypterids - blue; chondrosteans - red; teleosts - green; holosteans - yellow.

Homology of the opercular process of L.1696, Triassic–Jurassic actinopterygians, polypterids (Allis, 1922; Claeson *et al*. 2007), holosteans (e.g.

Ticinolepis, López-Arbarello *et al.*, 2016; *Calamopleurus*, Forey and Grande, 1998, Grande and Bemis, 1998; *Lepisosteus,* Grande, 2010) and teleosts (e.g. *Hiodon*, Hilton, 2002; *Luisiella*, Sferco, López-Arbarello and María Báez, 2015; *Heterotis*, Hilton, 2003) is unclear. Romano *et al.* (2019) suggested convergent evolution in ptycholepids and neopterygians, while Gardiner (1984) concluded convergent acquisition in polypterids and actinopterans. The pattern is complicated further by the presence of an opercular process in stem polypterids (Giles *et al.*, 2017) compared with absence in both stem (Hilton & Forey, 2009) and crown (Hilton *et al.*, 2011) chondrosteans and pycnodonts (Kriwet, 2001, 2005; Poyato-Ariza & Wenz, 2005). Whether opercular processes arose independently three times (*Ptycholepis* and L.1696; polypterids; neopterygians) or (with a subsequent loss in chondrosteans) remains uncertain. Unstable phylogenetic topologies amongst early actinopterygians, as well as the unclear monophyly and placement of groups such as ptycholepids, further muddy these waters. Additional CT-based descriptive work is likely to provide stability and clarity.

Other aspects of hyoid arch anatomy may also suggest an affinity between L.1696 and ptycholepids. Firstly, a splint-like process, termed an ‘anterior lamella’ by Wenz (1959, pl. 28), extends from the anterior margin of the ventral limb of the hyomandibula in both L.1696 and *Ptycholepis bollensis*. As far as we are aware, this has not been identified in any other early actinopterygian. Secondly, L.1696, *Boreosomus*, and *Ptycholepis* share the presence of two ossified accessory hyoid elements arranged in series between the hyomandibular and the ceratohyal (Véran, 1988). And lastly, two ceratohyal ossifications are present in L.1696—the only confirmed instance of this feature in Palaeozoic actinopterygians—and *Acrorhabdus*

(Stensiö, 1921), though *Boreosomus* has only a single ceratohyal (Nielsen, 1942) and the ceratohyals are unknown in *Ptycholepis*. The gill skeleton of *Acrorhabdus*, *Boreosomus* and *Ptycholepis* has not been described in great detail (Stensiö, 1921; Nielsen, 1942; Wenz, 1959; Gardiner, 1960; Schaeffer *et al.*, 1975; Véran, 1988; Bürgin, 1992), and CT-based accounts of their morphology represent a priority both for resolving early actinopterygian relationships and revealing more widespread occurrences of seemingly 'unique' hyoid and gill morphologies.

5.6.3 Phylogenetically forgotten fishes

L.1696 shares numerous morphological features with *Ptycholepis* and *Boreosomus*, and forms a monophyletic clade with them here. Brough (1939) grouped *Ptycholepis* and *Boreosomus* in the Ptycholepidae, a group of taxa which have been associated in the literature since the early 20th century, and were expanded to include *Acrorhabdus*, *Chungkingichthys* and *Yuchoulepis*, (Aldinger, 1937; Gardiner, 1967; Véran, 1988; Gardiner & Schaeffer, 1989; Bürgin, 1992; Mutter *et al.*, 2011; Romano *et al.*, 2019). However, the monophyly of this grouping has not been tested in a robust phylogenetic framework, with few ptycholepids present in most studies exploring actinopterygian relationships. *Ptycholepis* and *Boreosomus* were part of the 'Boreosomus group' of Gardiner & Schaeffer (1989), positioned among a haze of early actinopterygian groups. The only studies including more than one ptycholepid (Dietze, 2000; Mutter *et al.*, 2011) have largely non-overlapping, limited samples of extinct actinopterygian taxa (sharing only three taxa: *Acrolepis sedgwicki*, *Ptycholepis barboi* and *P. marshi*). Only *Boreosomus piveteaui* is routinely included in recent phylogenetic analyses of broader actinopterygian relationships (Coates, 1999; Gardiner *et al.*, 2005; Giles *et al.*, 2017; Latimer & Giles, 2018; Argyriou *et al.*, 2018, 2022; Figueroa *et al.*, 2019, 2021). The

placement of the Ptycholepidae relative to other stem-actinopterygians and extant clades remains unclear, and their addition to phylogenetic matrices represents a priority for future research.

A major expansion of existing phylogenetic matrices generally, encompassing much more of the Palaeozoic radiation of actinopterygians, is required. At present, ptycholepids (excepting *Boreosomus piveteaui*) are not the only group absent from taxon lists; numerous other groups of Palaeozoic actinopterygians that are supported on morphological grounds are also missing (e.g. Aeduellidae [Heyler, 1969, 1977, 2000; Gottfried, 1987; Štamberg, 2007, 2018; Mickle, 2011], Haplolepidae [Westoll, 1944; Lowney, 1980a, 1983; Huber, 1992; Elliott, 2014], Eurynotiformes [Sallan & Coates, 2013; Friedman *et al.*, 2018]). A broader sampling of these groups and the addition of specific characters capturing their synapomorphies will not only allow testing of their monophyly, but add greatly to our understanding of the Palaeozoic actinopterygian radiation. This greater taxon sampling will more accurately constrain node age estimates and, hopefully, robustness of phylogenetic hypotheses, with the potential to enable a wide range of downstream analyses (Soul & Wright, 2021).

5.7 Conclusion

L.1696 is a new Carboniferous actinopterygian with clear affinities to Triassic and Jurassic ptycholepids (*Boreosomus* and *Ptycholepis*) despite their separation by more than 60 million years. This seemingly generic fusiform Carboniferous actinopterygian was overlooked for more than 100 years yet represents a new taxon with unique features. This emphasises the importance of reinvestigating museum collections, particularly those outside national centres, and reinforces the power of CT scanning in

revealing novel morphologies seemingly hiding in plain sight. New morphologies provide additional data for phylogenetic analyses and addition of underrepresented actinopterygians to matrices will continue to recognise Palaeozoic actinopterygian radiations.

6 Summary and Future Directions

6.1 Summary

In this thesis I present a new through-Palaeozoic database of actinopterygian occurrences in order to examine trends in palaeodiversity, palaeogeography and sampling. I also utilise CT scanning to create digital models of Carboniferous actinopterygians, describing novel morphological features in long-known specimens.

In Chapter 2 (Henderson *et al.*, 2023), I showed that face-value taxonomic diversity is suggestive of a significant diversification of actinopterygians after the end-Devonian mass extinction event. This data augments past hypotheses (Sallan & Coates, 2010; Sallan & Friedman, 2012), however I also use the data to show that face-value diversity is tightly correlated with sampling metrics and that dividing occurrences into equal length intervals (rather than traditional ICS stages) challenges the hypothesis that actinopterygians continuously diversified throughout the early Carboniferous. I also quantify taxonomic biases resulting from prolific occurrences of poorly defined and wide-ranging genera that have existed since the 19th century (e.g. '*Elonichthys'*, *Palaeoniscum*, *Rhadinichthys* [Evans, 2005; Sallan, 2014; Mickle, 2017; Henderson *et al.*, 2023]). Despite their long history, revisions of these genera have not been forthcoming (but see Schindler [2017, 2018a] on *Elonichthys*), reflecting a broader oversight of long-known Carboniferous actinopterygian material generally.

In Chapters 2 and 3 (Henderson *et al.*, 2022, 2023), I show that fluctuations in diversity throughout the Carboniferous and Permian generally reflect biases, with uneven sampling and major spatial biases significantly influencing 'global' diversity

patterns. Chapter 3, in particular, shows how biases act to exacerbate the unevenness of occurrence distributions and confound estimation of diversity using sampling standardisation techniques. In both Chapter 2 and 3 I show clear geographic biases in research on Palaeozoic actinopterygians, demonstrating that occurrences and phylogenetic matrices are both centred around European and North American fishes. This modern bias translates to a palaeogeographic bias, with most occurrences restricted to a thin palaeolatitudinal band around the palaeoequator (Chapter 3). By dividing occurrences by palaeoenvironment I also confirm the major hiatus in the actinopterygian fossil record during the latest Carboniferous and early Permian (Friedman & Sallan, 2012).

In Chapters 4 and 5 I use CT data to redescribe two Carboniferous actinopterygians, one from the early Carboniferous (Tournaisian) and one from the late Carboniferous (Bashkirian). In redescribing these specimens, I corroborate prior work showing that that redescriptions have the potential to reveal significant taxonomic and morphological diversity (Sallan & Coates, 2013; Coates & Tietjen, 2018; Friedman *et al.*, 2018; Štamberg, 2023). I identify morphological diversity in the cranial features of a Tournaisian taxon (Chapter 4) and a new taxon in material known in the literature for more than 125 years (Chapter 5). I also conduct an expanded phylogenetic analysis and investigate different methods of phylogenetic inference, showing that Bayesian and parsimony methods largely explore different areas of treespace. I highlight instability in stem-actinopterygian relationships and discuss the oversight of many Carboniferous and Permian actinopterygians, which is evidenced by the absence of numerous clades from formal phylogenetic analyses.

My results reinforce that actinopterygians were significantly more diverse through the Carboniferous and Permian than in the Devonian and that they rose to dominate aquatic faunas by the Mesozoic. While the exact mode of this diversification across the Devonian-Carboniferous boundary and throughout the late Palaeozoic remains uncertain, the work presented in this thesis represents an important step forward in determining these patterns and teasing out the true underlying signal from obfuscating noise.

6.2 The importance of taxonomic and descriptive study

While not the 'flashiest' or most exciting field, taxonomic and descriptive studies are the foundation of palaeontological research. They fundamentally underpin all subsequent forms of investigation, such as diversity- and phylogeny-based research. New technology facilitates new discoveries and recognising hidden internal morphology among Palaeozoic actinopterygians (e.g. 319 million year old fossilised brains [Figueroa *et al.*, 2023]), proving that there is so much yet to learn about their evolution. A chief priority is the revision of prolific 'waste-basket' genera, as recently done for *Elonichthys* (Schindler, 2017, 2018a). Doing so, however, necessarily requires the revision of all species previously attributed to these genera. For example, over 40 species of '*Elonichthys*' (i.e. species not included in the genus following its recent revision) now require reinvestigation to determine whether they represent new taxa or belong to other existing genera. In tandem with these reinvestigations, it will be important to revisit historically overlooked collections of Carboniferous and Permian fishes with an eye to not only realise new taxonomic diversity, but to redescribe existing taxa in order to add important morphological data to phylogenetic studies.

Improving taxonomy will also be critical for future research on actinopterygian palaeodiversity. At present, significant taxonomic diversity is hidden by poorly defined genera and species that undoubtedly influence face-value diversity patterns. Nearly 150 species of Palaeozoic actinopterygians, representing almost a third of known species, belong to just six genera (Henderson *et al.*, 2022, 2023). This not only impacts face-value diversity; the related unevenness it causes in occurrence distributions causes issues with sampling standardisation techniques. While the scale of this problem seems vast, some clear opportunities present themselves. One suggested approach for countering the effect of spatial biases of studies of palaeodiversity is to concentrate on well-sampled, localised regions. Targeted taxonomic revisions of material from historically well-sampled regions, such as the Midland Valley of Scotland or Bohemian Massif of Central Europe, could be part of a concerted effort to understand regional palaeodiversity trends.

6.3 Future palaeodiversity studies

Despite a near 200-year history, the study of the diversity trends of early actinopterygians remains in its infancy. Collectors' curves do not appear to be reaching an asymptote and the rising rate of new descriptions continues to inflate counts of singletons (Chapters 2 and 3; Henderson *et al.*, 2022, 2023) – a clear indication of the early stage of research on Palaeozoic actinopterygian diversity. Increasing numbers of singletons are known to cause problems with richness estimators, though the use of sampling-standardised discovery curves (SSDCs [Close *et al.*, 2018]) may be a worthwhile avenue of research to pursue where sampling is adequate to accurately estimate diversity.

Unfortunately, most Palaeozoic intervals and sampled regions do not appear to be adequate for accurate actinopterygian diversity estimates at present (Chapters 2 and 3; Henderson *et al.*, 2022, 2023); increased sampling and alternative approaches will be necessary for future studies. Occurrence databases utilising publicly available resources such as the PBDB are currently the gold standard for examining palaeodiversity (Dillon *et al.*, 2023). However, future studies seeking to expand sampling will need to go beyond literature-based compilations of occurrences given how small a portion of the collected fossil record the literature covers (Allmon *et al.*, 2018; Marshall *et al.*, 2018). Most of the world is severely underrepresented in the actinopterygian (Chapters 2 and 3; Henderson *et al.*, 2022, 2023) and broader fossil records; the rest of the world is estimated to be around 45% as well sampled as Europe and North America (Ye & Peters, 2023). Exploration to discover new occurrences is one means of balancing this bias, though will necessarily be a slow process given the time involved in discovery of new fossil sites, description of specimens, and publication.

Collating data directly from museum collections may mitigate some biases more swiftly. Given that the majority of researchers are based at established universities and institutions in Europe and North America, this will continue to lead to literature and occurrence biases towards those regions (Raja *et al.*, 2022), as researchers are generally more likely to work on geographically localised material housed in nearby collections. For example, UK-based researchers are more likely to work on British museum collections, which contain a high proportion of British fossils (despite scientific colonialism resulting in non-British material finding its way to British collections). Accessing occurrences directly from collections in underrepresented regions lacking

the history of research, without as established research groups and with historically less funding will help to mitigate spatial bias towards North America and Europe, however it is vital that that local researchers drive this work and parachute science is avoided.

Given the significant spatial structuring of the fossil record, key to future studies on actinopterygian palaeodiversity research will be analyses focusing on specific, well-sampled regions in order to identify localised diversity dynamics. Prime candidates for this are the Carboniferous of Great Britain, the Carboniferous of North America, and the late Carboniferous to early Permian of Central Europe, given their long history of sampling and research (Traquair, 1877-1912; Frič, 1879; Rzehak, 1881; Newberry, 1889; Woodward, 1891; Eastman, 1902; Romer, 1945a; Dineley & Metcalf, 1999; Štamberg, 2006, 2007; Lloyd & Friedman, 2013), and reasonably well-constrained geochronology and stratigraphy (Breemen *et al.*, 1982; Monaghan & Parrish, 2006; Peters *et al.*, 2018). Building an accurate understanding of local trends will facilitate comparisons between regions, palaeoenvironments and across time, and potentially reveal patterns of provincialism or cosmopolitanism (Clapham & James, 2012; Qiao & Shen, 2014; Button *et al.*, 2017; Dai & Song, 2020). For example, comparison of localised trends in British, North American, and Central European diversity would allow plausible interpretations of how equatorial actinopterygian faunas changed during the Carboniferous and into the earliest Permian, which could be correlated with abiotic factors and biotic factors.

An alternative to occurrence-based diversity estimates would be to collate specimen-level databases (Schnetz *et al.*, 2022). Naturally, this task represents a much larger undertaking than an occurrence database, and so future studies could

focus initially on smaller geographic or temporal scales. Specimen-level data would allow for estimation of localised diversity dynamics at a finer resolution, though would likely need to be done in regions with temporally continuous fossil records to be of use regarding taxic diversity. Another possibility would be to categorise taxa by abundance, functional traits, and niche occupancy—in conjunction with the broader faunal assemblage (Bennett *et al.*, 2021)—in order to model ecosystem functions, trophic structure and biotic interactions (Keppeler *et al.*, 2020; Leuzinger & Rewald, 2021; Fraser *et al.*, 2021). By categorising by function rather than taxonomy, comparison of ecological diversity between regions and palaeoenvironments may be possible (Clarke, 2021). This kind of specimen-level data would also facilitate examination of actinopterygian diversity relative to other groups (e.g. chondrichthyans) (Schnetz, 2022; Schnetz *et al.*, 2022) across time and space.

6.4 Progress in phylogenetic investigation

Significant expansion of early actinopterygian representation in phylogenetic matrices is required. The latest time-scaled phylogenies place the origin of crown-actinopterygians close to the Devonian-Carboniferous boundary, crown-polypterids and crown-neopterygians in the late Carboniferous or early Permian, and crown-holosteans in the late Permian (Giles *et al.*, 2023). Despite this, the vast majority of species occupying the stems of extant clades occur in the Mesozoic. By more accurately constraining the sequence and tempo of character evolution, the addition of new Palaeozoic actinopterygians in future phylogenetic studies is likely to reveal both early crown-members and distinct radiations. The many clades hypothesised in the literature yet absent in most phylogenies represent the most obvious candidates for imminent inclusion (e.g. Aeduellidae [Heyler, 1969, 1977, 2000; Gottfried, 1987;

Štamberg, 2007, 2018; Mickle, 2011], Haplolepidae [Westoll, 1944; Lowney, 1980, 1983; Huber, 1992; Elliott, 2014], Ptycholepidae [Aldinger, 1937; Brough, 1939; Gardiner, 1967; Gardiner & Schaeffer, 1989; Bürgin, 1992; Romano *et al.*, 2019], Eurynotiformes [Sallan & Coates, 2013; Friedman *et al.*, 2018]). This will not only test the monophyly of these clades in a broader phylogenetic context but provide a more comprehensive representation of the morphological evolution of Palaeozoic actinopterygians. Recognition of well-supported clades defined by clear synapomorphies will also aid resolution of relationships between these clades, and in turn clarify the broader sequence of character acquisition and loss along the actinopterygian stem-lineage. Indeed, numerous studies have demonstrated how fossil data improves phylogenetic studies including extant lineages (Beck & Baillie, 2018; Asher *et al.*, 2019; Koch & Parry, 2020; Koch *et al.*, 2021).

In practice, this will require consolidation of characters and taxa from broad-scale phylogenetic matrices attempting to encompass the totality of the actinopterygian radiation (Giles *et al.*, 2017, 2023; Latimer & Giles, 2018; Argyriou *et al.*, 2018, 2022; Figueroa *et al.*, 2019, 2021; Stack & Gottfried, 2021) with those from finer-scale analyses of specific clades (Dietze, 2000; Poplin & Dutheil, 2005; Mickle *et al.*, 2009; Mutter *et al.*, 2011; Elliott, 2014, 2016). However, while they represent a priority, focus should not be limited to Palaeozoic actinopterygians. As evidenced by the recent realisation of scanilepiform and polypteriform affinity (Giles *et al.*, 2017), the relationships and character evolution of early crown-actinopterygians, such as stem- and crown-neopterygians (López-Arbarello & Sferco, 2018; Yuan *et al.*, 2022) and -chondrosteans (Grande & Bemis, 1991; Bemis *et al.*, 1997; Hilton *et al.*, 2011), will also have a bearing on those of earlier diverging clades. A coordinated approach from

the ‘top-down’ (i.e. adding early members of extant clades) and the ‘bottom-up’ (i.e. adding early stem-actinopterygian taxa and clades) represents the best way to develop phylogenetic hypotheses of the actinopterygian total group.

Novel methods of phylogenetic inference should also be used in tandem with updated data matrices. A fossilised birth-death model was recently implemented in an analysis of early actinopterygian phylogeny and divergence times (Giles *et al.*, 2023). However, this technique has recently been expanded to integrate information from fossil occurrences, either via the specification of stratigraphic ranges of in-group taxa (using multiple occurrences of the same species; Stadler *et al.*, 2018), incorporating stratigraphic age uncertainty (Barido-Sottani *et al.*, 2019, 2020), or providing information on sampling, birth and death rates, and the number of lineages (the occurrence birth-death process; Andréoletti *et al.*, 2022; Wright *et al.*, 2022). Expanded phylogenetic matrices could therefore be combined with recently compiled occurrence data for Palaeozoic actinopterygians. In addition, while many studies advocate for the superiority of Bayesian and likelihood-based methods of inference (Wright & Hillis, 2014; O’Reilly *et al.*, 2016, 2018; Puttick *et al.*, 2017b, 2019), parsimony methods also provide valuable information (Smith, 2019) especially when analysing discrete character datasets (Goloboff *et al*., 2018, 2019; Sansom *et al.*, 2018; Sookias, 2020). Extended implied weighting methods (Goloboff, 2014; Goloboff & Arias, 2019) may be useful with regard to early actinopterygian phylogeny due to the high levels of homoplasy and missing data.

Integration of new taxa into matrices and application of new methods raises the exciting prospect of generating robust phylogenetic hypotheses of early actinopterygian phylogeny. Together with the availability of occurrence data this would

open up a whole host of analytical techniques, such as phylogenetic comparative methods (Soul & Wright, 2021), used to explore evolutionary history. A conspicuous target for such analyses is the transition from the Devonian to Carboniferous and accurate identification of how actinopterygians rose to dominance. Robust phylogenetic hypotheses will not only help to clarify how many lineages crossed the end-Devonian mass extinction (Giles *et al.*, 2023), but facilitate interrogation of why those lineages persisted via explicit analysis of extinction selectivity and survivorship (Puttick *et al.*, 2017a; Soul & Friedman, 2017; Smithwick & Stubbs, 2018; Allen *et al.*, 2019; Lamsdell *et al.*, 2021). In turn, this will strengthen our understanding of the actinopterygian response to the extinction event and subsequent Carboniferous diversification (Sallan & Friedman, 2012; Sallan & Coates, 2013; Sallan & Galimberti, 2015). At present, it is unclear whether this represents an instance of adaptive radiation, a protracted extinction recovery, an ecological release facilitated by the extinction of placoderms and sarcopterygians, or some combination of all three (Schluter, 2000; Sallan & Coates, 2010; Sallan & Friedman, 2012; Friedman & Sallan, 2012; Slater, 2013; Holland, 2020). Analysis of evolutionary rates is an obvious first step (Simões & Pierce, 2021), which could be supplemented with simultaneous inspection of morphological disparity (Bault *et al.*, 2023) and ecological diversity (Cantalapiedra *et al.*, 2021) in a framework that can account for phylogenetic nonindependence and tease apart convergence (Speed & Arbuckle, 2017; Arbour & Zanno, 2020; Lautenschlager *et al.*, 2020).

An explicit phylogenetic framework is also critical for developing plausible sequences of habitat transition and biogeographic trends. While a marine origin of actinopterygians is almost certain (Betancur-R *et al.*, 2015), our understanding of

transitions to and from freshwater environments remains heavily reliant on crown actinopterygian data (Guinot & Cavin, 2018). Adequate representation of Palaeozoic taxa in similar analyses, though perhaps also exploring asymmetric transitions (Blackburn, 2015), has the potential to recognise alternate patterns of habitat colonisation in actinopterygian evolutionary history. In addition to habitat transitions, the ability to combine phylogenetic and occurrence data (Kubo, 2019) presents opportunities to examine drivers of diversification (such as vicariance; Capobianco and Friedman, 2019; Brikiatis, 2020), trends in bioregionalisation (Penn-Clarke & Harper, 2021; Dowding *et al.*, 2022; Pan *et al.*, 2022) and determinants of biogeographic variation (Button *et al.*, 2017; Dunne *et al.*, 2018; Dai & Song, 2020; Na *et al.*, 2022), though it will be critical to consider sampling biases alongside any such analysis (Maidment *et al.*, 2021).

Overall, the relative oversight of Palaeozoic actinopterygians compared with other vertebrates represents an opportunity. A wide range of novel analytical techniques are now available that await only the requisite data, and their application will help contemporary researchers to rework existing hypotheses about actinopterygian evolution. There are nascent signs that the next decade will be one of rapid improvement in our understanding of the origin and rise of the ray-finned fishes.

References

ÁDÁM T. KOCSIS & NUSSAÏBAH B. RAJA (2019) *chronosphere: Earth system history variables (pre-release) (Version 0.1.5).* Zenodo. http://doi.org/10.5281/zenodo.3525482. Zenodo.

AGASSIZ, L. (1833-1844) *Recherches sur les Poissons Fossiles*. Imprimerie de Petitpierre et Prince, Neuchâtel.

ALDINGER, H. (1937) Permische ganoidfische aus Ostgrönland. *Meddelelser om Grønland* **102**, 1–392.

ALDRICH, R. (2009) Colonial museums in a postcolonial Europe. *African and Black Diaspora: An International Journal* **2**, 137–156.

ALEKSEEV, A.A., LEBEDEV, O.A., BARSKOV, I.S., BARSKOVA, M.I., KONONOVA, L.I. & CHIZHOVA, V.A. (1994). On the stratigraphic position of the Famennian and Tournaisian fossil vertebrate beds in Andreyevka, Tula Region, Central Russia. *Proceedings of the Geologists' Association* **105**, 41–52.

ALLEN, B.J., STUBBS, T.L., BENTON, M.J. & PUTTICK, M.N. (2019). Archosauromorph extinction selectivity during the Triassic–Jurassic mass extinction. *Palaeontology* **62**, 211–224.

ALLEN, B.J., WIGNALL, P.B., HILL, D.J., SAUPE, E.E. & DUNHILL, A.M. (2020) The latitudinal diversity gradient of tetrapods across the Permo-Triassic mass extinction and recovery interval. *Proceedings of the Royal Society B: Biological Sciences* **287**, 20201125.

ALLIS, E. P. (1922) The cranial anatomy of *Polypterus*, with special reference to *Polypterus bichir*. *Journal of Anatomy* **56**, 189.

ALLISON, P.A. & BRIGGS, D.E.G. (1993) Paleolatitudinal sampling bias, Phanerozoic species diversity, and the end-Permian extinction. *Geology* **21**, 65–68.

ALLMON, W.D., DIETL, G.P., HENDRICKS, J.R. & ROSS, R.M. (2018) Bridging the two fossil records: Paleontology's "big data" future resides in museum collections. In *Museums at the Forefront of the History and Philosophy of Geology: History Made, History in the Making* (eds G.D. ROSENBURG & R. CLARY), Geological Society of America, Boulder, CO.

ALROY, J. (2009). Speciation and extinction in the fossil record of North American mammals. In *Speciation and Patterns of Diversity* (eds D. SCHLUTER, J. BRIDLE & R. BUTLIN), pp. 301–323. Cambridge University Press, Cambridge.

ALROY, J. (2010a) The Shifting Balance of Diversity Among Major Marine Animal Groups. *Science* **329**, 1191–1194.

ALROY, J. (2010b) Fair Sampling of Taxonomic Richness and Unbiased Estimation of Origination and Extinction Rates. *The Paleontological Society Papers* **16**, 55–80.

ALROY, J. (2010c) Geographical, environmental and intrinsic biotic controls on Phanerozoic marine diversification. *Palaeontology* **53**, 1211–1235.

ALROY, J. (2014) Accurate and precise estimates of origination and extinction rates. *Paleobiology* **40**, 374–397.

ALROY, J. (2017). Effects of habitat disturbance on tropical forest biodiversity. *Proceedings of the National Academy of Sciences* **114**, 6056–6061.

ALROY, J. (2018) Limits to species richness in terrestrial communities. *Ecology Letters* **21**, 1781–1789.

ALROY, J. (2020) On four measures of taxonomic richness. *Paleobiology* **46**, 158–175.

ALROY, J., ABERHAN, M., BOTTJER, D.J., FOOTE, M., FÜRSICH, F.T., HARRIES, P.J., HENDY, A.J.W., HOLLAND, S.M., IVANY, L.C., KIESSLING, W., KOSNIK, M.A., MARSHALL, C.R., MCGOWAN, A.J., MILLER, A.I., OLSZEWSKI, T.D., ET AL. (2008) Phanerozoic Trends in the Global Diversity of Marine Invertebrates. *Science* **321**, 97–100.

ANDERSON, J.S., SMITHSON, T., MANSKY, C.F., MEYER, T. & CLACK, J. (2015) A Diverse Tetrapod Fauna at the Base of 'Romer's Gap'. *PLOS ONE* **10**, e0125446.

ANDERSON, P.S.L., FRIEDMAN, M., BRAZEAU, M.D. & RAYFIELD, E.J. (2011) Initial radiation of jaws demonstrated stability despite faunal and environmental change. *Nature* **476**, 206–209.

ANDRÉOLETTI, J., ZWAANS, A., WARNOCK, R.C.M., AGUIRRE-FERNÁNDEZ, G., BARIDO-SOTTANI, J., GUPTA, A., STADLER, T. & MANCEAU, M. (2022) The Occurrence Birth–Death Process for Combined-Evidence Analysis in Macroevolution and Epidemiology. *Systematic Biology* **71**, 1440–1452.

ARBOUR, V.M. & ZANNO, L.E. (2020). Tail weaponry in Ankylosaurs and Glyptodonts: An example of a rare but strongly convergent phenotype. *The Anatomical Record* **303**, 988–998.

ARETZ, M., HERBIG, H.G., WANG, X.D., GRADSTEIN, F.M., AGTERBERG, F.P. & OGG, J.G. (2020) Chapter 23 - The Carboniferous Period. In *Geologic Time Scale 2020* (eds F.M. GRADSTEIN, J.G. OGG, M.D. SCHMITZ & G.M. OGG), pp. 811–874.

ARGYRIOU, T., GILES, S. & FRIEDMAN, M. (2022) A Permian fish reveals widespread distribution of neopterygian-like jaw suspension. *eLife* **11**, e58433.

ARGYRIOU, T., GILES, S., FRIEDMAN, M., ROMANO, C., KOGAN, I. & SÁNCHEZ-VILLAGRA, M.R. (2018) Internal cranial anatomy of Early Triassic species of †*Saurichthys* (Actinopterygii: †Saurichthyiformes): implications for the phylogenetic placement of †saurichthyiforms. *BMC Evolutionary Biology* **18**, 161.

ARRATIA, G. (1997) Basal teleosts and teleostean phylogeny. *Palaleo Ichthyologica* **7**, 1–168.

ARRATIA, G. (1999) The monophyly of Teleostei and stem-group teleosts. Consensus and disagreements. In *Mesozoic fishes 2: systematics and fossil record* (eds G. ARRATIA & H.-P. SCHULTZE), p. 604. Verlag Dr. Friedrich Pfeil, Munich.

ARRATIA, G. (2001) The sister-group of Teleostei: consensus and disagreements. *Journal of Vertebrate Paleontology* **21**, 767–773.

ARRATIA, G. (2013) Morphology, taxonomy, and phylogeny of Triassic pholidophorid fishes (Actinopterygii, Teleostei). *Journal of Vertebrate Paleontology* **33**, 1–138.

ARRATIA, G. & CIONE, A. (1996). The record of fossil fishes of southern South America. *Münchener Geowissenshaftliche Abhandlungen* **30**, 9–72.

ARRATIA, G. & CLOUTIER, R. (1996) Reassessment of the morphology of *Cheirolepis canadensis* (Cheirolepididae: Actinopterygii). In *Devonian fishes and plants of Miguasha, Quebec, Canada* (eds H.-P. SCHULTZE & R. CLOUTIER), pp. 165–197. Verlag Dr. Friedrich Pfeil, München, Germany.

ARRATIA, G. & CLOUTIER, R. (2004). A new cheirolepidid fish from the Middle-Devonian of Red Hill, Nevada, USA. In *Recent Advances in the Origin and Early Radiation of Vertebrates* (eds G. ARRATIA, M.V.H. WILSON & R. CLOUTIER), pp. 583–598. Verlag Dr. Friedrich Pfeil.

ASHER, R.J., SMITH, M.R., RANKIN, A. & EMRY, R.J. (2019) Congruence, fossils and the evolutionary tree of rodents and lagomorphs. *Royal Society Open Science* **6**, 190387.

ASSEMAT, A., GIRARD, C., JOACHIMSKI, M.M. & ADNET, S. (2022) Vertebrate diversity reveals perturbations in faunal communities prior to the Hangenberg event in the Montagne Noire (France). *Bulletin of Geosciences*, 109.

BAKAEV, A. & KOGAN, I. (2020) A new species of Burguklia (Pisces, Actinopterygii) from the Middle Permian of the Volga Region (European Russia). *PalZ* **94**, 93–106.

BANDYOPADHYAY, S. (1999). Gondwana vertebrate faunas of India. *Proceedings of the Indian National Science Academy* **A65**, 285–313.

BAPST, D.W. (2012) paleotree: an R package for paleontological and phylogenetic analyses of evolution. *Methods in Ecology and Evolution* **3**, 803–807.

BAPST, D.W., SCHREIBER, H.A. & CARLSON, S.J. (2018) Combined Analysis of Extant Rhynchonellida (Brachiopoda) using Morphological and Molecular Data. *Systematic Biology* **67**, 32–48.

BARDACK, D. (1979). Fishes of the Mazon Creek Fauna. In *Mazon Creek Fossils* (ed M.H. NITECKI), pp. 501–528. Academic Press.

BARDACK, D. (1992). Late Pennsylvanian paleonisciform fish from the Kinney Quarry, New Mexico. In *Geology and Paleontology of the Kinney Brick Quarry, Late Pennsylvanian, Central New Mexico* (ed J. ZIDEK), pp. 197–203.

BARIDO-SOTTANI, J., AGUIRRE-FERNÁNDEZ, G., HOPKINS, M.J., STADLER, T. & WARNOCK, R. (2019) Ignoring stratigraphic age uncertainty leads to erroneous estimates of species divergence times under the fossilized birth–death process. *Proceedings of the Royal Society B: Biological Sciences* **286**, 20190685.

BARIDO-SOTTANI, J., VAN TIEL, N.M.A., HOPKINS, M.J., WRIGHT, D.F., STADLER, T. & WARNOCK, R.C.M. (2020) Ignoring Fossil Age Uncertainty Leads to Inaccurate Topology and Divergence Time Estimates in Time Calibrated Tree Inference. *Frontiers in Ecology and Evolution* **8**.

BARNES, R. (2021). *dggridR: Discrete Global Grids for R*. C++.

BARNOSKY, A.D., CARRASCO, M.A. & DAVIS, E.B. (2005) The Impact of the Species–Area Relationship on Estimates of Paleodiversity. *PLoS Biology* **3**, e266.

BASDEN, A.M. & YOUNG, G.C. (2001) A primitive actinopterygian neurocranium from the Early Devonian of southeastern Australia. *Journal of Vertebrate Paleontology* **21**, 754–766.

BAULT, V., CRÔNIER, C. & MONNET, C. (2023) Coupling of taxonomic diversity and morphological disparity in Devonian trilobites? *Historical Biology* **0**, 1–12.

BECK, R.M.D. & BAILLIE, C. (2018) Improvements in the fossil record may largely resolve current conflicts between morphological and molecular estimates of mammal phylogeny. *Proceedings of the Royal Society B: Biological Sciences* **285**, 20181632.

BEHRENSMEYER, A.K. (1988) Vertebrate preservation in fluvial channels. *Palaeogeography, Palaeoclimatology, Palaeoecology* **63**, 183–199.

BELLWOOD, D.R. (2003) Origins and escalation of herbivory in fishes: a functional perspective. *Paleobiology* **29**, 71–83.

BELTAN, L. (1978) Decouverte d'une ichtyofaune dans le Carbonifere superieur d'Uruguay. Rapports avec les faunes ichtyologiques contemporaines des autres regions du Gondwana. *Annales de la Societe Geologique du Nord* **97, 351–355**, pls 58-60.

BELTAN, L. (1981). *Coccocephalichthys tessellatus* n.sp. (Pisces, Actinopterygii) from the Upper Carboniferous of Uruguay. *2nd Congresso Latino-Americano de Paleontologia, Porto Alegre*, 95–105.

BELTAN, L. (1989). New Permian actinopterygian families from Uruguay. *Acta Musei Reginaehradecensis, Series A, Scientiae Naturales* **22**, 79–86.

BEMIS, W.E., FINDEIS, E.K. & GRANDE, L. (1997) An overview of Acipenseriformes. *Environmental Biology of Fishes* **48**, 25–71.

BENDER, P. (2001). A new actinopterygian fish species from the late Permian Beaufort Group, South Africa. *Palaeontologia Africana* **37**, 25–40.

BENDER, P. (2002). A new Late Permian ray-finned (Actinopterygian) fish from the Beaufort Group, South Africa. *Palaeontologia Africana* **38**, 33–47.

BENDER, P. (2004). Late Permian actinopterygian (palaeoniscid) fishes from the Beaufort Group, South Africa: biostratigraphic and biogeographic implications. *Council for Geoscience Bulletin* **135**, 1–84.

BENDER, P. (2005). A new deep-bodied Late Permian actinopterygian fish from the Beaufort Group, South Africa. *Palaeontologia Africana* **41**, 7–22.

BENFIELD, M.C., COOK, S., SHARUGA, S. & VALENTINE, M.M. (2013) Five in situ observations of live oarfish Regalecus glesne (Regalecidae) by remotely operated vehicles in the oceanic waters of the northern Gulf of Mexico. *Journal of Fish Biology* **83**, 28–38.

BENNETT, C.E., KEARSEY, T.I., DAVIES, S.J., LENG, M.J., MILLWARD, D., SMITHSON, T.R., BRAND, P.J., BROWNE, M.A.E., CARPENTER, D.K., MARSHALL, J.E.A., DULSON, H. & CURRY, L. (2021) Palaeoecology and palaeoenvironment of Mississippian coastal lakes and marshes during the early terrestrialisation of tetrapods. *Palaeogeography, Palaeoclimatology, Palaeoecology* **564**, 110194.

BENNETT, C.V., UPCHURCH, P., GOIN, F.J. & GOSWAMI, A. (2018). Deep time diversity of metatherian mammals: implications for evolutionary history and fossil-record quality. *Paleobiology* **44**, 171–198.

BENSON, R.B.J. (2018). Dinosaur Macroevolution and Macroecology. *Annual Review of Ecology, Evolution, and Systematics* **49**, 379–408.

BENSON, R.B.J., BUTLER, R., CLOSE, R.A., SAUPE, E. & RABOSKY, D.L. (2021) Biodiversity across space and time in the fossil record. *Current Biology* **31**, R1225–R1236.

BENSON, R.B.J. & BUTLER, R.J. (2011) Uncovering the diversification history of marine tetrapods: ecology influences the effect of geological sampling biases. *Geological Society, London, Special Publications* **358**, 191–208.

BENSON, R.B.J., BUTLER, R.J., ALROY, J., MANNION, P.D., CARRANO, M.T. & LLOYD, G.T. (2016) Near-Stasis in the Long-Term Diversification of Mesozoic Tetrapods. *PLOS Biology* **14**, e1002359.

BENSON, R.B.J., BUTLER, R.J., LINDGREN, J. & SMITH, A.S. (2010). Mesozoic marine tetrapod diversity: mass extinctions and temporal heterogeneity in geological megabiases affecting vertebrates. *Proceedings of the Royal Society B: Biological Sciences* **277**, 829–834.

BENTON, M.J. (1993) *The Fossil Record 2*. Chapman and Hall.

BENTON, M.J. (2014). *Vertebrate Palaeontology*. Wiley-Blackwell, Chapman & Hall, London.

BENTON, M.J. (2015). Palaeodiversity and formation counts: redundancy or bias? *Palaeontology* **58**, 1003–1029.

BENTON, M.J., DUNHILL, A.M., LLOYD, G.T. & MARX, F.G. (2011). Assessing the quality of the fossil record: insights from vertebrates. *Geological Society, London, Special Publications* **358**, 63–94.

BENTON, M.J., RUTA, M., DUNHILL, A.M. & SAKAMOTO, M. (2013). The first half of tetrapod evolution, sampling proxies, and fossil record quality. *Palaeogeography, Palaeoclimatology, Palaeoecology* **372**, 18–41.

BERG, L.S. (1958). Early Carboniferous fishes from the Achinsk Region. *Voprosy Ihtiologii* **11**, 142–153.

BETANCUR-R, R., ORTÍ, G. & PYRON, R.A. (2015). Fossil-based comparative analyses reveal ancient marine ancestry erased by extinction in ray-finned fishes. *Ecology Letters* **18**, 441–450.

BETANCUR-R, R., WILEY, E.O., ARRATIA, G., ACERO, A., BAILLY, N., MIYA, M., LECOINTRE, G. & ORTÍ, G. (2017). Phylogenetic classification of bony fishes. *BMC Evolutionary Biology* **17**, 162.

BLACKBURN, D.G. (2015). Evolution of viviparity in squamate reptiles: Reversibility reconsidered. *Journal of Experimental Zoology Part B: Molecular and Developmental Evolution* **324**, 473–486.

BLAINVILLE, H.-M.D. DE (1818) Sur les ichthyolites ou les poissons fossiles. *Nouveau Dictionnaire d'Histoire Naturelle, appliquee aux Arts, a l'Agriculture, a l'Economie rurale et domestique, a la Medicine, etc. Nouvelle Edition* **27**, 310–395.

BLAINVILLE, H.-M.D. DE (1822) Analyse des principaux Traveaux dans les Sciences physiques, publiés dans l'année 1821. *Journal de physique, de chimie, d'histoire naturelle* **94**.

BLIECK, A. (2011) The André Dumont medallist lecture: From adaptive radiations to biotic crises in Palaeozoic vertebrates: a geobiological approach. *Geologica Belgica* **14**, 203–227.

BOLTON, H. (1895) The animal life of the Lancashire Coal Measures. *Transactions of the Manchester Microscopical Society*, 1–13.

BOLTON, H. (1904) The Palaeontology of the Lancashire Coal Measures. *Transactions of the Manchester Geological Society* **28**.

BOND, D.P.G., ZATOŃ, M., WIGNALL, P.B. & MARYNOWSKI, L. (2013) Evidence for shallow-water 'Upper Kellwasser' anoxia in the Frasnian–Famennian reefs of Alberta, Canada. *Lethaia* **46**, 355–368.

BOTELLA, H., BLOM, H., DORKA, M., AHLBERG, P.E. & JANVIER, P. (2007) Jaws and teeth of the earliest bony fishes. *Nature* **448**, 583–586.

BRAZEAU, M.D. (2011). Problematic character coding methods in morphology and their effects. *Biological Journal of the Linnean Society* **104**, 489–498.

BRAZEAU, M.D. & FRIEDMAN, M. (2015) The origin and early phylogenetic history of jawed vertebrates. *Nature* **520**, 490–497.

BRAZEAU, M.D., GUILLERME, T. & SMITH, M.R. (2019). An algorithm for Morphological Phylogenetic Analysis with Inapplicable Data. *Systematic Biology* **68**, 619–631.

BREEMEN, O. VAN, AFTALION, M., BOWES, D.R., DUDEK, A., MÍSAŘ, Z., POVONDRA, P. & VRÁNA, S. (1982) Geochronological studies of the Bohemian massif, Czechoslovakia, and their significance in the evolution of Central Europe. *Earth and Environmental Science Transactions of The Royal Society of Edinburgh* **73**, 89–108.

BRETT, C.E. (1995). Sequence stratigraphy, biostratigraphy, and taphonomy in shallow marine environments. *PALAIOS* **10**, 597–616.

BRIGGS, D.E.G. & GALL, J.-C. (1990). The continuum in soft-bodied biotas from transitional environments: A quantitative comparison of Triassic and Carboniferous Konservat-Lagerstatten. *Paleobiology* **16**, 204–218.

BRIGNON, A. (2019) The nomenclatural status of *Palaeothrissum inaequilobum* BLAINVILLE, 1818, *P. parvum* BLAINVILLE, 1818, and *Aeduella blainvillei* (AGASSIZ, 1833) (Actinopterygii, Aeduellidae). *Carnets Geol.* **19**, 141.

BRIKIATIS, L. (2020) An early Pangaean vicariance model for synapsid evolution. *Scientific Reports* **10**, 13091.

BRITO, P.M., ALVARADO-ORTEGA, J. & MEUNIER, F.J. (2017) Earliest known lepisosteoid extends the range of anatomically modern gars to the Late Jurassic. *Scientific Reports* **7**, 17830.

BROCKLEHURST, N. (2015) A simulation-based examination of residual diversity estimates as a method of correcting for sampling bias. *Palaeontologia Electronica* **18**, 1–15.

BROCKLEHURST, N. (2021) The First Age of Reptiles? Comparing Reptile and Synapsid Diversity, and the Influence of Lagerstätten, During the Carboniferous and Early Permian. *Frontiers in Ecology and Evolution* **9**, 507.

BROCKLEHURST, N. & FRÖBISCH, J. (2014). Current and historical perspectives on the completeness of the fossil record of pelycosaurian-grade synapsids. *Palaeogeography, Palaeoclimatology, Palaeoecology* **399**, 114–126.

BROCKLEHURST, N., KAMMERER, C.F. & FRÖBISCH, J. (2013). The early evolution of synapsids, and the influence of sampling on their fossil record. *Paleobiology* **39**, 470–490.

BROCKLEHURST, N., PANCIROLI, E., BENEVENTO, G.L. & BENSON, R.B., 2021. Mammaliaform extinctions as a driver of the morphological radiation of Cenozoic mammals. *Current Biology* **31(13)**, 2955-2963.

BROUGH, J. (1939) *The Triassic fishes of Besano, Lombardy*. Trustees of the British Museum, London [England].

BROUGHTON, R.E., BETANCUR-R., R., LI, C., ARRATIA, G. & ORTÍ, G. (2013) Multi-locus phylogenetic analysis reveals the pattern and tempo of bony fish evolution. *PLoS Currents* **5**.

BROWN, E.E., CASHMORE, D.D., SIMMONS, N.B. & BUTLER, R.J. (2019). Quantifying the completeness of the bat fossil record. *Palaeontology* **62**, 757–776.

BROWN, C.M., EVANS, D.C., CAMPIONE, N.E., O'BRIEN, L.J. & EBERTH, D.A. (2013) Evidence for taphonomic size bias in the Dinosaur Park Formation (Campanian, Alberta), a model Mesozoic terrestrial alluvial-paralic system. *Palaeogeography, Palaeoclimatology, Palaeoecology* **372**, 108–122.

BÜRGIN, T. (1992) *Basal Ray-finned Fishes (Osteichthyes; Actinopterygii) from the Middle Triassic of Monte San Giorgio (Canton Tessin, Switzerland): Systematic Palaeontology with Notes on Functional Morphology and Palaeoecology*. Birkhäuser.

BURROW, C. (1995) A new palaeoniscoid from the Lower Devonian Trundle beds of Australia. *Geobios* **28**, 319–325.

BUSH, A.M., MARKEY, M.J. & MARSHALL, C.R. (2004) Removing bias from diversity curves: the effects of spatially organized biodiversity on sampling-standardization. *Paleobiology* **30**, 666–686.

BUTLER, R.J., BENSON, R.B.J. & BARRETT, P.M. (2013) Pterosaur diversity: Untangling the influence of sampling biases, Lagerstätten, and genuine biodiversity signals. *Palaeogeography, Palaeoclimatology, Palaeoecology* **372**, 78–87.

BUTLER, R.J., BENSON, R.B.J., CARRANO, M.T., MANNION, P.D. & UPCHURCH, P. (2011). Sea level, dinosaur diversity and sampling biases: investigating the 'common cause' hypothesis in the terrestrial realm. *Proceedings of the Royal Society B: Biological Sciences* **278**, 1165–1170.

BUTTON, D.J., LLOYD, G.T., EZCURRA, M.D. & BUTLER, R.J. (2017). Mass extinctions drove increased global faunal cosmopolitanism on the supercontinent Pangaea. *Nature Communications* **8**, 733.

CAILLIEZ, F., 1983. The analytical solution of the additive constant problem. *Psychometrika* **48(2)**, 305-308.

CAMPBELL, K.S.W. & PHUOC, L.D. (1983). A Late Permian actinopterygian fish from Australia. *Palaeontology* **26**, 33–70.

CANTALAPIEDRA, J.L., DOMINGO, M.S. & DOMINGO, L. (2018). Multi-scale interplays of biotic and abiotic drivers shape mammalian sub-continental diversity over millions of years. *Scientific Reports* **8**, 13413.

CANTALAPIEDRA, J.L., SANISIDRO, Ó., ZHANG, H., ALBERDI, M.T., PRADO, J.L., BLANCO, F. & SAARINEN, J. (2021). The rise and fall of proboscidean ecological diversity. *Nature Ecology & Evolution*, 1–7.

CAPOBIANCO, A. & FRIEDMAN, M. (2019) Vicariance and dispersal in southern hemisphere freshwater fish clades: a palaeontological perspective. *Biological Reviews* **94**, 662–699.

CARMICHAEL, S.K., WATERS, J.A., SUTTNER, T.J., KIDO, E. & DEREUIL, A.A. (2014) A new model for the Kellwasser Anoxia Events (Late Devonian): Shallow water anoxia in an open oceanic setting in the Central Asian Orogenic Belt. *Palaeogeography, Palaeoclimatology, Palaeoecology* **399**, 394–403.

CARRETE VEGA, G. & WIENS, J.J. (2012). Why are there so few fish in the sea? *Proceedings of the Royal Society B: Biological Sciences* **279**, 2323–2329.

CARROLL, R.L. (1988). *Vertebrate paleontology and evolution*. Freeman, New York, N.Y.

CASHMORE, D.D., MANNION, P.D., UPCHURCH, P. & BUTLER, R.J. (2020). Ten more years of discovery: revisiting the quality of the sauropodomorph dinosaur fossil record. *Palaeontology* **63**, 951–978.

CAVIN, L. (2008). Palaeobiogeography of Cretaceous bony fishes (Actinistia, Dipnoi and Actinopterygii). *Geological Society, London, Special Publications* **295**, 165–183.

DE CELIS, A., NARVÁEZ, I., ARCUCCI, A. & ORTEGA, F. (2021) Lagerstätte effect drives notosuchian palaeodiversity (Crocodyliformes, Notosuchia). *Historical Biology* **33**, 3031–3040.

CHANG, M. (1982) The braincase of Youngolepis, a Lower Devonian crossopterygian from Yunnan, south-western China. PhD Thesis, Stockholm University, Stockholm.

CHAO, A. (1984). Nonparametric estimation of the number of classes in a population. *Scandinavian Journal of Statistics* **11**, 265–270.

CHAO, A., COLWELL, R.K., LIN, C.-W. & GOTELLI, N.J. (2009) Sufficient sampling for asymptotic minimum species richness estimators. *Ecology* **90**, 1125–1133.

CHAO, A. & JOST, L. (2012) Coverage-based rarefaction and extrapolation: standardizing samples by completeness rather than size. *Ecology* **93**, 2533–2547.

CHOO, B. (2012) Revision of the actinopterygian genus *Mimipiscis* (= *Mimia*) from the Upper Devonian Gogo Formation of Western Australia and the interrelationships of the early Actinopterygii. *Earth and Environmental Science Transactions of the Royal Society of Edinburgh* **102**, 77–104.

CHOO, B. (2015) A new species of the Devonian actinopterygian *Moythomasia* from Bergisch Gladbach, Germany, and fresh observations on *M. durgaringa* from the Gogo Formation of Western Australia. *Journal of Vertebrate Paleontology* **35**, e952817.

CHOO, B., LONG, J.A. & TRINAJSTIC, K. (2009) A new genus and species of basal actinopterygian fish from the Upper Devonian Gogo Formation of Western Australia. *Acta Zoologica* **90**, 194–210.

CHOO, B., LU, J., GILES, S., TRINAJSTIC, K. & LONG, J.A. (2019) A new actinopterygian from the Late Devonian Gogo Formation, Western Australia. *Papers in Palaeontology* **5**, 343–363.

CIONE, A.L., GOUIRIC-CAVALLI, S., MENNUCCI, J.A., CABRERA, D.A. & FREIJE, R.H. (2010). First vertebrate body remains from the Permian of Argentina (Elasmobranchii and Actinopterygii). *Proceedings of the Geologists' Association* **121**, 301–312.

CLACK, J.A. (2012) *Gaining Ground, Second Edition: The Origin and Evolution of Tetrapods*. Indiana University Press.

CLACK, J.A., BENNETT, C.E., DAVIES, S.J., SCOTT, A.C., SHERWIN, J.E. & SMITHSON, T.R. (2019). A Tournaisian (earliest Carboniferous) conglomerate-preserved non-marine faunal assemblage and its environmental and sedimentological context. *PeerJ* **6**, e5972.

CLAESON, K.M., BEMIS, W.E. & HAGADORN, J.W. (2007). New interpretations of the skull of a primitive bony fish *Erpetoichthys calabaricus* (Actinopterygii: Cladistia. *Journal of Morphology* **268**, 1021–1039.

CLAPHAM, M.E. & JAMES, N.P. (2012) Regional-scale marine faunal change in Eastern Australia during Permian climate fluctuations and its relationship to local community restructuring. *PALAIOS* **27**, 627–635.

CLAPHAM, M.E., KARR, J.A., NICHOLSON, D.B., ROSS, A.J. & MAYHEW, P.J. (2016). Ancient origin of high taxonomic richness among insects. *Proceedings of the Royal Society B: Biological Sciences* **283**, 20152476.

CLAPHAM, M.E., SHEN, S. & BOTTJER, D.J. (2009) The double mass extinction revisited: reassessing the severity, selectivity, and causes of the end-Guadalupian biotic crisis (Late Permian). *Paleobiology* **35**, 32–50.

CLARK, G. & JACKS, D. (2007) Coal and the Industrial Revolution, 1700–1869. *European Review of Economic History* **11**, 39–72.

CLARKE, J.T. (2021) Evidence for general size-by-habitat rules in actinopterygian fishes across nine scales of observation. *Ecology Letters* **24**, 1569–1581.

CLARKE, J.T. & FRIEDMAN, M. (2018) Body-shape diversity in Triassic–Early Cretaceous neopterygian fishes: sustained holostean disparity and predominantly gradual increases in teleost phenotypic variety. *Paleobiology* **44**, 402–433.

CLARKE, J.T., LLOYD, G.T. & FRIEDMAN, M. (2016) Little evidence for enhanced phenotypic evolution in early teleosts relative to their living fossil sister group. *Proceedings of the National Academy of Sciences* **113**, 11531–11536.

CLEAL, C.J. & THOMAS, B.A. (2005) Palaeozoic tropical rainforests and their effect on global climates: is the past the key to the present? *Geobiology* **3**, 13–31.

CLEARY, T.J., BENSON, R.B.J., EVANS, S.E. & BARRETT, P.M. (2018) Lepidosaurian diversity in the Mesozoic–Palaeogene: the potential roles of sampling biases and environmental drivers. *Royal Society Open Science* **5**, 171830.

CLEARY, T.J., BENSON, R.B.J., HOLROYD, P.A. & BARRETT, P.M. (2020) Tracing the patterns of non-marine turtle richness from the Triassic to the Palaeogene: from origin to global spread. *Palaeontology* **63**, 753–774.

CLEARY, T.J., MOON, B.C., DUNHILL, A.M. & BENTON, M.J. (2015) The fossil record of ichthyosaurs, completeness metrics and sampling biases. *Palaeontology* **58**, 521–536.

CLEMENT, A.M., KING, B., GILES, S., CHOO, B., AHLBERG, P.E., YOUNG, G.C. & LONG, J.A. (2018) Neurocranial anatomy of an enigmatic Early Devonian fish sheds light on early osteichthyan evolution. *eLife* **7**, e34349.

CLEMENTS, T., PURNELL, M. & GABBOTT, S. (2019). The Mazon Creek Lagerstätte: a diverse late Paleozoic ecosystem entombed within siderite concretions. *Journal of the Geological Society* **176**, 1–11.

CLOSE, R.A., BENSON, R.B.J., ALROY, J., BEHRENSMEYER, A.K., BENITO, J., CARRANO, M.T., CLEARY, T.J., DUNNE, E.M., MANNION, P.D., UHEN, M.D. & BUTLER, R.J. (2019) Diversity dynamics of Phanerozoic terrestrial tetrapods at the local-community scale. *Nature Ecology & Evolution* **3**, 590–597.

CLOSE, R.A., BENSON, R.B.J., ALROY, J., CARRANO, M.T., CLEARY, T.J., DUNNE, E.M., MANNION, P.D., UHEN, M.D. & BUTLER, R.J. (2020a) The apparent exponential radiation of Phanerozoic land vertebrates is an artefact of spatial sampling biases. *Proceedings of the Royal Society B: Biological Sciences* **287**, 20200372.

CLOSE, R.A., BENSON, R.B.J., SAUPE, E.E., CLAPHAM, M.E. & BUTLER, R.J. (2020b) The spatial structure of Phanerozoic marine animal diversity. *Science* **368**, 420–424.

CLOSE, R.A., BENSON, R.B.J., UPCHURCH, P. & BUTLER, R.J. (2017) Controlling for the species-area effect supports constrained long-term Mesozoic terrestrial vertebrate diversification. *Nature Communications* **8**, 15381.

CLOSE, R.A., EVERS, S.W., ALROY, J. & BUTLER, R.J. (2018) How should we estimate diversity in the fossil record? Testing richness estimators using sampling-standardised discovery curves. *Methods in Ecology and Evolution* **9**, 1386–1400.

CLOSE, R.A., FRIEDMAN, M., LLOYD, G.T. & BENSON, R.B.J. (2015). Evidence for a Mid-Jurassic Adaptive Radiation in Mammals. *Current Biology* **25**, 2137–2142.

CLOUTIER, R. & AHLBERG, P. (1996). Morphology, characters, and the interrelationships of basal sarcopterygians. In *Interrelationships of fishes.* pp. 445-80. Academic Press, San Diego.

CLOUTIER, R. & ARRATIA, G. (2004) Early diversification of actinopterygians. In *Recent Advances in the Origin and Early Radiation of Vertebrates* pp. 217–270. Verlag Dr. Friedrich Pfeil, München.

CLOUTIER, R., PROUST, J.N. & TESSIER, B., 2011. The Miguasha Fossil-Fish-Lagerstätte: a consequence of the Devonian land–sea interactions. *Palaeobiodiversity and Palaeoenvironments* **91**, 293-323.

Coates, M.I. (1993). New actinopterygian fish from the Namurian Manse Burn Formation of Bearsden, Scotland. *Palaeontology* **36**, 123–146.

COATES, M.I. (1998) Actinopterygians from the Namurian of Bearsden, Scotland, with comments on early actinopterygian neurocrania. *Zoological Journal of the Linnean Society* **122**, 27–59.

COATES, M.I. (1999) Endocranial preservation of a Carboniferous actinopterygian from Lancashire, UK, and the interrelationships of primitive actinopterygians. *Philosophical Transactions of the Royal Society of London. Series B: Biological Sciences* **354**, 435–462.

COATES, M.I. & TIETJEN, K. (2018) 'This strange little palaeoniscid': a new early actinopterygian genus, and commentary on pectoral fin conditions and function. *Earth and Environmental Science Transactions of the Royal Society of Edinburgh* **109**, 15–31.

COHEN, K.M., HARPER, D.A.T. & GIBBARD, P.L. (2021). ICS International Chronostratigraphic Chart 2021/05. International Commission on Stratigraphy, IUGS. www.stratigraphy.org [accessed 26 July 2021].

COLWELL, R.K., CODDINGTON, J.A. & HAWKSWORTH, D.L. (1994) Estimating terrestrial biodiversity through extrapolation. *Philosophical Transactions of the Royal Society of London. Series B: Biological Sciences* **345**, 101–118.

COOPER, R.A., MAXWELL, P.A., CRAMPTON, J.S., BEU, A.G., JONES, C.M. & MARSHALL, B.A. (2006). Completeness of the fossil record: Estimating losses due to small body size. *Geology* **34**, 241–244.

COPPER, P. & SCOTESE, C.R. (2003) Megareefs in Middle Devonian supergreenhouse climates. In *Extreme depositional environments: mega end members in geologic time* (eds M.A. CHAN & A.W. ARCHER). Geological Society of America.

COX, C.B. & HUTCHINSON, P. (1991). Fishes and amphibians from the late Permian Pedra de Fogo formation of northern Brazil. *Fishes and amphibians from the late Permian Pedra de Fogo formation of northern Brazil* **34**, 561–573.

CRAMPTON, J.S., BEU, A.G., COOPER, R.A., JONES, C.M., MARSHALL, B. & MAXWELL, P.A. (2003). Estimating the rock volume bias in paleobiodiversity studies. *Science* **301**, 358–360.

DAESCHLER, E.B. (2000) An Early Actinopterygian Fish from the Catskill Formation (Late Devonian, Famennian) in Pennsylvania, U.S.A. *Proceedings of the Academy of Natural Sciences of Philadelphia* **150**, 181–192.

DAI, X. & SONG, H. (2020) Toward an understanding of cosmopolitanism in deep time: a case study of ammonoids from the middle Permian to the Middle Triassic. *Paleobiology* **46**, 533–549.

DALQUEST, W.W. & KOCURKO, M.J. (1988). Notes on Permian fishes from Lake Kemp, Baylor County, Texas, with a synopsis of Texas palaeonisciform fishes. *The Southwestern Naturalist* **33**, 263–274.

DAS, S. & LOWE, M. (2018) Nature Read in Black and White: decolonial approaches to interpreting natural history collections. *Journal of Natural Science Collections* **6**, 4–14.

DAY, M.O., RAMEZANI, J., BOWRING, S.A., SADLER, P.M., ERWIN, D.H., ABDALA, F. & RUBIDGE, B.S. (2015) When and how did the terrestrial mid-Permian mass extinction occur? Evidence from the tetrapod record of the Karoo Basin, South Africa. *Proceedings of the Royal Society B: Biological Sciences* **282**, 20150834.

DEAKIN, W.J., ANDERSON, P.S.L., DEN BOER, W., SMITH, T.J., HILL, J.J., RÜCKLIN, M., DONOGHUE, P.C.J. & RAYFIELD, E.J. (2022) Increasing morphological disparity and decreasing optimality for jaw speed and strength during the radiation of jawed vertebrates. *Science Advances* **8**, eabl3644.

DEAN, C.D., CHIARENZA, A.A. & MAIDMENT, S.C.R. (2020) Formation binning: a new method for increased temporal resolution in regional studies, applied to the Late Cretaceous dinosaur fossil record of North America. *Palaeontology* **63**, 881–901.

DERYCKE, C., CLOUTIER, R. & CANDILIER, A.-M. (1995). Palaeozoic vertebrates of northern France and Belgium: Part II. Chondrichthyes; Acanthodii; Actinopterygii (uppermost Silurian to Carboniferous). *Geobios* **28**, 343–350.

DIAS, E.V. (2012). A new deep-bodied fossil fish (Actinopterygii) from the Rio do Rasto Formation, Paraná Basin, Brazil. *Zootaxa* **3192**, 1–23.

DIEDRICH, C.G. (2009). A coelacanthid-rich site at Hasbergen (NW Germany): taphonomy and palaeoenvironment of a first systematic excavation in the Kupferschiefer (Upper Permian, Lopingian). *Palaeobiodiversity and Palaeoenvironments* **1–2**, 67–94.

DIETZE, K. (2000) A Revision Of Paramblypterid And Amblypterid Actinopterygians From Upper Carboniferous–Lower Permian Lacustrine Deposits Of Central Europe. *Palaeontology* **43**, 927–966.

DILLON, E.M., DUNNE, E.M., WOMACK, T.M., KOUVARI, M., LARINA, E., CLAYTOR, J.R., IVKIĆ, A., JUHN, M., CARMONA, P.S.M., ROBSON, S.V., SAHA, A., VILLAFAÑA, J.A. & ZILL, M.E. (2023) Challenges and directions in analytical paleobiology. *Paleobiology*, 1–17.

DINELEY, D.L. & METCALF, S.J. (1999). *Fossil fishes of Great Britain*. Joint Nature Conservation Committee, Peterborough, UK.

DORNBURG, A. & NEAR, T.J. (2021) The Emerging Phylogenetic Perspective on the Evolution of Actinopterygian Fishes. *Annual Review of Ecology, Evolution, and Systematics* **52**, 427–452.

DOWDING, E.M. & EBACH, M.C. (2019) Evaluating Devonian bioregionalization: quantifying biogeographic areas. *Paleobiology* **45**, 636–651.

DOWDING, E.M., EBACH, M.C. & MAVRODIEV, E.V. (2022) Validating marine Devonian biogeography: a study in bioregionalization. *Palaeontology* **65**, e12578.

DRISCOLL, D.A., DUNHILL, A.M., STUBBS, T.L. & BENTON, M.J. (2019). The mosasaur fossil record through the lens of fossil completeness. *Palaeontology* **62**, 51–75.

DUNHILL, A.M., BENTON, M.J., NEWELL, A.J. & TWITCHETT, R.J. (2013). Completeness of the fossil record and the validity of sampling proxies: a case study from the Triassic of England and Wales. *Journal of the Geological Society* **170**, 291–300.

DUNHILL, A.M., BENTON, M.J., TWITCHETT, R.J. & NEWELL, A.J. (2012). Completeness of the fossil record and the validity of sampling proxies at outcrop level. *Palaeontology* **55**, 1155–1175.

DUNHILL, A.M., HANNISDAL, B. & BENTON, M.J. (2014) Disentangling rock record bias and common-cause from redundancy in the British fossil record. *Nature Communications* **5**, 4818.

DUNHILL, A.M., HANNISDAL, B., BROCKLEHURST, N. & BENTON, M.J. (2018) On formation-based sampling proxies and why they should not be used to correct the fossil record. *Palaeontology* **61**, 119–132.

DUNKLE, D.H. (1946). A new palaeoniscoid fish from the Lower Permian of Texas. *Journal of the Washington Academy of Sciences* **36**, 402–409.

DUNKLE, D.H. (1964). Preliminary description of a paleoniscoid fish from the Upper Devonian of Ohio. *Scientific Publications of the Cleveland Museum of Natural History* **3**, 1–24.

DUNKLE, D.H. & SCHAEFFER, B. (1973) *Tegeolepis clarki* (Newberry), a palaeonisciform from the Upper Devonian Ohio Shale. *Palaeontographica Abteilung A* **143**, 151–158.

DUNNE, E.M. (2020) Patterns and drivers of tetrapod diversity and biogeography in the late Palaeozoic and early Mesozoic. PhD Thesis, University of Birmingham.

DUNNE, E.M., CLOSE, R.A., BUTTON, D.J., BROCKLEHURST, N., CASHMORE, D.D., LLOYD, G.T. & BUTLER, R.J. (2018) Diversity change during the rise of tetrapods and the impact of the 'Carboniferous rainforest collapse'. *Proceedings of the Royal Society B: Biological Sciences* **285**, 20172730.

DUTHEIL, D.B. (1999) The first articulated fossil cladistian: Serenoichthys kemkemensis, gen. et sp. nov., from the Cretaceous of Morocco. *Journal of Vertebrate Paleontology* **19**, 243–246.

EASTMAN, C.R. (1902) The Carboniferous Fish-Fauna of Mazon Creek, Illinois. *The Journal of Geology* **10**, 535–541.

EGERTON, P. DE M.G. (1850) Palichthyologic Notes. No. 3.—On the Ganoidei Heterocerci. *Quarterly Journal of the Geological Society* **6**, 1–10.

EGERTON, P. DE M.G. (1856) Note on the fish remains from Styl Krans, South Africa. *Transactions of the Geological Society (London)* **2**, 226–227.

EICHWALD, C.E. VON (1861) *Palaeontology of Russia. Ancient Period: II. Fauna of the Greywacke. Calcareous and Copper Shale Formations of Russia.* tipografija Ya. Ionsona [E. Pratz or R. Golike], St. Petersburg.

ELLIOTT, F.M. (2014) A new haplolepid fauna (Osteichthyes: Actinopterygii) from the Lower Coal Measures of Scotland: Westphalian A; Langsettian, *Carbonicola communis* chronozone (Bashkirian). *Earth and Environmental Science Transactions of the Royal Society of Edinburgh* **105**, 207–225.

ELLIOTT, F.M. (2016) An early actinopterygian ichthyofauna from the Scottish Lower Coal Measures Formation: Westphalian A (Bashkirian). *Earth and Environmental Science Transactions of the Royal Society of Edinburgh* **107**, 351–394.

ESIN, D.N. (1990) The scale cover of Amblypterina costata (Eichwald) and the paleoniscid taxonomy based on isolated scales. *Palaeontological Journal* **2**, 90–98.

ESIN, D.N. (1995). Late Permian palaeoniscids of the European part of Russia [Posdnepermskiye paleoniscidy evropejskoj chasti Rossii]. PhD Thesis, Lomonossov State University, Moscow.

EVANS, F.J. (2005). Taxonomy, palaeoecology and palaeobiogeography of some palaeozoic fish of Southern Gondwana. PhD Thesis, University of Stellenbosch.

EZCURRA, M.D. & BUTLER, R.J. (2018). The rise of the ruling reptiles and ecosystem recovery from the Permo-Triassic mass extinction. *Proceedings of the Royal Society B: Biological Sciences* **285**, 20180361.

FAN, J., SHEN, S., ERWIN, D.H., SADLER, P.M., MACLEOD, N., CHENG, Q., HOU, X., YANG, J., WANG, X., WANG, Y., ZHANG, H., CHEN, X., LI, G., ZHANG, Y., SHI, Y., ET AL. (2020) A high-resolution summary of Cambrian to Early Triassic marine invertebrate biodiversity. *Science* **367**, 272–277.

FELICE, R.N. & GOSWAMI, A. (2018). Developmental origins of mosaic evolution in the avian cranium. *Proceedings of the National Academy of Sciences* **115**, 555–560.

FIGUEIREDO, F.J. & CARVALHO, B.C.M.C. (2004). A new actinopterygian fish from the Late Permian of the Paraná Basin, Southern Brazil. *Archivos do Museu Nacional do Rio de Janeiro.* **62**, 531–547.

FIGUEROA, R.T., FRIEDMAN, M. & GALLO, V. (2019) Cranial anatomy of the predatory actinopterygian *Brazilichthys macrognathus* from the Permian (Cisuralian) Pedra de Fogo Formation, Parnaíba Basin, Brazil. *Journal of Vertebrate Paleontology* **39**, e1639722.

FIGUEROA, R.T., GOODVIN, D., KOLMANN, M.A., COATES, M.I., CARON, A.M., FRIEDMAN, M. & GILES, S. (2023) Exceptional fossil preservation and evolution of the ray-finned fish brain. *Nature* **614**, 486–491.

FIGUEROA, R.T., WEINSCHÜTZ, L.C. & FRIEDMAN, M. (2021) The oldest Devonian circumpolar ray-finned fish? *Biology Letters* **17**, 20200766.

FLAMMANG, B.E., SUVARNARAKSHA, A., MARKIEWICZ, J. & SOARES, D. (2016) Tetrapod-like pelvic girdle in a walking cavefish. *Scientific Reports* **6**, 23711.

FLANNERY SUTHERLAND, J.T., MOON, B.C., STUBBS, T.L. & BENTON, M.J. (2019) Does exceptional preservation distort our view of disparity in the fossil record? *Proceedings of the Royal Society B: Biological Sciences* **286**, 20190091.

FLANNERY-SUTHERLAND, J.T., SILVESTRO, D. & BENTON, M.J. (2022) Global diversity dynamics in the fossil record are regionally heterogeneous. *Nature Communications* **13**, 2751.

FOOTE, M. (1994) Temporal variation in extinction risk and temporal scaling of extinction metrics. *Paleobiology* **20**, 424–444.

FOREY, P.L. & GRANDE, L. (1998) An African twin to the Brazilian Calamopleurus (Actinopterygii: Amiidae). *Zoological Journal of the Linnean Society* **123**, 179–195.

FOREY, P.L. & YOUNG, V.T. (1985). Upper Stephanian fishes from the Puertollano Basin, Ciudad Real, Spain (special volume). In *Papers on the Carboniferous of Iberian Peninsula (Sedimentology, Stratigraphy, Paleontology, Tectonics and Geochronology* (eds R.H. WAGNER & M.J.L. SOUSA), pp. 233–244. Anais Faculdade Ciencias Univ. Porto.

FRASER, D., SOUL, L.C., TÓTH, A.B., BALK, M.A., ERONEN, J.T., PINEDA-MUNOZ, S., SHUPINSKI, A.B., VILLASEÑOR, A., BARR, W.A., BEHRENSMEYER, A.K., DU, A., FAITH, J.T., GOTELLI, N.J., GRAVES, G.R., JUKAR, A.M., ET AL. (2021) Investigating Biotic Interactions in Deep Time. *Trends in Ecology & Evolution* **36**, 61–75.

FREY, L., RÜCKLIN, M., KORN, D. & KLUG, C. (2018). Late Devonian and Early Carboniferous alpha diversity, ecospace occupation, vertebrate assemblages and bio-events of southeastern Morocco. *Palaeogeography, Palaeoclimatology, Palaeoecology* **496**, 1–17.

FRIČ, A. (1879) *Fauna der Gaskohle und der Kalksteine der Permformation Böhmens*. In pp. 1–318. Selbstverlag—in commission bei Fr. Řivnáč, Prague.

FRICKE, R., ESCHMEYER, W.N. & VAN DER LAAN, R. (2023) ESHMEYER'S CATALOG OF FISHES: GENERA, SPECIES, REFERENCES.

http://researcharchive.calacademy.org/research/ichthyology/catalog/fishcatmain.asp [accessed 10 March 2023].

FRIEDMAN, M. (2015) The early evolution of ray-finned fishes. *Palaeontology* **58**, 213–228.

FRIEDMAN, M. (2022) The Macroevolutionary History of Bony Fishes: A Paleontological View. *Annual Review of Ecology, Evolution, and Systematics* **53**, 353–377.

FRIEDMAN, M. & BLOM, H. (2006). A new actinopterygian from the Famennian of East Greenland and the interrelationships of Devonian ray-finned fishes. *Journal of Paleontology* **80**, 1186–1204.

FRIEDMAN, M. & BRAZEAU, M.D. (2010) A reappraisal of the origin and basal radiation of the Osteichthyes. *Journal of Vertebrate Paleontology* **30**, 36–56.

FRIEDMAN, M., PIERCE, S.E., COATES, M. & GILES, S. (2018) Feeding structures in the ray-finned fish *Eurynotus crenatus* (Actinopterygii: Eurynotiformes): implications for trophic diversification among Carboniferous actinopterygians. *Earth and Environmental Science Transactions of the Royal Society of Edinburgh* **109**, 33–47.

FRIEDMAN, M. & SALLAN, L.C. (2012) Five hundred million years of extinction and recovery: a Phanerozoic survey of large-scale diversity patterns in fishes. *Palaeontology* **55**, 707–742.

GARDINER, B.G. (1960) A revision of certain Actinopterygian and Coelacanth fishes, chiefly from the Lower Lias. *Bulletin of the British Museum (Natural History), Geology* **4**, 239–384.

GARDINER, B.G. (1963) Certain palaeoniscoid fishes and the evolution of the snout in actinopterygians. *Bulletin of the British Museum (Natural History), Geology Series* **8(6), 257–325**, 2 pls.

GARDINER, B.G. (1967) Further notes on palaeoniscoid fishes with a classification of the Chondrostei. *Bulletin of the British Museum (Natural History), Geology Series* **14**, 146–206.

GARDINER, B.G. (1969) New palaeoniscoid fish from the Witteberg series of South Africa. *Zoological Journal of the Linnean Society* **48**, 423–452.

GARDINER, B.G. (1984) Devonian palaeoniscid fishes: new specimens of *Mimia* and *Moythomasia* from the Upper Devonian of Western Australia. *Bulletin of the British Museum of Natural History (Geology Series)* **37**, 173–428.

GARDINER, B.G. (1985) Actinopterygian fish from the Dinantian of Foulden, Berwickshire, Scotland. *Earth and Environmental Science Transactions of The Royal Society of Edinburgh* **76**, 61–66.

GARDINER, B.G. (1993). Osteichthyes: basal actinopterygians. In *The Fossil Record 2* (ed. M.J. BENTON). pp. 610-619, Chapman and Hall, London.

GARDINER, B.G. & BARTRAM, A.W.H. (1977). The homologies of ventral cranial fissures in osteichthyans. In *Problems in Early Vertebrate Evolution* (eds S.M. ANDREWS, R.S. MILES & A.D. WALKER), pp. 227–245. Academic Press, London, UK.

GARDINER, B.G. & SCHAEFFER, B. (1989) Interrelationships of lower actinopterygian fishes. *Zoological Journal of the Linnean Society* **97**, 135–187.

GARDINER, B.G., SCHAEFFER, B. & MASSERIE, J.A. (2005) A review of the lower actinopterygian phylogeny. *Zoological Journal of the Linnean Society* **144**, 511–525.

GARDNER, J.D., SURYA, K. & ORGAN, C.L. (2019) Early tetrapodomorph biogeography: Controlling for fossil record bias in macroevolutionary analyses. *Comptes Rendus Palevol* **18**, 699–709.

GERRINGER, M.E., LINLEY, T.D., JAMIESON, A.J., GOETZE, E. & DRAZEN, J.C. (2017) *Pseudoliparis swirei* sp. nov.: A newly-discovered hadal snailfish (Scorpaeniformes: Liparidae) from the Mariana Trench. *Zootaxa* **4358**, 161–177.

GESS, R.W. & WHITFIELD, A.K. (2020). Estuarine fish and tetrapod evolution: insights from a Late Devonian (Famennian) Gondwanan estuarine lake and a southern African Holocene equivalent. *Biological Reviews* **95**, 865–888.

GIEBEL, C. (1848) *Gaea excursoria germanica: Deutschlands Geologie, Geognosie und Paläontologie als unentbehrlicher Leitfaden auf Excursionen und beim Selbststudium*. E. Kummer.

GILES, S., COATES, M.I., GARWOOD, R.J., BRAZEAU, M.D., ATWOOD, R., JOHANSON, Z. & FRIEDMAN, M. (2015a) Endoskeletal structure in *Cheirolepis* (Osteichthyes, Actinopterygii), an early ray-finned fish. *Palaeontology* **58**, 849–870.

GILES, S., DARRAS, L., CLÉMENT, G., BLIECK, A. & FRIEDMAN, M. (2015b) An exceptionally preserved Late Devonian actinopterygian provides a new model for primitive cranial anatomy in ray-finned fishes. *Proceedings of the Royal Society B: Biological Sciences* **282**, 20151485.

GILES, S., FEILICH, K., PIERCE, S. & FRIEDMAN, M. (2021) High lineage survivorship across the end-Devonian Mass Extinction suggested by a remarkable new Late Devonian actinopterygian. bioRxiv. https://www.biorxiv.org/content/10.1101/2021.09.02.458676v2 [accessed 17 May 2022].

GILES, S., FEILICH, K., WARNOCK, R.C.M., PIERCE, S.E. & FRIEDMAN, M. (2023) A Late Devonian actinopterygian suggests high lineage survivorship across the end-Devonian mass extinction. *Nature Ecology & Evolution* **7**, 10–19.

GILES, S. & FRIEDMAN, M. (2014) Virtual reconstruction of endocast anatomy in early ray-finned fishes (Osteichthyes, Actinopterygii). *Journal of Paleontology* **88**, 636–651.

GILES, S., FRIEDMAN, M. & BRAZEAU, M.D. (2015c) Osteichthyan-like cranial conditions in an Early Devonian stem gnathostome. *Nature* **520**, 82–85.

GILES, S., XU, G.-H., NEAR, T.J. & FRIEDMAN, M. (2017) Early members of 'living fossil' lineage imply later origin of modern ray-finned fishes. *Nature* **549**, 265–268.

GINTER, M. & WILK, O., 2021. Middle Palaeozoic chondrichthyans and the associated ichthyofauna from southern Poland: a review. *Annales Societatis Geologorum Poloniae* **91(3)**, 253-286.

GOLOBOFF, P.A. (2014) Extended implied weighting. *Cladistics* **30**, 260–272.

GOLOBOFF, P.A. & ARIAS, J.S. (2019) Likelihood approximations of implied weights parsimony can be selected over the Mk model by the Akaike information criterion. *Cladistics* **35**, 695–716.

GOLOBOFF, P.A., LAET, J.D., RÍOS-TAMAYO, D. & SZUMIK, C.A. (2021). A reconsideration of inapplicable characters, and an approximation with step-matrix recoding. *Cladistics* **37(5)**, 596–629.

GOLOBOFF, P. & MORALES, M. (2023) TNT version 1.6, with a graphical interface for MacOS and Linux, including new routines in parallel. *Cladistics* **39**.

GOLOBOFF, P.A., PITTMAN, M., POL, D. & XU, X. (2019) Morphological Data Sets Fit a Common Mechanism Much More Poorly than DNA Sequences and Call Into Question the Mkv Model. *Systematic Biology* **68**, 494–504.

GOLOBOFF, P.A., TORRES, A. & ARIAS, J.S. (2018) Weighted parsimony outperforms other methods of phylogenetic inference under models appropriate for morphology. *Cladistics* **34**, 407–437.

GOLUBEV, V.K. (2001). Event stratigraphy and correlation of Kazanian marine deposits in the stratotype area. *Stratigraphy and Geological Correlation* **9**, 454–472.

GOOD, I.J. (1953) The population frequencies of species and the estimation of population parameters. *Biometrika* **40**, 237–264.

GOTTFRIED, M.D. (1987) A Pennsylvanian aeduelliform (Osteichthyes, Actinopterygii) from North America with comments on aeduelliform interrelationships. *Paläontologische Zeitschrift* **61**, 141–148.

GOTTFRIED, M.D. (1992). A new deep-scaled “palaeoniscoid” from the Kinney Quarry, Late Pennsylvanian of New Mexico. *New Mexico Bureau of Mines and Mineral Resources, Bulletin* **138**, 189–196.

GRADSTEIN, F.M., OGG, J.G., SCHMITZ, M.D. & OGG, G.M. (2020) *Geologic Time Scale 2020*. Elsevier.

GRANDE, L. (2010) An empirical synthetic pattern study of gars (Lepisosteiformes) and closely related species, based mostly on skeletal anatomy. The resurrection of Holostei. *Copeia* **10**, 1–871.

GRANDE, L. & BEMIS, W.E. (1991) Osteology and Phylogenetic Relationships of Fossil and Recent Paddlefishes (Polyodontidae) with Comments on the Interrelationships of Acipenseriformes. *Journal of Vertebrate Paleontology* **11**, 1–121.

GRANDE, L. & BEMIS, W.E. (1998) A Comprehensive Phylogenetic Study of Amiid Fishes (Amiidae) Based on Comparative Skeletal Anatomy. an Empirical Search for Interconnected Patterns of Natural History. *Journal of Vertebrate Paleontology* **18**, 1–696.

GRANDE, L. & HILTON, E.J. (2006) An Exquisitely Preserved Skeleton Representing a Primitive Sturgeon from the Upper Cretaceous Judith River Formation of Montana

(Acipenseriformes: Acipenseridae: N. gen. and sp.). *Memoir (The Paleontological Society)* **65**, 1–39.

GRANDE, L., JIN, F., YABUMOTO, Y. & BEMIS, W.E. (2002) Protopsephurus liui, a well-preserved primitive paddlefish (Acipenseriformes: Polyodontidae) from the Lower Cretaceous of China. *Journal of Vertebrate Paleontology* **22**, 209–237.

GREIG, D.C. (1988) *Geology of the Eyemouth district: memoir for 1:50 000 geological sheet 34 (Scotland)*. HMSO, Edinburgh.

GRIFFIS, N., MUNDIL, R., MONTAÑEZ, I., LE HERON, D., DIETRICH, P. & IANNUZZI, R. (2023) A Carboniferous apex for the late Paleozoic icehouse. *Geological Society, London, Special Publications* **535**, SP535-2022–2256.

GROGAN, E. & LUND, R. (2002). The geological and biological environment of the Bear Gulch Limestone (Mississippian of Montana, USA) and a model for its deposition. *Geodiversitas* **24**.

GROGAN, E.D. & LUND, R. (2015). Two new Actinopterygii (Vertebrata, Osteichthyes) with cosmine from the Bear Gulch Limestone (Heath Fm., Serpukhovian, Mississippian) of Montana USA. *Proceedings of the Academy of Natural Sciences of Philadelphia* **164**, 111–132.

GROSS, W. (1953) Devonische Palaeonisciden-Reste in Mittel-und Osteuropa. *Paläontologische Zeitschrift* **27**, 85–112.

GROSSNICKLE, D.M., SMITH, S.M. & WILSON, G.P., 2019. Untangling the multiple ecological radiations of early mammals. *Trends in ecology & evolution* **34(10)**, 936-949.

GUILLERME, T. & COOPER, N. (2018) Time for a rethink: time sub-sampling methods in disparity-through-time analyses. *Palaeontology* **61**, 481–493.

GUINOT, G. & CAVIN, L. (2018). Body size evolution and habitat colonization across 100 million years (Late Jurassic-Paleocene) of the actinopterygian evolutionary history. *Fish and Fisheries* **19**, 577–597.

GÜRICH, G. (1923). *Acrolepis lotzi* und andere Ganoiden aus den Dwyka-Schichten von Ganikobis, Südwestafrika. *Beiträge zur Geologischen Erforschung der Deutschen Schutzgebiete* **19**, 26–73.

HALLAM, A. & WIGNALL, P.B. (1999). Mass extinctions and sea-level changes. *Earth-Science Reviews* **48**, 217–250.

HALLIDAY, T.J.D., DOS REIS, M., TAMURI, A.U., FERGUSON-GOW, H., YANG, Z. & GOSWAMI, A. (2019). Rapid morphological evolution in placental mammals post-dates the origin of the crown group. *Proceedings of the Royal Society B: Biological Sciences* **286**, 20182418.

HALLIDAY, T.J.D., UPCHURCH, P. & GOSWAMI, A., 2016. Eutherians experienced elevated evolutionary rates in the immediate aftermath of the Cretaceous–Palaeogene mass extinction. *Proceedings of the Royal Society B: Biological Sciences* **283(1833)**, 20153026.

HAMEL, M.-H. (2005). A New Lower Actinopterygian from the Early Permian of the Paraná Basin, Brazil. *Journal of Vertebrate Paleontology* **25**, 19–26.

HAMPE, O., HAIRAPETIAN, V., DORKA, M., WITZMANN, F., AKBARI, A.M. & KORN, D. (2013). A first Late Permian fish fauna from Baghuk Mountain (Neo-Tethyan shelf, central Iran). *Bulletin of Geosciences* **88**, 1–20.

HANCOCK, A. & ATTHEY, T. (1872) XXVI.—Descriptive notes on a nearly entire specimen of *Pleurodus Rankinii*, on two new species of *Platysomus* and a new *Amphicentrum*, with remarks on a few other Fish remains found in the Coal-measures at Newsham. *Annals and Magazine of Natural History* **9**, 249–262.

HANCOCK, A. & HOWSE, R. (1870) On Dorypterus Hoffmanni, Germar, from the Marl-slate of Midderidge, Durham. *Quarterly Journal of the Geological Society* **26**, 623–641.

HANNIBAL, J.T. (2020). Berea sandstone: A heritage stone of international significance from Ohio, USA. *Geological Society, London, Special Publications* **486**, 177–204.

HANNISDAL, B., HAAGA, K.A., REITAN, T., DIEGO, D. & LIOW, L.H. (2017) Common species link global ecosystems to climate change: dynamical evidence in the planktonic fossil record. *Proceedings of the Royal Society B: Biological Sciences* **284**, 20170722.

HANNISDAL, B. & PETERS, S.E. (2011) Phanerozoic Earth System Evolution and Marine Biodiversity. *Science* **334**, 1121–1124.

HARPER, D.A.T., CASCALES-MIÑANA, B. & SERVAIS, T. (2020). Early Palaeozoic diversifications and extinctions in the marine biosphere: a continuum of change. *Geological Magazine* **157**, 5–21.

HAUBOLD, H. & SCHAUMBERG, G. (1985) *Die Fossilien des Kupferschiefers: Pflanzen-und Tierwelt zu Beginn des Zechsteins, eine Erzlagerstätte und ihre Paläontologie*. A. Ziemsen Verlag, Wittenberg Litherstadt.

HENDERSON, S., DUNNE, E.M., FASEY, S.A. & GILES, S. (2023) The early diversification of ray-finned fishes (Actinopterygii): hypotheses, challenges and future prospects. *Biological Reviews* **98**, 284–315.

HENDERSON, S., DUNNE, E.M. & GILES, S. (2021) The early diversification of ray-finned fishes (Actinopterygii): hypotheses, challenges and future prospects. EarthArXiv.

HENDERSON, S., DUNNE, E.M. & GILES, S. (2022) Sampling biases obscure the early diversification of the largest living vertebrate group. *Proceedings of the Royal Society B*, **289**, 20220916.

HENDY, A.J.W. (2011) Taphonomic Overprints on Phanerozoic Trends in Biodiversity: Lithification and Other Secular Megabiases. In *Taphonomy: Process and Bias Through Time* (eds P.A. ALLISON & D.J. BOTTJER), pp. 19–77.

HEYLER, D. (1969) Vertebres de l'Autunien de France. *Cahiers de Paleontologie*. Editions du Centre National de la Recherche Scientifique.

HEYLER, D. (1977) Sur Bourbonnella sottyi, un nouvel Aeduellidae (poisson Actinoptérygien). Stéphanien du Bassin de Blanzy-Montceau. *Compte Rendu sommaire de la Société Géologique de France* **1**, 21–23.

HEYLER, D. (2000) Les actinoptérygiens Stéphaniens et Autuniens du Massif Central (France) dans les collections du M.N.H.N. (Paris) et du Muséum d'Autun: compléments, mises au point, bilan. . *Bulletin de la Société d'Histoire Naturelle d'Autun* **169**, 7–44.

HILL, J.J., PUTTICK, M.N., STUBBS, T.L., RAYFIELD, E.J. & DONOGHUE, P.C.J. (2018) Evolution of jaw disparity in fishes. *Palaeontology* **61**, 847–854.

HILTON, E.J. (2002) Osteology of the extant North American fishes of the genus Hiodon Lesueur, 1818 (Teleostei: Osteoglossomorpha: Hiodontiformes). *Fieldiana*, **100**. 1–133.

HILTON, E.J. (2003) Comparative osteology and phylogenetic systematics of fossil and living bony-tongue fishes (Actinopterygii, Teleostei, Osteoglossomorpha). *Zoological Journal of the Linnean Society* **137**, 1–100.

HILTON, E.J. & FOREY, P.L. (2009) Redescription of †Chondrosteus acipenseroides Egerton, 1858 (Acipenseriformes, †Chondrosteidae) from the lower Lias of Lyme Regis (Dorset, England), with comments on the early evolution of sturgeons and paddlefishes. *Journal of Systematic Palaeontology* **7**, 427–453.

HILTON, E.J., GRANDE, L. & BEMIS, W.E. (2011) Skeletal Anatomy of the Shortnose Sturgeon, Acipenser brevirostrum Lesueur, 1818, and the Systematics of Sturgeons (Acipenseriformes, Acipenseridae). *Fieldiana Life and Earth Sciences* **2011**, 1–168.

HODNETT, J.-P.M., ELLIOTT, D.K., OLSON, T.J. & WITTKE, J.H. (2012) Ctenacanthiform sharks from the Permian Kaibab Formation, northern Arizona. *Historical Biology* **24**, 381–395.

HODNETT, J.-P. & LUCAS, S. (2015). Paleozoic fishes of New Mexico: a review. *Bulletin of the New Mexico Museum of Natural History and Science* **68**, 51–63.

HOLLAND, S.M. (2020) The Stratigraphy of Mass Extinctions and Recoveries. *Annual Review of Earth and Planetary Sciences* **48**, 75–97.

HOLLAND, T.M., LONG, J.A., WARREN, A. & GARVEY, J.M. (2006). Second specimen of the lower actinopterygian *Novogonatodus kasantsevae* Long 1988 from the Early Carboniferous of Mansfield, Victoria. *Proceedings of the Royal Society of Victoria* **118**, 1–10.

HOLZAPFEL, H.W. & MALZAHN, E. (1984). Die Fischreste der küstennahen Sedimente des unteren Zechstein 1 Westdeutschlands. *Geologica et Palaeontologica* **18**, 81–99.

HOOK, R.W. & BAIRD, D. (1986). The Diamond Coal Mine of Linton, Ohio, and its Pennsylvanian-age vertebrates. *Journal of Vertebrate Paleontology* **6**, 174–190.

HOSGÖR, I. & ŠTAMBERG, S. (2014). A first record of late Middle Permian actinopterygian fish from Anatolia, Turkey. *Acta Geologica Polonica* **64**, 147–159.

HOU, H., MA, X., ZHOU, H., OGG, J.G. & SHEN, Y. (2022) The End-Devonian Hangenberg Event and its aftermath in South China: Stratigraphic and sedimentary records from shallow to deep water facies. *Earth-Science Reviews* **232**, 104137.

HOUDE, P., BRAUN, E.L. & ZHOU, L., 2020. Deep-time demographic inference suggests ecological release as driver of neoavian adaptive radiation. *Diversity* **12(4)**, 164.

HSIEH, T.C., MA, K.H. & CHAO, A. (2016) iNEXT: an R package for rarefaction and extrapolation of species diversity (Hill numbers). *Methods in Ecology and Evolution* **7**, 1451–1456.

HUANG, C., JOACHIMSKI, M.M. & GONG, Y. (2018) Did climate changes trigger the Late Devonian Kellwasser Crisis? Evidence from a high-resolution conodont δ18OPO4 record from South China. *Earth and Planetary Science Letters* **495**, 174–184.

HUBER, P. (1992) *Pyritocephalus lowne*yae n. sp., the youngest haplolepiform (Pisces: Actinopterygii) from the Pennsylvanian of central New Mexico. *New Mexico Bureau of Mines Bulletin 138* **138**.

HUGHES, L.C., ORTÍ, G., HUANG, Y., SUN, Y., BALDWIN, C.C., THOMPSON, A.W., ARCILA, D., BETANCUR-R, R., LI, C., BECKER, L., BELLORA, N., ZHAO, X., LI, X., WANG, M., FANG, C., ET AL. (2018) Comprehensive phylogeny of ray-finned fishes (Actinopterygii) based on transcriptomic and genomic data. *Proceedings of the National Academy of Sciences* **115**, 6249–6254.

HURLEY, I.A., MUELLER, R.L., DUNN, K.A., SCHMIDT, E.J., FRIEDMAN, M., HO, R.K., PRINCE, V.E., YANG, Z., THOMAS, M.G. & COATES, M.I. (2007) A new time-scale for ray-finned fish evolution. *Proceedings of the Royal Society B: Biological Sciences* **274**, 489–498.

IVANOV, A.O. & LUCAS, S.G., 2019. Late Pennsylvanian fish assemblage from the Robledo Mountains and new records of Paleozoic chondrichthyans in New Mexico, USA. *Bulletin of Geosciences* **94(2)**, 235-255.

IVANOV, A.O., NESTELL, G.P. & NESTELL, M.K. (2013). Fish assemblages from the Capitanian (Middle Permian) of the Apache Mountains, West Texas, USA. In *The Carboniferous-Permian Transition: Bulletin 60* (eds S.G. LUCAS, W.A. DIMICHELE, J.E. BARRICK, J.W. SCHNEIDER & J.A. SPIELMANN), pp. 152–160. New Mexico Museum of Natural History and Science.

IVANOV, A.O., NESTELL, M.K., NESTELL, G.P. & BELL, G.L. (2020). New fish assemblages from the Middle Permian from the Guadalupe Mountains, West Texas, USA. *Palaeoworld* **29**, 239–256.

JACKSON, C.T. (1851). Report on the Albert Coal Mine. In *Reports on the geological relations, chemical analysis and microscopic examination of the Albert Coal Mining Company situated in Albert County, New Brunswick* p. 48. C. Vinten, New York.

JANVIER, P. (2007). Living primitive fishes and fishes from deep time. In *Fish Physiology* pp. 1–51. Academic Press.

JANVIER, P. & MAISEY, J.G. (2010). The Devonian vertebrates of South America and their biogeographical relationships. In *Morphology, Phylogeny and Paleobiogeography of Fossil Fishes* (eds G. ARRATIA, M.V.H. WILSON & R. CLOUTIER), pp. 431–459. Verlag Dr. Friedrich Pfeil, Munich.

JESSEN, H. (1968) *Moythomasia nitida* Gross und *M.* cf. *striata* Gross, devonische Palaeonisciden aus dem Oberen Plattenkalk der Bergisch-Gladbach --- Paffrather Mulde (Rheinisches Schiefergebirge). *Palaeontographica Abteilung A*, 87–114.

JOACHIMSKI, M.M., BREISIG, S., BUGGISCH, W., TALENT, J.A., MAWSON, R., GEREKE, M., MORROW, J.R., DAY, J. & WEDDIGE, K. (2009) Devonian climate and reef evolution: Insights from oxygen isotopes in apatite. *Earth and Planetary Science Letters* **284**, 599–609.

JOACHIMSKI, M.M. & BUGGISCH, W. (2002) Conodont apatite δ18O signatures indicate climatic cooling as a trigger of the Late Devonian mass extinction. *Geology* **30**, 711–714.

JONES, L.A., DEAN, C.D., MANNION, P.D., FARNSWORTH, A. & ALLISON, P.A. (2021). Spatial sampling heterogeneity limits the detectability of deep time latitudinal biodiversity gradients. *Proceedings of the Royal Society B: Biological Sciences* **288**, 20202762.

JOST, L. (2010) The Relation between Evenness and Diversity. *Diversity* **2**, 207–232.

JUBB, R.A. & GARDINER, B.G. (1975). A preliminary catalogue of identifiable fossil fish material from southern Africa. *Annals of the South African Museum* **67**, 381–440.

KAVEMBE, G.D., KAUTT, A.F., MACHADO-SCHIAFFINO, G. & MEYER, A. (2016) Eco-morphological differentiation in Lake Magadi tilapia, an extremophile cichlid fish living in hot, alkaline and hypersaline lakes in East Africa. *Molecular Ecology* **25**, 1610–1625.

KAZANTSEVA-SELEZNEVA, A.A. (1980). Permian Palaeonisci of central Siberia. *Paleontological Journal* **14**, 80–87.

KAZANTSEVA-SELEZNEVA, A.A. (1981). Late Palaeozoic Palaeonisci of East Kazakhstan [Pozdnepaleozoiskie paleoniski Vostochnogo Kazakhstana]. *Trudy Paleontologicheskogo Instituta Akademii Nauk SSSR* **180**, 1–140.

KEPPELER, F.W., MONTAÑA, C.G. & WINEMILLER, K.O. (2020) The relationship between trophic level and body size in fishes depends on functional traits. *Ecological Monographs* **90**, e01415.

KIESSLING, W., SIMPSON, C. & FOOTE, M. (2010). Reefs as cradles of evolution and sources of biodiversity in the Phanerozoic. *Science* **327**, 196–198.

KING, W. (1850) A Monograph of the Permian Fossils of England. *Monographs of the Palaeontographical Society* **3**, ix–258.

KIRKBY, J.W. (1864) On some Remains of Fish and Plants from the “Upper Limestone” of the Permian Series of Durham. *Quarterly Journal of the Geological Society of London* **20**, 345–358.

KNICK HARLEY, C. (1989) Coal exports and British shipping, 1850–1913. *Explorations in Economic History* **26**, 311–338.

KOCH, N.M., GARWOOD, R.J. & PARRY, L.A. (2021) Fossils improve phylogenetic analyses of morphological characters. *Proceedings of the Royal Society B: Biological Sciences* **288**, 20210044. Royal Society.

KOCH, N.M. & PARRY, L.A. (2020) Death is on Our Side: Paleontological Data Drastically Modify Phylogenetic Hypotheses. *Systematic Biology* **69**, 1052–1067.

KOOT, M.B. (2013). Effects of the late Permian mass extinction on chondrichthyan palaeobiodiversity and distribution patterns. PhD Thesis, Plymouth University.

KOTTELAT, M. (2012) Conspectus cobitidum*: an inventory of the loaches of the world (Teleostei: Cypriniformes: Cobitoidei). *The Raffles Bulletin of Zoology* **26**, 1–199.

KRIWET, J. (2005) A comprehensive study of the skull and dentition of pycnodont fishes. *Zitteliana* **45**, 135–188.

KRIWET, Ü. (2001) Feeding mechanisms and ecology of pycnodont fishes (Neopterygii, Pycnodontiformes). *Fossil Record* **4**, 139–165.

KSEPKA, D.T., STIDHAM, T.A. & WILLIAMSON, T.E., 2017. Early Paleocene landbird supports rapid phylogenetic and morphological diversification of crown birds after the K–Pg mass extinction. *Proceedings of the National Academy of Sciences* **114(30)**, 8047-8052.

KUBO, T. (2019). Biogeographical network analysis of Cretaceous terrestrial tetrapods: A phylogeny-based approach. *Systematic Biology* **68**, 1034–1051.

LAGOMARCINO, A.J. & MILLER, A.I. (2012). The relationship between genus richness and geographic area in Late Cretaceous marine biotas: epicontinental sea versus open-ocean-facing settings. *PLOS ONE* **7**, e40472.

LAKIN, J.A., MARSHALL, J.E.A., TROTH, I. & HARDING, I.C. (2016). Greenhouse to icehouse: a biostratigraphic review of latest Devonian–Mississippian glaciations and their global effects. *Geological Society, London, Special Publications* **423**, 439–464.

LAMBERS, P.H. (1999) The actinopterygian fish fauna of the Late Kimmeridgian and Early Tithonian 'Plattenkalke' near Solnhofen (Bavaria, Germany): state of the art. *Geologie en Mijnbouw* **78**, 215–229.

LAMSDELL, J.C. (2016). Horseshoe crab phylogeny and independent colonizations of fresh water: ecological invasion as a driver for morphological innovation. *Palaeontology* **59**, 181–194.

LAMSDELL, J.C., CONGREVE, C.R., HOPKINS, M.J., KRUG, A.Z. & PATZKOWSKY, M.E. (2017). Phylogenetic paleoecology: tree-thinking and ecology in deep time. *Trends in Ecology & Evolution* **32**, 452–463.

LATIMER, A.E. & GILES, S. (2018) A giant dapediid from the Late Triassic of Switzerland and insights into neopterygian phylogeny. *Royal Society Open Science* **5**, 180497.

LAUTENSCHLAGER, S., FIGUEIRIDO, B., CASHMORE, D.D., BENDEL, E.-M. & STUBBS, T.L. (2020) Morphological convergence obscures functional diversity in sabre-toothed carnivores. *Proceedings of the Royal Society B: Biological Sciences* **287**, 20201818.

LEBEDEV, O.A. (1996). Fish assemblages in the Tournaisian-Viséan environments of the East European Platform. *Geological Society, London, Special Publications* **107**, 387–415.

LEE, M.S.Y. & YATES, A.M. (2018). Tip-dating and homoplasy: reconciling the shallow molecular divergences of modern gharials with their long fossil record. *Proceedings of the Royal Society B: Biological Sciences* **285**, 20181071.

LEUZINGER, S. & REWALD, B. (2021) The Who or the How? Species vs. Ecosystem Function Priorities in Conservation Ecology. *Frontiers in Plant Science* **12**.

LEWIS, P.O. (2001) A Likelihood Approach to Estimating Phylogeny from Discrete Morphological Character Data. *Systematic Biology* **50**, 913–925.

LINLEY, T.D., GERRINGER, M.E., YANCEY, P.H., DRAZEN, J.C., WEINSTOCK, C.L. & JAMIESON, A.J. (2016) Fishes of the hadal zone including new species, in situ observations and depth records of Liparidae. *Deep Sea Research Part I: Oceanographic Research Papers* **114**, 99–110.

LIU, X.T. & WEI, F. (1988). A new saurichthyid from the Upper Permian of Zhejiang, China. *Vertebrata Palasiatica* **26**, 77–89.

LLOYD, G.T. (2011) A refined modelling approach to assess the influence of sampling on palaeobiodiversity curves: new support for declining Cretaceous dinosaur richness. *Biology Letters* **8**, 123–126.

LLOYD, G.T. & FRIEDMAN, M. (2013) A survey of palaeontological sampling biases in fishes based on the Phanerozoic record of Great Britain. *Palaeogeography, Palaeoclimatology, Palaeoecology* **372**, 5–17.

LLOYD, G.T., YOUNG, J.R. & SMITH, A.B. (2012*a*). Comparative quality and fidelity of deep-sea and land-based nannofossil records. *Geology* **40**, 155–158.

LLOYD, G.T., YOUNG, J.R. & SMITH, A.B. (2012*b*). Taxonomic structure of the fossil record is shaped by sampling bias. *Systematic Biology* **61**, 80–80.

LONG, J.A. (1988) New palaeoniscoid fishes from the late Devonian and early Carboniferous of Victoria. *Memoirs of the Association of Australasian Palaeontologists* **7**, 1–64.

LONG, J.A., CHOO, B. & YOUNG, G.C. (2008) A new basal actinopterygian fish from the Middle Devonian Aztec Siltstone of Antarctica. *Antarctic Science* **20**, 393–412.

LONG, J.A. & TRINAJSTIC, K. (2010) The Late Devonian Gogo Formation Lägerstatte of Western Australia: Exceptional Early Vertebrate Preservation and Diversity. *Annual Review of Earth and Planetary Sciences* **38**, 255–279.

LONG, J.A. & TRINAJSTIC, K.M. (2017) A review of recent discoveries of exceptionally preserved fossil fishes from the Gogo sites (Late Devonian, Western Australia). *Earth and Environmental Science Transactions of the Royal Society of Edinburgh* **108**, 111–117.

LÓPEZ-ARBARELLO, A., BÜRGIN, T., FURRER, H. & STOCKAR, R. (2016) New holostean fishes (Actinopterygii: Neopterygii) from the Middle Triassic of the Monte San Giorgio (Canton Ticino, Switzerland). *PeerJ* **4**, e2234.

LÓPEZ-ARBARELLO, A. & SFERCO, E. (2018) Neopterygian phylogeny: the merger assay. *Royal Society Open Science* **5**, 172337.

LOWNEY, K.A. (1980a) A Revision of the Family Haplolepidae (Actinopterygii, Paleonisciformes) from Linton, Ohio (Westphalian D, Pennsylvanian). *Journal of Paleontology* **54**, 942–953.

LOWNEY, K.A. (1980b). Certain Bear Gulch (Namurian A, Montana) Actinopterygii (Osteichthyes) and a reevaluation of the evolution of the Palaeozoic actinopterygians. PhD Thesis, New York University, New York, N.Y.

LOWNEY, K.A. (1983) The earliest known (Namurian A, E_1) haplolepids (Osteichthyes: Actinopterygii). *Transactions of the Royal Society of Edinburgh: Earth Sciences* **74**, 69–78.

LU, J., GILES, S., FRIEDMAN, M., DEN BLAAUWEN, J.L. & ZHU, M. (2016) The Oldest Actinopterygian Highlights the Cryptic Early History of the Hyperdiverse Ray-Finned Fishes. *Current Biology* **26**, 1602–1608.

LU, L.-W. (2002). A new Namurian palaeoniscoid fish from Zhongwei, Ningxia. *Vertebrata Palasiatica* **40**, 1–8.

LU, J. & ZHU, M. (2009) An onychodont fish (Osteichthyes, Sarcopterygii) from the Early Devonian of China, and the evolution of the Onychodontiformes. *Proceedings of the Royal Society B: Biological Sciences* **277**, 293–299.

LUCAS, S.G. (2017) Permian tetrapod extinction events. *Earth-Science Reviews* **170**, 31–60.

LUCAS, S.G., DIMICHELE, W.A. & ALLEN, B.D. (2021). *The Kinney Brick Quarry Lagerstätte, Late Pennsylvanian of New Mexico*. New Mexico Museum of Natural History and Science.

LUND, R. (2000). The new actinopterygian order Guildayichthyiformes from the lower Carboniferous of Montana (USA). *Geodiversitas* **22(2)**, 171–206.

LUND, R., GREENFEST-ALLEN, E. & GROGAN, E.D. (2012). Habitat and diversity of the Bear Gulch fish: Life in a 318 million year old marine Mississippian bay. *Palaeogeography, Palaeoclimatology, Palaeoecology* **342–343**, 1–16.

LUND, R. & MELTON, W.G. (1982). *Paratarrasius hibbardi* new genus and species (Actinopterygii, Tarrasiiformes) from the Namurian Bear Gulch Limestone of Montana, USA. *Palaeontology* **25**, 485–498.

LUND, R. & POPLIN, C. (1997) The rhadinichthyids (paleoniscoid actinopterygians) from the Bear Gulch Limestone of Montana (USA, Lower Carboniferous). *Journal of Vertebrate Paleontology* **17**, 466–486.

LUND, R. & POPLIN, C. (1999) Fish diversity of the Bear Gulch Limestone, Namurian, Lower Carboniferous of Montana, USA. *Geobios* **32**, 285–295.

LUND, R. & POPLIN, C. (2002). Cladistic analysis of the relationships of the tarrasiids (Lower Carboniferous actinopterygians). *Journal of Vertebrate Paleontology* **22(3)**, 480-486.

LUND, R., POPLIN, C. & MCCARTHY, K. (1995). Preliminary analysis of the interrelationships of some Paleozoic Actinopterygii. *Geobios* **28**, 215–220.

MAIDMENT, S.C.R., DEAN, C.D., MANSERGH, R.I. & BUTLER, R.J. (2021) Deep-time biodiversity patterns and the dinosaurian fossil record of the Late Cretaceous Western Interior, North America. *Proceedings of the Royal Society B: Biological Sciences* **288**, 20210692.

MALABARBA, M.C.L. (1988). A new genus and species of stem group actinopteran fish from the Lower Permian of Santa Catarina State, Brazil. *Zoological Journal of the Linnean Society* **94**, 287–299.

MANIAS, C. (2015) Building Baluchitherium and Indricotherium: Imperial and International Networks in Early-Twentieth Century Paleontology. *Journal of the History of Biology* **48**, 237–278.

MANNION, P.D., CHIARENZA, A.A., GODOY, P.L. & CHEAH, Y.N. (2019). Spatiotemporal sampling patterns in the 230 million year fossil record of terrestrial crocodylomorphs and their impact on diversity. *Palaeontology* **62**, 615–637.

MANNION, P.D. & UPCHURCH, P. (2010). Completeness metrics and the quality of the sauropodomorph fossil record through geological and historical time. *Paleobiology* **36**, 283–302.

MANNION, P.D., UPCHURCH, P., CARRANO, M.T. & BARRETT, P.M. (2011). Testing the effect of the rock record on diversity: a multidisciplinary approach to elucidating the generic richness of sauropodomorph dinosaurs through time. *Biological Reviews* **86**, 157–181.

MARK-KURIK, E. (2000). The Middle Devonian fishes of the Baltic States (Estonia, Latvia) and Belarus. *CFS Courier Forschungsinstitut Senckenberg* **223**, 309–324.

MARSHALL, C.R., FINNEGAN, S., CLITES, E.C., HOLROYD, P.A., BONUSO, N., CORTEZ, C., DAVIS, E., DIETL, G.P., DRUCKENMILLER, P.S., ENG, R.C., GARCIA, C., ESTES-SMARGIASSI, K., HENDY, A., HOLLIS, K.A., LITTLE, H., ET AL. (2018) Quantifying the dark data in museum fossil collections as palaeontology undergoes a second digital revolution. *Biology Letters* **14**, 20180431.

MÄRSS, T. (2001) Andreolepis (Actinopterygii) in the Upper Silurian of northern Eurasia. *Proceedings of the Estonian Academy of Sciences* **50**, 174-189.

MARTHA, R. (2002). A ray-finned fish (Osteichthyes) from the Late Permian of the State of Santa Catarina (Parana Basin), southern Brazil. *Revista Brasileira de Paleontologia* **3**, 56–61.

MARX, F.G. (2009). Marine mammals through time: when less is more in studying palaeodiversity. *Proceedings of the Royal Society B: Biological Sciences* **276**, 887–892.

MATVEEVA, A.A. (1958). Paleonistzidu Izuikchul'skogho ghorizonta Minusinskoi Kotlovinui. *Vprosy Ikhtiologii* **11**, 154–161.

MCGHEE, G.R., SHEEHAN, P.M., BOTTJER, D.J. & DROSER, M.L. (2012) Ecological ranking of Phanerozoic biodiversity crises: The Serpukhovian (early Carboniferous) crisis had a greater ecological impact than the end-Ordovician. *Geology* **40**, 147–150.

MCGOWAN, A.J. & SMITH, A.B. (2008) Are global Phanerozoic marine diversity curves truly global? A study of the relationship between regional rock records and global Phanerozoic marine diversity. *Paleobiology* **34**, 80–103.

MICKLE, K.E. (2011) The early actinopterygian fauna of the Manning Canyon Shale Formation (upper Mississippian, lower Pennsylvanian) of Utah, U.S.A. *Journal of Vertebrate Paleontology* **31**, 962–980.

MICKLE, K.E. (2012). Unravelling the systematics of palaeoniscoid fishes--lower actinopterygians in need of a complete phylogenetic revision. PhD Thesis, University of Kansas.

MICKLE, K.E. (2017) The lower actinopterygian fauna from the Lower Carboniferous Albert shale formation of New Brunswick, Canada – a review of previously described taxa and a description of a new genus and species. *Fossil Record* **20**, 47–67.

MICKLE, K.E. (2018) A new lower actinopterygian fish from the Upper Mississippian Bluefield Formation of West Virginia, USA. *PeerJ* **6**, e5533.

MICKLE, K.E., LUND, R. & GROGAN, E.D. (2009) Three new palaeoniscoid fishes from the Bear Gulch Limestone (Serpukhovian, Mississippian) of Montana (USA) and the relationships of lower actinopterygians. *Geodiversitas* **31**, 623–668.

MINIKH, A.V. & MINIKH, M.G. (2009) *Ikhtiofauna permi Evropeiskoi Rossii (Permian Ichthyofauna of the European Russia)*. Tsentr Nauka, Saratov.

MINIKH, A.V., MINIKH, M.G. & YANKEVICH, D.I. (2016). Permian and Triassic Fish Holotypes Kept in the Earth Sciences Museum at the Saratov State University. Article 2. Actinopterygian Fishes. *Известия Саратовского университета. Новая серия. Серия Науки о Земле* **16**, 178–187. Федеральное государственное бюджетное образовательное учреждение высшего образования «Саратовский национальный исследовательский государственный университет имени Н. Г. Чернышевского», Россия, Саратов.

MINIKH, M.G. (1992). New deep-bodied fishes from the Upper Permian deposits of the East European Plate. In *Questions of Palaeontology: the Inter-University Collection* (ed D.L. STEPANOV), pp. 137–146. Peterburgskii Gos. Universitet, St. Petersburg.

MINIKH, M.G. (1998). Late Permian and Triassic ichthyofauna of European Russia (taxonomy, stages of development, stratigraphic significance). PhD Thesis, Saratov State University, Saratov.

MITCHELL, J.S. (2015) Preservation is predictable: quantifying the effect of taphonomic biases on ecological disparity in birds. *Paleobiology* **41**, 353–367.

MIYASHITA, T., COATES, M.I., FARRAR, R., LARSON, P., MANNING, P.L., WOGELIUS, R.A., EDWARDS, N.P., ANNÉ, J., BERGMANN, U., PALMER, A.R. & CURRIE, P.J. (2019) Hagfish from the Cretaceous Tethys Sea and a reconciliation of the morphological–molecular conflict in early vertebrate phylogeny. *Proceedings of the National Academy of Sciences* **116**, 2146–2151. Proceedings of the

MONAGHAN, A.A., BROWNE, M.A.E. & BARFOD, D.N. (2014) An improved chronology for the Arthur's Seat volcano and Carboniferous magmatism of the Midland Valley of Scotland. *Scottish Journal of Geology* **50**, 165–172.

MONAGHAN, A.A. & PARRISH, R.R. (2006) Geochronology of Carboniferous–Permian magmatism in the Midland Valley of Scotland: implications for regional

tectonomagmatic evolution and the numerical time scale. *Journal of the Geological Society* **163**, 15–28.

MONTAÑEZ, I.P. (2016) A Late Paleozoic climate window of opportunity. *Proceedings of the National Academy of Sciences* **113**, 2334–2336. Proceedings of the

MONTAÑEZ, I.P. & POULSEN, C.J. (2013) The Late Paleozoic Ice Age: An Evolving Paradigm. *Annual Review of Earth and Planetary Sciences* **41**, 629–656.

MOY-THOMAS, J.A. (1938) Carboniferous Palaeoniscids from Northumberland and Berwickshire. *Geological Magazine* **75**, 308–318.

MOY-THOMAS, J.A. & DYNE, M.B. (1938) XVII.—The Actinopterygian Fishes from the Lower Carboniferous of Glencartholm, Eskdale, Dumfriesshire. *Earth and Environmental Science Transactions of The Royal Society of Edinburgh* **59**, 437–480. Royal Society of Edinburgh Scotland Foundation.

MURRAY, A.M. (2000). The Palaeozoic, Mesozoic and Early Cenozoic fishes of Africa. *Fish and Fisheries* **1**, 111–145.

MUSCENTE, A.D., SCHIFFBAUER, J.D., BROCE, J., LAFLAMME, M., O'DONNELL, K., BOAG, T.H., MEYER, M., HAWKINS, A.D., HUNTLEY, J.W., MCNAMARA, M., MACKENZIE, L.A., STANLEY, G.D., HINMAN, N.W., HOFMANN, M.H. & XIAO, S. (2017) Exceptionally preserved fossil assemblages through geologic time and space. *Gondwana Research* **48**, 164–188.

MUTTER, R.J., UPCHURCH, P., MCGOWAN, A.J. & SLATER, C.S.C. (2011) A case study of the palaeobiogeography of Early Mesozoic actinopterygians. In *Palaeogeography and Palaeobiogeography: Biodiversity in Space and Time* p. CRC Press.

NA, L., KOCSIS, Á.T., LI, Q. & KIESSLING, W. (2022) Coupling of geographic range and provincialism in Cambrian marine invertebrates. *Paleobiology*, 1–12.

NEAR, T.J., EYTAN, R.I., DORNBURG, A., KUHN, K.L., MOORE, J.A., DAVIS, M.P., WAINWRIGHT, P.C., FRIEDMAN, M. & SMITH, W.L. (2012) Resolution of ray-finned fish phylogeny and timing of diversification. *Proceedings of the National Academy of Sciences* **109**, 13698–13703.

NELSEN, M.P., DIMICHELE, W.A., PETERS, S.E. & BOYCE, C.K. (2016) Delayed fungal evolution did not cause the Paleozoic peak in coal production. *Proceedings of the National Academy of Sciences* **113**, 2442–2447. Proceedings of the

NELSON, J.S., GRANDE, T.C. & WILSON, M.V.H. (2016) *Fishes of the World*. John Wiley & Sons, Hoboken, N.J.

NEVES, R., GUEINN, K.J., CLAYTON, G., IOANNIDES, N.S., NEVILLE, R.S.W. & KRUSZEWSKA, K. (1973) Palynological Correlations within the Lower Carboniferous of Scotland and Northern England. *Earth and Environmental Science Transactions of The Royal Society of Edinburgh* **69**, 23–70. Royal Society of Edinburgh Scotland Foundation.

NEWBERRY, J.S. (1856) Description of several new genera and species of fossil fishes from the Carboniferous strata of Ohio. *Proceedings of the Academy of Natural Sciences of Philadelphia* **8**, 96–100.

NEWBERRY, J.S. (1889) *The Paleozoic fishes of North America*. U.S. Government Printing Office, Washington.

NEWBERRY, J.S. & WORTHEN, A.H. (1870) Part II - Paleontology of Illinois - Section I - Description of fossil vertebrates. In *Geology and Paleontology* (ed A.H. WORTHEN), pp. 345–374. Authority of the Legislature of Illinois, Chicago.

NEWMAN, M., BURROW, C., BLAAUWEN, J. DEN & GILES, S. (2021) A new actinopterygian Cheirolepis jonesi nov. sp. from the Givetian of Spitsbergen, Svalbard. *Norwegian Journal of Geology* **101**, 202103. Geological Society of Norway.

NIELSEN, E. (1942) Studies on Triassic fishes from East Greenland. I. *Glaucolepis* and *Boreosomus*. *Meddelelser om Grønland* **138**, 1–403.

NIELSEN, E. (1949) Studies on Triassic fishes from East Greenland. II. *Australosomus* and *Birgeria*. *Meddelelser om Grønland* **146**, 1–309.

NIEUWENHUYS, R. (1982) An Overview of the Organization of the Brain of Actinopterygian Fishes. *American Zoologist* **22**, 287–310.

NURGALIEV, D.K., SILANTIEV, V.V. & NIKOLAEVA, S.V. (eds) (2015) *Type and Reference Sections of the Middle and Upper Permian of the Volga and Kama River Regions*. Kazan University Press, Kazan.

O'REILLY, J.E., PUTTICK, M.N., PARRY, L., TANNER, A.R., TARVER, J.E., FLEMING, J., PISANI, D. & DONOGHUE, P.C.J. (2016) Bayesian methods outperform parsimony but at the expense of precision in the estimation of phylogeny from discrete morphological data. *Biology Letters* **12**, 20160081.

O'REILLY, J.E., PUTTICK, M.N., PISANI, D. & DONOGHUE, P.C.J. (2018) Probabilistic methods surpass parsimony when assessing clade support in phylogenetic analyses of discrete morphological data. *Palaeontology* **61**, 105–118.

OLIVE, S., CLÉMENT, G., DAESCHLER, E.B. & DUPRET, V. (2015*a*). Characterization of the placoderm (Gnathostomata) assemblage from the tetrapod-bearing locality of Strud (Belgium, upper Famennian). *Palaeontology* **58**, 981–1002.

OLIVE, S., CLÉMENT, G., DAESCHLER, E.B. & DUPRET, V. (2016). Placoderm Assemblage from the Tetrapod-Bearing Locality of Strud (Belgium, Upper Famennian) Provides Evidence for a Fish Nursery. *PLOS ONE* **11**, e0161540.

OLIVE, S., CLÉMENT, G., DENAYER, J., DERYCKE, C., DUPRET, V., GERRIENNE, P., GUERIAU, P., MARION, J.-M., MOTTEQUIN, B. & PRESTIANI, C. (2015*b*). Flora and fauna from a new Famennian (Upper Devonian) locality at Becco, eastern Belgium. *Geologica Belgica* **18**.

OLIVE, S., LEROY, Y., DAESCHLER, E.B., DOWNS, J.P., LADEVÈZE, S. & CLÉMENT, G. (2020). Tristichopterids (Sarcopterygii, Tetrapodomorpha) from the Upper Devonian tetrapod-bearing locality of Strud (Belgium, upper Famennian), with phylogenetic and paleobiogeographic considerations. *Journal of Vertebrate Paleontology* **40**, e1768105.

OLIVE, S., PRADEL, A., MARTINEZ-PÉREZ, C., JANVIER, P., LAMSDELL, J.C., GUERIAU, P., RABET, N., DURANLEAU-GAGNON, P., CÁRDENAS-ROZO, A.L., ZAPATA RAMÍREZ, P.A. & BOTELLA,

H. (2019). New insights into Late Devonian vertebrates and associated fauna from the Cuche Formation (Floresta Massif, Colombia). *Journal of Vertebrate Paleontology* **39**, e1620247.

OLSON, E.C. (1967). Early Permian vertebrates of Oklahoma. University of Oklahoma.

OPLUŠTIL, S. & CLEAL, C.J. (2007) A comparative analysis of some Late Carboniferous basins of Variscan Europe. *Geological Magazine* **144**, 417–448.

ØRVIG, T. (1960). New finds of acanthodians, arthrodires, crossopterygians, ganoids and dipnoans in the Upper Middle Devonian Calcareous Flags (Oberer Plattenkalk) of the Bergisch Gladbach-Paffrath Trough. *Paläontologische Zeitschrift* **34**, 295–335.

OTOO, B.K.A., CLACK, J.A., SMITHSON, T.R., BENNETT, C.E., KEARSEY, T.I. & COATES, M.I. (2019) A fish and tetrapod fauna from Romer's Gap preserved in Scottish Tournaisian floodplain deposits. *Palaeontology* **62**, 225–253.

PAGE, B.W. (1977) Collections and collectors of note: 14. The Manchester Museum. *Newsletter of the Geological Curators Group* **2**.

PAIS DE REZENDE, J.M., FIGUEROA, R.T., PONCIANO, L.C.M. DE O. & GALLO, V. (2021). A new Late Devonian fish fauna from Northeastern Brazil. *Historical Biology*, 1–10.

PAN, Z.-H., NIU, Z.-B., MENG, F.-Y. & ZHU, M. (2022) New insights from network analysis on the biogeography of antiarchs (jawed stem-Gnathostomata). *Palaeoworld*.

PARADIS, E., CLAUDE, J. & STRIMMER, K. (2004) APE: Analyses of Phylogenetics and Evolution in R language. *Bioinformatics* **20**, 289–290.

PARDO, J.D., LENNIE, K. & ANDERSON, J.S. (2020). Can we reliably calibrate deep nodes in the tetrapod tree? Case studies in deep tetrapod divergences. *Frontiers in Genetics* **11**.

PARDO, J.D., SMALL, B.J., MILNER, A.R. & HUTTENLOCKER, A.K. (2019) Carboniferous–Permian climate change constrained early land vertebrate radiations. *Nature Ecology & Evolution* **3**, 200–206.

PATES, S., WOLFE, J.M., LEROSEY-AUBRIL, R., DALEY, A.C. & ORTEGA-HERNÁNDEZ, J. (2022) New opabiniid diversifies the weirdest wonders of the euarthropod stem group. *Proceedings of the Royal Society B: Biological Sciences* **289**, 20212093.

PATTERSON, C. (1982) Morphology and Interrelationships of Primitive Actinopterygian Fishes. *American Zoologist* **22**, 241–259.

PATTERSON, C. (1994) Bony Fishes. *Short Courses in Paleontology* **7**, 57–84.

PEARSON, D.M. & WESTOLL, T.S. (1979) The Devonian actinopterygian Cheirolepis Agassiz. *Earth and Environmental Science Transactions of The Royal Society of Edinburgh* **70**, 337–399. Royal Society of Edinburgh Scotland Foundation.

PEARSON, M.R., BENSON, R.B.J., UPCHURCH, P., FRÖBISCH, J. & KAMMERER, C.F. (2013). Reconstructing the diversity of early terrestrial herbivorous tetrapods. *Palaeogeography, Palaeoclimatology, Palaeoecology* **372**, 42–49.

PENN-CLARKE, C.R. & HARPER, D.A.T. (2021) Early–Middle Devonian brachiopod provincialism and bioregionalization at high latitudes: A case study from southwestern Gondwana. *GSA Bulletin* **133**, 819–836.

PERRIER, V. & CHARBONNIER, S. (2014). The Montceau-les-Mines Lagerstätte (Late Carboniferous, France). *Comptes Rendus Palevol* **13**, 353–367.

PETERS, S.E. (2005) Geologic constraints on the macroevolutionary history of marine animals. *Proceedings of the National Academy of Sciences* **102**, 12326–12331.

PETERS, S.E. (2006). Genus extinction, origination, and the durations of sedimentary hiatuses. *Paleobiology* **32**, 387–407.

PETERS, S.E. (2007). The problem with the Paleozoic. *Paleobiology* **33**, 165–181.

PETERS, S.E. & FOOTE, M. (2001). Biodiversity in the Phanerozoic: a reinterpretation. *Paleobiology* **27**, 583–601.

PETERS, S.E. & HEIM, N.A. (2010) The geological completeness of paleontological sampling in North America. *Paleobiology* **36**, 61–79.

PETERS, S.E. & HEIM, N.A. (2011). Stratigraphic distribution of marine fossils in North America. *Geology* **39**, 259–262.

PETERS, S.E., HUSSON, J.M. & CZAPLEWSKI, J. (2018). Macrostrat: A platform for geological data integration and deep-time earth crust research. *Geochemistry, Geophysics, Geosystems* **19**, 1393–1409.

PLOTNICK, R.E. & WAGNER, P.J. (2006) Round up the usual suspects: common genera in the fossil record and the nature of wastebasket taxa. *Paleobiology* **32**, 126–146.

POINTON, M.A., CHEW, D.M., OVTCHAROVA, M., SEVASTOPULO, G.D. & CROWLEY, Q.G. (2012) New high-precision U–Pb dates from western European Carboniferous tuffs; implications for time scale calibration, the periodicity of late Carboniferous cycles and stratigraphical correlation. *Journal of the Geological Society* **169**, 713–721.

POPLIN, C. (1974). *Étude de quelques paléoniscidés pennsylvaniens du Kansas*. Cahiers de Paléontologie, C.N.R.S. Paris.

POPLIN, C., WANG, N.-C., RICHTER, M. & SMITH, M. (1991). An enigmatic actinopterygian (Pisces: Osteichthyes) from the Upper Permian of China. *Zoological Journal of the Linnean Society* **103**, 1–20.

POPLIN, C. & DUTHEIL, D. (2005). Les Aeduellidae (Pisces, Actinopterygii) carbonifères et permiens: systématique et étude phylogénétique préliminaire. *Geodiversitas* **27**, 17–33.

POPLIN, C. & LUND, R. (2000). Two new deep-bodied palaeoniscoid actinopterygians from Bear Gulch (Montana, USA, Lower Carboniferous). *Journal of Vertebrate Paleontology* **20**, 428–449.

POPLIN, C.M. & LUND, R. (2002). Two Carboniferous fine-eyed palaeoniscoids (Pisces, Actinopterygii) from Bear Gulch (USA). *Journal of Paleontology* **76**, 1014–1028.

POPLIN, M.C. & VÉRAN, M. (1996) A revision of the actinopterygian fish Coccocephalus wildi from the Upper Carboniferous of Lancashire. *Special Papers in Palaeontology* **52**, 7–30.

POWELL, M.G. (2009) The Latitudinal Diversity Gradient of Brachiopods over the Past 530 Million Years. *The Journal of Geology* **117**, 585–594.

POYATO-ARIZA, F.J. & WENZ, S. (2005) Akromystax tilmachiton gen. et sp. nov., a new pycnodontid fish from the Lebanese Late Cretaceous of Haqel and En Nammoura. *Journal of Vertebrate Paleontology* **25**, 27–45.

PRADEL, A., MAISEY, J.G., MAPES, R.H. & KRUTA, I. (2016). First evidence of an intercalar bone in the braincase of "palaeonisciform" actinopterygians, with a virtual reconstruction of a new braincase of *Lawrenciella* Poplin, 1984 from the Carboniferous of Oklahoma. *Geodiversitas* **38**, 489–504.

PROKOFIEV, A.M. (2002) First finding of an articulated actinopterygian skeleton from the Upper Devonian of Siberia and a reappraisal of the family Moythomasiidae Kazantseva, 1971 (Osteichthyes). *Paleontological Research* **6**, 321–327.

PROKOFIEV, A.M. (2005). An interesting new palaeoniscoid actinopterygian (Osteichthyes) from the Lower Permian of Southeastern Kazakhstan. *Paleontological Research* **9**, 85–92.

PURNELL, M.A., DONOGHUE, P.J.C., GABBOTT, S.E., MCNAMARA, M.E., MURDOCK, D.J.E. & SANSOM, R.S. (2018) Experimental analysis of soft-tissue fossilization: opening the black box. *Palaeontology* **61**, 317–323.

PUTTICK, M.N., KRIWET, J., WEN, W., HU, S., THOMAS, G.H. & BENTON, M.J. (2017a) Body length of bony fishes was not a selective factor during the biggest mass extinction of all time. *Palaeontology* **60**, 727–741.

PUTTICK, M.N., O'REILLY, J.E., PISANI, D. & DONOGHUE, P.C.J. (2019) Probabilistic methods outperform parsimony in the phylogenetic analysis of data simulated without a probabilistic model. *Palaeontology* **62**, 1–17.

PUTTICK, M.N., O'REILLY, J.E., TANNER, A.R., FLEMING, J.F., CLARK, J., HOLLOWAY, L., LOZANO-FERNANDEZ, J., PARRY, L.A., TARVER, J.E., PISANI, D. & DONOGHUE, P.C.J. (2017b) Uncertain-tree: discriminating among competing approaches to the phylogenetic analysis of phenotype data. *Proceedings of the Royal Society B: Biological Sciences* **284**, 20162290.

QIAO, L. & SHEN, S. (2014) Global paleobiogeography of brachiopods during the Mississippian—Response to the global tectonic reconfiguration, ocean circulation, and climate changes. *Gondwana Research* **26**, 1173–1185.

QIAO, T., KING, B., LONG, J.A., AHLBERG, P.E. & ZHU, M. (2016) Early Gnathostome Phylogeny Revisited: Multiple Method Consensus. *PLOS ONE* **11**, e0163157.

QIE, W., ALGEO, T.J., LUO, G. & HERRMANN, A. (2019) Global events of the Late Paleozoic (Early Devonian to Middle Permian): A review. *Palaeogeography, Palaeoclimatology, Palaeoecology* **531**, 109259.

R CORE TEAM (2020) *R: A language and environment for statistical computing.* R Foundation for Statistical Computing, Vienna, Austria.

RAJA, N.B., DUNNE, E.M., MATIWANE, A., KHAN, T.M., NÄTSCHER, P.S., GHILARDI, A.M. & CHATTOPADHYAY, D. (2022) Colonial history and global economics distort our understanding of deep-time biodiversity. *Nature Ecology & Evolution* **6**, 145–154.

RAMBAUT, A., DRUMMOND, A.J., XIE, D., BAELE, G. & SUCHARD, M.A. (2018) Posterior Summarization in Bayesian Phylogenetics Using Tracer 1.7. *Systematic Biology* **67**, 901–904.

RAMPINO, M.R. & SHEN, S.-Z. (2021) The end-Guadalupian (259.8 Ma) biodiversity crisis: the sixth major mass extinction? *Historical Biology* **33**, 716–722.

RAUP, D.M. (1972) Taxonomic Diversity during the Phanerozoic. *Science* **177**, 1065–1071.

RAUP, D.M. (1976) Species Diversity in the Phanerozoic: An Interpretation. *Paleobiology* **2**, 289–297.

REN, Y. & XU, G.-H. (2021) A new species of Pteronisculus from the Middle Triassic (Anisian) of Luoping, Yunnan, China, and phylogenetic relationships of early actinopterygian fishes. *Vertebrata Palasiatica* **59**.

RICHTER, M. & BREITKREUZ, C. (1997). Permian fish-remains from the north Chilean Peine Formation. *Modern Geology* **21**, 175–188.

ROBINSON, D.F. & FOULDS, L.R., 1981. Comparison of phylogenetic trees. *Mathematical Biosciences* **53(1-2)**, 131-147.

ROMANO, C., KOOT, M.B., KOGAN, I., BRAYARD, A., MINIKH, A.V., BRINKMANN, W., BUCHER, H. & KRIWET, J. (2016) Permian-Triassic Osteichthyes (bony fishes): diversity dynamics and body size evolution: Diversity and size of Permian-Triassic bony fishes. *Biological Reviews* **91**, 106–147.

ROMANO, C., LÓPEZ-ARBARELLO, A., WARE, D., JENKS, J.F. & BRINKMANN, W. (2019) Marine Early Triassic Actinopterygii from the Candelaria Hills (Esmeralda County, Nevada, USA). *Journal of Paleontology* **93**, 971–1000.

ROMER, A.S. (1945a) The late Carboniferous vertebrate fauna of Kounova (Bohemia) compared with that of the Texas Redbeds. *American Journal of Science* **243**, 417–442.

ROMER, A.S. (1945b) *Vertebrate Paleontology*, 2nd edition. University of Chicago Press, Chicago.

ROMER, A.S. (1956). The early evolution of land vertebrates. *Proceedings of the American Philosophical Society* **100**, 157–167.

ROMER, A.S. (1966) *Vertebrate Paleontology*, 3rd edition. University of Chicago Press, Chicago.

RONQUIST, F., TESLENKO, M., VAN DER MARK, P., AYRES, D.L., DARLING, A., HÖHNA, S., LARGET, B., LIU, L., SUCHARD, M.A. & HUELSENBECK, J.P. (2012) MrBayes 3.2: Efficient Bayesian

Phylogenetic Inference and Model Choice Across a Large Model Space. *Systematic Biology* **61**, 539–542.

RYGEL, M.C., CALDER, J.H., GIBLING, M.R., GINGRAS, M.K. & MELROSE, C.S.A. (2006). Tournaisian forested wetlands in the Horton Group of Atlantic Canada. In *Wetlands Through Time* (eds S.F. GREB & W.A. DIMICHELE). Geological Society of America.

RZEHAK, A. (1881) Die Fauna des mährischen Rothliegenden. *Verhandlungen der Kaiserl.-Königl. geologischen Reichsanstalt* **5**, 78–79.

SAHNEY, S., BENTON, M.J. & FERRY, P.A. (2010). Links between global taxonomic diversity, ecological diversity and the expansion of vertebrates on land. *Biology Letters* **6**, 544–547.

SAKAMOTO, M., VENDITTI, C. & BENTON, M.J. (2017) 'Residual diversity estimates' do not correct for sampling bias in palaeodiversity data. *Methods in Ecology and Evolution* **8**, 453–459.

SALLAN, L.C. (2012) Tetrapod-like axial regionalization in an early ray-finned fish. *Proceedings of the Royal Society B: Biological Sciences* **279**, 3264–3271.

SALLAN, L.C. (2014) Major issues in the origins of ray-finned fish (Actinopterygii) biodiversity: Ray-finned fish (Actinopterygii) origins. *Biological Reviews* **89**, 950–971.

SALLAN, L.C. & COATES, M.I. (2010) End-Devonian extinction and a bottleneck in the early evolution of modern jawed vertebrates. *Proceedings of the National Academy of Sciences* **107**, 10131–10135.

SALLAN, L.C. & COATES, M.I. (2013) Styracopterid (Actinopterygii) ontogeny and the multiple origins of post-Hangenberg deep-bodied fishes. *Zoological Journal of the Linnean Society* **169**, 156–199.

SALLAN, L.C. & FRIEDMAN, M. (2012) Heads or tails: staged diversification in vertebrate evolutionary radiations. *Proceedings of the Royal Society B: Biological Sciences* **279**, 2025–2032.

SALLAN, L. & GALIMBERTI, A.K. (2015) Body-size reduction in vertebrates following the end-Devonian mass extinction. *Science* **350**, 812–815.

SALLAN, L., FRIEDMAN, M., SANSOM, R.S., BIRD, C.M. & SANSOM, I.J. (2018). The nearshore cradle of early vertebrate diversification. *Science* **362**, 460–464.

SALLAN, L.C., KAMMER, T.W., AUSICH, W.I. & COOK, L.A. (2011) Persistent predator-prey dynamics revealed by mass extinction. *Proceedings of the National Academy of Sciences* **108**, 8335–8338.

SANDERS, H.L. (1968) Marine Benthic Diversity: A Comparative Study. *The American Naturalist* **102**, 243–282.

SANSOM, R.S., CHOATE, P.G., KEATING, J.N. & RANDLE, E. (2018) Parsimony, not Bayesian analysis, recovers more stratigraphically congruent phylogenetic trees. *Biology Letters* **14**, 20180263.

SANSOM, R.S., RANDLE, E. & DONOGHUE, P.C.J. (2015) Discriminating signal from noise in the fossil record of early vertebrates reveals cryptic evolutionary history. *Proceedings of the Royal Society B: Biological Sciences* **282**, 20142245.

SAWAI, E. & NYEGAARD, M. (2022) A review of giants: Examining the species identities of the world's heaviest extant bony fishes (ocean sunfishes, family Molidae). *Journal of Fish Biology* **100**, 1345–1364.

SCHACHAT, S., BARESCH, A., BUI, T., FALCON-LANG, H.J., CHANEY, D.S., NELSON, W.J., ELRICK, S.D., KERP, H., LUCAS, S.G. & DIMICHELE, W.A. (2023) Vegetational change during the Middle–Late Pennsylvanian transition in western Pangaea. *Geological Society, London, Special Publications* **535**, 535-2022–2281.

SCHAEFFER, B., DUNKLE, D.H. & MCDONALD, N.G. (1975) Ptycholepis marshi Newberry : a chondrostean fish from the Newark group of Eastern North America. *Fieldiana - Geology* **33**.

SCHINDLER, T. (2017) Neubeschreibung, Rekonstruktion, Paläoökologie und Paläobiogeografe von Elonichthys fritschi Friedrich, 1878 (Osteichthyes, Actinopterygii; Unterperm, Deutschland). *Mainzer naturwissenschaftliches Archiv* **54**, 5–47.

SCHINDLER, T. (2018*a*). Neubeschreibung und erste Rekonstruktion von *Elonichthys germari* Giebel, 1848. *Hallesches Jahrbuch für Geowissenschaften* **41**, 1–33.

SCHINDLER, T. (2018*b*). Revision of *Rhabdolepis macropterus* (Bronn, 1829) (Osteichthyes, lower Actinopterygii; Lower Permian, SW Germany). *PalZ* **92**, 651–660.

SCHLIEP, K.P. (2011) phangorn: phylogenetic analysis in R. *Bioinformatics* **27**, 592–593.

SCHLUTER, D. (2000). *The ecology of adaptive radiation*. Oxford University Press, Oxford.

SCHNETZ, L. (2022) Completeness and diversity patterns of Palaeozoic chondrichthyans. PhD Thesis, University of Birmingham, Birmingham, UK.

SCHNETZ, L., BUTLER, R.J., COATES, M.I. & SANSOM, I.J. (2022) Skeletal and soft tissue completeness of the acanthodian fossil record. *Palaeontology* **65**, e12616.

SCHRAM, F.R. (1983) Lower Carboniferous biota of Glencartholm, Eskdale, Dumfriesshire. *Scottish Journal of Geology* **19**, 1–15.

SCHULTZE, H.-P. (1968) Palaeoniscoidea-Schuppen aus dem Unterdevon Australiens und Kanadas und aus dem Mitteldevon Spitzbergens. *Bulletin of the British Museum (Natural History)* **16**, 343–368.

SCHULTZE, H.-P. & BARDACK, D. (1987). Diversity and size changes in palaeonisciform fishes (Actinopterygii, Pisces) from the Pennsylvanian Mazon Creek fauna, Illinois, U.S.A. *Journal of Vertebrate Paleontology* **7**, 1–23.

SCHULTZE, H.-P. & CUMBAA, S.L. (2001) *Dialipina* and the characters of basal actinopterygians. In *Major Events in Early Vertebrate Evolution*. CRC Press.

SCHULTZE, H.-P. & MÄRSS, T. (2004) Revisiting Lophosteus, a primitive osteichthyan. *Acta Universitatis Latviensis* **679**, 57–78.

SCOTESE, C.R. (2021). An atlas of Phanerozoic paleogeographic maps: the seas come in and the seas go out. *Annual Review of Earth and Planetary Sciences* **49**, 679–728.

SEPKOSKI, J.J. (1976) Species diversity in the Phanerozoic: species-area effects. *Paleobiology* **2**, 298–303.

SEPKOSKI, J.J. (1981) A factor analytic description of the Phanerozoic marine fossil record. *Paleobiology* **7**, 36–53.

SEPKOSKI, J.J. (1996) Patterns of Phanerozoic Extinction: a Perspective from Global Data Bases. In *Global Events and Event Stratigraphy in the Phanerozoic: Results of the International Interdisciplinary Cooperation in the IGCP-Project 216 "Global Biological Events in Earth History"* (ed O.H. WALLISER), pp. 35–51. Springer, Berlin, Heidelberg.

SEPKOSKI, J.J. (2002). A compendium of fossil marine animal genera. *Bulletins of American Paleontology* **363**, 1–560.

SEPKOSKI, J.J., BAMBACH, R.K., RAUP, D.M. & VALENTINE, J.W. (1981) Phanerozoic marine diversity and the fossil record. *Nature* **293**, 435–437.

SFERCO, E., LÓPEZ-ARBARELLO, A. & MARÍA BÁEZ, A. (2015) Anatomical description and taxonomy of †*Luisiella feruglioi* (Bordas), new combination, a freshwater teleost (Actinopterygii, Teleostei) from the Upper Jurassic of Patagonia. *Journal of Vertebrate Paleontology* **35**, e924958.

SIMÕES, T.R. & PIERCE, S.E. (2021) Sustained high rates of morphological evolution during the rise of tetrapods. *Nature Ecology & Evolution* **5**, 1403–1414. Nature Publishing Group.

SIMÕES, T.R., VERNYGORA, O., CALDWELL, M.W. & PIERCE, S.E. (2020). Megaevolutionary dynamics and the timing of evolutionary innovation in reptiles. *Nature Communications* **11**, 3322.

ŠIMŮNEK, Z. & CLEAL, C.J. (2020). The systematic and palaeoecological significance of *Neuropteris ovata* (Medullosales) cuticles from the Stephanian Stage of the Puertollano Basin, Spain. *Spanish Journal of Palaeontology* **31**, 231–243.

SLATER, G.J. (2013). Phylogenetic evidence for a shift in the mode of mammalian body size evolution at the Cretaceous-Palaeogene boundary. *Methods in Ecology and Evolution* **4**, 734–744.

SMITH, A.B. (2001) Large–scale heterogeneity of the fossil record: implications for Phanerozoic biodiversity studies. *Philosophical Transactions of the Royal Society of London. Series B: Biological Sciences* **356**, 351–367.

SMITH, A.B., LLOYD, G.T. & MCGOWAN, A.J. (2012) Phanerozoic marine diversity: rock record modelling provides an independent test of large-scale trends. *Proceedings of the Royal Society B: Biological Sciences* **279**, 4489–4495.

SMITH, A.B. & MCGOWAN, A.J. (2007) The Shape of the Phanerozoic Marine Palaeodiversity Curve: How Much Can Be Predicted from the Sedimentary Rock Record of Western Europe? *Palaeontology* **50**, 765–774.

SMITH, A.B. & MCGOWAN, A.J. (2011) The ties linking rock and fossil records and why they are important for palaeobiodiversity studies. *Geological Society, London, Special Publications* **358**, 1–7.

SMITH, G.R., STEARLEY, R.F. & BADGLEY, C.E. (1988). Taphonomic bias in fish diversity from Cenozoic floodplain environments. *Palaeogeography, Palaeoclimatology, Palaeoecology* **63**, 263–273.

SMITH, M.R. (2019) Bayesian and parsimony approaches reconstruct informative trees from simulated morphological datasets. *Biology Letters* **15**, 20180632.

SMITHSON, T.R., RICHARDS, K.R. & CLACK, J.A. (2016) Lungfish diversity in Romer's Gap: reaction to the end-Devonian extinction. *Palaeontology* **59**, 29–44.

SMITHSON, T.R., WOOD, S.P., MARSHALL, J.E.A. & CLACK, J.A. (2012) Earliest Carboniferous tetrapod and arthropod faunas from Scotland populate Romer's Gap. *Proceedings of the National Academy of Sciences* **109**, 4532–4537.

SMITHWICK, F.M. & STUBBS, T.L. (2018). Phanerozoic survivors: Actinopterygian evolution through the Permo-Triassic and Triassic-Jurassic mass extinction events. *Evolution* **72**, 348–362.

SOLER-GIJÓN, R. & MORATALLA, J.J. (2001). Fish and tetrapod trace fossils from the Upper Carboniferous of Puertollano, Spain. *Palaeogeography, Palaeoclimatology, Palaeoecology* **171**, 1–28.

SOOKIAS, R.B. (2020) Exploring the effects of character construction and choice, outgroups and analytical method on phylogenetic inference from discrete characters in extant crocodilians. *Zoological Journal of the Linnean Society* **189**, 670–699.

SOUL, L.C. & FRIEDMAN, M. (2017). Bias in phylogenetic measurements of extinction and a case study of end-Permian tetrapods. *Palaeontology* **60**, 169–185.

SOUL, L.C. & WRIGHT, D.F. (2021) Phylogenetic Comparative Methods: A User's Guide for Paleontologists. *Elements of Paleontology*.

SPEED, M.P. & ARBUCKLE, K. (2017). Quantification provides a conceptual basis for convergent evolution. *Biological Reviews* **92**, 815–829.

STACK, J. & GOTTFRIED, M.D. (2021) A new, exceptionally well-preserved Permian actinopterygian fish from the Minnekahta Limestone of South Dakota, USA. *Journal of Systematic Palaeontology* **19**, 1271–1302.

STACK, J., HODNETT, J.-P., LUCAS, S.G. & SALLAN, L. (2021) Tanyrhinichthys mcallisteri, a long-rostrumed Pennsylvanian ray-finned fish (Actinopterygii) and the simultaneous appearance of novel ecomorphologies in Late Palaeozoic fishes. *Zoological Journal of the Linnean Society* **191**, 347–374.

STADLER, T., GAVRYUSHKINA, A., WARNOCK, R.C.M., DRUMMOND, A.J. & HEATH, T.A. (2018) The fossilized birth-death model for the analysis of stratigraphic range data under different speciation modes. *Journal of Theoretical Biology* **447**, 41–55.

ŠTAMBERG, S. (1991) Actinopterygians of the Central Bohemian Carboniferous Basins. *Acta Musei Nationalis Pragae, Series B* **47**, 25–102.

ŠTAMBERG, S. (2006). Carboniferous-Permian actinopterygian fishes of the continental basins of the Bohemian Massif, Czech Republic: An overview. *Geological Society, London, Special Publications* **265**, 217–230.

ŠTAMBERG, S. (2007) *Permo-Carboniferous Actinopterygians of the Boskovice Graben, Part 1* - Neslovicela, Bourbonnella, Letovichthys, Elonichthys. Museum of Eastern Bohemia, Hradec Králové.

ŠTAMBERG, S. (2010). Taxonomic remarks on *Rhabdolepis saarbrueckensis* Gardiner, 1963 (Osteichthyes: Actinopterygii) and its relationships to some actinopterygians from the Late Carboniferous of the Bohemian Massif, Czech Republic. *Journal of the National Museum (Prague), Natural History Series* **179**, 153–170.

ŠTAMBERG, S. (2013). Knowledge of the Carboniferous and Permian actinopterygian fishes of the Bohemian Massif - 100 years after Antonín Frič. *Acta Musei Nationalis Pragae, Series A - Historia* **67**, 159–182.

ŠTAMBERG, S. (2016a) Actinopterygians of the Stephanian sediments of the Krkonoše Piedmont Basin (Bohemian Massif) and their palaeobiogeographic relationship. *Bulletin of Geosciences* **91**, 169–186.

ŠTAMBERG, S. (2016b) A new actinopterygian species of Igornichthys Heyler, 1972 from the Permian of the Krkonoše Piedmont Basin (Bohemian Massif, Czech Republic), and its relationship to the actinopterygians of other European Permo-Carboniferous basins. *Geodiversitas* **38**, 475–488. Muséum national d'Histoire naturelle, Paris.

ŠTAMBERG, S. (2018) Actinopterygians of the Permian locality Buxières-Les-Mines (Bourbon l'archambault Basin, France) and their relationship to other early actinopterygians. *Fossil Imprint* **74**, 245–291.

ŠTAMBERG, S. (2021). Actinopterygians of the Broumov Formation (Permian) in the Czech part of the Intra-Sudetic Basin (the Czech Republic). *Fossil Imprint* **77**, 73–101.

ŠTAMBERG, S. (2023) Actinopterygian fish *Paramblypterus rohani* (Heckel & Kner, 1861) from the Permian sediments of the Bohemian Massif (the Czech Republic) and its relationships to *Paramblypterus duvernoyi* (Agassiz, 1833) and other Amblypteridae. *Acta Musei Reginaehradecensis, Series A, Scientiae Naturales* **40**, 61–96.

ŠTAMBERG, S. & STEYER, J.-S. (2021). New actinopterygians from the Permian of the Brive Basin, and the ichthyofaunas of the French Massif Central. *Fossil Imprint* **77**, 145–165.

ŠTAMBERG, S. & ZAJÍC, J. (2008) *Carboniferous and Permian faunas and their occurence in the limnic basins of the Czech Republic*. Museum of Eastern Bohemia, Hradec Králové.

STAMPFLI, G.M., HOCHARD, C., VÉRARD, C., WILHEM, C. & VONRAUMER, J. (2013) The formation of Pangea. *Tectonophysics* **593**, 1–19.

STARRFELT, J. & LIOW, L.H. (2016) How many dinosaur species were there? Fossil bias and true richness estimated using a Poisson sampling model. *Philosophical Transactions of the Royal Society B: Biological Sciences* **371**, 20150219.

STENSIÖ, E.A. (1921) *Triassic fishes from Spitzbergen - Part 1*. A. Holzhausen, Vienna.

STIGALL, A.L., BAUER, J.E., LAM, A.R. & WRIGHT, D.F. (2017). Biotic immigration events, speciation, and the accumulation of biodiversity in the fossil record. *Global and Planetary Change* **148**, 242–257.

STONE, P., MCMILLAN, A.A., FLOYD, J.D., BARNES, R.P., PHILLIPS, E.R., DEAN, M.T., KIMBELL, G.S., MERRITT, J.W., DOCHARTAIGH, B.E.O. & RUSHTON, A.W.A. (2012) *British Regional Geology: South of Scotland*, 4th edition. British Geological Survey, Nottingham, UK.

SWARTZ, B.A. (2009). Devonian actinopterygian phylogeny and evolution based on a redescription of *Stegotrachelus finlayi*. *Zoological Journal of the Linnean Society* **156**, 750–784.

TAVERNE, L.P. (1997) *Osorioichthys marginis*, 'paléonisciforme' du Famennien de Belgique, et la phylogénie des actinoptérygiens dévoniens (Pisces). *Bulletin de l'Institut Royal des Sciences Naturelles de Belgique* **67**, 57–78.

THOMSON, K.S. (1977) The Pattern of Diversification Among Fishes. In *Developments in Palaeontology and Stratigraphy* (ed A. HALLAM), pp. 377–404.

TINTORI, A., SUN, Z., NI, P., LOMBARDO, C., JIANG, D. & MOTANI, R. (2015) Oldest stem Teleostei from the Late Ladinian (Middle Triassic) of Southern China. *Rivista Italiana di Paleontologia e Stratigrafia* **121**, 285–296.

TOLOKONNIKOVA, Z. & ERNST, A. (2021) Richness of Famennian-Tournaisian (Late Devonian-early Carboniferous) bryozoans in shallow areas of Palaeotethys and Palaeoasian oceans. *Palaeobiodiversity and Palaeoenvironments* **101**, 885–906.

TRAQUAIR, R.H. (1875) XXX.—On the structure and systematic position of the genus Cheirolepis. *Annals and Magazine of Natural History* **15**, 237–249.

TRAQUAIR, R.H. (1877-1912) *The Ganoid Fishes of the British Carboniferous Formations*. The Palaeontographical Association, London.

TRAQUAIR, R.H. (1877b) The Ganoid Fishes of the British Carboniferous Formations. Part 1. Palæoniscidæ. Pages 1–60; Plates I–VII. *Monographs of the Palaeontographical Society* **31**, 1–60.

TRAQUAIR, R.H. (1879). On the Structure and Affinities of the Platysomidæ. *Geological Magazine* **6**, 576–576. Cambridge University Press.

TRAQUAIR, R.H. (1881) III.— Report on Fossil Fishes collected by the Geological Survey of Scotland in Eskdale and Liddesdale. Part I.—Ganoidei. *Transactions of the Royal Society of Edinburgh* **30**, 15–71.

TRAQUAIR, R.H. (1886) II.—New Palæoniscidæ from the English Coal-measures. *Geological Magazine* **3**, 440–442.

TRAQUAIR, R.H. (1890). LXI.— Observations on some fossil fishes from the lower Carboniferous Rocks of Eskdale, Dumfriesshire. *Annals and Magazine of Natural History* **6**, 491–494.

TRAQUAIR, R.H. (1901) The Ganoid Fishes of the British Carboniferous Formations. Part I. Palæoniscidæ. Pages 61–87; Plates VIII–XVIII. *Monographs of the Palaeontographical Society* **55**, 61–87.

TRAQUAIR, R.H. (1908). IV.—Report on Fossil Fishes collected by the Geological Survey of Scotland from Shales exposed on the Shore near Gullane, East Lothian. *Earth and Environmental Science Transactions of The Royal Society of Edinburgh* **46**, 103–117.

TRAQUAIR, R.H. (1909) The Ganoid Fishes of the British Carboniferous Formations. Part I, No. 4. Palæoniscidæ. Pages 107–122; Plates XXIV–XXX. *Monographs of the Palaeontographical Society* **63**, 107–122.

TRAQUAIR, R.H. (1912). The Ganoid Fishes of the British Carboniferous Formations. Part I, No. 6. Palæoniscidæ. Pages 159–180; Plates XXXVI–XL. *Monographs of the Palaeontographical Society* **65**, 159–180.

TRINAJSTIC, K. (1999a) Scales of palaeoniscoid fishes (Osteichthyes: Actinopterygii) from the Late Devonian of Western Australia. *Records of the Western Australian Museum: Supplement* **57**, 93–106.

TRINAJSTIC, K. (1999b) Scale morphology of the Late Devonian palaeoniscoid Moythomasia durgaringa Gardiner and Bartram, 1977. *Alcheringa: An Australasian Journal of Palaeontology* **23**, 9–19.

TRINAJSTIC, K., BRIGGS, D.E.G. & LONG, J.A. (2022) The Gogo Formation Lagerstätte: a view of Australia's first great barrier reef. *Journal of the Geological Society* **179**.

TUTIN, S.L. & BUTLER, R.J. (2017). The completeness of the fossil record of plesiosaurs, marine reptiles from the Mesozoic. *Acta Palaeontologica Polonica* **62**, 563–573.

TVERDOKHLEBOV, V.P., TVERDOKHLEBOVA, G.I., MINIKH, A.V., SURKOV, M.V. & BENTON, M.J. (2005) Upper Permian vertebrates and their sedimentological context in the South Urals, Russia. *Earth-Science Reviews* **69**, 27–77.

UPCHURCH, P., MANNION, P.D., BENSON, R.B.J., BUTLER, R.J. & CARRANO, M.T. (2011) Geological and anthropogenic controls on the sampling of the terrestrial fossil record: a case study from the Dinosauria. *Geological Society, London, Special Publications* **358**, 209–240.

VALENTINE, J.W. (1968) Climatic Regulation of Species Diversification and Extinction. *GSA Bulletin* **79**, 273–276.

VALENTINE, J.W. & PEDDICORD, R.G. (1967) Evaluation of Fossil Assemblages by Cluster Analysis. *Journal of Paleontology* **41**, 502–507.

VÁZQUEZ, P. & CLAPHAM, M.E. (2017) Extinction selectivity among marine fishes during multistressor global change in the end-Permian and end-Triassic crises. *Geology* **45**, 395–398.

VÉRAN, M. (1988) Les éléments accessoires de l'arc hyoïdien des poissons téléostomes (Acanthodiens et Osteichthyens) fossiles et actuels. *Mémoires Du Museum National d'histoire Naturelle* **54**, 1–98.

VERMEIJ, G.J. & LEIGHTON, L.R. (2003) Does global diversity mean anything? *Paleobiology* **29**, 3–7.

VILHENA, D.A. & SMITH, A.B. (2013) Spatial Bias in the Marine Fossil Record. *PLOS ONE* **8**, e74470.

VOGEL, G. (2019) Countries demand their fossils back, forcing natural history museums to confront their past. *Science*.

WALKER, F.M., DUNHILL, A.M. & BENTON, M.J. (2020). Variable preservation potential and richness in the fossil record of vertebrates. *Palaeontology* **63**, 313–329.

WALL, P.D., IVANY, L.C. & WILKINSON, B.H. (2011) Impact of outcrop area on estimates of Phanerozoic terrestrial biodiversity trends. *Geological Society, London, Special Publications* **358**, 53–62.

WANG, N.N. & DONG, Z.Z. (1989) Discovery of Late Silurian microfossils of Agnatha and fishes from Yunnan, China. *Acta palaeontologica Sinica* **28**, 192–206.

WANG, N.-Z., JIN, F., WANG, W. & ZHU, X.-S. (2007). Actinopterygian fishes from the Permian-Triassic boundary beds in Zhejiang and Jiangxi Provinces, South China, and fish mass extinction, recovery and radiation. *Vertebrata Palasiatica* **45**, 307.

WANG, W., QU, Q.-M. & ZHU, M. (2010). A brief review of the Middle Palaeozoic vertebrates from Southeast Asia. *Palaeoworld* **19**, 27–36.

WANG, X., QIE, W., SHENG, Q., QI, Y., WANG, Y., LIAO, Z., SHEN, S. & UENO, K. (2013) Carboniferous and Lower Permian sedimentological cycles and biotic events of South China. *Geological Society, London, Special Publications* **376**, 33–46.

WARD, P., LABANDEIRA, C., LAURIN, M. & BERNER, R.A. (2006). Confirmation of Romer's Gap as a low oxygen interval constraining the timing of initial arthropod and vertebrate terrestrialization. *Proceedings of the National Academy of Sciences* **103**, 16818–16822.

WATERS, C.N., BROWNE, M.A.E., JONES, N.S. & SOMERVILLE, I.D. (2011a) Midland Valley of Scotland. In *A revised correlation of Carboniferous rocks in the British Isles* (ed C. WATERS), pp. 96–102. Geological Society of London, London.

WATERS, C.N., DEAN, M.T., JONES, N.S. & SOMERVILLE, I.D. (2011b) Northumberland Trough and Solway Basin. In *A revised correlation of Carboniferous rocks in the British Isles* (ed C. WATERS), pp. 89–95. Geological Society of London, London.

WATERS, C.N., JONES, N.S., COLLINSON, J.D. & CLEAL, C.J. (2011c) Craven Basin and southern Pennines. In *A revised correlation of Carboniferous rocks in the British Isles* (ed C. WATERS), p. 74-81. Geological Society of London, London.

WATSON, D.M.S. (1925) The Structure of Certain Palæoniscids and the Relationships of that Group with other Bony Fish. *Proceedings of the Zoological Society of London* **95**, 815–870.

WATSON, W. & WALKER, H.J. (2004) The world's smallest vertebrate, *Schindleria brevipinguis*, a new paedomorphic species in the family Schindleriidae (Perciformes: Gobioidei). *Records of the Australian Museum* **56**, 139–142.

WEEMS, R.E. & WINDOLPH, J.F.J. (1986). A new actinopterygian fish (Paleonisciformes) from the Upper Mississippian Bluestone Formation of West Virginia. *Proceedings of the Biological Society of Washington* **99**, 584–601.

WENZ, S. (1959) Etude de Ptycholepis bollensis, poisson du Lias superieur de l'Yonne et du Wurtemberg. *Bulletin de la Société Géologique de France* **S7-I**, 916–928.

WESTOLL, T.S. (1934). The Permian palaeoniscid fishes of Northumberland and Durham. PhD Thesis, Durham University.

WESTOLL, T.S. (1941*a*). The age of certain Permian fish-bearing strata. *Geological Magazine* **78**, 37–44.

WESTOLL, T.S. (1941*b*). The Permian fishes *Dorypterus* and *Lekanichthys*. *Proceedings of the Zoological Society of London* **B111**, 39–58.

WESTOLL, T.S. (1944) The Haplolepidae, a new family of late Carboniferous bony fishes : a study in taxonomy and evolution. Bulletin of the AMNH ; v. 83, article 1. New York : [American Museum of Natural History].

WHALEN, C.D. & BRIGGS, D.E.G. (2018). The Palaeozoic colonization of the water column and the rise of global nekton. *Proceedings of the Royal Society B: Biological Sciences* **285**, 20180883.

WHITAKER, A.F. & KIMMIG, J. (2020) Anthropologically introduced biases in natural history collections, with a case study on the invertebrate paleontology collections from the middle Cambrian Spence Shale Lagerstätte. *Palaeontologia Electronica* **23**, 1–26.

WHITE, E.I. (1927) XI.—The Fish-Fauna of the Cementstones of Foulden, Berwickshire. *Earth and Environmental Science Transactions of The Royal Society of Edinburgh* **55**, 255–287.

WILLIAMS, S.C. & LUCAS, S.G. (2013) Taphonomy and paleoecology of Pennsylvanian fishes from the Kinney Brick Quarry, New Mexico, USA. In *The Carboniferous-Permian Transition: Bulletin 60* (eds S.G. LUCAS, W.A. DIMICHELE, J.E. BARRICK, J.W. SCHNEIDER & J.A. SPIELMANN), pp. 371–389.

WILLIAMSON, I.A. (1999) The Burnley Coalfield. *British Mining - Memoirs* **63**.

WILSON, C.D., PARDO, J.D. & ANDERSON, J.S. (2018) A primitive actinopterygian braincase from the Tournaisian of Nova Scotia. *Royal Society Open Science* **5**, 171727.

WOMACK, T.M., CRAMPTON, J.S. & HANNAH, M.J. (2021). Spatial scaling of beta diversity in the shallow-marine fossil record. *Paleobiology* **47**, 39–53.

WOOD, M. (2017) Glencartholm revisited: describing for the first time Stan Wood's discovery and excavation of Mumbie Quarry, adjacent to the important Palaeozoic fossil site of Glencartholm. *Earth and Environmental Science Transactions of The Royal Society of Edinburgh* **108**, 47–54. Royal Society of Edinburgh Scotland Foundation.

WOODWARD, A.S. (1889) *Catalogue of the Fossil Fishes in the British Museum. IV volumes*. Trustees of the British Museum, London.

WOODWARD, A.S. (1891) *Catalogue of the Fossil Fishes in the British Museum (Natural History), Part II*. British Museum (Natural History), London.

WOODWARD, A.S. (1931). XLVII.—On *Urosthenes*, a fossil fish from the Upper Coal Measures of Lithgow, New South Wales. *Annals and Magazine of Natural History* **8**, 365–367.

WOODWARD, A.S. (1940). XLIX.—A Palæoniscid Fish (*Elonichthys davidi*, sp. n.) from the Newcastle Coal Measures, New South Wales. *Annals and Magazine of Natural History* **6**, 462–464.

WRIGHT, A.M., BAPST, D.W., BARIDO-SOTTANI, J. & WARNOCK, R.C.M. (2022) Integrating Fossil Observations Into Phylogenetics Using the Fossilized Birth–Death Model. *Annual Review of Ecology, Evolution, and Systematics* **53**, 251–273.

WRIGHT, A.M. & HILLIS, D.M. (2014) Bayesian Analysis Using a Simple Likelihood Model Outperforms Parsimony for Estimation of Phylogeny from Discrete Morphological Data. *PLOS ONE* **9**, e109210.

WRIGHT, A.M., LLOYD, G.T. & HILLIS, D.M. (2016) Modeling Character Change Heterogeneity in Phylogenetic Analyses of Morphology through the Use of Priors. *Systematic Biology* **65**, 602–611.

XU, G.-H. & GAO, K.-Q. (2011) A new scanilepiform from the Lower Triassic of northern Gansu Province, China, and phylogenetic relationships of non-teleostean Actinopterygii. *Zoological Journal of the Linnean Society* **161**, 595–612.

XU, G.-H., GAO, K.-Q. & FINARELLI, J.A. (2014) A revision of the Middle Triassic scanilepiform fish *Fukangichthys longidorsalis* from Xinjiang, China, with comments on the phylogeny of the Actinopteri. *Journal of Vertebrate Paleontology* **34**, 747–759.

YANKEVICH, D.I. & MINIKH, M.G. (1998). Ichthyofauna. In *Biota of East European Russia at the Early/Late Permian boundary (International Symposium "Upper Permian stratotypes of the Volga region")* (eds T.A. GRUNT, N.K. ESAULOVA & G.P. KANEV). Moscow.

YE, S. & PETERS, S.E. (2023) Bedrock geological map predictions for Phanerozoic fossil occurrences. *Paleobiology*, 1–20.

YOUNG, J. (1866) On the Affinities of Platysomus and allied Genera. *Quarterly Journal of the Geological Society* **22**, 301–317.

YUAN, Z., XU, G.-H., DAI, X., WANG, F., LIU, X., JIA, E., MIAO, L. & SONG, H. (2022) A new perleidid neopterygian fish from the Early Triassic (Dienerian, Induan) of South China, with a reassessment of the relationships of Perleidiformes. *PeerJ* **10**, e13448.

ZAJÍC, J. (2014) Permian Fauna of the Krkonoše Piedmont Basin (Bohemian Massif, Central Europe). *Acta Musei Nationalis Pragae, Series B* **70**, 131–142.

ZHANG, F., DAHL, T.W., LENTON, T.M., LUO, G., SHEN, S., ALGEO, T.J., PLANAVSKY, N., LIU, J., CUI, Y., QIE, W., ROMANIELLO, S.J. & ANBAR, A.D. (2020) Extensive marine anoxia

associated with the Late Devonian Hangenberg Crisis. *Earth and Planetary Science Letters* **533**, 115976.

ZHU, M. & FAN, J. (1995) Youngolepis from the Xishancun Formation (Early Lochkovian) of Qujing; China. *Geobios* **28**, 293–299.

ZHU, M. & SCHULTZE, H.-P. (1997). The oldest sarcopterygian fish. *Lethaia* **30(4)**, 293-304.

ZHU, M. & SCHULTZE, H.-P. (2001). Interrelationships of basal osteichthyans. In *Major events in early vertebrate evolution, paleontology, phylogeny, genetics and development* (ed. AHLBERG, P.). Taylor and Francis, London.

ZHU, M. & YU, X. (2002) A primitive fish close to the common ancestor of tetrapods and lungfish. *Nature* **418**, 767–770.

ZHU, M., WANG, W. & YU, X. (2010) *Meemannia eos*, a basal sarcopterygian fish from the Lower Devonian of China –expanded description and significance. In *Morphology, Phylogeny and Paleobiogeography of Fossil Fishes* pp. 199–214.

ZHU, M., YU, X. & JANVIER, P. (1999). A primitive fossil fish sheds light on the origin of bony fishes. *Nature* **397**, 607-610.

ZHU, M., YU, X., WANG, W., ZHAO, W. & JIA, L. (2006) A primitive fish provides key characters bearing on deep osteichthyan phylogeny. *Nature* **441**, 77–80.

ZHU, M., ZHAO, W., JIA, L., LU, J., QIAO, T. & QU, Q. (2009). The oldest articulated osteichthyan reveals mosaic gnathostome characters. *Nature* **458**, 469–474.

ZHU, Y., LI, Q., LU, J., CHEN, Y., WANG, J., GAI, Z., ZHAO, W., WEI, G., YU, Y., AHLBERG, P.E. & ZHU, M. (2022) The oldest complete jawed vertebrates from the early Silurian of China. *Nature* **609**, 954–958.

ZIDEK, J. (1992). Late Pennsylvanian Chondrichthyes, Acanthodii, and deep-bodied Actinopterygii from the Kinney Quarry, Manzanita Mountains, New Mexico. *New Mexico Bureau of Mines & Mineral Resources Bulletin* **138**, 145–182.

ZOHAR, I., BELMAKER, M., NADEL, D., GAFNY, S., GOREN, M., HERSHKOVITZ, I. & DAYAN, T. (2008). The living and the dead: How do taphonomic processes modify relative abundance and skeletal completeness of freshwater fish? *Palaeogeography, Palaeoclimatology, Palaeoecology* **258**, 292–316.

ZUSCHIN, M., HARZHAUSER, M. & MANDIC, O. (2011) Disentangling palaeodiversity signals from a biased sedimentary record: an example from the Early to Middle Miocene of Central Paratethys Sea. *Geological Society, London, Special Publications* **358**, 123–139.

Appendices

A Supplementary Information from Henderson *et al.* (2023)

Appendix A consists of the Supplementary Information from the following paper, corresponding to Chapter 2 of this thesis:

HENDERSON, S., DUNNE, E.M., FASEY, S.A. and GILES, S., 2023. The early diversification of ray-finned fishes (Actinopterygii): hypotheses, challenges and future prospects. *Biological Reviews*, 98(1), 284-315. https://doi.org/10.1111/brv.12907.

A.1 Occurrence and interval data

Occurrences of Palaeozoic actinopterygians (ma, million years ago; myr, million years), downloadable in .csv format here: https://onlinelibrary.wiley.com/action/downloadSupplement?doi=10.1111%2Fbrv.12907&file=brv12907-sup-0002-TableS1.csv

Description of the roughly equal-length time intervals into which occurrence data were placed (ma, million years ago; myr, million years), downloaded in .csv format here: https://onlinelibrary.wiley.com/action/downloadSupplement?doi=10.1111%2Fbrv.12907&file=brv12907-sup-0003-TableS2.csv

A.2 Supplementary Figures

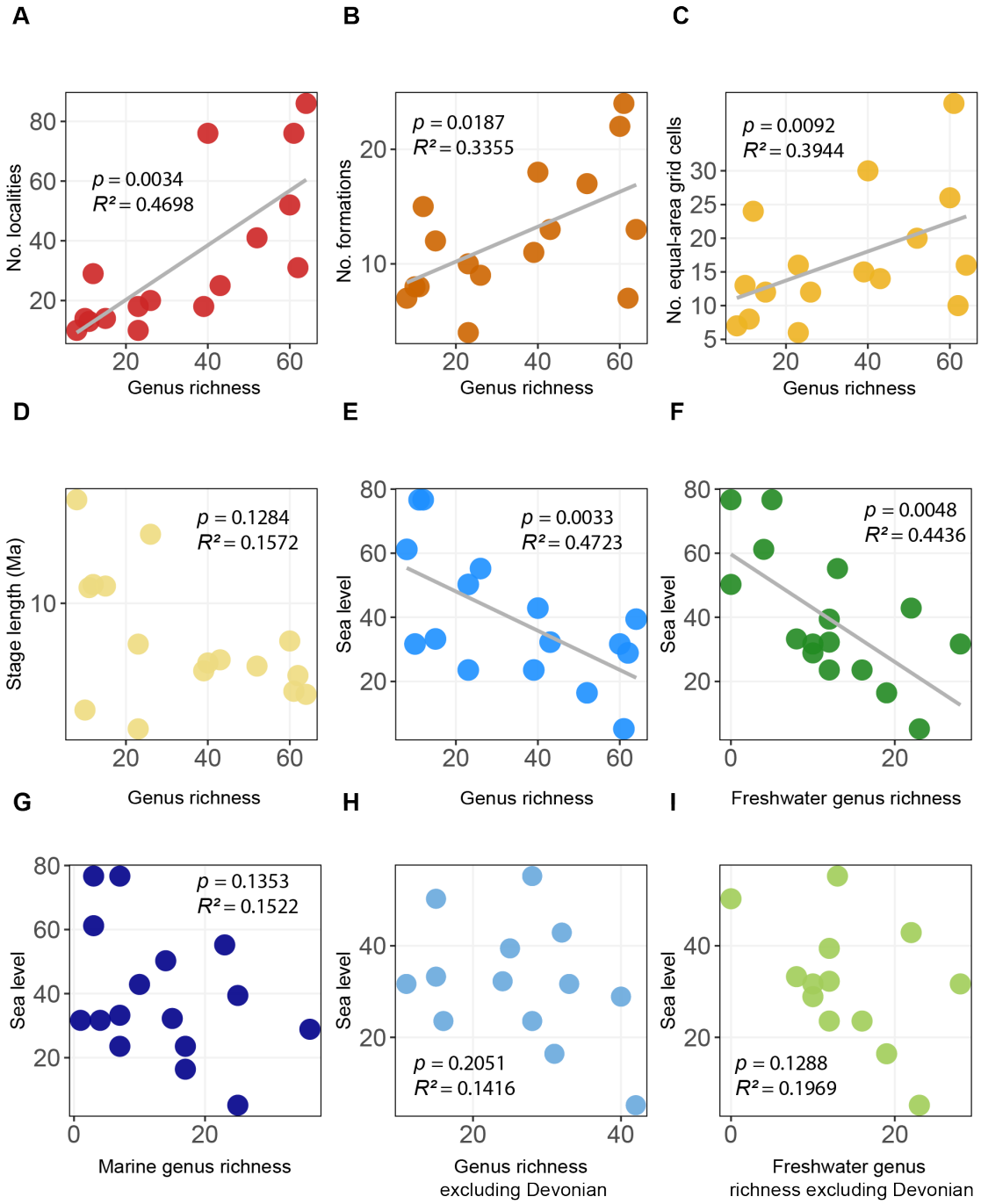


Fig. A.1: Regressions of total genus richness in individual equal-length stages with (A) number of localities, (B) number of geological formations, (C) number of occupied equal-area grid cells, (D) stage length, and (E) sea level; and regressions of freshwater genus richness (F) and marine genus richness (G) with sea level, including Devonian stages, and of overall genus richness (H) and freshwater genus richness (I) with sea level, excluding Devonian stages.

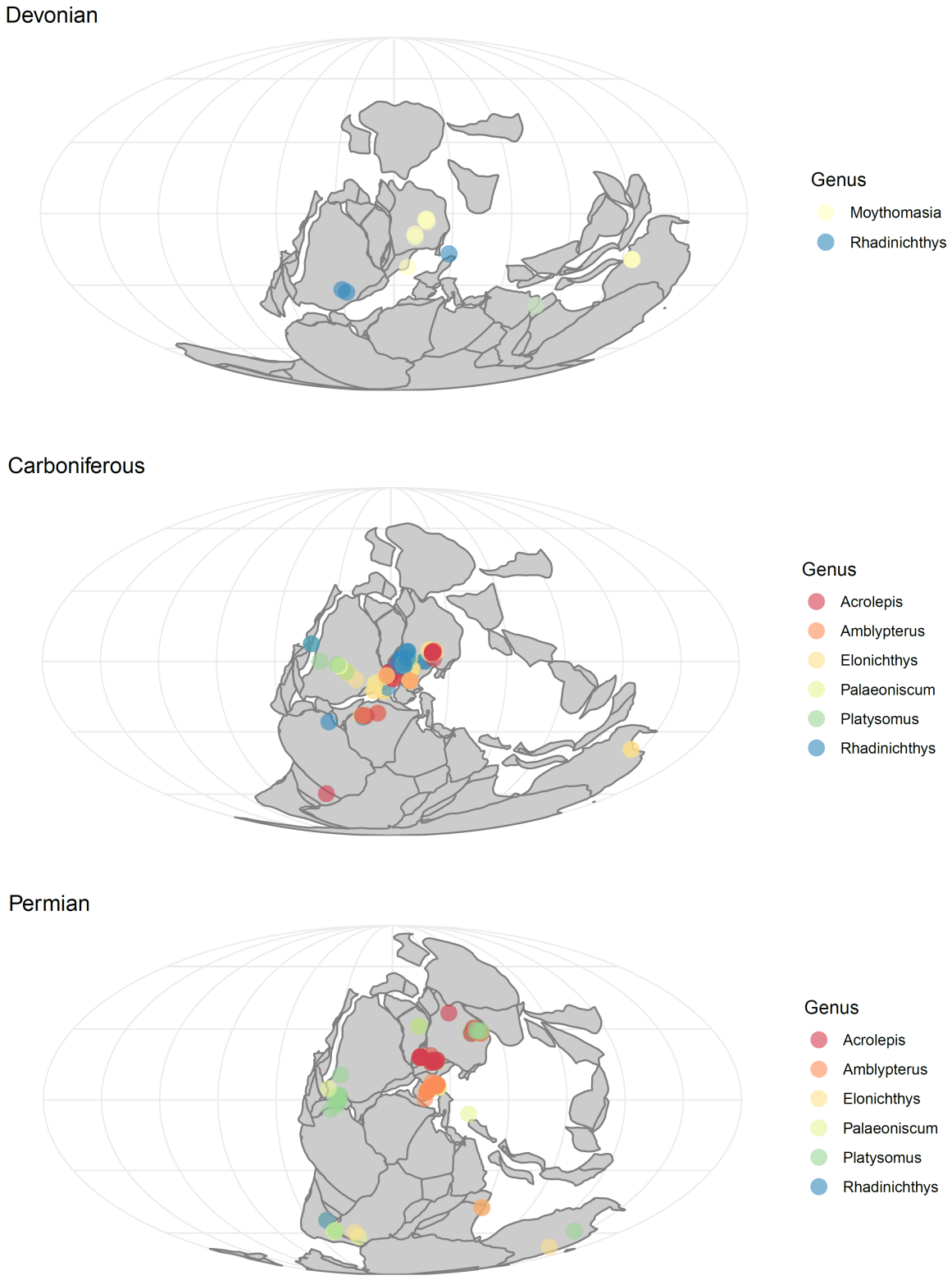


Fig. A.2: Palaeomaps showing occurrences of Devonian, Carboniferous and Permian waste-basket genera.

B Supplemental Material from Henderson *et al*. (2022)

Appendix B consists of the Supplemental Material from the following paper, corresponding to Chapter 3 of this thesis:

HENDERSON, S., DUNNE, E.M. and GILES, S., 2022. Sampling biases obscure the early diversification of the largest living vertebrate group. Proceedings of the Royal Society B, 289(1985), 20220916. https://doi.org/10.1098/rspb.2022.0916.

B.1 Occurrence data and code

Occurrences of Palaeozoic actinopterygians (ma, million years ago; myr, million years) in .csv format and R script to run analyses are downloadable here: https://doi.org/10.6084/m9.figshare.c.6238460.v1

B.2 Supplementary Figures

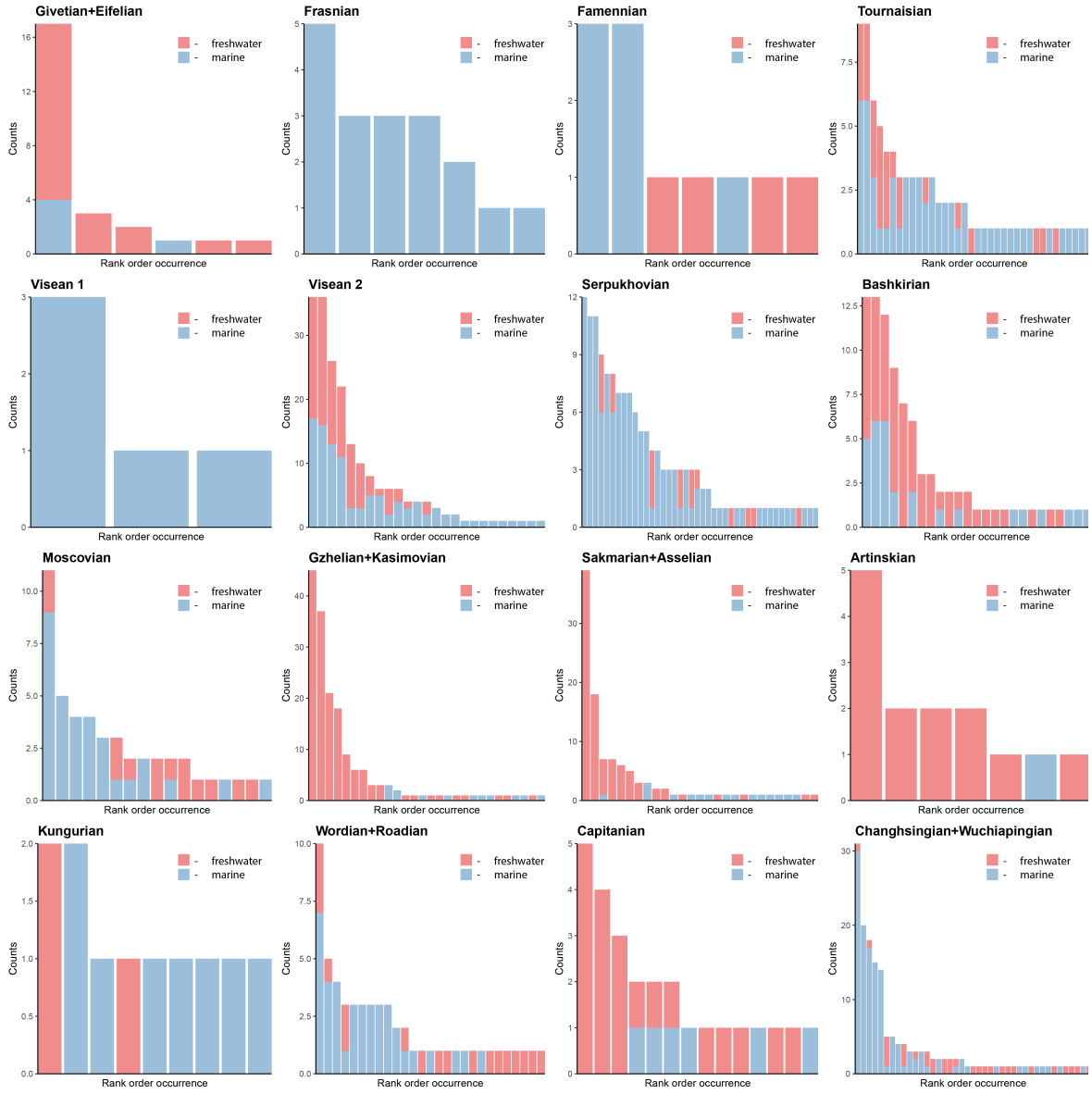


Figure B.1: Rank order occurrence distributions of the sampled equal-length intervals at genus level (coloured by palaeoenvironment, blue – marine and brackish; red – freshwater).

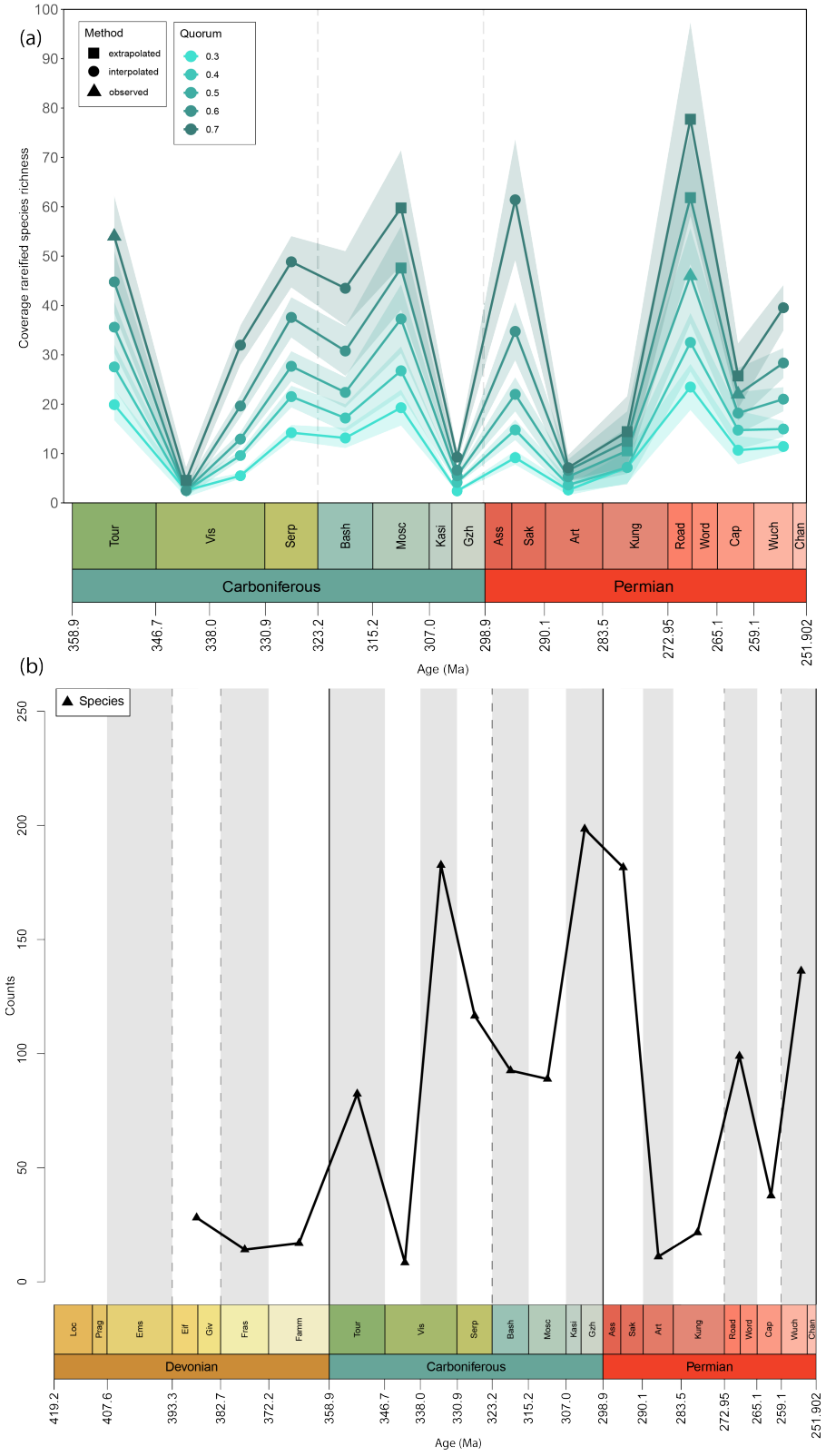


Figure B.2: Species-level trends for (a) coverage-based rarefaction estimates, and (b) squares estimates.

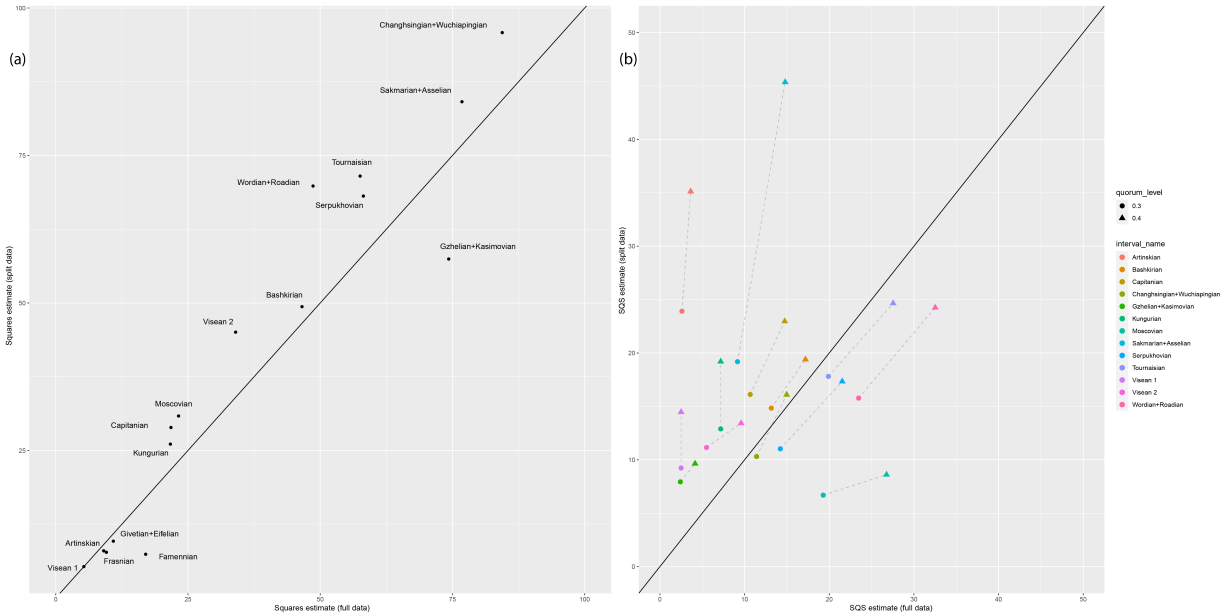


Figure B.3: Comparison of (a) squares and (b) coverage-rarefied richness applied to the complete dataset and split-analysed-and-summed subsets (split by palaeoenvironment).

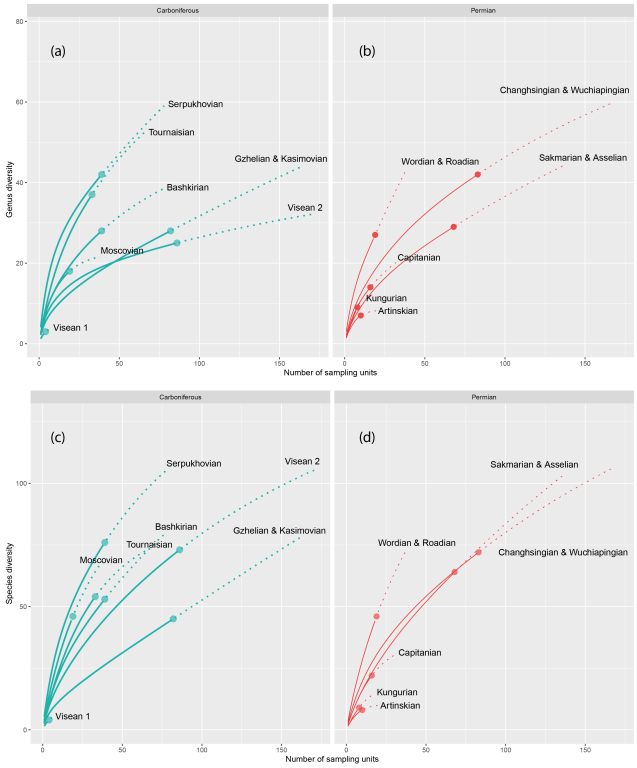


Figure B.4: Size-based rarefaction curves for (a) Carboniferous genus-level occurrences, (b) Permian genus-level occurrences, (c) Carboniferous species-level occurrences, (d) Permian genus-level occurrences.

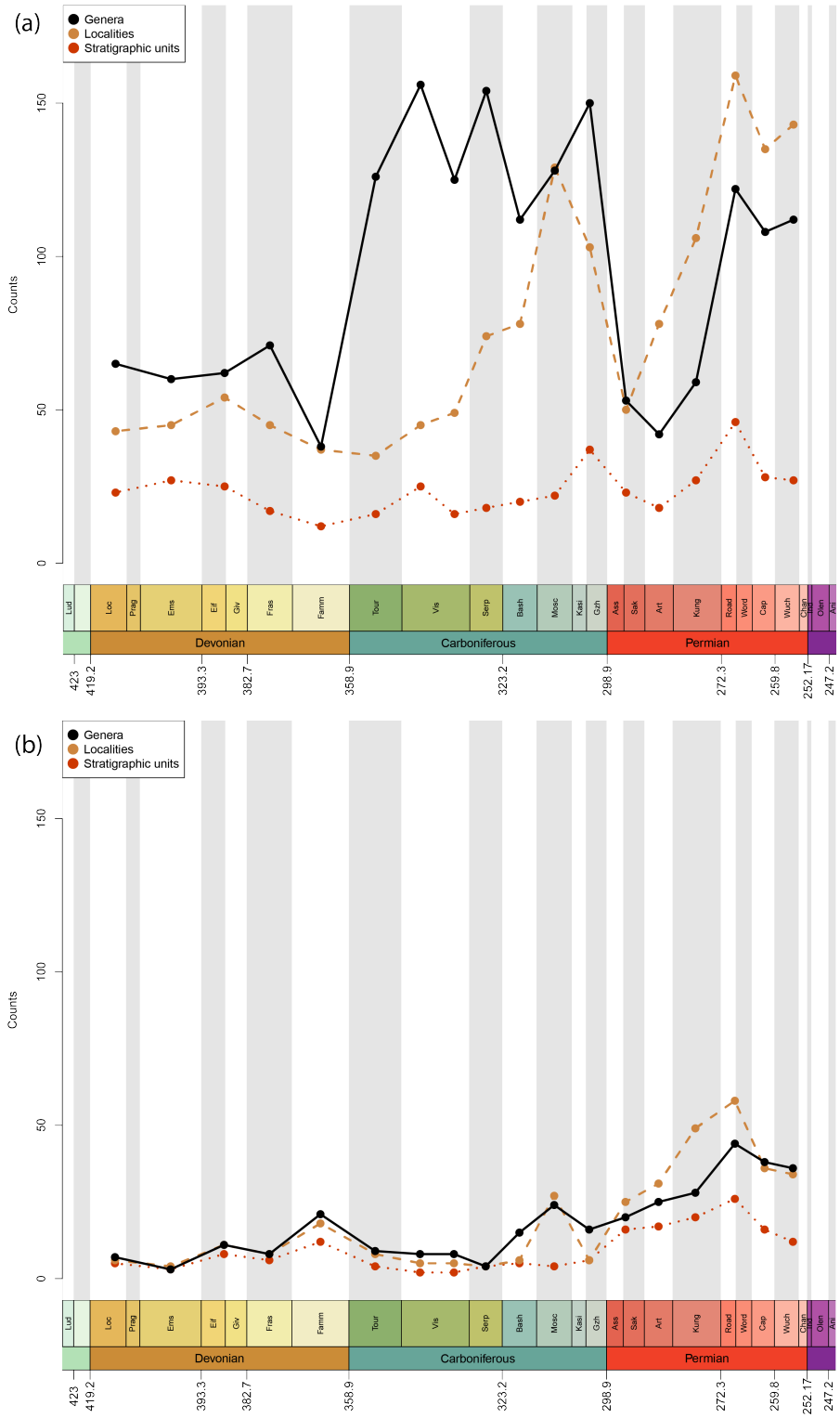


Figure B.5: Raw counts of Palaeozoic gnathostome genera (black, solid line), collections (brown, short dashed line) and formations (red, dotted line) entered in the PBDB that are classified as having a marine or brackish palaeoenvironment (a) or a freshwater or terrestrial palaeoenvironment (b).

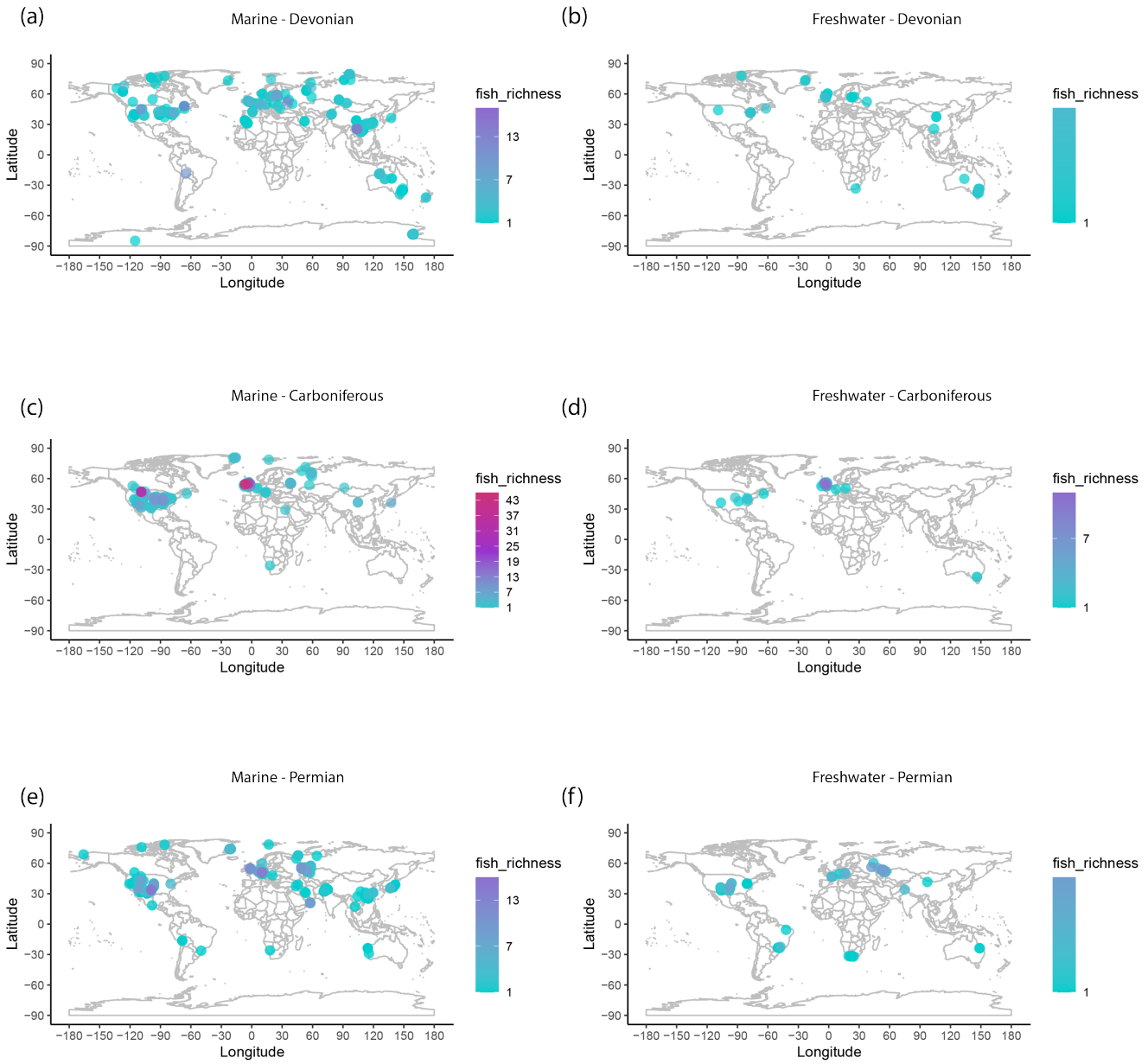


Figure B.6: Geographic distribution of Palaeozoic gnathostome genera entered in the PBDB partitioned by geological period (Devonian – a-b; Carboniferous – c-d; Permian – e-f) and palaeoenvironment (marine – a, c, e; freshwater – b, d, f). Colour scales correspond to the richness of localities, ranging from low (light blue) to high (pink) richness.

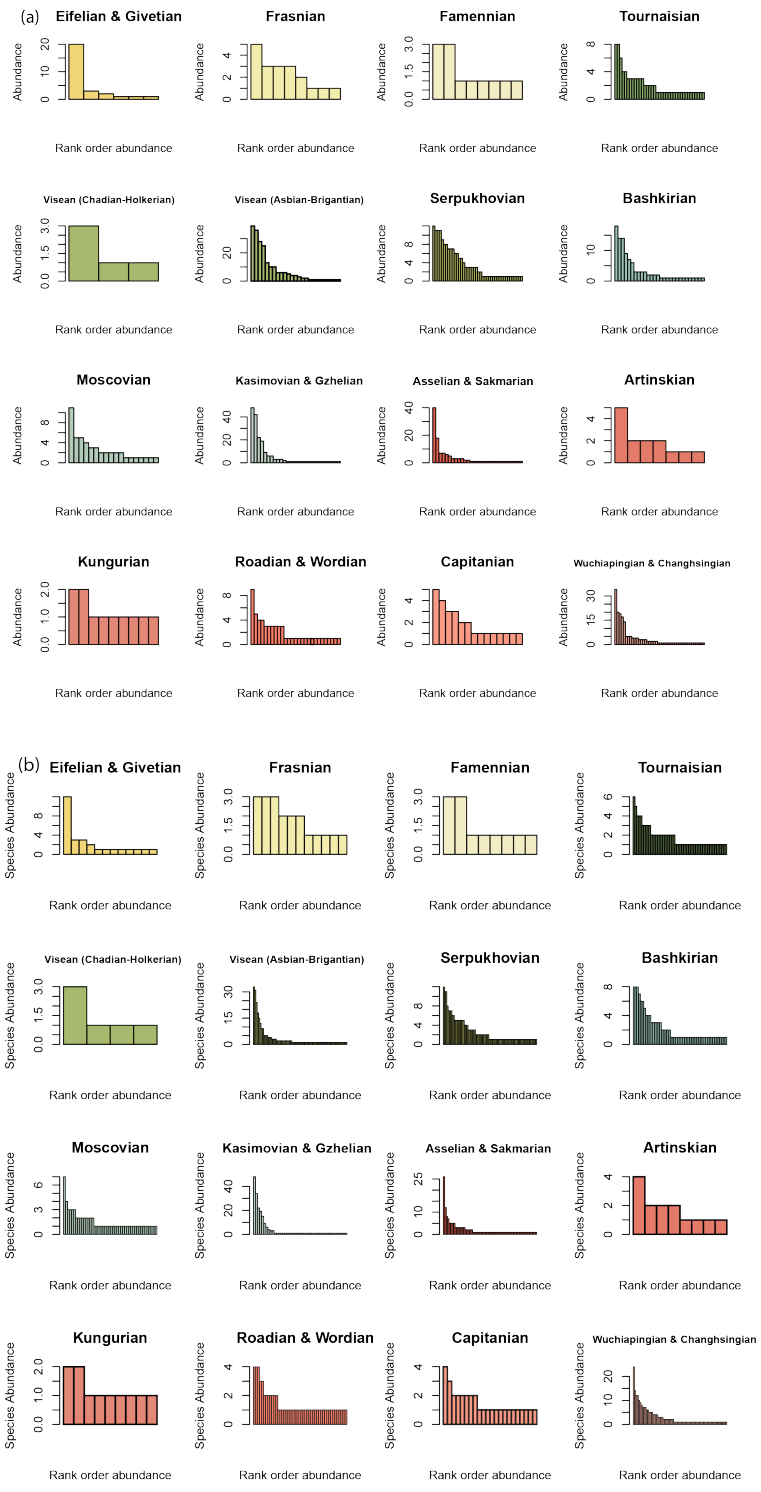


Figure B.7: Rank order occurrence distributions of the sampled equal-length intervals (colours correspond with the International Commission on Stratigraphy; ICS) at (a) genus-level occurrences and (b) species-level occurrences.

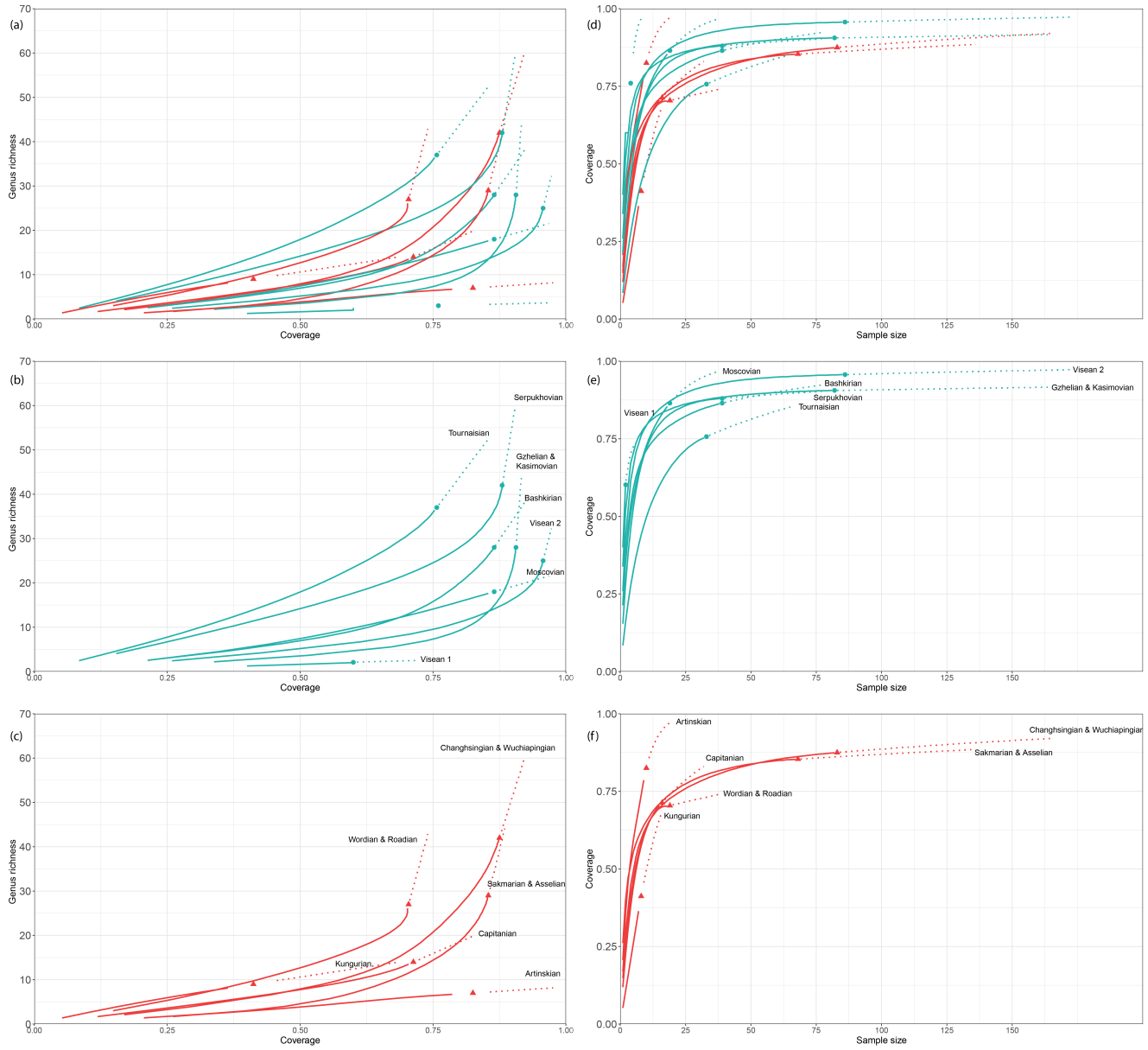


Figure B.8: Genus-level coverage-based rarefaction curves (a-c) and sample completeness (d-f) for Carboniferous (b and e) and Permian (c and f) intervals. Solid lines are interpolated measures, points are observed data and dotted lines are extrapolated estimates. Carboniferous intervals are in green and Permian intervals are in red according to the ICS colours.

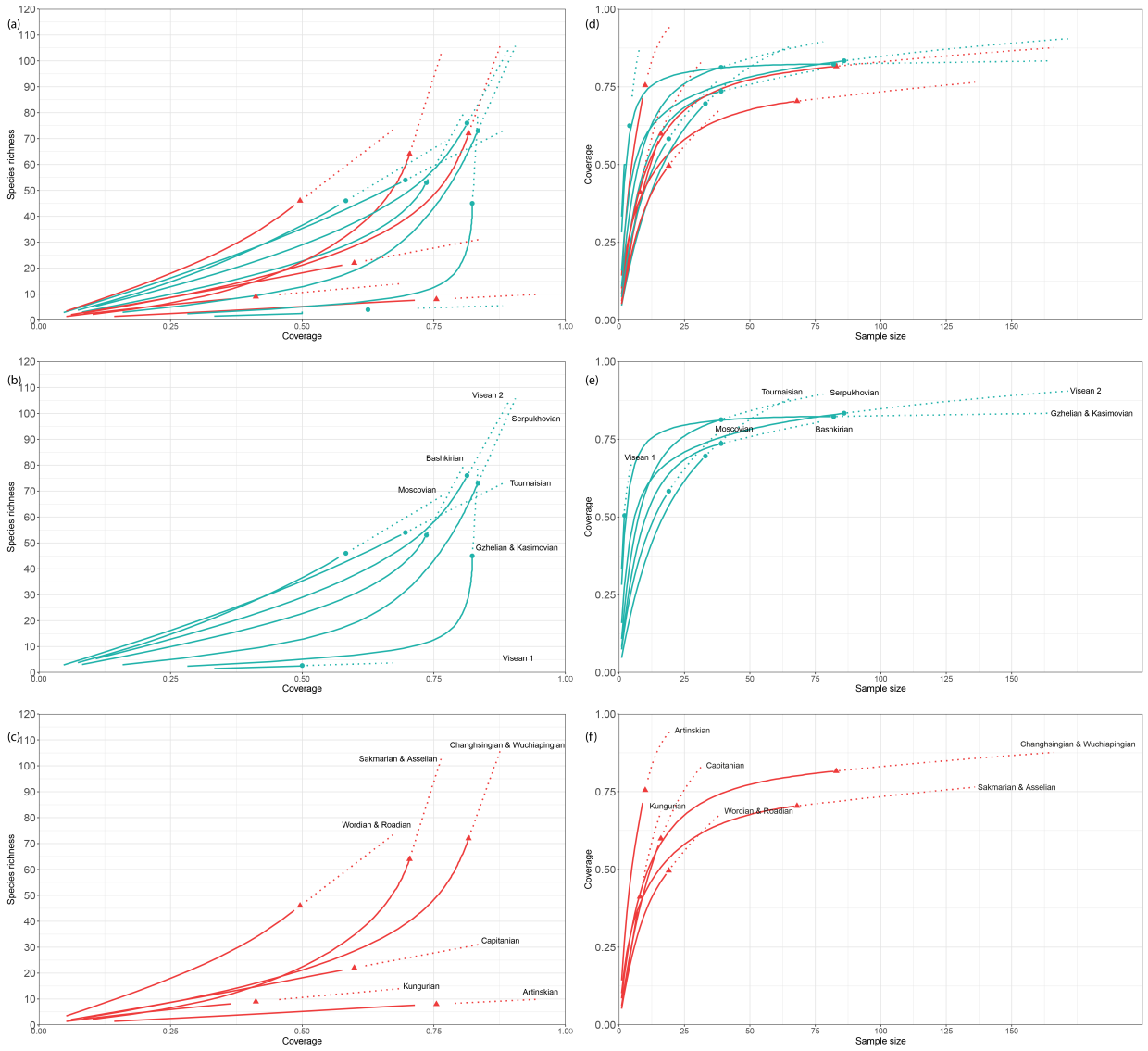


Figure B.9: Species-level coverage-based rarefaction curves (a-c) and sample completeness (d-f) for Carboniferous (b and e) and Permian (c and f) intervals. Solid lines are interpolated measures, points are observed data and dotted lines are extrapolated estimates. Carboniferous intervals are in green and Permian intervals are in red according to the ICS colours.

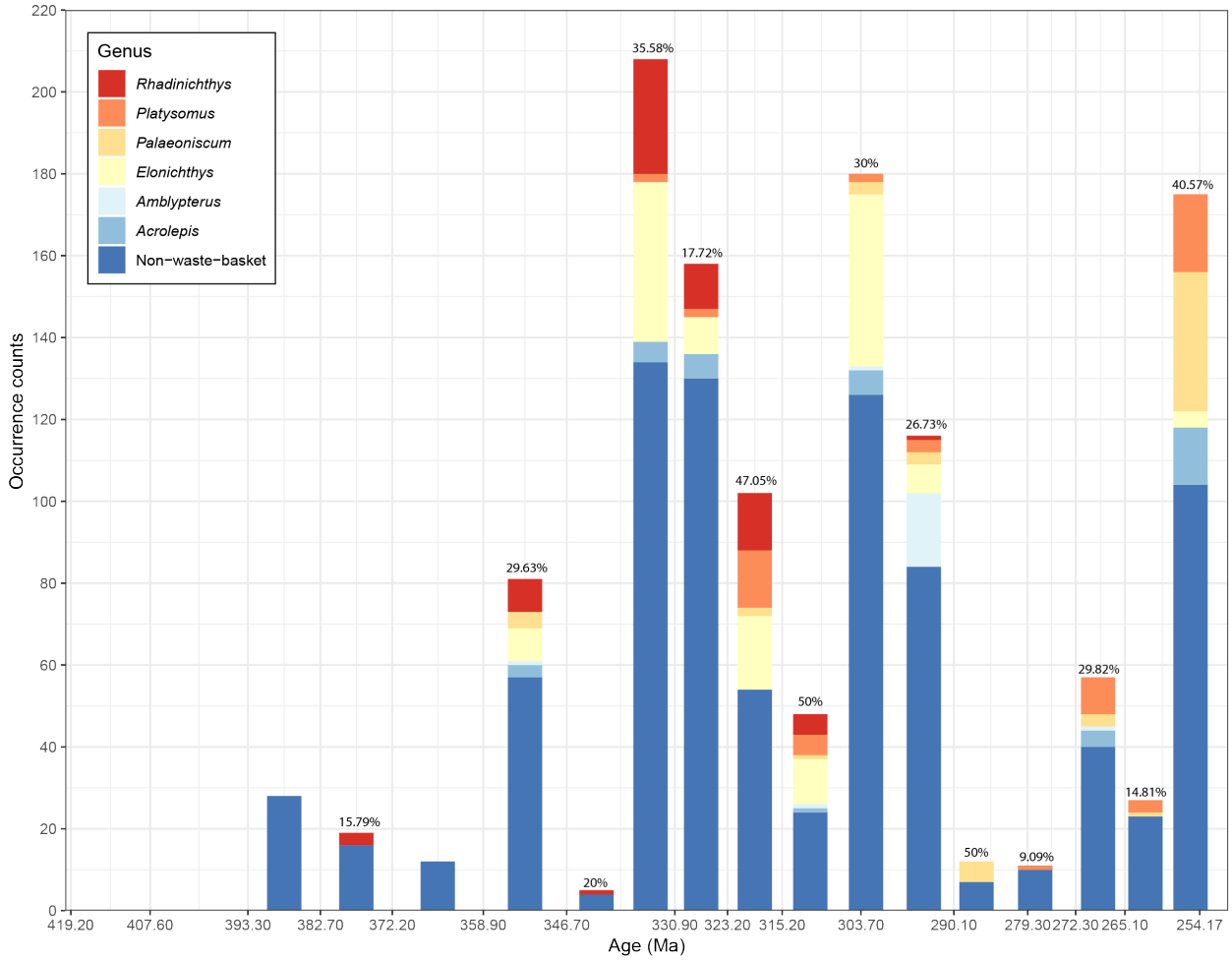


Figure B.10: Occurrences of 'waste-basket' genera (*Acrolepis, Amblypterus, Elonichthys, Palaeoniscus, Platysomus* and *Rhadinichthys*) versus non-'waste-basket' genera through the Palaeozoic, showing the total percentage of 'waste-basket' occurrences in each interval.

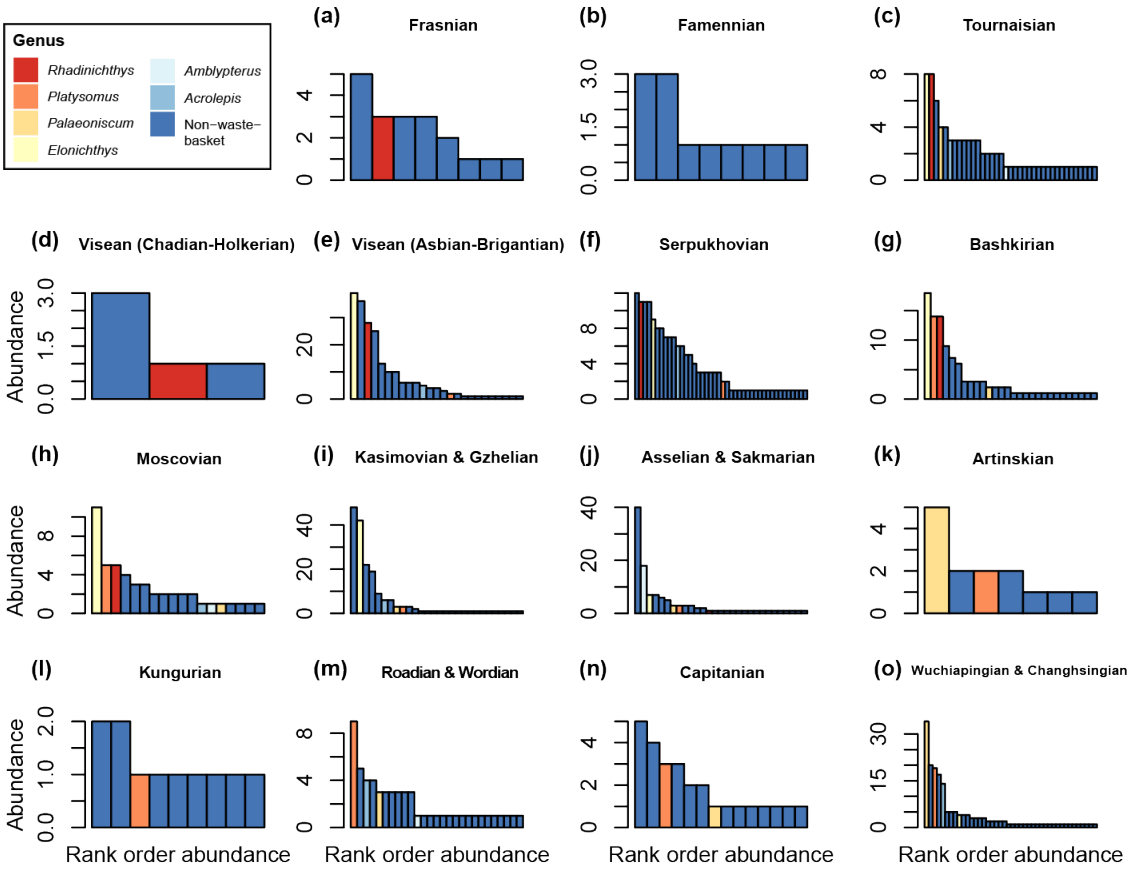


Figure B.11: Rank order occurrence distributions of the sampled equal-length intervals at genus level (colours show ‘waste-basket’ genera versus non-‘waste-basket’ genera).

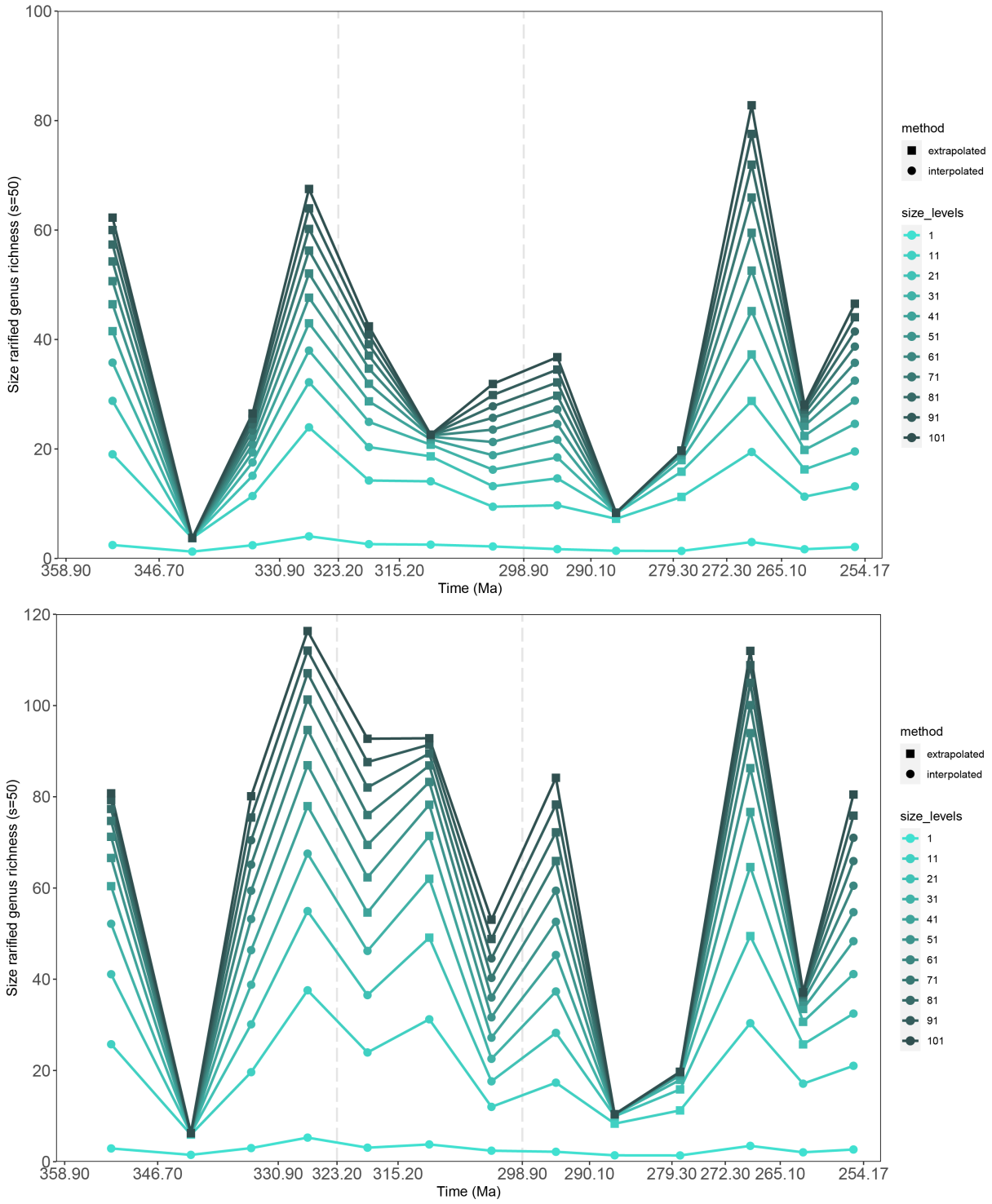


Figure B.12: Estimates of Carboniferous and Permian actinopterygian diversity using size-based (classical) rarefaction of (a) occurrences of genera and (b) occurrences of species, showing estimates for different sample sizes.

C Supplementary Information for description and phylogenetic analyses of MM L.1696

C.1 Additional images of MM L.1696

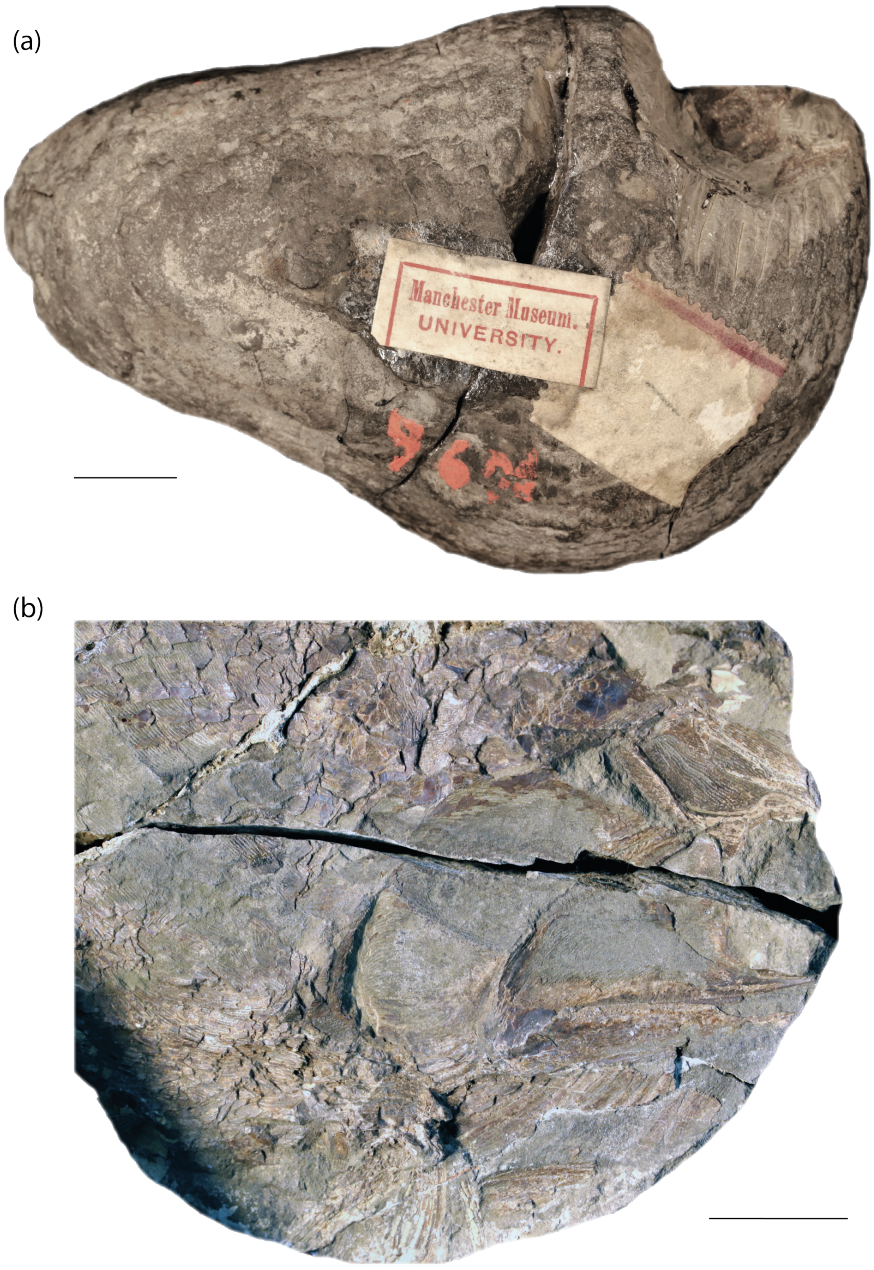


Figure C.1: Additional images of MM L.1696 showing (a) the reverse of the nodule, and (b) the anterior region of the counterpart. Scale bars = 10 mm.

C.2 Taxon list for phylogenetic analyses

Taxon	Source
Acanthodes bronni	Miles, 1973; Davis *et al*., 2012.
Acipenser brevirostrum	Nieuwenhuys, 1982; Hilton *et al*., 2011.
Aesopichthys erinaceus	Poplin & Lund, 2000.
Aetholepis mirablis	Woodward 1895.
Amia calva	Grande & Bemis, 1998; Sallan, 2014.
Amphicentrum granulosum	Traquair, 1875; Bradley-Dyne, 1939.
Arduafrons prominoris	Nursall 1999.
Atractosteus spatula	Grande, 2010.
Austelliscus ferox	Figueroa *et al*., 2021.
Australosomus kochi	Nielsen, 1949.
Avonichthys manskyi	Wilson et al. 2018.
Beagiascus pulcherrimus	Mickle *et al.*, 2009.
Beishanichthys brevicaudalis	Xu & Gao, 2011.
Birgeria groenlandica	Nielsen, 1949.
Bobasatrania groenlandica	Stensiö, 1932.
Boreosomus piveteaui	Nielsen, 1942.
Boreosomus reuterskioldi	Stensiö, 1921; Nielsen, 1942; Romano *et al*., 2019; Argyriou *et al*., 2022.
Brazilichthys macrognathus	Figeruoa *et al*., 2019
Brembodus ridens	Tintori 1981.
Caturus furcatus	Patterson, 1975; Lambers, 1994; Grande & Bemis, 1998.
Cheirolepis canadensis	Arratia & Cloutier, 1996; Arratia, 2009.
Cheirolepis schultzei	Arratia & Cloutier, 2004.
Cheirolepis trailli	Pearson & Westoll, 1979; Giles *et al*., 2015a.
Chondrosteus acipenseroides	Hilton & Forey 2009; Hilton *et al*., 2011.
Cladodoides wildungensis	Maisey, 2005.
Coccocephalichthys wildi	Poplin, 1974; Poplin & Véran, 1996.
Cosmoptychius striatus	Gardiner; 1963; Schaeffer, 1971; Coates, 1999.
Cuneognathus gardineri	Friedman & Blom, 2006.
Cyranorhis bergeraci	Lund *et al.,* 1997.
Dandya ovalis	Tintori 1983.
Dapedium caelatum	Thies & Hauff, 2008; Thies & Herzog, 1999.
Dapedium noricum	Tintori 1983.
Dapedium pholidotum	Patterson, 1975; Thies & Herzog, 1999; Thies *et al*., 2015.

Dapedium punctatum	Thies & Herzog, 1999; Thies & Hauff, 2011; Thies & Waschewitz, 2015.
Dapedium sp. (Lias)	Rayner 1948; Patterson 1975.
Dapedium stollorum	Thies & Herzog, 1999; Thies & Hauff, 2011; Thies & Waschewitz, 2015.
Dialipina salguerioensis	Schultze, 1968; Schultze & Cumbaa, 2001.
Dicksonosteus arcticus	Goujet, 1975
Diplocercides kayseri	Stensiö, 1922a,b; Forey, 1996.
Dipteronotus ornatus	Nielsen, 1949; Bürgin, 1992.
Discoserra pectinodon	Lund, 2000; Hurley *et al*., 2007.
Donnrosenia schaefferi	Long et al., 2008.
Dorsetichthys bechei	Patterson, 1968; Patterson, 1973; Patterson, 1975; Grande & Bemis, 1998.
Ebenaqua ritchei	Campbell & Le Duy Phuoc, 1983.
Elops hawaiensis	Forey, 1973.
Entelognathus primordialis	Zhu *et al.,* 2013.
Eomesodon liassicus	Gardiner 1960.
Erpetoichthys calabaricus	Claeson *et al*., 2007; Claeson & Hagadorn, 2008; Giles *et al*. 2017.
Eusthenopteron foordi	Jarvik, 1980.
Evenkia eunoptera	Berg, 1942; Selenzneva, 1985; Sytchevskaya, 1999.
Fouldenia ischiptera	Sallan & Coates, 2013.
Fukangichthys longidorsalis	Xu *et al*., 2014.
Gibbodon cenensis	Tintori 1981.
Glyptolepis groenlandica	Jarvik, 1972; Jarvik, 1980.
Gogonasus andrewsae	Long *et al*., 1997; Long *et al*., 2006; Holland, 2014.
Gogosardina coatesi	Choo *et al.,* 2009.
Guiyu oneiros	Zhu *et al.*, 2009; Qiao & Zhu, 2010.
Hemicalypterus weiri	Schaeffer, 1967; Gibson 2013, 2016.
Heterostrophus phillipsi	Woodward 1928, 1929.
Hiodon alosoides	Hilton, 2002.
Howqualepis rostridens	Long, 1988; Choo, 2009.
Hulettia americana	Schaeffer & Patterson, 1984.
Ichthyokentema purbeckensis	Griffith & Patterson, 1963.
Kalops monophyrum	Poplin & Lund 2002.
Kansasiella eatoni	Poplin, 1974.
Kentuckia deani	Rayner, 1951; Giles & Friedman, 2014.
Kentuckia hlavini	Dunkle, 1964; Feldman, 1996.
Krasnoyarichthys jesseni	Prokofiev, 2002.
Lambeia pectinatus	Mickle 2017.
Lawrenciella schaefferi	Poplin, 1984; Hamel & Poplin, 2008.
Lepisosteus osseus	Balfour & Parker, 1882; Mathiesen & Popper, 1987; Grande, 2010.
Leptolepis bronni	Rayner, 1937.
“Ligulalepis”	Basden *et al*., 2000; Basden & Young, 2001; Clement *et al*., 2018.
Limnomis delaneyi	Daeschler, 2000.
Luederia kempi	Schaeffer & Dalquest, 1978.

Luganoia lepidosteoides	Bürgin, 1992.
Macrepistius arenatus	Schaeffer, 1960; Schaeffer, 1971.
Macrosemimimus lennieri	Jain & Robinson, 1963; Wenz, 1967; Patterson, 1875; Schröder *et al*., 2012.
Macrosemius rostratus	Bartram, 1977.
Meemannia eos	Zhu *et al*., 2006, 2010; Lu *et al*. 2016.
Mesonichthys aitkeni	Traquair, 1886, 1901; Watson, 1925; Gardiner, 1963.
Melanecta anneae	Coates, 1998.
Mesturus sp.	Nursall 1999.
Mesturus verrucosus	Nursall 1999.
Miguashaia bureaui	Cloutier, 1996.
Mimipiscis bartrami	Gardiner, 1984; Choo, 2011.
Mimipiscis toombsi	Gardiner, 1984; Choo, 2011; Giles & Friedman, 2014.
Moythomasia durgaringa	Gardiner, 1984; Long & Trinajstic, 2010; Choo 2015.
Moythomasia lineata	Jessen, 1968; Choo 2015.
Moythomasia nitida	Jessen, 1968; Choo 2015.
Moythomasia perforata	Gross, 1942.
Neoproscinetes penalvai	Nursall & Maisey, 1987; Machado, 2008.
Novogonatodus kasantsevae	Long, 1998; Holland *et al.*, 2007.
Obaichthys decoratus	Grande, 2010.
Onychodus jandemarrai	Andrews *et al.*, 2006.
Osorioichthys marginis	Taverne, 1997.
Osteolepis macrolepidotus	Jarvik 1948.
Ozarcus mapesae	Pradel *et al*., 2014.
Palaeoneiros clackorum	Giles *et al.*, 2023.
Paradapedium egertoni	Jain 1973.
Peltopleurus lissocephalus	Bürgin, 1992.
Platysomus superbus	Moy-Thomas & Bradley-Dyne, 1938.
Polyodon spathula	Argyriou *et al*., 2018
Polypterus bichir	Allis 1922; Jollie 1984; Bjerring 1991; Bartsch & Gemballa 1992; Bartsch *et al*. 1997; Grande 2010.
Porolepis sp.	Jarvik, 1972; Jarvik, 1980.
Propterus elongatus	Bartram, 1977.
Psarolepis romeri	Yu, 1998; Zhu *et al*., 1999; Zhu & Yu, 2009; Qu *et al.,* 2013.
Pteronisculus stensioi	Nielsen 1942; Coates, 1998.
Ptycholepis bollensis	Woodward 1895; Aldinger, 1937; Wenz, 1959, 1968; Schaeffer *et al*., 1975; Veran, 1988; Veran 1998; Garbelli & Tintori, 2015.
Raynerius splendens	Giles *et al.,* 2015b.
Sargodon tomicus	Tintori 1983.
Saurichthys madagascarensis	Kogan *et al.*, 2016.
Saurichthys ornatus	Stensiö, 1925; Argyriou *et al*., 2018.
Scanilepis dubia	Aldinger, 1937; Lehman, 1979.
Scopulipiscis saxciput	Latimer & Giles, 2018.
Semionotus elegans	Olsen & McCune, 1991.
Stegotrachelus finlayi	Gardiner, 1963; Swartz, 2009.

Styloichthys changae	Zhu & Yu, 2002; Zhu *et al*., 2006; Friedman, 2007.
Styracopterus fulcratus	Sallan & Coates, 2013.
Tanaocrossus kalliokoskii	Schaeffer, 1967; Schaeffer & Donald, 1978.
Tegeolepis clarki	Gardiner, 1963; Dunkle & Schaeffer, 1973.
Tetragonolepis oldhami	Jain 1973.
Tetragonolepis semicincta	Thies, 1991.
Trawdenia planti	Coates, 1999; Coates & Tietjen 2018.
Venusichthys comptus	Xu & Zhao, 2016.
Watsonulus eugnathoides	Olsen, 1984; Grande & Bemis, 1998.
Wendyichthys dicksoni	Lund & Poplin, 1997.
Woodichthys bearsdeni	Coates, 1998.
Yelangichthys macrocephalus	Wu *et al*., 2013; Argyriou *et al*., 2018.

C.3 Character list for phylogenetic analyses

1. Large dermal plates - (Forey, 1980; Gardiner, 1984; Zhu & Schultze, 2001; Zhu et al., 2001; Zhu & Yu, 2002; Zhu et al., 2006; Friedman, 2007; Brazeau, 2009; Zhu et al., 2009; Friedman & Brazeau; 2010; Davis et al., 2012; Zhu et al., 2013; Brazeau & Friedman, 2014; Giles et al., 2015b,c; Giles et al., 2017; Argyriou et al., 2018; Latimer & Giles, 2018; Wilson et al., 2019; Figueroa et al., 2021.)

0 absent
1 present

2. Sensory lines - (Brazeau, 2009; Zhu et al., 2013; Giles et al., 2015b; Giles et al., 2017; Argyriou et al., 2018; Latimer & Giles, 2018; Wilson et al., 2019; Figueroa et al., 2021.)

0 preserved as open grooves
1 pass through canals

3. Premaxilla as distinct ossification - (Hurley et al. 2007; Xu et al. 2014; Giles et al., 2017; Argyriou et al., 2018; Latimer & Giles, 2018; Wilson et al., 2019; Figueroa et al., 2021. Typically, the premaxilla is a short, paired or median bone that contributes to the orbital margin anterior to the maxilla. However, considerable variation is present, and we have attempted to consistently code this variation as laid out here and in the following character descriptions. A premaxilla may be completely absent (e.g. *Acipenser*, *Cyranorhis*) or dorsally expanded into a midline bone (possibly fused with the rostral; e.g. *Bobasatrania*, *Styracopterus*). These two latter states are coded as 1 here.)

0 present
1 absent

4. Premaxillae, contact at midline - (Cloutier & Ahlberg, 1996; Taverne, 1997; Schultze & Cumbaa, 2001; Zhu & Schultze, 2001; Zhu & Yu, 2002; Cloutier & Arratia, 2004; Friedman & Blom, 2006; Zhu et al., 2006; Friedman, 2007; Long et al., 2008; Swartz, 2009; Choo, 2011; Giles et al., 2017; Argyriou et al., 2018; Latimer & Giles, 2018; Wilson et al., 2019; Figueroa et al., 2021. Coded as inapplicable in taxa lacking any ossification in the position typically occupied by the premaxilla (e.g. *Acipenser*, *Cyranorhis*) and where the premaxilla appears fused with the rostral (e.g. *Bobasatrania*, *Styracopterus*).)

0 present
1 absent

5. Premaxilla fused at midline - (Xu et al., 2011; Xu et al., 2015; Xu & Zhao, 2016; Giles et al., 2017; Argyriou et al., 2018; Latimer & Giles, 2018; Wilson et al., 2019; Figueroa et al., 2021. Coded as inapplicable in taxa lacking any ossification in the position typically occupied by the premaxilla (e.g. *Acipenser*, *Cyranorhis*) and where the premaxilla appears fused with the rostral (e.g. *Bobasatrania*, *Styracopterus*) and where the premaxilla appears fused with the rostral (e.g. *Bobasatrania*, *Styracopterus*).)

0 absent
1 present

6. Premaxilla - (Friedman, 2007; Giles et al., 2015b; Giles et al., 2017; Argyriou et al., 2018; Latimer & Giles, 2018; Wilson et al., 2019; Figueroa et al., 2021. Coded as inapplicable in taxa lacking any ossification in the position typically occupied by the premaxilla (e.g. *Acipenser*, *Cyranorhis*) and in taxa where the premaxillae do not contact at the midline.)

0 Reaches or extends past anterior margin of orbit

1 Confined to region anterior to orbit

7. Premaxilla contributes to orbital margin - (Cloutier & Ahlberg, 1996; Schultze & Cumbaa, 2001; Zhu & Schultze, 2001; Zhu et al., 2001; Zhu & Yu, 2002; Cloutier & Arratia, 2004; Zhu et al., 2006; Friedman, 2007; Long et al., 2008; Swartz, 2009; Zhu et al., 2009; Xu & Gao, 2011; Zhu et al., 2013; Xu et al., 2014; Giles et al., 2017; Argyriou et al., 2018; Latimer & Giles, 2018; Wilson et al., 2019; Figueroa et al., 2021. Coded as inapplicable in taxa lacking any ossification in the position typically occupied by the premaxilla (e.g. *Acipenser*, *Cyranorhis*), where the premaxilla appears fused with the rostral (e.g. *Bobosatrania*, *Styracopterus*), and where the premaxilla is restricted anterior to the orbit.)
    0 absent
    1 present

8. Teeth on premaxillae - (Cloutier & Arratia 2004, Xu et al. 2014; Giles et al., 2017; Argyriou et al., 2018; Latimer & Giles, 2018; Wilson et al., 2019; Figueroa et al., 2021. Coded as inapplicable in taxa lacking any ossification in the position typically occupied by the premaxilla (e.g. *Acipenser*, *Cyranorhis*).)
    0 present
    1 absent

9. Mobile premaxilla - (Arratia 1999; Cavin & Suteethorn 2006; Hurley et al. 2007; Giles et al., 2017; Argyriou et al., 2018; Latimer & Giles, 2018; Wilson et al., 2019; Figueroa et al., 2021. Coded as inapplicable in taxa lacking any ossification in the position typically occupied by the premaxilla (e.g. *Acipenser*, *Cyranorhis*) and where the premaxilla appears fused with the rostral (e.g. *Bobasatrania*, *Styracopterus*))
    0 absent
    1 present

10. Olfactory nerve pierces premaxilla - (Grande 2010; Xu et al., 2015; Xu & Shen, 2015; Xu & Zhao, 2016; Giles et al., 2017; Argyriou et al., 2018; Latimer & Giles, 2018; Wilson et al., 2019; Figueroa et al., 2021. Coded as inapplicable in taxa lacking any ossification in the position typically occupied by the premaxilla (e.g. *Acipenser*, *Cyranorhis*) and where the premaxilla appears fused with the rostral (e.g. *Bobasatrania*, *Styracopterus*).)
    0 absent
    1 present

11. Nasal process of premaxilla - (Gardiner & Schaeffer 1989; Olsen & McCune 1991; Gardiner et al. 1996; Gardiner et al. 2005; Cavin & Suteethorn 2006; Hurley et al. 2007; Grande 2010; LÓpez-Arbarello 2012; Xu & Wu 2012; Xu et al. 2014; Bermúdez-Rochas & Poyato-Ariza 2015; Poyato-Ariza 2015; Thies & Waschkewitz, 2015; Xu & Shen, 2015; Gibson 2016; Xu & Zhao, 2016; Giles et al., 2017; López-Arbarello & Sferco 2018; Argyriou et al., 2018; Latimer & Giles, 2018; Wilson et al., 2019; Figueroa et al., 2021. Coded as inapplicable in taxa lacking any ossification in the position typically occupied by the premaxilla (e.g. *Acipenser*, *Cyranorhis*) and where the premaxilla appears fused with the rostral (e.g. *Bobasatrania*, *Styracopterus*).)
    0 absent
    1 short
    2 long, reaches skull roof

12. Sensory canal on premaxilla - (Giles et al., 2017; Argyriou et al., 2018; Latimer & Giles, 2018; Wilson et al., 2019; Figueroa et al., 2021. Coded as inapplicable in taxa lacking any ossification

in the position typically occupied by the premaxilla (e.g. *Acipenser*, *Cyranorhis*) and where the premaxilla appears fused with the rostral (e.g. *Bobasatrania*, *Styracopterus*).)

0 present
1 absent

13. Postrostrals (element[s] immediately anterior to frontals but not in contact with premaxillae) - (Cloutier & Ahlberg, 1996; Taverne, 1997; Lund, 2000; Schultze & Cumbaa, 2001; Zhu & Schultze, 2001; Lund & Poplin, 2002; Cloutier & Arratia, 2004; Friedman & Blom, 2006; Long et al., 2008; Swartz, 2009; Choo, 2011; Xu et al., 2014; Giles et al., 2015b; Giles et al., 2017; Argyriou et al., 2018; Latimer & Giles, 2018; Wilson et al., 2019; Figueroa et al., 2021.)

0 present
1 absent

14. Single median dermal bone capping snout - (Gardiner & Schaeffer, 1989; Taverne, 1997; Friedman & Blom, 2006; Long et al., 2008; Swartz, 2009; Choo, 2011; Giles et al., 2015b; Poyato-Ariza 2015; Giles et al., 2017; Argyriou et al., 2018; Latimer & Giles, 2018; Wilson et al., 2019; Figueroa et al., 2021.)

0 absent
1 present

15. Median rostral - (Gardiner et al. 1996; Hurley et al. 2007; Giles et al., 2017; Argyriou et al., 2018; Latimer & Giles, 2018; Wilson et al., 2019; Figueroa et al., 2021.)

0 plate-like
1 tube-like

16. Pores for rostral organ - (Friedman, 2007; Giles et al., 2015b; Giles et al., 2017; Argyriou et al., 2018; Latimer & Giles, 2018; Wilson et al., 2019; Figueroa et al., 2021.)

0 absent
1 present

17. Nasal bone as single consolidated ossification (i.e. bone(s) carrying supraorbital canal between premaxilla and anterior margin of frontals) - (Taverne, 1997; Schultze & Cumbaa, 2001; Friedman & Blom, 2006; Long et al., 2008; Swartz, 2009; Choo, 2011; Giles et al., 2015b; Giles et al., 2017; Argyriou et al., 2018; Latimer & Giles, 2018; Wilson et al., 2019; Figueroa et al., 2021.)

0 absent
1 present

18. Contact of nasals on midline - (Giles et al., 2017; Argyriou et al., 2018; Latimer & Giles, 2018; Wilson et al., 2019; Figueroa et al., 2021.)

0 separated by dermal bones
1 contacting or separated by gap unfilled by bone

19. Nasal contributes to orbital margin - (Xu & Wu 2012; Xu et al. 2014; Xu & Zhao, 2016; Giles et al., 2017; López-Arbarello & Sferco 2018; Argyriou et al., 2018; Latimer & Giles, 2018; Wilson et al., 2019; Figueroa et al., 2021.)

0 absent
1 present

20. Mesial margin of (anterior) nasal - (Lund et al., 1995; Ahlberg & Johanson, 1998; Ahlberg et al., 2000; Lund, 2000; Poplin & Lund, 2000; Schultze & Cumbaa, 2001; Lund & Poplin, 2002; Cloutier & Arratia, 2004; Zhu & Ahlberg, 2004; Daeschler et al., 2006; Long et al., 2006; Zhu et al., 2006; Zhu et al., 2009; Choo, 2011; Giles et al., 2015b; Giles et al., 2017; López-Arbarello & Sferco 2018; Argyriou et al., 2018; Latimer & Giles, 2018; Wilson et al., 2019; Figueroa et al., 2021.)
    0 not notched
    1 notched

21. Posterior nostril in complete communication with orbital fenestra - (Friedman & Blom, 2006; Long et al., 2008; Choo, 2011; Giles et al., 2015b; Giles et al., 2017; Argyriou et al., 2018; Latimer & Giles, 2018; Wilson et al., 2019; Figueroa et al., 2021. This character refers to the opening of the posterior nostril with reference to the surrounding dermal bones.)
    0 absent
    1 present

22. Posterior nostril: contribution to margin by premaxillae - (Friedman & Blom, 2006; Long et al., 2008; Choo, 2011; Giles et al., 2015b; Giles et al., 2017; Argyriou et al., 2018; Latimer & Giles, 2018; Wilson et al., 2019; Figueroa et al., 2021.)
    0 absent
    1 present

23. Tectals (sensu Cloutier & Ahlberg 1996, not counting the posterior tectal of Jarvik) (Lund et al., 1995; Cloutier & Ahlberg, 1996; Lund, 2000; Schultze & Cumbaa, 2001; Zhu & Schultze, 2001; Zhu et al., 2001; Lund & Poplin, 2002; Zhu & Yu, 2002; Cloutier & Arratia, 2004; Zhu et al., 2006; Friedman, 2007; Swartz, 2009; Zhu et al., 2009; Zhu et al., 2013; Giles et al., 2015b; Giles et al., 2017; Argyriou et al., 2018; Latimer & Giles, 2018; Wilson et al., 2019; Figueroa et al., 2021.)
    0 absent
    1 present

24. Dermal intracranial joint - (Cloutier & Ahlberg, 1996; Ahlberg & Johanson, 1998; Zhu & Ahlberg, 2004; Zhu & Schultze, 2001; Zhu et al., 2001; Zhu & Yu, 2002; Daeschler et al., 2006; Long et al., 2006; Zhu et al., 2006; Friedman, 2007; Brazeau, 2009; Zhu et al., 2009; Choo, 2011; Davis et al., 2012; Zhu et al., 2013; Giles et al., 2015b; Giles et al., 2017; Argyriou et al., 2018; Latimer & Giles, 2018; Wilson et al., 2019; Figueroa et al., 2021.)
    0 absent
    1 present

25. Pineal foramen - (Cloutier & Ahlberg, 1996; Taverne, 1997; Schultze & Cumbaa, 2001; Zhu & Schultze, 2001; Zhu & Yu, 2002; Friedman & Blom, 2006; Friedman, 2007; Long et al., 2008; Brazeau, 2009; Swartz, 2009; Davis et al., 2012; Zhu et al., 2013; Xu et al., 2014; Giles et al., 2015b,c; Giles et al., 2017; Argyriou et al., 2018; Latimer & Giles, 2018; Wilson et al., 2019; Figueroa et al., 2021. A pineal foramen is variably present in *Cheirolepis canadensis* (Pearson & Westoll, 1979; Arratia & Cloutier, 1996), *C. trailli* (Pearson & Westoll, 1979), *Kentuckia deani* (Rayner, 1951) and *Meemannia* (Zhu et al., 2010), and these taxa are coded '0/1' to reflect this polymorphism.)
    0 present
    1 absent

26. Pineal eminence - (Friedman, 2007; Zhu et al., 2009; Giles et al., 2015b; Giles et al., 2017; Argyriou et al., 2018; Latimer & Giles, 2018; Wilson et al., 2019; Figueroa et al., 2021. Can only be coded in taxa that lack a pineal foramen.)
    0 absent
    1 present

27. Shape of parietals (sarcopterygian postparietals) - (Dietze, 2000; Schultze & Cumbaa, 2001; Cloutier & Arratia, 2004; Friedman & Blom, 2006; Long et al., 2008; Swartz, 2009; Choo, 2011; Xu et al., 2014; Giles et al., 2015b; Giles et al., 2017; Argyriou et al., 2018; Latimer & Giles, 2018; Wilson et al., 2019; Figueroa et al., 2021.)
    0 rectangular, with long axis parallel to midline
    1 quadrate

28. Relative lengths of frontals and parietals (sarcopterygian parietals and postparietals) - (Lund et al., 1995; Taverne, 1997; Dietze, 2000; Lund, 2000; Poplin & Lund, 2000; Schultze & Cumbaa, 2001; Lund & Poplin, 2002; Cloutier & Arratia, 2004; Friedman & Blom, 2006; Zhu et al., 2006; Long et al., 2008; Swartz, 2009; Choo, 2011; López-Arbarello 2012; Xu et al., 2014; Bermúdez-Rochas & Poyato-Ariza 2015; Thies & Waschkewitz, 2015; Gibson 2016; Giles et al., 2015b; Giles et al., 2017; López-Arbarello & Sferco 2018; Argyriou et al., 2018; Latimer & Giles, 2018; Wilson et al., 2019; Figueroa et al., 2021.)
    0 frontal shorter than parietal
    1 frontal approximately equal to parietal
    2 frontal longer than parietal

29. Frontals broad posteriorly and tapering anteriorly - (Arratia 1999; López-Arbarello 2012; Bermúdez-Rochas & Poyato-Ariza 2015; Thies & Waschkewitz, 2015; Gibson 2016; Giles et al., 2017; López-Arbarello & Sferco 2018; Argyriou et al., 2018; Latimer & Giles, 2018; Wilson et al., 2019; Figueroa et al., 2021.)
    0 absent
    1 present

30. Anterior pit line - (Giles et al., 2015b,c; Giles et al., 2017; Argyriou et al., 2018; Latimer & Giles, 2018; Wilson et al., 2019; Figueroa et al., 2021. Although not figured, an anterior pit line is described for *Miguashaia* (Cloutier 1996).)
    0 absent
    1 present

31. Otic canal extends through parietals - (Giles et al., 2015b,c; Giles et al., 2017; Argyriou et al., 2018; Latimer & Giles, 2018; Wilson et al., 2019; Figueroa et al., 2021.)
    0 absent
    1 present

32. Junction between supraorbital and infraorbital canals - alter the refer exactly to the posterior junction? - (López-Arbarello 2012; Bermúdez-Rochas & Poyato-Ariza 2015; Poyato-Ariza 2015; Giles et al., 2017; López-Arbarello & Sferco 2018; Argyriou et al., 2018; Latimer & Giles, 2018; Wilson et al., 2019; Figueroa et al., 2021. The supraorbital canal may terminate in the frontal/parietal, or it may become confluent with the infraorbital canal. The exact position of this junction is highly variable, and typically occurs in the region of the frontal, dermosphenotic, dermopterotic.)
    0 absent

1 present

33. Anterior branch of infraorbital sensory canal - (Giles et al., 2017; Argyriou et al., 2018; Latimer & Giles, 2018; Wilson et al., 2019; Figueroa et al., 2021. In some taxa (e.g. *Dapedium*), the infraorbital canal continues anteriorly above the orbit a short way.)
    0 absent
    1 present

34. Tabular - (Lund et al., 1995; Cloutier & Ahlberg, 1996; Schultze & Cumbaa, 2001; Zhu & Schultze, 2001; Cloutier & Arratia, 2004; Long et al., 2008; Swartz, 2009; Giles et al., 2015b; Giles et al., 2017; Argyriou et al., 2018; Latimer & Giles, 2018; Wilson et al., 2019; Figueroa et al., 2021.)
    0 present
    1 absent

35. Tabular pit line - (Giles et al., 2015b,c; Giles et al., 2017; Argyriou et al., 2018; Latimer & Giles, 2018; Wilson et al., 2019; Figueroa et al., 2021.)
    0 absent
    1 present

36. Number of bones carrying otic portion of lateral line canal between dermosphenotic and posterior edge of skull roof. - (Gardiner & Schaeffer 1989; Cloutier & Arratia, 2004; Hurley et al. 2007; Choo, 2011; Giles et al., 2015b; Xu & Zhao, 2016; Giles et al., 2017; Argyriou et al., 2018; Latimer & Giles, 2018; Wilson et al., 2019; Figueroa et al., 2021. This character is reformulated from Choo's character 'Dermopterotic: present/absent'. Rather than designating bones as an intertemporal (or supratemporal or dermosphenotic) a priori, we consider the number of bones carrying the otic portion of the lateral line canal between the dermosphenotic and the posterior edge of the skull roof. Where two bones are present, these are treated as the intertemporal and supratemporal; where only one is present, this is treated as the dermopterotic. Anamestic bones between the dermosphenotic and frontal are not included in this count.))
    0 at least two (i.e. intertemporal and supratemporal)
    1 one (i.e. dermopterotic)

37. Intertemporal: relative length - (Taverne, 1997; Friedman & Blom, 2006; Choo, 2011; Giles et al., 2015b; Giles et al., 2017; Argyriou et al., 2018; Latimer & Giles, 2018; Wilson et al., 2019; Figueroa et al., 2021. Coded as inapplicable in taxa with a dermopterotic. Coded as inapplicable in taxa with a dermopterotic.)
    0 shorter than supratemporal
    1 of similar length to supratemporal
    2 longer than supratemporal

38. Intertemporal: contact with supratemporal anterior to that between frontal and parietal - (Friedman & Blom, 2006; Choo, 2011; Giles et al., 2015b; Giles et al., 2017; Argyriou et al., 2018; Latimer & Giles, 2018; Wilson et al., 2019; Figueroa et al., 2021. Coded as inapplicable in taxa with a dermopterotic.)
    0 absent
    1 present

39. Intertemporal contacts nasal - (Xu & Gao, 2011; Xu et al., 2014; Giles et al., 2015b; Giles et al., 2017; Argyriou et al., 2018; Latimer & Giles, 2018; Wilson et al., 2019; Figueroa et al., 2021. Coded as inapplicable in taxa with a dermopterotic.)
    0 absent
    1 present

40. Supratemporal: narrow anterolateral flange forming ventral margin of spiracular opening - (Choo, 2011; Giles et al., 2015b; Giles et al., 2017; Argyriou et al., 2018; Latimer & Giles, 2018; Wilson et al., 2019; Figueroa et al., 2021. Coded as inapplicable in taxa with a dermopterotic.)
    0 absent
    1 present

41. Parietal fused to dermopterotic - (Xu & Gao 2011; Xu et al. 2014; Giles et al., 2017; Argyriou et al., 2018; Latimer & Giles, 2018; Wilson et al., 2019; Figueroa et al., 2021. Coded as inapplicable in taxa with a separate intertemporal and supertemporal, and in taxa lacking these bones entirely.)
    0 absent
    1 present

42. Bone carrying otic portion of lateral line canal extends past posterior margin of parietals - (Lu et al. 2016; Giles et al., 2017; Argyriou et al., 2018; Latimer & Giles, 2018; Wilson et al., 2019; Figueroa et al., 2021.)
    0 absent
    1 present

43. Number of paired extrascapulars - (Gardiner & Schaeffer, 1989; Lund et al., 1995; Cloutier & Ahlberg, 1996; Grande & Bemis 1998; Coates, 1998; Lund, 2000; Poplin & Lund, 2000; Schultze & Cumbaa, 2001; Zhu & Schultze, 2001; Lund & Poplin, 2002; Cloutier & Arratia, 2004; Friedman & Blom, 2006; Long et al., 2008; Swartz, 2009; Choo, 2011; López-Arbarello 2012; Zhu et al., 2013; Bermúdez-Rochas & Poyato-Ariza 2015; Poyato-Ariza 2015; Giles et al., 2015b; Thies & Waschkewitz, 2015; Xu et al., 2015; Gibson 2016; Xu & Zhao, 2016; Giles et al., 2017; López-Arbarello & Sferco 2018; Argyriou et al., 2018; Latimer & Giles, 2018; Wilson et al., 2019; Figueroa et al., 2021.)
    0 one pair
    1 two pairs
    2 three or more pairs

44. Extrascapular reaches lateral edge of skull roof - (Giles et al., 2015b,c; Giles et al., 2017; Argyriou et al., 2018; Latimer & Giles, 2018; Wilson et al., 2019; Figueroa et al., 2021. The skull roof of *Moythomasia* as shown in Fig. 103 (Gardiner, 1984) is a restoration (see also Choo 2015: fig. 13). The only skull roof directly figured by Gardiner does not preserve the extrascapulars in situ (fig. 83). However, in specimens viewed by us, as well as in published photos of articulated material (e.g. Choo 2015: fig 8), the lateral extrascapular of *M. durgaringa* is clearly excluded from the lateral margin of the skull roof.)
    0 absent
    1 present

45. Single median extrascapular - (Dietze, 2000; Cloutier & Arratia, 2004; Long et al., 2008; Swartz, 2009; Choo, 2011; Xu & Gao, 2011; Zhu et al., 2013; Xu et al., 2014; Giles et al., 2015b; Giles

et al., 2017; Argyriou et al., 2018; Latimer & Giles, 2018; Wilson et al., 2019; Figueroa et al., 2021.)

0 present
1 absent

46. Extrascapulae contact each other at midline - (Giles et al., 2015b,c; Giles et al., 2017; Argyriou et al., 2018; Latimer & Giles, 2018; Wilson et al., 2019; Figueroa et al., 2021. Inapplicable for taxa that possess a median extrascapular, as it is logically impossible for the lateral extrascapulae to meet in the midline.)

0 absent
1 present

47. Medially-directed branch of sensory canal in extrascapulae - (Choo, 2011; Giles et al., 2015b; Giles et al., 2017; Argyriou et al., 2018; Latimer & Giles, 2018; Wilson et al., 2019; Figueroa et al., 2021.)

0 present
1 absent

48. Extratemporal - (Cloutier & Ahlberg, 1996; Ahlberg & Johanson, 1998; Zhu & Schultze, 2001; Zhu et al., 2001; Zhu & Yu, 2002; Zhu & Ahlberg, 2004; Daeschler et al., 2006; Long et al., 2006; Zhu et al., 2006; Friedman, 2007; Zhu et al., 2009; Giles et al., 2015b; Giles et al., 2017; Argyriou et al., 2018; Latimer & Giles, 2018; Wilson et al., 2019; Figueroa et al., 2021.)

0 absent
1 present

49. Antorbital bone - (Gardiner & Schaeffer 1989; Lund et al. 2000; Cloutier & Arratia, 2004; Hurley et al. 2007; Choo, 2011; Xu & Gao, 2011; Xu et al., 2014; Giles et al., 2015b; Giles et al., 2017; López-Arbarello & Sferco 2018; Argyriou et al., 2018; Latimer & Giles, 2018; Wilson et al., 2019; Figueroa et al., 2021.)

0 absent
1 present

50. Tube-like canal bearing anterior arm of antorbital - could include another state here for elongated antorbitals (e.g. Amia) - (Grande 2010; Xu & Wu 2012; Xu et al. 2014; Poyato-Ariza 2015; Xu & Shen, 2015; Xu & Zhao, 2016; Giles et al., 2017; López-Arbarello & Sferco 2018; Argyriou et al., 2018; Latimer & Giles, 2018; Wilson et al., 2019; Figueroa et al., 2021.)

0 absent
1 present

51. Infraorbitals - (Cloutier & Arratia, 2004; Gardiner et al., 2005; Choo, 2011; Xu & Gao, 2011; Xu et al., 2014; Giles et al., 2015b; Giles et al., 2017; López-Arbarello & Sferco 2018; Argyriou et al., 2018; Latimer & Giles, 2018; Wilson et al., 2019; Figueroa et al., 2021.)

0 one
1 two
2 more than two

52. Anterior expansion of lacrimal - (Taverne, 1997; Friedman & Blom, 2006; Long et al., 2008; Swartz, 2009; Choo, 2011; Giles et al., 2015b; Giles et al., 2017; Argyriou et al., 2018; Latimer & Giles, 2018; Wilson et al., 2019; Figueroa et al., 2021.)

0 absent

1 present

53. Notch in anterior margin of jugal - (Cloutier & Arratia, 2004; Friedman & Blom, 2006; Long et al., 2008; Swartz, 2009; Choo, 2011; Giles et al., 2015b; Giles et al., 2017; Xu et al., 2014; Argyriou et al., 2018; Latimer & Giles, 2018; Wilson et al., 2019; Figueroa et al., 2021.)
    0 absent
    1 present

54. Suborbitals (non-canal bearing ossifications separating jugal and maxilla) - (Gardiner & Schaeffer 1989; Olsen & McCune 1991; Taverne, 1997; Schultze & Cumbaa, 2001; Friedman & Blom, 2006; Long et al., 2008; Choo, 2011; López-Arbarello 2012; Xu & Gao 2011; Bermúdez-Rochas & Poyato-Ariza 2015; Poyato-Ariza 2015; Giles et al., 2015b; Thies & Waschkewitz, 2015; Xu et al., 2015; Gibson 2016; Xu & Zhao, 2016; Giles et al., 2017; López-Arbarello & Sferco 2018; Argyriou et al., 2018; Latimer & Giles, 2018; Wilson et al., 2019; Figueroa et al., 2021.)
    0 absent
    1 one
    2 two
    3 three
    4 four or more

55. Multiple rami of infraorbital canal in jugal - (Giles et al., 2015b,c; Giles et al., 2017; Argyriou et al., 2018; Latimer & Giles, 2018; Wilson et al., 2019; Figueroa et al., 2021. Multiple branches radiate from the infraorbital canal in the jugal of many Carboniferous and younger actinopterygians, as well as the new taxon described here.)
    0 absent
    1 present

56. Dermosphenotic with distinct posterior ramus - (Gardiner & Schaeffer, 1989; Coates, 1998; Schultze & Cumbaa, 2001; Cloutier & Arratia, 2004; Friedman & Blom, 2006; Zhu et al., 2006; Long et al., 2008; Zhu et al., 2009; Choo, 2011; Giles et al., 2015b; Xu et al., 2015; Giles et al., 2017; Argyriou et al., 2018; Latimer & Giles, 2018; Wilson et al., 2019; Figueroa et al., 2021. The dermosphenotic of *Moythomasia* illustrated by (Gardiner 1984, fig 69) lacks a posterior limb, but this is from a small individual and most likely reflects ontogenetic variability, with a posterior limb being developed in larger individuals (B. Choo, pers. comm.; Choo 2015: fig. 8). The posterior limb of the dermosphenotic is variably developed in *Mesopoma* (Coates, 1999), so this taxon is scored '0/1' to reflect this polymorphism.)
    0 absent
    1 present

57. Dermosphenotic: contact with frontals blocked by intertemporal or dermopterotic - (Friedman & Blom, 2006; Choo, 2011; Giles et al., 2015b; Giles et al., 2017; Argyriou et al., 2018; Latimer & Giles, 2018; Wilson et al., 2019; Figueroa et al., 2021.)
    0 absent
    1 present

58. Supraorbital - (Gardiner & Schaeffer 1989; Grande & Bemis 1998; Hurley et al. 2007; Xu & Gao 2011; Xu et al. 2014; Poyato-Ariza 2015; Xu et al., 2015; Xu & Zhao, 2016; Giles et al., 2017; López-Arbarello & Sferco 2018; Argyriou et al., 2018; Latimer & Giles, 2018; Wilson et al., 2019; Figueroa et al., 2021.)

0 absent
1 one or two
2 three or more

59. Anterior-most infraorbital anterior to orbit (i.e. does not contribute to orbital margin) - (Olsen & McCune 1991; Cavin & Suteethorn 2006; López-Arbarello 2012; Bermúdez-Rochas & Poyato-Ariza 2015; Thies & Waschkewitz, 2015; Gibson 2016; Giles et al., 2017; López-Arbarello & Sferco 2018; Argyriou et al., 2018; Latimer & Giles, 2018; Wilson et al., 2019; Figueroa et al., 2021.)
    0 absent
    1 present

60. Three or more lachrymals - (Grande 2010; Xu & Wu 2012; Xu et al. 2014, 2015; Bermódez-Rochas & Poyato-Ariza 2015; Poyato-Ariza 2015; Thies & Waschkewitz, 2015; Gibson 2016; Xu & Zhao, 2016; Giles et al., 2017; Argyriou et al., 2018; Latimer & Giles, 2018; Wilson et al., 2019; Figueroa et al., 2021. The first lachrymal is regarded here as the anteriormost canal-bearing bone that contributes to orbital margin.)
    0 absent
    1 present

61. Circumorbital ring - (Wiley 1976; Lopez-Arbarello 2010.Wiley 1976; López-Arbarello 2012; Bermúdez-Rochas & Poyato-Ariza 2015; Poyato-Ariza 2015; Thies & Waschkewitz, 2015; Gibson 2016; Giles et al., 2017; López-Arbarello & Sferco 2018; Argyriou et al., 2018; Latimer & Giles, 2018; Wilson et al., 2019; Figueroa et al., 2021.)
    0 Supraorbitals do not contact infraorbitals at the anterior rim of the orbit.
    1 Supraorbitals contact infraorbitals, closing the orbit.

62. Jugal canal - (Patterson, 1982; Lauder & Liem, 1983; Gardiner, 1984; Cloutier & Arratia, 2004; Brazeau, 2009; Friedman & Brazeau, 2010; Choo, 2011; Davis et al., 2012; Zhu et al., 2013; Giles et al., 2015b,c; Giles et al., 2017; Argyriou et al., 2018; Latimer & Giles, 2018; Wilson et al., 2019; Figueroa et al., 2021.)
    0 absent
    1 present

63. Dermohyal - (Patterson, 1982; Gardiner & Schaeffer, 1989; Lund et al., 1995; Cloutier & Ahlberg, 1996; Coates, 1998; Dietze, 2000; Lund, 2000; Schultze & Cumbaa, 2001; Zhu & Schultze, 2001; Zhu et al., 2001; Lund & Poplin, 2002; Zhu & Yu, 2002; Cloutier & Arratia, 2004; Gardiner et al., 2005; Friedman & Blom, 2006; Zhu et al., 2006; Friedman, 2007; Long et al., 2008; Swartz, 2009; Zhu et al., 2009; Choo, 2011; Xu & Gao, 2011; Xu et al., 2014; 2015; Giles et al., 2015b; Xu & Zhao, 2016; Giles et al., 2017; Argyriou et al., 2018; Latimer & Giles, 2018; Wilson et al., 2019; Figueroa et al., 2021. This region of the cheek is missing in *Coccocephalichthys* (Poplin, 1974; Poplin & Véran, 1996), and was presumably removed by Watson (1925) when he first described the specimen. It is unclear from the surviving cast whether a dermohyal and/or accessory operculum were present, and as such this taxon is coded as ?.)
    0 absent
    1 present

64. Head of dermohyal projects above dorsal margin of operculum - (Giles et al., 2015b,c; Giles et al., 2017; Argyriou et al., 2018; Latimer & Giles, 2018; Wilson et al., 2019; Figueroa et al., 2021.

The dermohyal is not preserved in *Melanecta* (Coates, 1998), but it is clear from the surrounding bones that it would not have projected above the dorsal surface of the operculum.)

0 absent
1 present

65. Dermohyal - (Gardiner et al., 2005; Coates, 1999; Xu & Gao, 2011; Xu et al., 2014; Giles et al., 2015b; Giles et al., 2017; Argyriou et al., 2018; Latimer & Giles, 2018; Wilson et al., 2019; Figueroa et al., 2021.)

0 fused to hyomandibular
1 separate from hyomandibular

66. Complete enclosure of spiracle by bones bearing otic and infraorbital canals - (Friedman, 2007; Zhu et al., 2009; Giles et al., 2015b; Giles et al., 2017; Argyriou et al., 2018; Latimer & Giles, 2018; Wilson et al., 2019; Figueroa et al., 2021.)

0 absent
1 present

67. Maxilla - (Zhu & Yu, 2002; Friedman, 2007; Xu et al., 2014, 2015; Giles et al., 2015b; Xu & Zhao, 2016; Giles et al., 2017; López-Arbarello & Sferco 2018; Argyriou et al., 2018; Latimer & Giles, 2018; Wilson et al., 2019; Figueroa et al., 2021.)

0 absent
1 present

68. Expanded dorsal lamina of maxilla - (Lund et al., 1995; Lund, 2000; Poplin & Lund, 2000; Schultze & Cumbaa, 2001; Zhu & Schultze, 2001; Zhu et al., 2001; Zhu & Yu, 2002; Lund & Poplin, 2002; Cloutier & Arratia, 2004; Zhu et al., 2006; Friedman, 2007; Zhu et al., 2009; Zhu et al., 2013; Giles et al., 2015b,c; Giles et al., 2017; López-Arbarello & Sferco 2018; Argyriou et al., 2018; Latimer & Giles, 2018; Wilson et al., 2019; Figueroa et al., 2021.)

0 absent
1 present

69. Contribution by maxilla to posterior margin of cheek - (Friedman, 2007; Zhu et al., 2009; Zhu et al., 2013; Giles et al., 2015b,c; Giles et al., 2017; López-Arbarello & Sferco 2018; Argyriou et al., 2018; Latimer & Giles, 2018; Wilson et al., 2019; Figueroa et al., 2021.)

0 absent
1 present

70. Sensory canal/pit line associated with maxilla - (Grande & Bemis 1998; Friedman, 2007; Zhu et al., 2009; Zhu et al., 2013; Giles et al., 2015b; Giles et al., 2017; Argyriou et al., 2018; Latimer & Giles, 2018; Wilson et al., 2019; Figueroa et al., 2021.)

0 absent
1 present

71. Teeth on maxilla - (Poyato-Ariza & Wenz, 2002; Cloutier & Arratia, 2004; López-Arbarello 2012; Xu et al. 2014, 2015; Bermúdez-Rochas & Poyato-Ariza 2015; Poyato-Ariza 2015; Thies & Waschkewitz, 2015; Gibson 2016; Xu & Zhao, 2016; Giles et al., 2017; Cawley & Kriwet 2018; López-Arbarello & Sferco 2018; Argyriou et al., 2018; Latimer & Giles, 2018; Wilson et al., 2019; Figueroa et al., 2021.)

0 present
1 absent

72. Mobile maxilla in cheek - (Patterson 1973; Gardiner & Schaeffer 1989; Olsen & McCune 1991; Gardiner et al. 1996; Gardiner et al. 2005; Coates 1999; Hurley et al. 2007; Xu & Gao 2011; Poyato-Ariza 2015; Xu et al. 2014, 2015; Xu & Zhao, 2016; Giles et al., 2017; Argyriou et al., 2018; Latimer & Giles, 2018; Wilson et al., 2019; Figueroa et al., 2021.)
    0 absent
    1 present

73. Peg-like anterior process of maxilla - (Grande 2010; Xu & Wu 2012; Xu et al. 2014; Poyato-Ariza 2015; Giles et al., 2017; Argyriou et al., 2018; Latimer & Giles, 2018; Wilson et al., 2019; Figueroa et al., 2021.)
    0 absent
    1 present

74. Posterior maxillary notch - (Grande & Bemis 1998; Xu & Wu 2012; Xu et al. 2014, 2015. Arratia 2013; Xu & Zhao, 2016; Giles et al., 2017; López-Arbarello & Sferco 2018; Argyriou et al., 2018; Latimer & Giles, 2018; Wilson et al., 2019; Figueroa et al., 2021.)
    0 absent
    1 present

75. Supramaxilla - (Grande & Bemis 1998; Gardiner & Schaeffer 1989; Olsen & McCune 1991; Gardiner et al. 1996; Gardiner et al. 2005; Coates 1999; Hurley et al. 2007; Xu & Gao 2011; Xu et al. 2014, 2015; Bermúdez-Rochas & Poyato-Ariza 2015; Poyato-Ariza 2015; Xu & Shen, 2015; Thies & Waschkewitz, 2015; Gibson 2016; Xu & Zhao, 2016; Giles et al., 2017; López-Arbarello & Sferco 2018; Argyriou et al., 2018; Latimer & Giles, 2018; Wilson et al., 2019; Figueroa et al., 2021.)
    0 absent
    1 one
    2 two

76. Course of mandibular canal - (Friedman & Blom, 2006; Long et al., 2008; Swartz, 2009; Choo, 2011; Giles et al., 2015b; Giles et al., 2017; Argyriou et al., 2018; Latimer & Giles, 2018; Wilson et al., 2019; Figueroa et al., 2021.)
    0 traces ventral margin of jaw along entire length
    1 arches dorsally in anterior half of jaw

77. Mandibular canal reaches anterior margin of mandible - (Giles et al., 2015b,c; Giles et al., 2017; Argyriou et al., 2018; Latimer & Giles, 2018; Wilson et al., 2019; Figueroa et al., 2021.)
    0 present
    1 absent

78. Mandibular canal - (Patterson, 1982; Cloutier & Ahlberg, 1996; Coates, 1998; Schultze & Cumbaa, 2001; Zhu & Schultze, 2001; Zhu et al., 2001; Zhu & Yu, 2002; Cloutier & Arratia, 2004; Zhu et al., 2006; Friedman, 2007; Zhu et al., 2009; Choo, 2011; Zhu et al., 2013; Giles et al., 2015b; Giles et al., 2017; Argyriou et al., 2018; Latimer & Giles, 2018; Wilson et al., 2019; Figueroa et al., 2021.)
    0 primarily carried by infradentaries
    1 primarily carried by dentary

79. Relative length of dentary - (Ahlberg & Johanson, 1998; Zhu et al., 2001; Zhu & Yu, 2002; Zhu & Ahlberg, 2004; Friedman, 2007; Zhu et al., 2009; Giles et al., 2015b; Giles et al., 2017; Argyriou et al., 2018; Latimer & Giles, 2018; Wilson et al., 2019; Figueroa et al., 2021.)
    0 long (constitutes most of the length of the lower jaw)
    1 short (constitutes less than half of jaw length)

80. Teeth on dentary - (Cloutier & Arratia 2004, Xu et al. 2014; Giles et al., 2017; López-Arbarello & Sferco 2018; Argyriou et al., 2018; Latimer & Giles, 2018; Wilson et al., 2019; Figueroa et al., 2021.)
    0 present
    1 absent

81. Dentary with conspicuously reflexed distal tip - (Friedman & Blom, 2006; Long et al., 2008; Swartz, 2009; Choo, 2011; Giles et al., 2015b; Giles et al., 2017; Argyriou et al., 2018; Latimer & Giles, 2018; Wilson et al., 2019; Figueroa et al., 2021.)
    0 absent
    1 present

82. Enlarged series of parasymphysial teeth on dentary - (Friedman & Blom, 2006; Long et al., 2008; Swartz, 2009; Choo, 2011; Giles et al., 2017; Argyriou et al., 2018; Latimer & Giles, 2018; Wilson et al., 2019; Figueroa et al., 2021.)
    0 absent
    1 present

83. Facet for parasymphysial tooth-whorl on anterior dentary - (Choo, 2011; Giles et al., 2015b; Giles et al., 2017; Argyriou et al., 2018; Latimer & Giles, 2018; Wilson et al., 2019; Figueroa et al., 2021.)
    0 present
    1 absent

84. Teeth of outer dental arcade - (Friedman, 2007; Giles et al., 2015b; Poyato-Ariza 2015; Giles et al., 2017; López-Arbarello & Sferco 2018; Argyriou et al., 2018; Latimer & Giles, 2018; Wilson et al., 2019; Figueroa et al., 2021. Coates (1998) states that the maxilla of *Melanecta* bears large teeth interspersed with smaller teeth, but it is unclear how these teeth are arranged. As such, this taxon is coded '?'.)
    0 several rows of disorganized teeth
    1 two rows, with large teeth lingually and small teeth labially
    2 single row of teeth

85. Jaw margins overlain by lateral lamina - (Giles et al. 2017; Argyriou et al., 2018; Latimer & Giles, 2018; Wilson et al., 2019; Figueroa et al., 2021. In *Styracopterus*, *Fouldenia* and *Amphicentrum*, a lateral lamina of bone obscures the maxillary dentition (Sallan & Coates 2013).)
    0 absent
    1 present

86. Acrodin caps on teeth - (Patterson, 1982; Gardiner, 1984; Maisey, 1986; Gardiner & Schaeffer, 1989; Cloutier & Ahlberg, 1996; Taverne, 1997; Coates, 1999; Poplin & Lund, 2000; Schultze & Cumbaa, 2001; Zhu & Schultze, 2001; Zhu et al., 2001; Zhu & Yu, 2002; Cloutier & Arratia, 2004; Gardiner et al., 2005; Friedman & Blom, 2006; Zhu et al., 2006; Friedman, 2007; Long et al., 2008; Zhu et al., 2009; Friedman & Brazeau, 2010; Choo, 2011; Xu & Gao, 2011; Zhu et al.,

2013; Xu et al., 2014; Giles et al., 2015b,c; Giles et al., 2017; Argyriou et al., 2018; Latimer & Giles, 2018; Wilson et al., 2019; Figueroa et al., 2021.)

0 absent
1 present

87. Plicidentine - (Zhu & Yu 2002; Friedman 2007; López-Arbarello 2012; Bermúdez-Rochas & Poyato-Ariza 2015; Poyato-Ariza 2015; Thies & Waschkewitz, 2015; Gibson 2016; Giles et al., 2017; López-Arbarello & Sferco 2018; Argyriou et al., 2018; Latimer & Giles, 2018; Wilson et al., 2019; Figueroa et al., 2021.)

0 absent
1 present

88. Ossification of mentomeckelian region: - (Friedman & Blom, 2006; Long et al., 2008; Swartz, 2009; Grande 2010; Choo, 2011; Xu et al., 2014; Giles et al., 2015b; Poyato-Ariza 2015; Giles et al., 2017; Argyriou et al., 2018; Latimer & Giles, 2018; Wilson et al., 2019; Figueroa et al., 2021.)

0 present
1 absent

89. Number of infradentaries - (Friedman & Blom, 2006; Friedman, 2007; Long et al., 2008; Choo, 2011; Xu & Gao, 2011; Xu et al., 2014; Giles et al., 2015b; Poyato-Ariza 2015; Giles et al., 2017; López-Arbarello & Sferco 2018; Argyriou et al., 2018; Latimer & Giles, 2018; Wilson et al., 2019; Figueroa et al., 2021.)

0 more than two
1 two (angular and surangular)
2 one (angular only)

90. Coronoids (sensu stricto, excluding parasymphysial tooth whorl or anterior coronoid) - (Schultze and Cumbaa, 2001; Zhu and Schultze, 2001; Zhu et al., 2001; Zhu and Yu, 2002; Zhu et al., 2006; Friedman, 2007; Zhu et al., 2009; Giles et al., 2015b,c; Poyato-Ariza 2015; Giles et al., 2017; López-Arbarello & Sferco 2018; Argyriou et al., 2018; Latimer & Giles, 2018; Wilson et al., 2019; Figueroa et al., 2021.)

0 present
1 absent

91. Number of coronoids - (Ahlberg & Clack, 1998; Daeschler et al., 2006; Long et al., 2006; Friedman, 2007; Zhu et al., 2009; Zhu et al., 2013; Giles et al., 2015b; Giles et al., 2017; Argyriou et al., 2018; Latimer & Giles, 2018; Wilson et al., 2019; Figueroa et al., 2021. A single specimen of *Pteronisculus stensioi* has at least five or six coronoids anterior to the prearticular region. However, these appear to correspond to the three coronoids present in most specimens, so the taxon is coded here as '2'. Two coronoids are reported in *Boreosomus* (Nielsen, 1942).)

0 five
1 four or more
2 three
3 two
4 one

92. Posterior coronoid - (Cloutier & Ahlberg, 1996; Ahlberg & Johanson, 1998; Zhu & Ahlberg, 2004; Daeschler et al., 2006; Long et al., 2006; Giles et al., 2015b; Giles et al., 2017; Argyriou et al., 2018; Latimer & Giles, 2018; Wilson et al., 2019; Figueroa et al., 2021.)

0 morphologically similar to anterior coronoids
1 expanded

93. Coronoid process of lower jaw - (Patterson 1973; Gardiner & Schaeffer 1989; Olsen & McCune 1991; Poyato-Ariza & Wenz, 2002; Zhu & Yu, 2002; Friedman, 2007; Friedman, 2007; Xu & Gao 2011; Xu et al. 2014, 2015; Giles et al., 2015b; Poyato-Ariza 2015; Xu & Zhao, 2016; Giles et al., 2017; Cawley & Kriwet 2018; Cawley & Kriwet 2018; López-Arbarello & Sferco 2018; Argyriou et al., 2018; Latimer & Giles, 2018; Wilson et al., 2019; Figueroa et al., 2021.)
    0 absent
    1 present

94. Coronoid process contributed to by - (Modified from Patterson 1973; Olsen & McCune 1991; Gardiner et al. 2005; Poyato-Ariza 2015; Giles et al., 2017; López-Arbarello & Sferco 2018; Argyriou et al., 2018; Latimer & Giles, 2018; Wilson et al., 2019; Figueroa et al., 2021.)
    0 prearticular only
    1 surangular only
    2 dentary plus postdentary bones
    3 angular only

95. Leptolepid notch - (Arratia 2013; Giles et al., 2017; López-Arbarello & Sferco 2018; Argyriou et al., 2018; Latimer & Giles, 2018; Wilson et al., 2019; Figueroa et al., 2021. A distinct notch in the posterior margin of the dentary is seen in taxa such as *Leptolepis*.)
    0 absent
    1 present

96. Accessory hyoid element involvement in jaw joint - modified according to Argyriou et al. 2022 - (Grande & Bemis 1998; Olsen & McCune 1991; Grande 2010; Xu & Wu 2012; Xu et al. 2014, 2015; López-Arbarello 2012; Bermúdez-Rochas & Poyato-Ariza 2015; Poyato-Ariza 2015; Thies & Waschkewitz, 2015; Gibson 2016; Xu & Zhao, 2016; Giles et al., 2017; López-Arbarello & Sferco 2018; Argyriou et al., 2018; Latimer & Giles, 2018; Wilson et al., 2019; Figueroa et al., 2021.)
    0 absent
    1 present

97. Retroarticular process - (Friedman, 2007; Giles et al., 2015b; Giles et al., 2017; Argyriou et al., 2018; Latimer & Giles, 2018; Wilson et al., 2019; Figueroa et al., 2021.)
    0 present
    1 absent

98. Palatal bite - (Giles et al., 2017; Argyriou et al., 2018; Latimer & Giles, 2018; Wilson et al., 2019; Figueroa et al., 2021.)
    0 absent
    1 present

99. Palatal articulation with basipterygoid process - (Revised from Friedman, 2007; Brazeau, 2009; Zhu et al., 2009; Friedman & Brazeau, 2010; Davis et al., 2012; Zhu et al., 2013; Giles et al., 2015b,c; Giles et al., 2017; López-Arbarello & Sferco 2018; Argyriou et al., 2018; Latimer & Giles, 2018; Wilson et al., 2019; Figueroa et al., 2021. This character is expanded from previous formulations, which only considered whether a basipterygoid fenestra was absent or present. Where a basipterygoid process is absent, the dorsal margin of the palate may be flat, or the

metapterygoid may bear a distinct notch. This character was altered from Giles *et al.,* 2022 which made having a metapterygoid process and basipterygoid fenestra exclusive characters despite some taxa possessing both.).

0 articulation not obvious
1 via basipterygoid fenestra
2 via notch in palatoquadrate

100. Dorsal process in metapterygoid region of palatoquadrate (new character) – (Some taxa (e.g. *Pteronisculus*, *Raynerius*) have a dorsal process posterior to the basipterygoid fenestra/notch in the metapterygoid region of the palatoquadrate. Others lack any noticeable metapterygoid extension, e.g. *Cheirolepis*)

0 absent
1 present

101. Palatoquadrate ossifications - (Giles et al., 2017; Argyriou et al., 2018; Latimer & Giles, 2018; Wilson et al., 2019; Figueroa et al., 2021.)

0 comineralized
1 separate ossification centers

102. Lateral process of ectopterygoid - (Giles et al., 2017; Argyriou et al., 2018; Latimer & Giles, 2018; Wilson et al., 2019; Figueroa et al., 2021.)

0 absent
1 present

103. Palatoquadrate symphysis - (Giles et al., 2017; Argyriou et al., 2018; Latimer & Giles, 2018; Wilson et al., 2019; Figueroa et al., 2021. This character captures whether the palatoquadrates contact at the midline.)

0 absent
1 present

104. Dorsal margin of palate - (Giles et al., 2017; Argyriou et al., 2018; Latimer & Giles, 2018; Wilson et al., 2019; Figueroa et al., 2021.)

0 high posterior extension
1 flat dorsal margin

105. Metapterygoid posterior to quadrate - (Giles et al., 2017; Argyriou et al., 2018; Latimer & Giles, 2018; Wilson et al., 2019; Figueroa et al., 2021.)

0 absent
1 present

106. Number of dermopalatines - (Friedman, 2007; Giles et al., 2015b; Giles et al., 2017; Argyriou et al., 2018; Latimer & Giles, 2018; Wilson et al., 2019; Figueroa et al., 2021.)

0 multiple
1 single

107. Prearticular - (Poyato-Ariza 2015; Giles et al., 2017; López-Arbarello & Sferco 2018; Argyriou et al., 2018; Latimer & Giles, 2018; Wilson et al., 2019; Figueroa et al., 2021.)

0 present
1 absent

108. Vomers - (Patterson 1973; Olsen & McCune 1991; López-Arbarello 2012; Arratia 2013; Xu & Wu, 2012; Bermúdez-Rochas & Poyato-Ariza 2015; Poyato-Ariza 2015; Thies & Waschkewitz, 2015; Gibson 2016; Xu & Zhao, 2016; Giles et al., 2017; López-Arbarello & Sferco 2018; Argyriou et al., 2018; Latimer & Giles, 2018; Wilson et al., 2019; Figueroa et al., 2021.)

0 paired
1 single

109. Vomer sutured to parasphenoid - (Patterson 1973; Olsen & McCune 1991; Hurley et al. 2007; Giles et al., 2017; Argyriou et al., 2018; Latimer & Giles, 2018; Wilson et al., 2019; Figueroa et al., 2021.)

0 absent
1 present

110. Operculum - (Argyriou et al., 2018; Argyriou et al., 2022.).

0 absent
1 present

111. Posterior process of operculum

0 absent
1 present

112. Facet on the opercular for articulation with the opercular process of hyomandibular (new character).

0 absent
1 present

113. Accessory operculum - We here consider the antoperculum as an accessory operculum (Schultze & Cumbaa, 2001; Cloutier & Arratia, 2004; Friedman & Blom, 2006; Long et al., 2008; Swartz, 2009; Giles et al., 2015b; Giles et al., 2017; Argyriou et al., 2018; Latimer & Giles, 2018; Wilson et al., 2019; Figueroa et al., 2021. This region of the cheek was removed in *Coccocephalichthys* (Poplin, 1974; Poplin & Véran, 1996), presumably by Watson (1925) when he first described the specimen. It is unclear from the surviving cast whether a dermohyal and/or accessory operculum were present, and as such this taxon is coded as ?.)

0 absent
1 present

114. Operculum - relative size - (Modified from Lund et al., 1995; Lund, 2000; Lund & Poplin, 2002; Cloutier & Arratia, 2004; Long et al., 2008; Swartz, 2009; Choo, 2011; López-Arbarello 2012; Bermúdez-Rochas & Poyato-Ariza 2015; Xu et al., 2015; Giles et al., 2015b; Thies & Waschkewitz, 2015; Gibson 2016; Xu & Zhao, 2016; Giles et al., 2017; López-Arbarello & Sferco 2018; Argyriou et al., 2018; Latimer & Giles, 2018; Wilson et al., 2019; Figueroa et al., 2021.)

0 at least twice as high as subopercular
1 subequal
2 smaller than subopercular

115. Subopercle - (Poyato-Ariza & Wenz, 2002; Xu et al. 2014; Giles et al., 2017; Cawley & Kriwet 2018; Argyriou et al., 2018; Latimer & Giles, 2018; Wilson et al., 2019; Figueroa et al., 2021.)

0 present

1 absent

116. Anterodorsal process of suboperculum - (Long et al., 2008; Choo, 2011; López-Arbarello 2012; Bermúdez-Rochas & Poyato-Ariza 2015; Giles et al., 2015b; Thies & Waschkewitz, 2015; Poyato-Ariza 2015; Gibson 2016; Giles et al., 2017; López-Arbarello & Sferco 2018; Argyriou et al., 2018; Latimer & Giles, 2018; Wilson et al., 2019; Figueroa et al., 2021. An anterodorsal process is present some non-neopterygian actinopterygians and 'semionotiforms'. Although these processes do not appear to be homologous they are coded within the character.)
0 absent
1 present

117. Anteroventral process of suboperculum - (Giles et al., 2017; Argyriou et al., 2018; Latimer & Giles, 2018; Wilson et al., 2019; Figueroa et al., 2021.)
0 absent
1 present

118. Number of cheek bones bearing pre-opercular canal posterior to jugal - (Friedman, 2007; Zhu et al., 2009; Zhu et al., 2013; Giles et al., 2015b; Xu & Zhao, 2016; Giles et al., 2017; Argyriou et al., 2018; Latimer & Giles, 2018; Wilson et al., 2019; Figueroa et al., 2021.)
0 one
1 multiple
2 series of small ossicles

119. Preoperculum orientation - (Modified from Patterson 1973; Olsen & McCune 1991; Grande & Bemis 1998; Gardiner et al., 2005; Swartz 2009; López-Arbarello 2012; Bermúdez-Rochas & Poyato-Ariza 2015; Thies & Waschkewitz, 2015; Poyato-Ariza 2015; Gibson 2016; Giles et al., 2017; López-Arbarello & Sferco 2018; Argyriou et al., 2018; Latimer & Giles, 2018; Wilson et al., 2019; Figueroa et al., 2021. This character is reformulated from its original (compound) formulation, which considered both maxilla and preoperculum shape. Primitively in actinopterygians the preoperculum is wholly or partially developed dorsal to the maxilla as an anterodorsal-posteroventrally oriented bone, either with (e.g. *Mimipiscis, Moythomasia*) or without (e.g. *Cheirolepis*) a dorsoventrally oriented limb. The preoperculum may also be near-vertical, with no distinct anterodorsal or anteroventral extensions (e.g. *Boreosomus, Peltopleurus*), or developed as an anteroventral-posterodorsally-directed bone largely ventral to the maxilla (e.g. *Discoserra, Propterus*).)
0 prounounced dorsal limb
1 vertical
2 pronounced ventral limb

120. Junction between preopercular and more anterior cheek bones - (Modified from López-Arbarello 2012; Bermúdez-Rochas & Poyato-Ariza 2015; Poyato-Ariza 2015; Thies & Waschkewitz, 2015; Gibson 2016; Giles et al., 2017; López-Arbarello & Sferco 2018; Argyriou et al., 2018; Latimer & Giles, 2018; Wilson et al., 2019; Figueroa et al., 2021.)
0 Infraorbitals (including jugal) or suborbitals suture with or abut preopercular
1 Infraorbitals (including jugals) and suborbitals broadly overlap preopercular
2 completely obscure

121. Posterior border of preopeculum notched ventrally - (López-Arbarello 2012; Bermúdez-Rochas & Poyato-Ariza 2015; Giles et al., 2017; Thies & Waschkewitz, 2015; Gibson 2016;

López-Arbarello & Sferco 2018; Argyriou et al., 2018; Latimer & Giles, 2018; Wilson et al., 2019; Figueroa et al., 2021.)

0 absent
1 present

122. Interopercle - (Patterson 1973; Grande & Bemis 1998; Gardiner & Schaeffer 1989; Olsen & McCune 1991; Poyato-Ariza & Wenz, 2002; Xu & Gao 2011; Xu et al. 2014, 2015. Gardiner & Schaeffer 1989; Olsen & McCune 1991; Gardiner et al. 1996; Gardiner et al. 2005; Cavin & Suteethorn 2006; Hurley et al. 2007; López-Arbarello 2012; Bermúdez-Rochas & Poyato-Ariza 2015; Poyato-Ariza 2015; Thies & Waschkewitz, 2015; Gibson 2016; Xu & Zhao, 2016; Giles et al., 2017; Cawley & Kriwet 2018; López-Arbarello & Sferco 2018; Argyriou et al., 2018; Latimer & Giles, 2018; Wilson et al., 2019; Figueroa et al., 2021.)

0 absent
1 present

123. Branchiostegal rays - dorsal-most in series - (Lund et al., 1995; Cloutier & Arratia, 2004; Choo, 2011; Giles et al., 2015b; Giles et al., 2017; Argyriou et al., 2018; Latimer & Giles, 2018; Wilson et al., 2019; Figueroa et al., 2021.)

0 of similar depth to adjacent branchiostegal ray
1 deeper than adjacent branchiostegal ray

124. Lateral gulars - (Olsen & McCune 1991; Xu et al., 2014; Giles et al., 2017; Argyriou et al., 2018; Latimer & Giles, 2018; Wilson et al., 2019; Figueroa et al., 2021.)

0 present
1 absent

125. Lateral gulars - (Gardiner & Schaeffer, 1989; Cloutier & Ahlberg, 1996; Taverne, 1997; Lund & Poplin, 1997; Coates, 1999; Schultze & Cumbaa, 2001; Zhu & Schultze, 2001; Cloutier & Arratia, 2004; Friedman & Blom, 2006; Long et al., 2008; Swartz, 2009; Brazeau, 2009; Xu & Gao, 2011; Davis et al., 2012; Zhu et al., 2013; Xu et al., 2014; Giles et al., 2015b,c; Giles et al., 2017; Argyriou et al., 2018; Latimer & Giles, 2018; Wilson et al., 2019; Figueroa et al., 2021. The condition in *Boreosomus* (Nielsen, 1942) is unique: instead of lateral gulars flanking a median gular, there appears to be a second median gular. This may well represent a fusion of the two, longer lateral gulars, is coded as such.)

0 extending most of the length of the lower jaw
1 restricted to the anterior third of the lower jaw (no longer than the width of three branchiostegals)

126. Median gular - (Olsen & McCune 1991; Lund et al., 1995; Cloutier & Ahlberg, 1996; Coates, 1999; Lund, 2000; Schultze & Cumbaa, 2001; Zhu & Schultze, 2001; Zhu et al., 2001: Lund & Poplin, 2002; Zhu & Yu, 2002; Cloutier & Arratia, 2004; Zhu et al., 2006; Friedman, 2007; Zhu et al., 2009; Xu & Gao, 2011; López-Arbarello 2012; Zhu et al., 2013; Bermúdez-Rochas & Poyato-Ariza 2015; Poyato-Ariza 2015; Xu et al., 2014, 2015; Giles et al., 2015b,c; Thies & Waschkewitz, 2015; Xu & Zhao, 2015; Gibson 2016; Giles et al., 2017; López-Arbarello & Sferco 2018; Argyriou et al., 2018; Latimer & Giles, 2018; Wilson et al., 2019; Figueroa et al., 2021. Pearson & Westoll (1979: p. 365) state that a median gular is not known in *Cheirolepis canadensis*. Although a median gular is reconstructed by Cloutier & Arratia (1996: fig. 7), this bone is not present in any specimen photos and is not mentioned in the text. As such, this taxon is coded as ?.)

0 absent

1 present

127. Relative length of median gular - (Giles et al., 2015b,c; Giles et al., 2017; Argyriou et al., 2018; Latimer & Giles, 2018; Wilson et al., 2019; Figueroa et al., 2021. The condition in *Boreosomus* (Nielsen, 1942) is unique: instead of lateral gulars flanking a median gular, there appears to be a second median gular. This may well represent a fusion of the two, longer lateral gulars, and is coded as such.)

0 much shorter than jaw length
1 more than half of law length

128. Fenestra ventrolateralis - (Schultze & Cumbaa, 2001; Zhu & Schultze, 2001; Zhu et al., 2001; Zhu & Yu, 2002; Zhu et al., 2006; Friedman, 2007; Zhu et al., 2009; Zhu et al., 2013; Giles et al., 2015b; Giles et al., 2017; Argyriou et al., 2018; Latimer & Giles, 2018; Wilson et al., 2019; Figueroa et al., 2021.)

0 absent
1 present

129. Palatal opening surrounded by premaxilla, maxilla, dermopalatine and vomer (choana) - (Zhu & Yu, 2002; Friedman, 2007; Giles et al., 2015b; Giles et al., 2017; Argyriou et al., 2018; Latimer & Giles, 2018; Wilson et al., 2019; Figueroa et al., 2021. Character can only be coded in taxa which possess all of these bones.)

0 absent
1 present

130. Internasal cavity - (Ahlberg & Johanson, 1998; Zhu & Yu, 2002; Zhu & Ahlberg, 2004; Daeschler et al., 2006; Long et al., 2006; Friedman, 2007; Zhu et al., 2009; Zhu et al., 2013; Giles et al., 2015b,c; Giles et al., 2017; Argyriou et al., 2018; Latimer & Giles, 2018; Wilson et al., 2019; Figueroa et al., 2021.)

0 absent
1 present

131. Interorbital septum - (Friedman, 2007; Zhu et al., 2009; Brazeau, 2009; Friedman & Brazeau, 2010; Davis et al., 2012; Zhu et al., 2013; Giles et al., 2015b,c; Giles et al., 2017; Argyriou et al., 2018; Latimer & Giles, 2018; Wilson et al., 2019; Figueroa et al., 2021.)

0 broad
1 narrow

132. Optic foramen - (Giles et al., 2017; Argyriou et al., 2018; Latimer & Giles, 2018; Wilson et al., 2019; Figueroa et al., 2021. Primitively in actinopts, the optic nerve exits the cranial cavity into the orbit through paired foramina approximately halfway up the orbital wall. In many Carboniferous and younger taxa, much of the orbital wall is unossified (the optic fenestra). The optic nerves may exit through openings just posterior to (e.g. *Pteronisculus*) or confluent with (e.g. *Pholidophorus*) the optic fenestra. In polypterids and *Fukangichthys*, the optic nerve exits ventrally through paired foramina that abut the parasphenoid.)

0 dorsally positioned
1 ventrally positioned (i.e. abuts parasphenoid)

133. Pronounced median anterior crista on dorsal surface of braincase - (Giles et al., 2015b,c; Giles et al., 2017; Argyriou et al., 2018; Latimer & Giles, 2018; Wilson et al., 2019; Figueroa et al., 2021. Carboniferous and younger actinopts such as *Lawrenciella* (Hamel &

Poplin, 2008) have a median crista anterior to the anterior dorsal fontanelle upon which the skull roof sits.)

0 absent
1 present

134. Expanded anterior dorsal fontanelle - (Giles et al., 2015b,c; Giles et al., 2017; Argyriou et al., 2018; Latimer & Giles, 2018; Wilson et al., 2019; Figueroa et al., 2021. The anterior dorsal fontanelle of many Carboniferous and younger actinopts is greatly expanded, in contrast to the smaller fontanelle of Devonian taxa such as *Mimipiscis* (Gardiner, 1984).)

0 absent
1 present

135. Endoskeletal intracranial joint - (Cloutier & Ahlberg, 1996; Ahlberg & Johanson, 1998; Zhu & Ahlberg, 2004; Zhu et al., 2001; Zhu & Yu, 2002; Daeschler et al., 2006; Long et al., 2006; Friedman, 2007; Brazeau, 2009; Zhu et al., 2009; Friedman & Brazeau, 2010; Davis et al., 2013; Zhu et al., 2013; Giles et al., 2015b,c; Giles et al., 2017; Argyriou et al., 2018; Latimer & Giles, 2018; Wilson et al., 2019; Figueroa et al., 2021.)

0 absent
1 present

136. Eye stalk or unfinished area for similar structure - (Zhu & Schultze, 2001; Zhu et al., 2001; Zhu & Yu, 2002; Zhu et al., 2006; Friedman, 2007; Zhu et al., 2009; Zhu et al., 2013; Giles et al., 2015b,c; Giles et al., 2017; Argyriou et al., 2018; Latimer & Giles, 2018; Wilson et al., 2019; Figueroa et al., 2021. This character is coded as absent for taxa that possess a large interorbital fenestra (e.g. *Pteronisculus*, *Coccocephalichthys*, *Kentuckia deani*), as, if present, the eyestalk area would be visible posterior to the opening for the optic nerve.)

0 absent
1 present

137. Roof of posterior myodome perforated by palatine branch of facial nerve (VII) (Coates, 1999; Giles et al., 2015b; Giles et al., 2017; Argyriou et al., 2018; Latimer & Giles, 2018; Wilson et al., 2019; Figueroa et al., 2021.)

0 absent
1 present

138. Roof of posterior myodome perforated by the abducens nerve (VI)

0 present
1 absent

139. Foramen for abducens nerve (VI) dorsally positioned (level with optic foramen (II)) - (Coates, 1999; Giles et al., 2015b; Giles et al., 2017; Argyriou et al., 2018; Latimer & Giles, 2018; Wilson et al., 2019; Figueroa et al., 2021.)

0 absent
1 present

140. Anterodorsal myodome - (Patterson 1973; Olsen & McCune 1991; Coates, 1999; Gardiner et al. 1996; Hurley et al. 2007; Xu & Gao, 2011; Xu et al., 2014, 2015; Giles et al., 2015b; Poyato-Ariza 2015; Xu & Zhao, 2016; Giles et al., 2017; Argyriou et al., 2018; Latimer & Giles, 2018; Wilson et al., 2019; Figueroa et al., 2021.)

0 paired
1 single
2 absent

141. Posterior myodome - (Modified from Patterson 1973; Olsen & McCune 1991; Coates, 1999; Xu et al., 2014. Wiley 1976; Gardiner, 1984; Gardiner & Schaeffer, 1989; Gardiner et al. 1996; Hurley et al. 2007; López-Arbarello 2012; Xu & Gao, 2011; Bermúdez-Rochas & Poyato-Ariza 2015; Xu et al. 2014, 2015; Giles et al., 2015b; Thies & Waschkewitz, 2015; Gibson 2016; Xu & Zhao, 2016; Giles et al., 2017; López-Arbarello & Sferco 2018; Argyriou et al., 2018; Latimer & Giles, 2018; Wilson et al., 2019; Figueroa et al., 2021.)
0 absent
1 paired
2 median

142. Basicranial fenestra - (Ahlberg & Johanson, 1998; Zhu et al., 2001; Zhu & Yu, 2002; Zhu & Ahlberg, 2004; Friedman, 2007; Zhu et al., 2009; Zhu et al., 2013; Giles et al., 2015b,c; Giles et al., 2017; Argyriou et al., 2018; Latimer & Giles, 2018; Wilson et al., 2019; Figueroa et al., 2021.)
0 absent
1 present

143. Endoskeletal spiracular canal - (Modified from Patterson, 1982; Gardiner, 1984; Gardiner & Schaeffer, 1989; Taverne, 1997; Coates, 1999; Gardiner et al., 2005; Xu & Gao, 2011; Xu et al., 2014; Giles et al., 2015b; Giles et al., 2017; López-Arbarello & Sferco 2018; Argyriou et al., 2018; Latimer & Giles, 2018; Wilson et al., 2019; Figueroa et al., 2021. Taxa that lack a groove on the lateral commissure are coded as inapplicable for this character.))
0 open
1 partial closure of spiracular bar
2 complete enclosure in canal

144. Basipterygoid process - (Gardiner et al., 2005; Xu & Gao, 2011; Xu et al., 2014, 2015; Giles et al., 2015b; Xu & Zhao, 2016; Giles et al., 2017; López-Arbarello & Sferco 2018; Argyriou et al., 2018; Latimer & Giles, 2018; Wilson et al., 2019; Figueroa et al., 2021.)
0 present
1 absent

145. Basipterygoid process with vertically oriented component - (Ahlberg & Johanson, 1998; Zhu & Schultze, 2001; Zhu et al., 2001; Zhu & Yu, 2002; Zhu & Ahlberg, 2004; Zhu et al., 2006; Friedman, 2007; Zhu et al., 2009; Davis et al., 2012; Zhu et al., 2013; Giles et al., 2015b,c; Giles et al., 2017; Argyriou et al., 2018; Latimer & Giles, 2018; Wilson et al., 2019; Figueroa et al., 2021.)
0 absent
1 present

146. Dermal component to basipterygoid process - (Gardiner, 1984; Gardiner & Schaeffer, 1989; Taverne, 1997; Coates, 1999; Giles et al., 2015b; Giles et al., 2017; Argyriou et al., 2018; Latimer & Giles, 2018; Wilson et al., 2019; Figueroa et al., 2021.)
0 absent
1 present

147. Hyoid facet - (Gardiner et al. 2005; Gardiner et al. 1996; Hurley et al. 2007; Xu & Gao 2011; Xu et al. 2015; Giles et al., 2017; López-Arbarello & Sferco 2018; Argyriou et al., 2018; Latimer & Giles, 2018; Wilson et al., 2019; Figueroa et al., 2021.)

0 directed posteroventrally
1 horizontal

148. Fossa bridgei - (Gardiner, 1984; Gardiner & Schaeffer, 1989; Taverne, 1997; Coates, 1999; Xu & Gao, 2011; Xu et al., 2014; Giles et al., 2015b; Giles et al., 2017; Argyriou et al., 2018; Latimer & Giles, 2018; Wilson et al., 2019; Figueroa et al., 2021.)

0 absent
1 present

149. Posttemporal fossae - (Zhu & Yu, 2002; Friedman, 2007; Argyriou et al., 2018; Latimer & Giles, 2018; Wilson et al., 2019; Figueroa et al., 2021.)

0 absent
1 present

150. Vestibular fontanelle - (Friedman, 2007; Brazeau, 2009; Zhu et al., 2009; Friedman & Brazeau, 2010; Davis et al., 2012; Zhu et al., 2013; Brazeau & Friedman, 2014; Giles et al., 2015b,c; Giles et al., 2017; Argyriou et al., 2018; Latimer & Giles, 2018; Wilson et al., 2019; Figueroa et al., 2021.)

0 absent
1 present

151. Ventral cranial fissure and vestibular fontanelle - (Coates, 1999; Giles et al., 2015b; Giles et al., 2017; Argyriou et al., 2018; Latimer & Giles, 2018; Wilson et al., 2019; Figueroa et al., 2021. We follow Coates (1999) in coding *Howqualepis* as '0' on the basis of Long 1988 fig. 16 and AMF65495 (pers. obs. S.G.), rather than the braincase reconstruction (Long, 1988: fig. 18.)

0 separated by bridge of bone
1 conflUent

152. Accessory fenestration in otic capsule - (Friedman, 2007; Zhu et al., 2009; Giles et al., 2015b; Giles et al., 2017; Argyriou et al., 2018; Latimer & Giles, 2018; Wilson et al., 2019; Figueroa et al., 2021.)

0 absent
1 present

153. Otoccipital fissure - (Friedman, 2007; Brazeau, 2009; Davis et al., 2012; Zhu et al., 2013; Giles et al., 2015b,c; Giles et al., 2017; Argyriou et al., 2018; Latimer & Giles, 2018; Wilson et al., 2019; Figueroa et al., 2021.)

0 absent
1 present

154. Median projection overhanging posterior part of posterior dorsal fontanelle - (Giles et al., 2015b; Giles et al., 2017; Argyriou et al., 2018; Latimer & Giles, 2018; Wilson et al., 2019; Figueroa et al., 2021. Variable in *Boreosomus*: the posterior dorsal fontanelle is closed in the specimen figured in Nielsen (1942: plate 25F), but developed in the specimen figured in plate 28. This taxon is coded ?0/1? to reflect this polymorphism.)

0 absent

1 present

155. Median projection overhanging anterior part of posterior dorsal fontanelle - (Giles et al., 2015b; Giles et al., 2017; Argyriou et al., 2018; Latimer & Giles, 2018; Wilson et al., 2019; Figueroa et al., 2021. This projection is somewhat reduced in *Pteronisculus* (Nielsen, 1942), but is coded '1' here. Variable in *Boreosomus*: the posterior dorsal fontanelle is closed in the specimen figured in Nielsen 1942 plate 25F, but developed in the specimen figured in plate 28. This taxon is coded ?0/1? to reflect this polymorphism. *Cheirolepis trailli* is coded '0' (2015a).)

0 absent
1 present

156. Dorsal aorta - (Coates & Sequeira, 1998; Coates & Sequeira, 2001a, b; Coates, 1999; Friedman, 2007; Zhu et al., 2009; Friedman & Brazeau, 2010; Zhu et al., 2013; Giles et al., 2015b,c; Giles et al., 2017; López-Arbarello & Sferco 2018; Argyriou et al., 2018; Latimer & Giles, 2018; Wilson et al., 2019; Figueroa et al., 2021. This character is coded as inapplicable in taxa that lack a canal for the dorsal aorta. *Cheirolepis trailli* is coded '0' (Giles et al., 2015a). The aortic canal of *Moythomasia* is not figured by Gardiner (1984), but a clear posterior notch in the aortic canal can be seen in Long & Trinajstic (2010:fig 5b). The neurocranium of *Gogosardina* is not yet described, but this character can be coded on the basis of Choo et al. (2009: fig. 9).)

0 open in groove
1 canal notched posteriorly
2 completely enclosed in canal

157. Dorsal aorta pierced by canal/s for exit of eff.a.2 - (Giles et al., 2015b; Giles et al., 2017; Argyriou et al., 2018; Latimer & Giles, 2018; Wilson et al., 2019; Figueroa et al., 2021. In *Mimipiscis bartrami* and *M. toombsi*, a groove for one of the efferent branchial arteries branches off from the lateral dorsal aorta immediately before the articular area for the first infrapharyngobranchial. However, it is uncertain which, so both taxa coded as '?' for these characters. The neurocranium of *Gogosardina* is not yet described, but this character can be coded on the basis of Choo et al. (2009: fig. 9).)

0 absent
1 present

158. Dorsal aorta pierced by canal/s for exit of eff.a.1 - (Giles et al., 2015b; Giles et al., 2017; Argyriou et al., 2018; Latimer & Giles, 2018; Wilson et al., 2019; Figueroa et al., 2021. In *Mimipiscis bartrami* and *M. toombsi*, a groove for one of the efferent branchial arteries branches off from the lateral dorsal aorta immediately before the articular area for the first infrapharyngobranchial. However, it is uncertain which, so both taxa coded as '?' for these characters. The neurocranium of *Gogosardina* is not yet described, but this character can be coded on the basis of Choo et al. (2009: fig. 9).)

0 absent
1 present

159. Bifurcation of dorsal aorta - (Coates & Sequeira, 1998; Coates & Sequeira, 2001a, b; Coates, 1999; Friedman, 2007; Zhu et al., 2009; Friedman & Brazeau, 2010; Zhu et al., 2013; Giles et al., 2015b,c; Giles et al., 2017; Argyriou et al., 2018; Latimer & Giles, 2018; Wilson et al., 2019; Figueroa et al., 2021.)

0 posterior to occiput
1 anterior to occiput

160. Birfurcation of dorsal aorta into lateral dorsal aortae - (Coates, 1999; Giles et al., 2015b; Giles et al., 2017; Argyriou et al., 2018; Latimer & Giles, 2018; Wilson et al., 2019; Figueroa et al., 2021. This character is coded as inapplicable in taxa that lack a canal for the dorsal aorta. In *Mimipiscis toombsi*, the bifurcation point of the dorsal aorta can be open (Giles & Friedman, 2014: fig. 2) or closed (Gardiner 1984: fig. 15). This taxon is coded '0/1' to reflect this polymorphism. The aortic canal of *Moythomasia* is not figured by Gardiner (1984), but the bifucation into the lateral dorsal aortae can be seen in Long & Trinajstic (2010:fig 5b).) State 2 was added following Argyriou et al. (2018; 2022).

0 open
1 enclosed in canal

161. Braincase ossifications differentiated - (Giles et al., 2017; Argyriou et al., 2018; Latimer & Giles, 2018; Wilson et al., 2019; Figueroa et al., 2021.)

0 absent
1 present

162. Basisphenoid - (Wiley 1976; López-Arbarello 2012; Bermúdez-Rochas & Poyato-Ariza 2015; Thies & Waschkewitz, 2015; Gibson 2016; Giles et al., 2017; López-Arbarello & Sferco 2018; Argyriou et al., 2018; Latimer & Giles, 2018; Wilson et al., 2019; Figueroa et al., 2021.)

0 present
1 absent or very reduced

163. Opisthotic-pterotic relationship - (Gardiner et al. 1996; Hurley et al. 2007; Giles et al., 2017; Argyriou et al., 2018; Latimer & Giles, 2018; Wilson et al., 2019; Figueroa et al., 2021. This character can only be coded when separate braincase ossifications can be identified.)

0 opisthotic larger than subotic
1 opisthotic and pterotic equal in size

164. Epioccipital - (Hurley et al. 2007; Giles et al., 2017; Argyriou et al., 2018; Latimer & Giles, 2018; Wilson et al., 2019; Figueroa et al., 2021. This character can only be coded when separate braincase ossifications can be identified.)

0 present
1 absent

165. Forward extension of the exoccipital around the vagus nerve - (Olsen & McCune 1991; Gardiner et al. 1996; Cavin & Suteethorn 2006; Hurley et al. 2007; López-Arbarello 2012; Bermúdez-Rochas & Poyato-Ariza 2015; Thies & Waschkewitz, 2015; Gibson 2016; Giles et al. 2017; López-Arbarello & Sferco 2018; Argyriou et al., 2018; Latimer & Giles, 2018; Wilson et al., 2019; Figueroa et al., 2021. This character can only be coded when separate braincase ossifications can be identified.)

0 absent
1 present

166. Spenotic with small dermal component - (Grande 2010; López-Arbarello 2012; Xu & Wu 2012; Xu et al. 2014, 2015; Arratia 2013; Bermúdez-Rochas & Poyato-Ariza 2015; Poyato-Ariza 2015; Thies & Waschkewitz, 2015; Gibson 2016; Xu & Zhao, 2016; Giles et al. 2017; López-Arbarello & Sferco 2018; Argyriou et al., 2018; Latimer & Giles, 2018; Wilson et al., 2019; Figueroa et al., 2021. This character can only be coded when separate braincase ossifications can be identified.)

0 absent
1 present

167. Pterotic - (Gardiner et al. 1996; Grande & Bemis, 1998; Hurley et al. 2007; Xu et al. 2014; Poyato-Ariza 2015; Xu & Shen, 2015; Xu & Zhao, 2016; Giles et al. 2017; López-Arbarello & Sferco 2018; Argyriou et al., 2018; Latimer & Giles, 2018; Wilson et al., 2019; Figueroa et al., 2021. This character can only be coded when separate braincase ossifications can be identified.)
0 present
1 absent

168. Opisthotic bone - (Wiley 1976; Olsen & McCune 1991; Grande & Bemis 1998; Cavin & Suteethorn 2006; Hurley et al. 2007; Grande 2010; López-Arbarello 2012; Bermúdez-Rochas & Poyato-Ariza 2015; Poyato-Ariza 2015; Thies & Waschkewitz, 2015; Xu et al., 2014, 2015; Gibson 2016; Xu & Zhao, 2016; Giles et al. 2017; López-Arbarello & Sferco 2018; Argyriou et al., 2018; Latimer & Giles, 2018; Wilson et al., 2019; Figueroa et al., 2021. This character can only be coded when separate braincase ossifications can be identified.)
0 present
1 absent

169. Intercalar - (Olsen & McCune 1991; Olsen 1994; Gardiner et al. 1996; López-Arbarello 2012; Xu et al. 2014; Poyato-Ariza 2015; Xu & Shen, 2015; Thies & Waschkewitz, 2015; Gibson 2016; Xu & Zhao, 2016; Giles et al. 2017; López-Arbarello & Sferco 2018; Argyriou et al., 2018; Latimer & Giles, 2018; Wilson et al., 2019; Figueroa et al., 2021. This character can only be coded when separate braincase ossifications can be identified.)
0 present
1 absent

170. Occipital region ossification pattern (Argyriou et al. 2018, 2022).
0 basioccipital and exoccipitals as separate ossifications
1 comineralized

171. Supraoccipital bone - (Grande 2010; Poyato-Ariza 2015; Xu et al. 2014, 2015; Xu & Zhao, 2016; Giles et al. 2017; López-Arbarello & Sferco 2018; Argyriou et al., 2018; Latimer & Giles, 2018; Wilson et al., 2019; Figueroa et al., 2021. This character can only be coded when separate braincase ossifications can be identified.)
0 absent
1 present

172. Membranous outgrowth of intercalar - (Patterson 1973; Olsen & McCune 1991; Gardiner et al. 1996; Hurley et al. 2007; Giles et al. 2017; López-Arbarello & Sferco 2018; Argyriou et al., 2018; Latimer & Giles, 2018; Wilson et al., 2019; Figueroa et al., 2021. This character can only be coded when separate braincase ossifications can be identified.)
0 absent
1 present

173. Post-temporal fossa - (Patterson 1973; Gardiner, 1984; Gardiner & Schaeffer, 1989; Olsen & McCune 1991; Coates, 1999; Hurley et al. 2007; López-Arbarello 2012; Xu & Gao, 2011; Xu et al. 2014, 2015; Bermúdez-Rochas & Poyato-Ariza 2015; Giles et al., 2015b; Poyato-

Ariza 2015; Thies & Waschkewitz, 2015; Gibson 2016; Xu & Zhao, 2016; Giles et al. 2017; Argyriou et al., 2018; Latimer & Giles, 2018; Wilson et al., 2019; Figueroa et al., 2021.)

0 absent
1 present

174. Sub-temporal fossa - (Gardiner, 1984; Gardiner & Schaeffer, 1989; Gardiner et al. 1996; Hurley et al. 2007; Xu & Gao, 2011; Xu et al. 2014, 2015; Xu & Zhao, 2016; Argyriou et al., 2018; Latimer & Giles, 2018; Wilson et al., 2019; Figueroa et al., 2021.)

0 absent
1 present

175. Dilatator fossa - (Gardiner, 1984; Gardiner & Schaeffer, 1989; Coates, 1999; Gardiner et al. 1996; Hurley et al. 2007; Xu & Gao, 2011; Xu et al. 2014, 2015; Xu & Zhao, 2016; Giles et al. 2017; Argyriou et al., 2018; Latimer & Giles, 2018; Wilson et al., 2019; Figueroa et al., 2021.)

0 absent
1 present

176. Parasphenoid - (Gardiner, 1984; Brazeau, 2009; Davis et al., 2012; Zhu et al., 2013; Giles et al., 2015b,c; Giles et al. 2017; Argyriou et al., 2018; Latimer & Giles, 2018; Wilson et al., 2019; Figueroa et al., 2021.)

0 absent
1 present

177. Parasphenoid - (Coates, 1999; Zhu & Yu, 2002; Gardiner et al., 2005; Friedman, 2007, Xu & Gao, 2011; Xu et al., 2014, 2015; Giles et al., 2015b; Xu & Zhao, 2016; Giles et al. 2017; López-Arbarello & Sferco 2018; Argyriou et al., 2018; Latimer & Giles, 2018; Wilson et al., 2019; Figueroa et al., 2021.)

0 terminates at/anterior to ventral otic fissure
1 extends across ventral otic fissure
2 extends to basioccipital

178. Ascending process of the parasphenoid - (Patterson, 1982; Coates, 1999; Dietze, 2000; Schultze & Cumbaa, 2001; Zhu & Schultze, 2001; Cloutier & Arratia, 2004; Gardiner et al., 2005; Friedman & Blom, 2006; Zhu et al., 2006; Zhu et al., 2009; Choo, 2011; Xu & Gao, 2011; Zhu et al., 2013; Xu et al., 2014; Giles et al., 2015b,c; Giles et al. 2017; López-Arbarello & Sferco 2018; Argyriou et al., 2018; Latimer & Giles, 2018; Wilson et al., 2019; Figueroa et al., 2021.)

0 absent
1 present

179. Parasphenoid with multifid anterior margin - (Friedman & Blom, 2006; Friedman, 2007; Zhu et al., 2009; Choo, 2011; Zhu et al., 2013; Giles et al., 2015b,c; Giles et al. 2017; Argyriou et al., 2018; Latimer & Giles, 2018; Wilson et al., 2019; Figueroa et al., 2021.)

0 absent
1 present

180. Buccohypophyseal canal pierces parasphenoid - (Giles et al., 2015b,c; Giles et al. 2017; Argyriou et al., 2018; Latimer & Giles, 2018; Wilson et al., 2019; Figueroa et al., 2021. The buccohypophyseal canal typically enters the dorsal surface of the parasphenoid, but

whether it exits via the ventral surface is more variable, and this distribution is captured by this character.)

0 present
1 absent

181. Parasphenoid teeth - (Arratia 2013; Giles et al. 2017; López-Arbarello & Sferco 2018; Argyriou et al., 2018; Latimer & Giles, 2018; Wilson et al., 2019; Figueroa et al., 2021.)

0 small
1 large
2 absent

182. Parasphenoid pierced by ascending common carotids (Argyriou et al. 2018, 2022).

0 absent
1 present

183. Parasphenoid pierced by internal carotid artery - (Gardiner et al. 1996; Hurley et al. 2007; Xu & Wu, 2012; Xu et al., 2015; Xu & Zhao, 2016; Giles et al. 2017; Argyriou et al., 2018; Latimer & Giles, 2018; Wilson et al., 2019; Figueroa et al., 2021.)

0 absent
1 present

184. Parasphenoid pierced by efferent pseudobranchial artery - (Gardiner et al. 1996; Hurley et al. 2007; Xu & Wu, 2012; Xu et al., 2015; Xu & Zhao, 2016; Giles et al. 2017; Argyriou et al., 2018; Latimer & Giles, 2018; Wilson et al., 2019; Figueroa et al., 2021.)

0 absent
1 present

185. Aortic notch in parasphenoid - (Modified from Gardiner et al. 2005; Giles et al. 2017; Argyriou et al., 2018; Latimer & Giles, 2018; Wilson et al., 2019; Figueroa et al., 2021.)

0 absent
1 present

186. Parabasal canal - (Xu and Gao 2011; Xu et al. 2014; Giles et al. 2017; Argyriou et al., 2018; Latimer & Giles, 2018; Wilson et al., 2019; Figueroa et al., 2021.)

0 present
1 absent

187. Anterolaterally divergent olfactory tracts - (Coates, 1999; Giles & Friedman, 2014; Giles et al., 2015b; Giles et al. 2017; Argyriou et al., 2018; Latimer & Giles, 2018; Wilson et al., 2019; Figueroa et al., 2021.)

0 absent
1 present

188. Elongate olfactory tract(s) - (Brazeau, 2009; Friedman & Brazeau 2010; Davis et al., 2012; Zhu et al., 2013; Brazeau & Friedman, 2014; Giles & Friedman, 2014; Giles et al., 2015b,c; Giles et al. 2017; Argyriou et al., 2018; Latimer & Giles, 2018; Wilson et al., 2019; Figueroa et al., 2021. The olfactory tracts of *Osorioichthys* are elongate (pers. obs. unpubl. scan data S.G.).)

0 absent

1 present

189. Olfactory nerves carried in a single tract - (Coates, 1999; Giles & Friedman, 2014; Giles et al., 2015b; Giles et al. 2017; Argyriou et al., 2018; Latimer & Giles, 2018; Wilson et al., 2019; Figueroa et al., 2021. The olfactory nerves are carried in separate tracts in *Osorioichthys* (pers. obs. unpubl. scan data S.G.).)
0 present
1 absent

190. Hypophyseal chamber - (Coates, 1999; Xu & Gao, 2011; Xu et al., 2014; Giles et al., 2015b; Giles et al. 2017; Argyriou et al., 2018; Latimer & Giles, 2018; Wilson et al., 2019; Figueroa et al., 2021.)
0 projects posteroventrally
1 projects ventrally or anteroventrally

191. Optic lobes - (Giles & Friedman, 2014; Giles et al., 2015b; Giles et al. 2017; Argyriou et al., 2018; Latimer & Giles, 2018; Wilson et al., 2019; Figueroa et al., 2021.)
0 narrower than cerebellum
1 same width or wider than cerebellum

192. Optic lobes - (Coates 1999; Hurley et al. 2007; Xu et al. 2014; Giles et al. 2017; Argyriou et al., 2018; Latimer & Giles, 2018; Wilson et al., 2019; Figueroa et al., 2021.)
0 smaller than telencephalon
1 larger than telencephalon

193. Optic tectum divided into bilateral halves - (Coates, 1999; Giles et al., 2015b; Giles et al. 2017; Argyriou et al., 2018; Latimer & Giles, 2018; Wilson et al., 2019; Figueroa et al., 2021.)
0 absent
1 present

194. Cerebellar corpus - (Giles et al., 2015b,c; Giles et al. 2017; Argyriou et al., 2018; Latimer & Giles, 2018; Wilson et al., 2019; Figueroa et al., 2021. The region posterior to the cerebellar auricles in *Lawrenciella* was considered to be the area octavolateralis by Hamel & Poplin (2005). However, we interpret it as the corpus cerebellum, and this taxon is coded '1'.)
0 absent
1 present

195. Cerebellar corpus - (Coates 1999; Hurley et al. 2007; Xu & Gao 2011; Xu et al. 2014; Giles et al. 2017; Argyriou et al., 2018; Latimer & Giles, 2018; Wilson et al., 2019; Figueroa et al., 2021.)
0 divided bilaterally
1 undivided

196. Position of cerebellar corpus - (Coates 1999; Hurley et al. 2007; Xu & Gao 2011; Xu et al. 2014; Giles et al. 2017; Argyriou et al., 2018; Latimer & Giles, 2018; Wilson et al., 2019; Figueroa et al., 2021.)
0 enters fourth ventricle
1 arches above fourth ventricle

197. Cerebellar corpus with median anteriorly projecting portion - (Coates 1999; Hurley et al. 2007; Xu & Gao 2011; Xu et al. 2014; Giles et al. 2017; Argyriou et al., 2018; Latimer & Giles, 2018; Wilson et al., 2019; Figueroa et al., 2021.)

0 absent
1 present

198. Horizontal semicircular canal - (Davis et al., 2012; Zhu et al., 2013; Giles & Friedman, 2014; Giles et al., 2015b,c; Giles et al. 2017; Argyriou et al., 2018; Latimer & Giles, 2018; Wilson et al., 2019; Figueroa et al., 2021.)

0 joins vestibular region dorsal to ampulla for the posterior semicircular canal
1 joins vestibular region level with ampulla for the posterior semicircular canal

199. Junction between ampulla of posterior semicircular canal and cranial cavity - (Giles et al., 2015b,c; Giles et al. 2017; Argyriou et al., 2018; Latimer & Giles, 2018; Wilson et al., 2019; Figueroa et al., 2021. In certain stem actinopterygians, such as *Mimipiscis* (Giles and Friedman, 2014), a short length of canal lies between the posterior ampulla and the remainder of the labyrinth.)

0 separated by short length of canal
1 confluent

200. Crus commune of anterior and posterior semicircular canal - (Giles & Friedman, 2014; Giles et al., 2015b; Giles et al. 2017; Argyriou et al., 2018; Latimer & Giles, 2018; Wilson et al., 2019; Figueroa et al., 2021.)

0 dorsal to endocranial roof
1 ventral to endocranial roof

201. Lateral cranial canal - (Gardiner, 1984; Gardiner & Schaeffer, 1989; Coates, 1999; Cloutier & Arratia, 2004; Gardiner et al., 2005; Zhu et al., 2006; Zhu et al., 2009; Zhu et al., 2013; Giles & Friedman, 2014; Xu et al., 2014; Giles et al., 2015b,c; Giles et al. 2017; Argyriou et al., 2018; Latimer & Giles, 2018; Wilson et al., 2019; Figueroa et al., 2021. The presence of a lateral cranial canal in *Ligulalepis* and *Psarolepis* is uncertain, but its presence in *Meemannia* is confirmed following Lu et al. (2016). *Erpetoichthys* is conservatively coded as '?'.)

0 absent
1 present

202. Lateral cranial canal connects to cranial cavity anteriorly - (Giles et al. 2017; Argyriou et al., 2018; Latimer & Giles, 2018; Wilson et al., 2019; Figueroa et al., 2021.)

0 absent
1 present

203. Enameloid on dermal bones and scales - (Giles et al., 2015b,c, 2017; Argyriou et al., 2018; Latimer & Giles, 2018; Wilson et al., 2019; Figueroa et al., 2021: Characters 147-150 form part of an atomisation of the compound characters 'ganoine' (typically defined as a single or multilayer enamel covering) and 'cosmine' (typically defined as a single layer of enamel with a well-defined pore canal network) (e.g. Cloutier & Ahlberg, 1996; Ahlberg & Johanson, 1998; Zhu & Ahlberg, 2004; Schultze & Cumbaa, 2001; Zhu & Schultze, 2001; Zhu et al., 2001; Zhu & Yu, 2002; Daeschler et al., 2006; Long et al., 2006; Zhu et al., 2006; Zhu et al., 2009; Davis et al., 2012; Zhu et al., 2013). A similar approach to atomization was taken by Friedman (2007), Brazeau & Friedman (2010) and Giles et al. (2015b). As detailed histological investigations have not been carried out for the majority of early actinopterygians (rather, they have simply been

described as being covered in/bearing ridges of ganoine), many of these characters cannot be coded for a number of taxa.)

0 absent
1 present

204. Extensive pore-canal network - (See notes above for c. 196.)

0 absent
1 present

205. Enamel - (See notes above for c. 196.)

0 single-layered
1 multi-layered

206. Enamel layers - (See notes above for c. 196.)

0 applied directly to one another
1 separated by layers of dentine

207. Scales on body - (Giles et al. 2017; Argyriou et al., 2018; Latimer & Giles, 2018; Wilson et al., 2019; Figueroa et al., 2021.)

0 present
1 absent

208. Scales - (Cloutier & Arratia, 2004; Friedman & Blom, 2006; Long et al., 2008; Swartz, 2009; Zhu et al., 2009; Choo, 2011; Giles et al., 2015b; Giles et al. 2017; Argyriou et al., 2018; Latimer & Giles, 2018; Wilson et al., 2019; Figueroa et al., 2021.)

0 micromeric
1 macromeric

209. Scales with 'peg and socket articulation' - (Maisey, 1986; Gardiner & Schaeffer, 1989; Cloutier & Ahlberg, 1996; Coates, 1999; Dietze, 2000; Poplin & Lund, 2000; Schultze & Cumbaa, 2001; Cloutier & Arratia, 2004; Friedman & Blom, 2006; Friedman, 2007; Long et al., 2008; Brazeau, 2009; Swartz, 2009; Zhu et al., 2009; Friedman & Brazeau, 2010; López-Arbarello 2012; Xu & Gao, 2011; Choo, 2011; Davis et al., 2012; Zhu et al., 2013; Xu et al., 2014; Giles et al., 2015b,c; Xu & Zhao, 2016; Giles et al. 2017; López-Arbarello & Sferco 2018; Argyriou et al., 2018; Latimer & Giles, 2018; Wilson et al., 2019; Figueroa et al., 2021. This character is coded only for taxa that possess rhombic scales.)

0 absent
1 present

210. Peg on rhomboid scale - (Patterson, 1982; Cloutier & Ahlberg, 1996; Dietze, 2000; Schultze & Cumbaa, 2001; Zhu & Schultze, 2001; Zhu et al., 2001: Zhu & Yu, 2002; Cloutier & Arratia, 2004; Friedman & Blom, 2006; Zhu et al., 2006; Friedman, 2007; Zhu et al., 2009; Giles et al. 2017; Argyriou et al., 2018; Latimer & Giles, 2018; Wilson et al., 2019; Figueroa et al., 2021. Although peg-and-socket articulation of is present between the scales of *Limnomis* (Daeschler, 2000), the nature of the peg is not described. As such, this taxon is conservatively coded '?'.)

0 narrow
1 broad

211. Anterodorsal process on scale - (Patterson, 1982; Gardiner, 1984; Gardiner & Schaeffer, 1989; Schultze & Cumbaa, 2001; Zhu & Schultze, 2001; Zhu et al., 2001; Zhu & Yu, 2002; Cloutier & Arratia, 2004; Friedman & Blom, 2006; Zhu et al., 2006; Friedman, 2007; Long et al., 2008; Swartz, 2009; Zhu et al., 2009; Choo, 2011; Zhu et al., 2013; Giles et al., 2015b,c; Giles et al. 2017; Argyriou et al., 2018; Latimer & Giles, 2018; Wilson et al., 2019; Figueroa et al., 2021.)

0 absent
1 present

212. Scales with well developed pores on surface - (Friedman & Blom 2006; Long et al., 2008; Swartz, 2009; Choo, 2011; Xu et al., 2014; Giles et al., 2015b; Giles et al. 2017; Argyriou et al., 2018; Latimer & Giles, 2018; Wilson et al., 2019; Figueroa et al., 2021. Scales from the posterior half of the flank in *Wendyichthys* bear pores on the enamel surface, whereas those from the anterior part of the flank lack these pores (Lund & Poplin, 1997: fig. 6). This taxon is scored '1'.)

0 absent
1 present

213. Small scales below dorsal fin - (Giles et al. 2017; Argyriou et al., 2018; Latimer & Giles, 2018; Wilson et al., 2019; Figueroa et al., 2021.)

0 absent
1 present

214. Lepidotrichia - (Friedman, 2007; Brazeau, 2009; Zhu et al., 2009; Friedman & Brazeau, 2010; Davis et al., 2012; Zhu et al., 2013; Brazeau & Friedman, 2014; Giles et al., 2015b,c; Giles et al. 2017; Argyriou et al., 2018; Latimer & Giles, 2018; Wilson et al., 2019; Figueroa et al., 2021.)

0 absent
1 present

215. Fringing fulcra - (Patterson, 1982; Gardiner & Schaeffer, 1989; Grande & Bemis 1998; Coates, 1999; Dietze, 2000; Schultze & Cumbaa, 2001; Poyato-Ariza & Wenz, 2002; Cloutier & Arratia, 2004; Friedman & Blom, 2006; Friedman, 2007; Long et al., 2008; Swartz, 2009; Zhu et al., 2009; Choo, 2011; Xu & Gao, 2011; López-Arbarello 2012; Zhu et al., 2013; Xu et al., 2014, 2015; Bermúdez-Rochas & Poyato-Ariza 2015; Poyato-Ariza 2015; Giles et al., 2015b; Thies & Waschkewitz, 2015; Gibson 2016; Xu & Zhao, 2016; Giles et al. 2017; Cawley & Kriwet 2018; López-Arbarello & Sferco 2018; Argyriou et al., 2018; Latimer & Giles, 2018; Wilson et al., 2019; Figueroa et al., 2021.)

0 absent
1 present

216. Double headed hyomandibular - (Cloutier & Ahlberg, 1996; Zhu & Schultze, 2001; Schultze & Cumbaa, 2001; Zhu et al., 2001; Zhu & Yu, 2002; Zhu et al., 2006; Friedman, 2007; Zhu et al., 2009; Friedman & Brazeau, 2010; Zhu et al., 2013; Giles et al., 2015b,c; Giles et al. 2017; López-Arbarello & Sferco 2018; Argyriou et al., 2018; Latimer & Giles, 2018; Wilson et al., 2019; Figueroa et al., 2021.)

0 absent
1 present

217. Perforate hyomandibula - (Friedman, 2007; Zhu et al., 2009; Friedman & Brazeau, 2010; Xu & Gao, 2011; Zhu et al., 2013; Brazeau & Friedman, 2014; Xu et al., 2014, 2015; Giles et al., 2015b; Xu & Zhao, 2016; Giles et al. 2017; Argyriou et al., 2018; Latimer & Giles, 2018; Wilson et al., 2019; Figueroa et al., 2021. Although Long (1988: p.24) mentions the presence of a depression for the hyomandibular nerve in *Howqualepis*, it is unclear whether this perforated the hyomandibula. This taxon is conservatively coded as '?'.)

0 absent
1 present

218. Opercular process - (Gardiner & Schaeffer, 1989 Poyato-Ariza & Wenz, 2002;; Giles et al., 2015b; Giles et al. 2017; Cawley & Kriwet 2018; López-Arbarello & Sferco 2018; Argyriou et al., 2018; Latimer & Giles, 2018; Wilson et al., 2019; Figueroa et al., 2021.). This character has been modified to more clearly separate taxa which have a very distinct opercular process for articulation of the hyomandibular with the opercular from those that have a small bump.

0 absent
1 present

219. Thin ventral process extending from the anterior margin of the hyomandibular. Only two taxa exhibit a very thin ventral process (also termed an ‘anterior lamella’; Wenz, 1959) extending from the anterior margin of the hyomandibular.

0 absent
1 present

220. Ceratohyal - (Gardiner et al., 2005; Xu & Gao, 2011; Giles et al., 2015b; Giles et al. 2017; Xu et al., 2014; Argyriou et al., 2018; Latimer & Giles, 2018; Wilson et al., 2019; Figueroa et al., 2021.)

0 single ossification
1 two ossifications

221. Anterior ossification of ceratohyal - (Revised from Coates, 1999; Giles et al., 2015b; Giles et al. 2017; López-Arbarello & Sferco 2018; Argyriou et al., 2018; Latimer & Giles, 2018; Wilson et al., 2019; Figueroa et al., 2021. The character captures whether the ceratohyal (or the anterior ossification if an anterior and posterior ceratohyal are present) is medially constricted (hourglass-shaped) or plate-like in lateral view.)

0 no medial constriction
1 medial constriction (hourglass-shaped)

222. Anterior ceratohyal - (Coates, 1999; Giles et al., 2015b; Giles et al. 2017; Argyriou et al., 2018; Latimer & Giles, 2018; Wilson et al., 2019; Figueroa et al., 2021. The groove for the afferent hyoidean artery in the ceratohyal of *Gogosardina* is visible in Choo 2009 (fig 6).)

0 no groove
1 groove for afferent hyoidean artery

223. Ossified accessory hyoid elements – (Argyriou et al., 2022 In most primitive gnathostomes and chondrichthyans, elements situated between the epihyal or hyomandibula the ceratohyal are completely absent.)

0 absent
1 present

224. If present, number of accessory hyoid elements – (Argyriou et al., 2022.)
0 one
1 two

225. Symplectic shape - (Giles et al. 2017; López-Arbarello & Sferco 2018; Argyriou et al., 2018; Latimer & Giles, 2018; Wilson et al., 2019; Figueroa et al., 2021.)
0 tube/splint like
1 hatchet
2 l-shaped

226. Hypohyal - (Friedman & Brazeau, 2010; Brazeau & Friedman, 2014; Giles et al., 2015b,c; Giles et al. 2017; Argyriou et al., 2018; Latimer & Giles, 2018; Wilson et al., 2019; Figueroa et al., 2021.)
0 absent
1 present

227. Basihyal - (Davis et al., 2012; Zhu et al., 2013; Giles et al., 2015b,c; Giles et al. 2017; López-Arbarello & Sferco 2018; Argyriou et al., 2018; Latimer & Giles, 2018; Wilson et al., 2019; Figueroa et al., 2021.)
0 absent
1 present

228. Gill arches - (Giles et al., 2015b,c; Giles et al. 2017; Argyriou et al., 2018; Latimer & Giles, 2018; Wilson et al., 2019; Figueroa et al., 2021.)
0 largely restricted to area under braincase
1 extend far posterior to braincase

229. Number of ossified basibranchials (new character) - Some extant actinopterygians possess multiple basibranchial elements, yet these remain cartilaginous (e.g. *Acipenser*, *Amia*). In extinct actinopterygians, the number of basibranchials is variable.
0 one
1 two
2 three
3 four
4 none

230. Number of ceratobranchials - (Giles et al. 2017; Argyriou et al., 2018; Latimer & Giles, 2018; Wilson et al., 2019; Figueroa et al., 2021.)
0 five
1 four

231. Ventral processes extending from anterior region of ceratobranchials (new character) – In MM L.1696 the 3rd and 4th ceratobranchials bear distinct ventral processes emanating from the ventral face near the anterior margin of the bone.
0 absent
1 present

232. Fifth ceratobranchial morphology (new character).

0 rod-like along entire length
1 bifurcates posteriorly
2 broad, plate-like
3 median flange proximally

233. Number of hypobranchials - (Grande, 2010; Xu & Wu, 2012; Xu et al., 2014, 2015; Xu & Zhao, 2016; Giles et al. 2017; López-Arbarello & Sferco 2018; Argyriou et al., 2018; Latimer & Giles, 2018; Wilson et al., 2019; Figueroa et al., 2021.). An additional state was added to account for the taxa which only possess two hypobranchials (e.g. *Mesonichthys aitkeni*, Watson, 1925).

0 three
1 four
2 two

234. Number of epibranchials (new character).

0 five
1 four
2 three
3 two
4 none

235. Uncinate processes on epibranchials - (Coates, 1999; Xu & Gao, 2011; Xu et al., 2014, 2015; Poyato-Ariza 2015; Xu & Zhao, 2016; Giles et al. 2017; López-Arbarello & Sferco 2018; Argyriou et al., 2018; Latimer & Giles, 2018; Wilson et al., 2019; Figueroa et al., 2021. An uncinate process is a dorsally-directed extension on the epibranchial that articulates with the pharyngobranchial skeleton.)

0 absent
1 present

236. Endoskeletal urohyal - (Friedman, 2007; Friedman & Brazeau, 2010; Giles et al., 2015b,c; Poyato-Ariza 2015; Giles et al. 2017; López-Arbarello & Sferco 2018; Argyriou et al., 2018; Latimer & Giles, 2018; Wilson et al., 2019; Figueroa et al., 2021.)

0 absent
1 present

237. Urohyal formed as a tendon bone of the sternohyoideus muscle - (Arratia 2013; Giles et al. 2017; Argyriou et al., 2018; Latimer & Giles, 2018; Wilson et al., 2019; Figueroa et al., 2021.)

0 absent
1 present

238. Presupracleithrum - (Patterson, 1982; Gardiner, 1984; Gardiner & Schaeffer, 1989; Taverne, 1997; Lund, 2000; Schultze & Cumbaa, 2001; Zhu & Schultze, 2001; Zhu et al., 2001; Lund & Poplin, 2002; Zhu & Yu, 2002; Cloutier & Arratia, 2004; Gardiner et al., 2005; Friedman & Blom, 2006; Zhu et al., 2006; Friedman, 2007; Long et al., 2008; Swartz, 2009; Zhu et al., 2009; Choo, 2011; Xu & Gao, 2011; Zhu et al., 2013; Xu et al., 2014; Giles et al., 2015b; Giles et al. 2017; López-Arbarello & Sferco 2018; Argyriou et al., 2018; Latimer & Giles, 2018; Wilson et al., 2019; Figueroa et al., 2021. An elongate bone termed the 'anocleithrum' is variably

present in *Wendyichthys* (Lund & Poplin, 1997) in the position occupied by the presupracleithrum in other taxa. We regard this as a positional homologue, and code the taxon '0/1' to reflect this polymorphism. Coded as '?' in *C. trailli* following arguments in Friedman & Blom (2006).)

0 absent
1 present

239. Presupracleithrum - Note that the postspiracular of some descriptions (e.g. Mickle et al. 2009) is here identified as a presupracleithrum (e.g. *Lineagruan* has presupracleithrum and a postspiracular in the description, but is here coded as having multiple presupracleithra). - (Xu et al. 2014; Giles et al. 2017; Argyriou et al., 2018; Latimer & Giles, 2018; Wilson et al., 2019; Figueroa et al., 2021.)

0 single
1 multiple

240. Dorsal margin of cleithrum - (Cloutier & Ahlberg, 1996; Schultze & Cumbaa, 2001; Zhu & Schultze, 2001; Zhu et al., 2001; Zhu & Yu, 2002; Cloutier & Arratia, 2004; Zhu et al., 2006; Friedman, 2007; Zhu et al., 2009; Giles et al., 2015b,c; Giles et al. 2017; Argyriou et al., 2018; Latimer & Giles, 2018; Wilson et al., 2019; Figueroa et al., 2021.)

0 pointed
1 broad and rounded

241. Medial wing on cleithrum - (Cavin & Suteethorn 2006; Poyato-Ariza 2015; Giles et al. 2017; López-Arbarello & Sferco 2018; Argyriou et al., 2018; Latimer & Giles, 2018; Wilson et al., 2019; Figueroa et al., 2021.)

0 absent
1 present

242. Anocleithrum - (Gardiner & Schaeffer, 1989; Lund et al., 1995; Cloutier & Ahlberg, 1996; Dietze, 2000; Poplin & Lund, 2000; Schultze & Cumbaa, 2001; Zhu & Schultze, 2001; Zhu et al., 2001; Zhu & Yu, 2002; Cloutier & Arratia, 2004; Zhu et al., 2006; Friedman, 2007; Zhu et al., 2009; Zhu et al., 2013; Giles et al., 2015b; Giles et al. 2017; López-Arbarello & Sferco 2018; Argyriou et al., 2018; Latimer & Giles, 2018; Wilson et al., 2019; Figueroa et al., 2021.)

0 bone developed as postcleithrum
1 bone developed as anocleithrum sensu stricto
2 bone absent

243. Clavicle - (Patterson 1973; Olsen & McCune 1991; Coates 1999; Xu & Gao 2011; Xu et al. 2014; Poyato-Ariza 2015; Xu & Zhao, 2016; Giles et al. 2017; López-Arbarello & Sferco 2018; Argyriou et al., 2018; Latimer & Giles, 2018; Wilson et al., 2019; Figueroa et al., 2021.)

0 present as a broad plate
1 much reduced or absent

244. Serrated organ - (Arratia 2013; Giles et al. 2017; López-Arbarello & Sferco 2018; Argyriou et al., 2018; Latimer & Giles, 2018; Wilson et al., 2019; Figueroa et al., 2021. The serrated organ (or appendage) is a small, elongate element, typically ornamented with serrated ridges, present near the anterior margin of the cleithrum.)

0 absent
1 present

245. Interclavicle - (Cloutier & Arratia, 2004; Giles et al. 2017; Xu et al., 2014; Argyriou et al., 2018; Latimer & Giles, 2018; Wilson et al., 2019; Figueroa et al., 2021.)

0 present
1 absent

246. Triradiate scapulocoracoid with distinct distal buttresses (*sensu* Coates and Tietjen, 2018) – (Olsen & McCune 1991; Zhu & Schultze, 2001; Zhu et al., 2001; Zhu & Yu, 2002; Zhu et al., 2006; Friedman, 2007; Zhu et al., 2009; Xu & Gao, 2011; Zhu et al., 2013; Xu et al., 2014; Giles et al., 2015b; Giles et al. 2017; Argyriou et al., 2018; Coates & Tietjen, 2018; Latimer & Giles, 2018; Wilson et al., 2019; Figueroa et al., 2021. Coates & Tietjen [2018] highlighted that a truly triradiate scapulocoracoid, with three distinct distal buttresses, is a sarcopterygian characteristic. The scapulocoracoid of actinopterygians lack distinct buttresses, though tend to be divided into three parts; 'tripartite').

0 absent
1 present

247. Tripartite scapulocoracoid with dorsal and ventral portions divided by a shelf-life middle region or bar (*sensu* Coates & Tietjen, 2018). (This character refers to the condition in some actinopterygians in which the scapulocoracoid has a dorsal and ventral portion separated by a shelf-life middle region or bar.).

0 absent
1 present

248. Posterior mesocoracoid process on scapulocoracoid. (This refers to a distinct, posteriorly or posteroventrally directed process on the scapulocoracoid, not the stout glenoid process of sarcopterygians. *Moythomasia durgargina* is labelled as having a mesocoracoid process, however this is a small dorsal extension, rather than the distinct process of later Carboniferous fishes).

0 absent
1 present

249. Perforate propterygium - (Patterson, 1982; Gardiner, 1984; Gardiner & Schaeffer, 1989; Rosen, 1989; Taverne, 1997; Coates, 1999; Zhu & Schultze, 2001; Zhu et al., 2001; Zhu & Yu, 2002; Zhu et al., 2006; Brazeau, 2009; Zhu et al., 2009; Friedman & Brazeau, 2010; Xu & Gao, 2011; Davis et al., 2012; Zhu et al., 2013; Xu et al., 2014; Giles et al., 2015b,c; Argyriou et al., 2018; Latimer & Giles, 2018; Wilson et al., 2019; Figueroa et al., 2021.)

0 absent
1 present

250. Anterior rays embrace propterygium - (Patterson, 1982; Gardiner, 1984; Gardiner & Schaeffer, 1989; Taverne, 1997; Coates, 1999; Schultze & Cumbaa, 2001; Zhu & Schultze, 2001; Friedman & Blom, 2006; Long et al., 2008; Swartz, 2009; Choo, 2011; Xu & Gao, 2011; Giles et al., 2015b; Giles et al. 2017; Argyriou et al., 2018; Latimer & Giles, 2018; Wilson et al., 2019; Figueroa et al., 2021.)

0 absent
1 present
2 fused

251. Propterygium fused to first ray - (Giles et al. 2017; López-Arbarello & Sferco 2018; Argyriou et al., 2018; Latimer & Giles, 2018; Wilson et al., 2019; Figueroa et al., 2021.)

0 absent
1 present

252. Pectoral fin endoskeleton - (Taverne, 1997; Coates, 1999; Friedman & Blom, 2006; Long et al., 2008; Swartz, 2009; Xu & Gao, 2011; Xu et al., 2014; Giles et al., 2015b; Giles et al. 2017; Argyriou et al., 2018; Latimer & Giles, 2018; Wilson et al., 2019; Figueroa et al., 2021.)
0 extends far beyond body wall (fins lobate)
1 barely extends beyond body wall (fins not lobate)

253. Pectoral fin radials - (Zhu & Yu, 2002; Friedman, 2007; Giles et al., 2015b; Giles et al. 2017. Two series of pectoral fin radials are described (but not figured) for Cheirolepis candensis (Arratia & Cloutier, 2004). Although we consider this arrangement to be unlikely, for now this taxon is coded '1'; Argyriou et al., 2018; Latimer & Giles, 2018; Wilson et al., 2019; Figueroa et al., 2021.)
0 unjointed
1 jointed

254. Fin articulation - (Zhu & Schultze, 2001; Zhu et al., 2001; Zhu & Yu, 2002; Zhu et al., 2006; Friedman, 2007; Zhu et al., 2009; Friedman & Brazeau, 2010; Zhu et al., 2013; Giles et al., 2015b,c; Giles et al. 2017; Argyriou et al., 2018; Latimer & Giles, 2018; Wilson et al., 2019; Figueroa et al., 2021.)
0 monobasal
1 polybasal

255. Pectoral fin-ray segmentation - (Coates, 1999; Friedman & Blom, 2006; Long et al., 2008; Choo, 2011; Xu & Gao, 2011; Xu et al., 2014; Giles et al., 2015b; Giles et al. 2017; Argyriou et al., 2018; Latimer & Giles, 2018; Wilson et al., 2019; Figueroa et al., 2021.)
0 roughly even segmentation to fin base
1 proximal segments elongate with terminal segmentation
2 no significant segmentation on pectoral fin
3 terminal segments elongate with proximal segmentation

256. Pectoral fin - (Giles et al., 2015b; Giles et al. 2017; Argyriou et al., 2018; Latimer & Giles, 2018; Wilson et al., 2019; Figueroa et al., 2021.)
0 [leaf-like]
1 (not leaf-like)

257. Paired fin spines - (Zhu et al., 2001; Zhu & Yu, 2002; Friedman, 2007; Zhu et al., 2009; Brazeau, 2009; Davis et al., 2012; Zhu et al., 2013; Giles et al., 2015b,c; Giles et al. 2017; Argyriou et al., 2018; Latimer & Giles, 2018; Wilson et al., 2019; Figueroa et al., 2021.)
0 absent
1 present

258. Pelvic fins - (Friedman & Blom, 2006; Friedman, 2007; Brazeau, 2009; Choo, 2011; Davis et al., 2012; Zhu et al., 2013; Brazeau & Friedman, 2014; Giles et al., 2015b,c; Giles et al. 2017; Argyriou et al., 2018; Latimer & Giles, 2018; Wilson et al., 2019; Figueroa et al., 2021.)
0 absent
1 present

259. Pelvic fin insertion - (Gardiner & Schaeffer, 1989; Coates, 1998; Coates, 1999; Lund, 2000; Schultze & Cumbaa, 2001; Cloutier & Arratia, 2004; Friedman & Blom, 2006; Zhu et al., 2006; Long et al., 2008; Swartz, 2009; Zhu et al., 2009; Choo, 2011; Xu et al., 2014; Giles et al., 2015b; Giles et al. 2017; Argyriou et al., 2018; Latimer & Giles, 2018; Wilson et al., 2019; Figueroa et al., 2021.)

0 shorter than fin depth (short based)
1 longer than fin depth (long based)

260. Basal scutes on fins - (Friedman, 2007; Zhu & Yu, 2002; López-Arbarello 2012; Bermúdez-Rochas & Poyato-Ariza 2015; Giles et al., 2015b; Thies & Waschkewitz, 2015; Gibson 2016; Giles et al. 2017; López-Arbarello & Sferco 2018; Argyriou et al., 2018; Latimer & Giles, 2018; Wilson et al., 2019; Figueroa et al., 2021.)

0 absent
1 present

261. Dorsal scutes anterior to dorsal fin - (Olsen & McCune 1991; Lund, 2000; Poplin & Lund, 2000; Poyato-Ariza & Wenz, 2002; Cloutier & Arratia, 2004; Friedman & Blom, 2006; Long et al., 2008; Swartz, 2009; Choo, 2011; Giles et al., 2015b; Thies & Waschkewitz, 2015; Gibson 2016; Giles et al. 2017; Cawley & Kriwet 2018; López-Arbarello & Sferco 2018; Argyriou et al., 2018; Latimer & Giles, 2018; Wilson et al., 2019; Figueroa et al., 2021.)

0 absent
1 few limited to region immediately anterior to fin (basal fulcra only)
2 many, extending to posterior of skull roof (complete set of dorsal ridge scales)

262. Ventral scutes between hypochordal lobe of caudal fin and anal fin (Patterson, 1982; Taverne, 1997; Friedman & Blom, 2006; Long et al., 2008; Choo, 2011; Giles et al., 2015b; Giles et al. 2017; López-Arbarello & Sferco 2018; Argyriou et al., 2018; Latimer & Giles, 2018; Wilson et al., 2019; Figueroa et al., 2021.)

0 absent
1 present

263. Ventral scutes anterior to anal fin - (Cloutier & Arratia, 2004; Friedman & Blom, 2006; Long et al., 2008; Swartz, 2009; Choo, 2011; Giles et al., 2015b; Giles et al. 2017; Argyriou et al., 2018; Latimer & Giles, 2018; Wilson et al., 2019; Figueroa et al., 2021.)

0 absent
1 present

264. Dorsal fin(s) - (Gardiner & Schaeffer, 1989; Schultze & Cumbaa, 2001; Zhu & Schultze, 2001; Zhu et al., 2001; Zhu & Yu, 2002; Cloutier & Arratia, 2004; Friedman & Blom, 2006; Zhu et al., 2006; Friedman, 2007; Long et al., 2008; Brazeau, 2009; Swartz, 2009; Zhu et al., 2009; Choo, 2011; Davis et al., 2012; Zhu et al., 2013; Giles et al., 2015b,c; Giles et al. 2017; Argyriou et al., 2018; Latimer & Giles, 2018; Wilson et al., 2019; Figueroa et al., 2021.)

0 two
1 one

265. Relative positions of anal and (second) dorsal fin - (Poplin & Lund, 2000; Cloutier & Arratia, 2004; Friedman & Blom, 2006; Long et al., 2008; Swartz, 2009; Choo, 2011; López-Arbarello 2012; Bermúdez-Rochas & Poyato-Ariza 2015; Giles et al., 2015b; Thies & Waschkewitz, 2015; Gibson 2016; Giles et al. 2017; López-Arbarello & Sferco 2018; Argyriou et al., 2018; Latimer & Giles, 2018; Wilson et al., 2019; Figueroa et al., 2021.)

0 anal shifted anteriorly relative to dorsal
1 fins opposite one another
2 anal shifted posteriorly relative to dorsal

266. Median fins (except caudal fin) - (Gardiner et al., 2005; Xu & Gao, 2011; Xu et al., 2014, 2015; Xu & Zhao, 2016; Giles et al. 2017; López-Arbarello & Sferco 2018; Argyriou et al., 2018; Latimer & Giles, 2018; Wilson et al., 2019; Figueroa et al., 2021.)
0 rays more numerous than radials
1 rays andradials equal

267. Proximal and middle radials of dorsal fin - (Giles et al. 2017; Argyriou et al., 2018; Latimer & Giles, 2018; Wilson et al., 2019; Figueroa et al., 2021.)
0 proximal and middle radials of similar size
1 proximal radials substantially enlarged

268. Posteriormost proximal radial of dorsal fin - (Giles et al. 2017; Argyriou et al., 2018; Latimer & Giles, 2018; Wilson et al., 2019; Figueroa et al., 2021.)
0 enlarged plate
1 smaller than more anterior radials

269. Epichordal lobe of caudal fin - (Patterson, 1982; Cloutier & Ahlberg, 1996; Coates, 1999; Schultze & Cumbaa, 2001; Zhu & Schultze, 2001; Friedman & Blom, 2006; Long et al., 2008; Swartz, 2009; Choo, 2011; Giles et al., 2015b; Giles et al. 2017; Argyriou et al., 2018; Latimer & Giles, 2018; Wilson et al., 2019; Figueroa et al., 2021.)
0 present
1 absent

270. Fulcra along dorsal ridge of caudal fin - (Patterson, 1982; Taverne, 1997; Gardiner & Schaeffer, 1989; Gardiner et al., 2005; Friedman & Blom, 2006; Long et al., 2008; Choo, 2011; López-Arbarello 2012; Bermúdez-Rochas & Poyato-Ariza 2015; Giles et al., 2015b; Giles et al. 2017; López-Arbarello & Sferco 2018; Argyriou et al., 2018; Latimer & Giles, 2018; Wilson et al., 2019; Figueroa et al., 2021.)
0 absent
1 present

271. Caudal fin geometry - (Modified from Gardiner et al., 2005; Giles et al. 2017; Argyriou et al., 2018; Latimer & Giles, 2018; Wilson et al., 2019; Figueroa et al., 2021. A long chordal lobe is considered to be present when the notochord reaches the posterior margin of the caudal fin.)
0 long chordal lobe
1 short chordal lobe

272. Posterior margin of caudal fin - (Grande & Bemis 1998; Xu & Gao 2011; Xu et al. 2014; Xu & Zhao, 2016; Giles et al. 2017; López-Arbarello & Sferco 2018; Argyriou et al., 2018; Latimer & Giles, 2018; Wilson et al., 2019; Figueroa et al., 2021.)
0 forked
1 unforked

273. Epineural processes (Arratia 2013; Argyriou et al. 2018, 2022).
0 absent

1 present

274. Diplospondyly in mid-caudal region - (Grande & Bemis 1998; Arratia 2013; Poyato-Ariza 2015; Giles et al. 2017; López-Arbarello & Sferco 2018; Argyriou et al., 2018; Latimer & Giles, 2018; Wilson et al., 2019; Figueroa et al., 2021.)
0 absent
1 present

275. Median neural spines in caudal region - (Coates 1999; Hurley et al. 2007; Xu et al. 2014; Giles et al. 2017; López-Arbarello & Sferco 2018; Argyriou et al., 2018; Latimer & Giles, 2018; Wilson et al., 2019; Figueroa et al., 2021.)
0 absent
1 present

276. Uroneural - (Pinna, 1996; Hurley et al., 2007; Xu & Wu, 2012, Xu et al., 2014; Xu & Zhao, 2016; Giles et al. 2017; López-Arbarello & Sferco 2018; Argyriou et al., 2018; Latimer & Giles, 2018; Wilson et al., 2019; Figueroa et al., 2021.)
0 absent
1 present

277. Division of hypurals into dorsal and ventral groups - (Pinna, 1996, Xu & Wu, 2012, Xu et al., 2014; Xu & Zhao, 2016; Giles et al. 2017; Argyriou et al., 2018; Latimer & Giles, 2018; Wilson et al., 2019; Figueroa et al., 2021.)
0 absent
1 present

278. Number of caudal lepidotrichs borne per hypural - (Giles et al. 2017; López-Arbarello & Sferco 2018; Argyriou et al., 2018; Latimer & Giles, 2018; Wilson et al., 2019; Figueroa et al., 2021.)
a. multiple (single)
b. single

279. Opistocoelous vertebrae - (Wiley, 1976; López-Arbarello 2012; Bermúdez-Rochas & Poyato-Ariza 2015; Thies & Waschkewitz, 2015; Poyato-Ariza 2015; Gibson 2016; Giles et al. 2017; López-Arbarello & Sferco 2018; Argyriou et al., 2018; Latimer & Giles, 2018; Wilson et al., 2019; Figueroa et al., 2021.)
0 absent
1 present

280. Ossified ribs - (Giles et al. 2017; Argyriou et al., 2018; Latimer & Giles, 2018; Wilson et al., 2019; Figueroa et al., 2021.)
0 present
1 absent

281. Antorbital deeper than anteriormost infraorbital - (L?pez-Arbarello 2012; Thies & Waschkewitz, 2015; Gibson 2016; Lóiiiiiiiiipez-Arbarello & Sferco 2018; Latimer & Giles, 2018.)
0 absent
1 present

282. Infraorbitals fragmented - (Latimer & Giles, 2018. The infraorbitals normally form as a single row partially surrounding the orbit. In some taxa, they may be fragmented into multiple irregular ossifications.)

0 absent
1 present

283. Suborbitals fragmented - (Grande & Bemis 1998; López-Arbarello 2011; López-Arbarello & Sferco 2018; Latimer & Giles, 2018. The suborbitals normally form as a single row partially surrounding the orbit, posterior and/or ventral to the infraorbitals. In some taxa, they may be fragmented into multiple irregular ossifications.)

0 absent
1 present

284. Suborbitals extend ventral to orbit - (López-Arbarello 2011; López-Arbarello & Sferco 2018; Latimer & Giles, 2018.)

0 absent
1 present

285. Coronoids contribute to lateral dentition field - (Latimer & Giles, 2018. Coronoids are normally restricted to the medial (lingual) surface of the jaw. In some dapediids, they may extend laterally to contribute to the labial tooth row.)

0 absent
1 present

286. Jaw articulation ventral to orbit - (López-Arbarello 2012; Bermúdez-Rochas & Poyato-Ariza 2015; Poyato-Ariza 2015; Thies & Waschkewitz, 2015; Gibson 2016; López-Arbarello & Sferco 2018; Latimer & Giles, 2018.)

0 absent
1 present

287. Parasphenoid wings around basiocciput - (Latimer & Giles, 2018. The parasphenoid is normally restricted to covering the ventral face of the braincase. In some taxa, extensions may extend dorsally and laterally to cloak the basiocciput.)

0 absent
1 present

288. Dorsal extension of parasphenoid between orbits - (Latimer & Giles, 2018. The parasphenoid extends dorsally between the orbits, contributing to the interorbital septum, in some taxa.)

0 absent
1 present

289. Ligament pit on posterior face of braincase - (Latimer & Giles, 2018. A deep ligament pit, dorsal to the foramen magnum, is found on the posterior face of the braincase in some taxa.)

0 absent
1 present

290. 'Hem-like' median fins - (Gibson 2016; Latimer & Giles, 2018.)

0 absent
1 present

291. Anal fin insertion - (Latimer & Giles, 2018.)
    0 short
    1 long

292. Denticulate ridge scales - (Latimer & Giles, 2018.)
    0 absent
    1 present

293. Ossified centra - (Poyato-Ariza & Wenz, 2002; Cawley & Kriwet 2018; Latimer & Giles, 2018.)
    0 absent
    1 present

294. Supratemporal commissure in parietal - (Poyato-Ariza & Wenz, 2002; Thies & Waschkewitz, 2015; Gibson 2016; Cawley & Kriwet 2018; López-Arbarello & Sferco 2018; Latimer & Giles, 2018. The supratemporal commissure is normally carried by the extrascapulars, but is sometimes borne in the parietal.)
    0 absent
    1 present

295. Enlarged vomerine teeth - (Poyato-Ariza & Wenz, 2002; Cawley & Kriwet 2018; López-Arbarello & Sferco 2018; Latimer & Giles, 2018.)
    0 absent
    1 present

296. Enlarged prearticular teeth - (Poyato-Ariza & Wenz, 2002; Cawley & Kriwet 2018; Latimer & Giles, 2018.)
    0 absent
    1 present

297. Prearticular symphysis - (Nursall 2010.; Latimer & Giles, 2018)
    0 absent
    1 present

298. Dermal supraoccipital - (Poyato-Ariza & Wenz, 2002; Cawley & Kriwet 2018; Latimer & Giles, 2018. A median bone, typically referred to as a dermal supraoccipital, is present between the parietals in some taxa.)
    0 absent
    1 present

299. Preoperculum taller than operculum - (Poyato-Ariza & Wenz, 2002; Cawley & Kriwet 2018; Latimer & Giles, 2018.)
    0 shorter
    1 taller

300. Preoperculum wider than operculum - (Poyato-Ariza & Wenz, 2002; Cawley & Kriwet 2018; Latimer & Giles, 2018.)
    0 narrower
    1 wider

301. Branchiostegals contact next in sequence - (Poyato-Ariza & Wenz, 2002; Cawley & Kriwet 2018; Latimer & Giles, 2018.)

0 absent
1 present

302. Dorsal lateral line - (Latimer & Giles, 2018.)

0 absent
1 present

303. Parasphenoid inflected ventrally below orbit - (Nursall 2010; Latimer & Giles, 2018.)

0 absent
1 present

304. Sagittal flange on neural spine - (Poyato-Ariza & Wenz, 2002; Cawley & Kriwet 2018; Latimer & Giles, 2018.)

0 absent
1 present

305. Sagittal flange on haemal spine - (Poyato-Ariza & Wenz, 2002; Cawley & Kriwet 2018; Latimer & Giles, 2018.)

0 absent
1 present

306. Pleural ribs alate - (Nursall 2010; Latimer & Giles, 2018.)

0 absent
1 present

307. Concavity on the ventral margin of the dentary forming the border of the lower jaw - (Figueroa et al. 2021; Latimer & Giles, 2018.)

0 absent
1 present

C.4 *Mesonichthys aitkeni* genus and species diagnoses

***Mesonichthys* genus diagnosis (Gardiner, 1963):** Body fusiform; dorsal fin arising well in front of anal, both fins triangular, acuminate and similar in size; caudal fin deeply cleft and inequilobate; pectoral fin long, with principal rays unjointed in proximal third of their length, pelvics short based; all fins have numerous fulcra anteriorly and lepidotrichia distally bifurcated. Snout rounded anteriorly and not produced into a rostrum. Jaw suspension only moderately oblique and opercular more than twice as high as subopercular. Orbit large with well developed sclerotic ring; dermohyal present but no accessory opercular; suborbitals present; angle of preopercular approximately 6o°; cranial roof bones and cheek bones ornamented with ridges of enamel; teeth of two sizes, larger conical laniaries being closely set with smaller tooth series interspersed; scales rhomboidal with pronounced ridges.

***Mesonichthys aitkeni* species diagnosis (Gardiner, 1963):** Fishes not exceeding 18 cm in total length, body fusiform, length of head contained five times and greatest depth of body four times in total body length. Lepidotrichia slender and smooth. Scales of moderate size, deeper than broad on the flank and ornamented with prominent striae which obliquely across the scale. Striae straight, rarely bifurcated or interpolated, and run parallel to one another.

C.5 Supplementary Figures

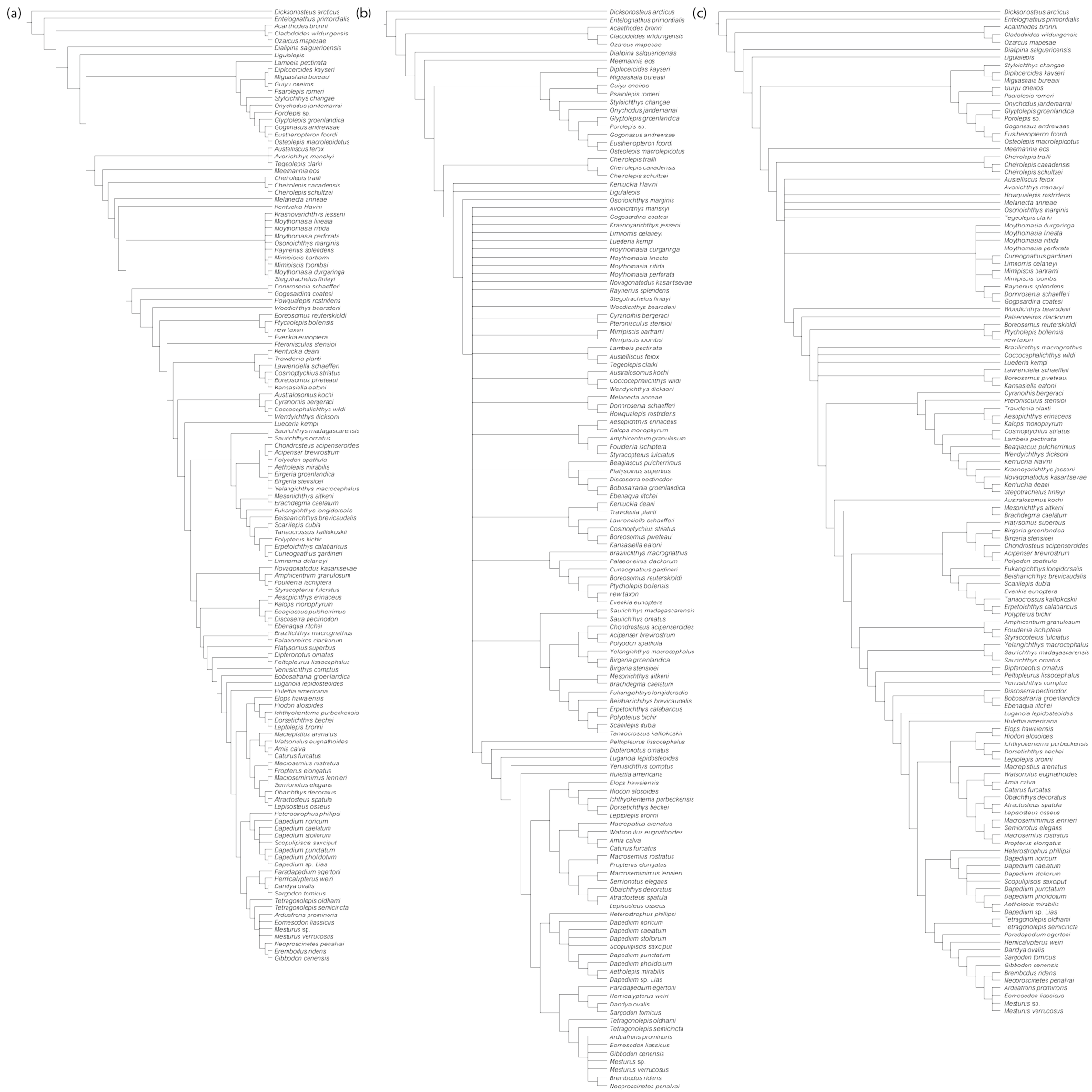


Figure C.2: Results of parsimony analysis. Strict consensus trees obtained from (a) implied weights (k = 1; tree length = 207.09175), (b) implied weights (k = 3; tree length = 153.30130), (c) implied weights (k = 12, tree length = 76.49224) with only outgroup constraint.

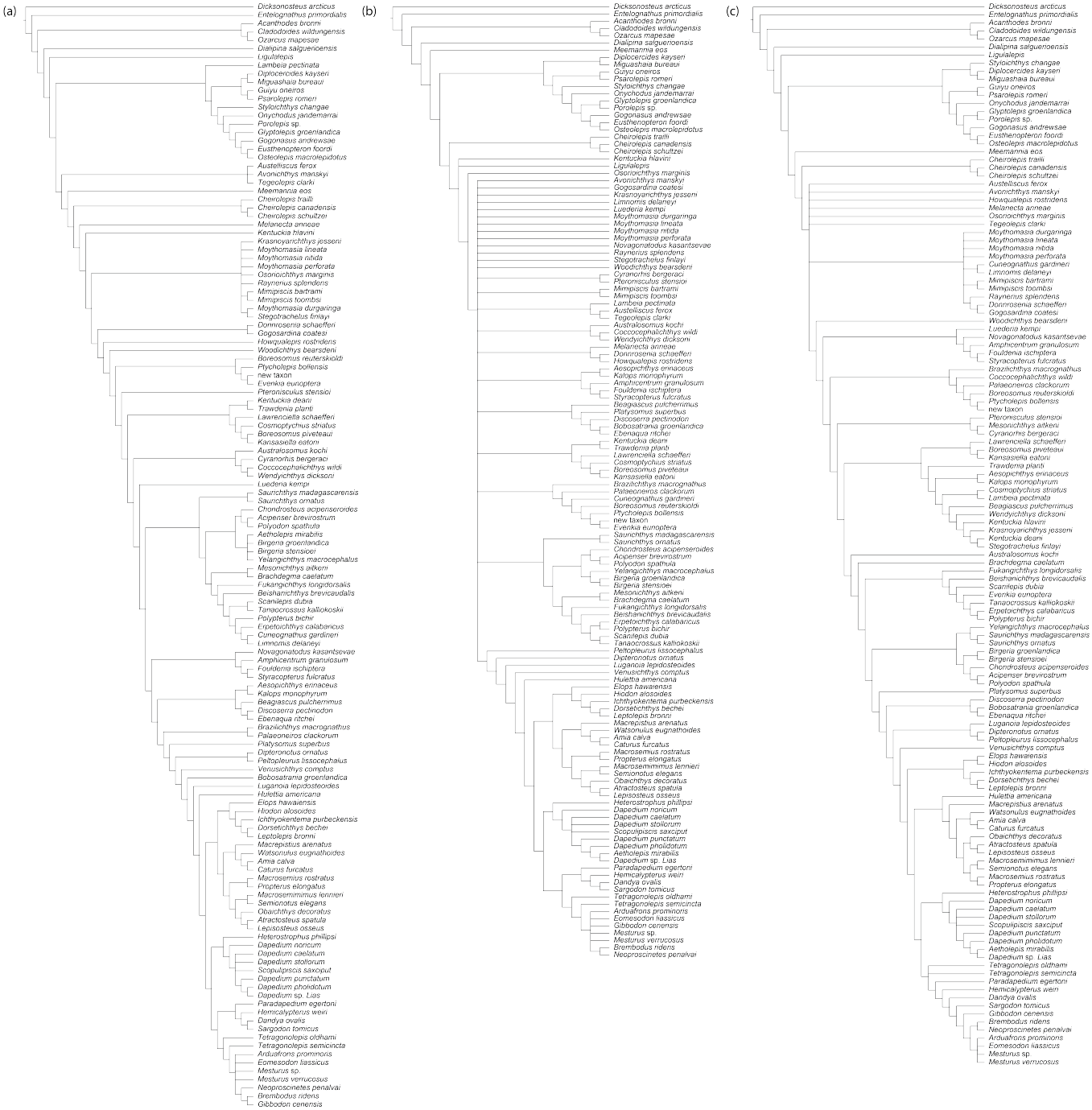


Figure C.3: Results of parsimony analysis. Strict consensus trees obtained from (a) implied weights (k = 1; tree length = 207.10725), (b) implied weights (k = 3; tree length = 153.30130), (c) implied weights (k = 12, tree length = 76.49819) with outgroup constraint and initial negative constraint on a polypteriform and chondrostean clade.